# Synthesis and Characterization of Multiphase Block Copolymers: Influence of Functional Groups on Macromolecular Architecture

Tomonori Saito

Dissertation submitted to the Faculty of the Virginia Polytechnic Institute and State University in Partial Fulfillment of the Requirements for the Degree

Doctor of Philosophy

In

Chemistry

Virginia Polytechnic Institute and State University

Submitted to:

Timothy E. Long, Chair

James E. McGrath

Judy S. Riffle

Garth L. Wilkes

Richey M. Davis

April 15, 2008
Blacksburg Virginia

Keywords: anionic polymerization, multiphase block copolymer, hydrogen-bonding, ionomer, morphology, structure-property relationship

# Synthesis and Characterization of Multiphase Block Copolymers: Influence of Functional Groups on Macromolecular Architecture

**Tomonori Saito**

## ABSTRACT

Low molecular weight liquid polybutadienes (1000 – 2000 g/mol) consisting of 60 mol% 1,2-polybutadiene repeating units were synthesized via anionic telomerization and conventional anionic polymerization. Maintaining the initiation and reaction temperature less than 70 °C minimized chain transfer and enabled the telomerization to occur in a living fashion, which resulted in well-controlled molecular weights and narrow polydispersity indices. MALDI-TOF mass spectrometry confirmed that the liquid polybutadienes synthesized via anionic telomerization contained one benzyl end and one protonated end.

Subsequently, 2-ureido-4[*1H*]-pyrimidone (UPy) quadruple hydrogen-bonding was introduced to telechelic poly(ethylene-*co*-propylene), and mechanical characterization of the composites with UPy-functionalized carbon nanotubes was performed. The composites enhanced the mechanical properties and the UPy-UPy association between the matrix polymer and carbon nanotubes prevented the decrease of an elongation at break. The matrix polymer was also reinforced without sacrificing the processability. Additionally, UPy groups were introduced to styrene-butadiene rubbers (SBRs). Introducing UPy groups to SBRs drastically changed the physical properties of these materials. Specifically, the SCMHB networks served as mechanically effective crosslinks, which raised $T_g$ and enhanced the mechanical performance of the SBRs.

Novel site-specific sulfonated graft copolymers, poly(methyl methacrylate)-*g*-(poly(sulfonic acid styrene)-*b*-poly(*tert*-butyl styrene)), poly(methyl methacrylate)-*g*-(poly(*tert*-butyl styrene)-*b*-poly(sulfonic acid styrene)), and the corresponding sodium sulfonate salts were successfully synthesized via living anionic polymerization, free radical graft copolymerization, and post-sulfonation strategies. The graft copolymers contained approximately 9 – 10 branches on average and 4 wt% of sulfonic acid or sodium sulfonate blocks adjacent to the backbone or at the branch terminus. The mobility of the sulfonated blocks located at the branch termini enabled the sulfonated blocks to more readily interact and form ionic aggregates. The glass transition temperatures ($T_g$) of the sulfonated graft copolymers with sulfonated blocks at the branch termini were higher than that of copolymers with sulfonated blocks adjacent to the backbone. More facile aggregation of sulfonated blocks at the branch termini resulted in the appearance of ionomer peaks in SAXS whereas ionomer peaks were not observed in sulfonated graft copolymers with sulfonated blocks adjacent to the backbone.

In addition, similar analogues, novel site-specific sulfonated graft copolymers, poly(methyl methacrylate)-*g*-(poly(sulfonic acid styrene)-*b*-poly(ethylene-*co*-propylene)) (PMMA-*g*-SPS-*b*-PEP), poly(methyl methacrylate)-*g*-(poly(ethylene-*co*-propylene)-*b*-poly(sulfonic acid styrene)) (PMMA-*g*-PEP-*b*-SPS), and the corresponding sodium sulfonate salts were successfully synthesized. Estimated $\chi N$ values predicted the phase separation of each block and differential scanning calorimetry (DSC) and dynamic mechanical analysis confirmed the phase separation of each block component of the graft copolymers. The aggregation of sulfonic acid or sodium sulfonate groups at the branch termini restricted the glass transition of the PEP block. This lack of the glass transition of

the PEP block resulted in higher storage modulus than a sulfonated graft copolymer with sulfonated blocks adjacent to the backbone. The location of sulfonated blocks in both sulfonic acid and sodium sulfonate graft copolymers significantly affected the thermal, mechanical and morphological properties.

Lastly, symmetric (16000 g/mol for each block) and asymmetric (14000 g/mol and 10000 g/mol for each block) poly(ethylene-*co*-propylene)-*b*-poly(dimehtylsiloxane) (PEP-*b*-PDMS) were synthesized using living anionic polymerization and subsequent hydrogenation. The onset of thermal degradation for the PEP-*b*-PDMS diblock copolymer was higher than 300 ºC and PEP-*b*-PDMS was more thermally stable than the precursor diblock copolymer, polyisoprene-*b*-PDMS. DSC analysis of PEP-*b*-PDMS provided $T_g$ of PDMS -125 ºC, $T_g$ of PEP -60 ºC, $T_c$ of PDMS -90 ºC, and $T_m$ of PDMS -46 and -38 ºC, respectively. Appearance of thermal transitions of each PEP and PDMS block revealed the formation of phase separation. Estimated $\chi N$ also supported the phase separation.

# Acknowledgements

I would like to thank my advisor Prof. Timothy E. Long for his guidance throughout my graduate school years and for his help in allowing me to come to Virginia Tech and grow as a polymer chemist. I would like to extend my gratitude to my committee members for their advice and guidance. I would also like to thank my collaborators in our research work, Dr. Frederick Beyer in the Army Research Laboratory, Prof. David Green in the University of Virginia, Drs. Robert Allen, Hiroshi Ito, and Jeff Gelorme at IBM, Dr. Carl Willis in Kraton Polymers, and Kim Harich and Stephen McCartney in Virginia Tech. The university staff was always helpful, including Millie Ryan, Laurie Good, and Jan McGinty.

I would like to recognize my fellow graduate students and postdocs in Prof. Tim Long's group for their help and support through the years; Qin Lin, Lars Kilian. Scott Trenor, Matt McKee, Ann Fornof, Serkan Unal, Afia Karikari, Amanda Willis, Matthew Cashion, Rebecca Huyck, John Layman, Andy Duncan, Matt Hunley, Sean Ramirez, Bill Heath and particularly the Hahn 3rd floor folks, Sharlene Williams, Gozde Ozturk, Akshay Kokil, Emily Anderson, Mana Tamami, Shijing Cheng, and Renlong Gao. I would like to thank Casey Elkins and Kalpana Viswanathan for mentoring me in my early years of a graduate school. I would also like to recognize my Japanese colleagues in the lab for their support, Keiichi Osano and Takeo Suga. Lastly, I would like to especially thank Brian Mather for his help and friendship where we grew together as a scientist.

Since I came to Blacksburg, I have gotten to know many people in school and in town. I have received support and prayer from those in Blacksburg as well as people from out of town and my home country, Japan. My uncle, Dr. Rikio Yokota, Mr. Paul Hergenrother, and Dr. John Connell helped me to come to Virginia Tech and I thank them for their guidance and support for my study here.

I would also like to thank my parents and my brother for their continuous support and love. And I would like to give biggest thanks to my wife, Holly, for loving me and

supporting me every day. Knowing her and spending time with her has been a main part of my life outside of school since my first year in Virginia Tech.

Lastly, I would like to give ultimate thanks to the Lord. He invited me and guided me to know him. I got to know him personally during my first year at Virginia Tech and I accepted Jesus Christ as my savior. The Lord has always guided me and encouraged me. I praise him for giving me a life and a purpose. I did not deserve but Lord Jesus paid the penalty for my sin upon the cross and the Holy Spirit lives in me. I am thankful for his love and continuous support. Every breath I take and every moment I have are because of him. I would like to express the deepest thanksgiving to the Lord and I pray he will continue to teach me and use me for his glory.

# List of Figures

# List of Schemes

# List of Tables

# Chapter 1: Dissertation Overview

This dissertation focuses on the synthesis and characterization of multiphase block copolymers with non-covalent interactions. The initial chapters focus on synthesis of well-defined polymers. The subsequent chapters discuss the influence of hydrogen-bonding interaction in a polymer matrix. The final chapters describe the structure-property relationships of site-specific sulfonated graft copolymers and synthesis of low $T_g$ diblock copolymers. The majority of synthesis utilized a living anionic polymerization to obtain well-defined polymers and the polymers were subsequently functionalized with hydrogen-bonding or sulfonic acid groups. The structure-property relationships of various novel multiphase copolymers with non-covalent interaction were also investigated.

Chapter 2 summarizes a literature review of the synthetic methodology to prepare well-defined macromolecular architectures, phase separation of block copolymers, and non-covalent interactions in macromolecular systems (hydrogen-bonding and ionic interactions), and the structure-property relationships of multiphase ionomers. The focus of Chapter 3 is on the synthesis and characterization of 1000 g/mol 60% 1,2-liquid polybutadienes via anionic telomerization. The influence of the initiation procedures, the reaction temperature, and the scale of reaction on the various telomerization processes were studied and compared to the properties of liquid polybutadiene synthesized using conventional anionic polymerization. The discussion of Chapter 4 transitions to an introduction of hydrogen-bondings to telechelic poly(ethylene-*co*-propylene) and mechanical properties of the composites with hydrogen-bonding functionalized carbon nanotubes. Chapter 5 describes introducing hydrogen-bondings to styrene butadiene

rubber and the influence of hydrogen-bondings on the mechanical performance. Chapters 6 and 7 investigate the influence of site-specific sulfonation in graft copolymers upon thermal, mechanical, and morphological properties. In addition, novel sulfonated graft copolymers with sulfonated blocks in precise location were synthesized and characterized. Lastly, Chapter 8 describes synthesis and characterization of low $T_g$ diblock copolymers.

# Chapter 2: Literature Review

## 2.1 Introduction

Precisely controlled chain polymerization has been a key factor for investigating the structure-property relationships of various novel multiphase copolymers with non-covalent interaction. This chapter will first describe the synthetic methodology to prepare well-defined macromolecular architecture (general aspects of living anionic polymerization). Secondly, this chapter will discuss phase separation of block copolymers and non-covalent interactions in macromolecular system (hydrogen-boding and ionic interaction). Lastly, this chapter will summarize research investigation for structure-property relationships of multiphase ionomers.

## 2.2 Living Anionic Polymerization

Living anionic polymerization possesses several important characteristics: controlled molecular weight, molecular weight distribution, controlled stereochemistry, functional termination capability, block copolymer synthesis, and star and branched copolymer synthesis. These five characteristics are all important criteria and will also be described in detail in this section. Among these characteristics, synthesis of well-defined homo and block copolymers play an important factor in this dissertation and will be discussed in detail. Living anionic polymerization has especially been the most advantageous strategy to prepare multiphase block copolymers. Therefore, the general concepts of living anionic polymerization are summarized and discussed.

### 2.2.1 General Concept of Living Polymerization

Living polymerization was developed and used in recent decades to prepare macromolecules with well-defined structures and low degrees of compositional

heterogeneity (homopolymers and each block segment).[1-8] The term "living" refers to no chain termination occurrence. The increase of molecular weight during the course of reaction depends on the initiation, propagation, and termination mechanisms. Figure 2.1 compares living polymerization to other polymerization method. A step-growth polymerization generally gives the rapid molecular weight increase at the end of the reaction due to the coupling reaction mechanism and the termination occurs based on the equilibrium nature of the reactivity of functional groups. On the other hand, a fast chain growth occurs in a conventional free-radical polymerization (Figure 2.1) and the chain-ends are terminated either by combination mechanism or disproportionation mechanism. The initiation step in a conventional free radical polymerization is slow, which results in the polymerization occurrence over a long period of time and plateau-out molecular weight over a certain reaction time.

Living polymerization is defined as a polymerization without termination and chain-transfer.[9, 10] The polymerized chains grow in a controlled linear fashion, which is shown in Figure 2.1. The initiated monomer species propagates until completing the monomer consumption. Intentional termination will be required to terminate the reaction. This living characteristic (no termination and no chain-transfer) produces a controlled molecular weight and a narrow molecular weight distribution. The molecular weight is readily calculated following the equation 2-1.

$$\text{Molecular Weight [g/mol]} = \frac{grams\ of\ monomer}{mols\ of\ initiator} \qquad (2\text{-}1)$$

Living polymerization using a monofunctional initiator follows the equation 2-1, whereas the denominator needs to be multiplied by 0.5 for living polymerization that utilizes a difunctional initiator.

The several types of living polymerization have been developed. The representative living polymerizations are classified as living anionic polymerization, living cationic polymerization, and living radical polymerization (stable free radical polymerization (SFRP), nitroxide mediated polymerization (NMP), atom transfer radical polymerization (ATRP), radical addition-fragmentation transfer (RAFT)).[11] Only living anionic polymerization will be focused here and further discussed in this dissertation.

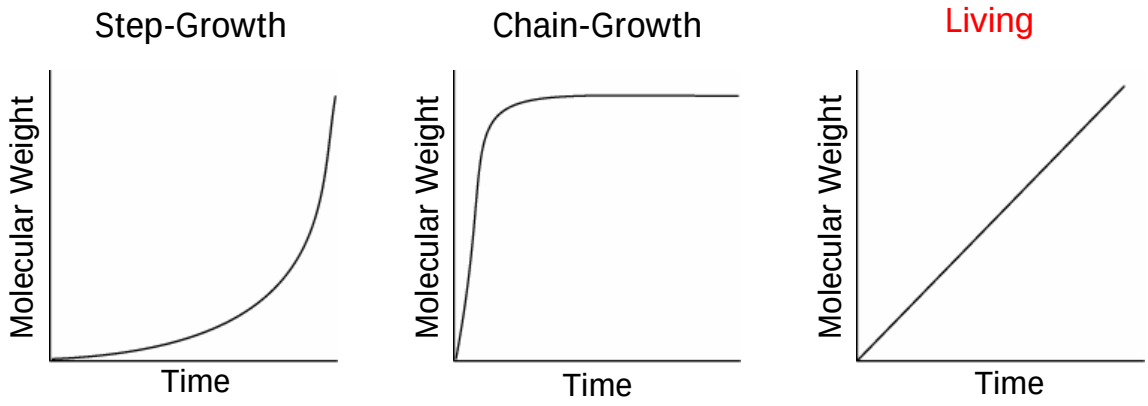


**Figure 2.1** Molecular weight growth of step-growth, chain-growth, and living polymerization

### 2.2.2 General Criteria of Living Anionic Polymerization

Living anionic polymerization is the earliest and most successful strategy among living polymerization strategies. Ziegler reported the polymerization of butadiene using *n*-butyllithium in 1929.[12, 13] In the report, Ziegler described termination and chain-transfer steps did not play a role in the polymerization mechanism. Later, Szwarc et al. named the term "living" for this kind of anionic polymerization.[9, 10] Living anionic polymerization of styrene is shown in Scheme 2.1 as a typical example. *sec*-Butyllithium initiates well-distilled styrene in cyclohexane. Rapid initiation occurs and the initiated styryllithium propagates until completing consumption of the styrene monomer. In styrene polymerization at 40 ºC in cyclohexane, 1 h reaction is sufficient for the complete

monomer consumption. The propagated styryllithium is terminated with a protic solvent such as methanol. Any protic compounds, e.g. water, will terminate the anionic polymerization, so that anionic polymerization requires a very clean and dry system in the polymerization. Monomer and solvent has to be well-distilled. In this styrene polymerization, styrene is first dried over calcium hydride and distilled under vacuum. Then, styrene is treated with an aliquot of dibutylmagnesium and distilled under vacuum. Cyclohexane is treated with sodium and distilled from the still or is passed through an activated molecular sieve column and activated alumina column immediately prior to use. For further details for various anionic polymerization, Hadjichristidis et al.[3] and Morton et al.[8] have summarized the techniques for distillation of monomers, solvent, and other technical issues for living anionic polymerization.

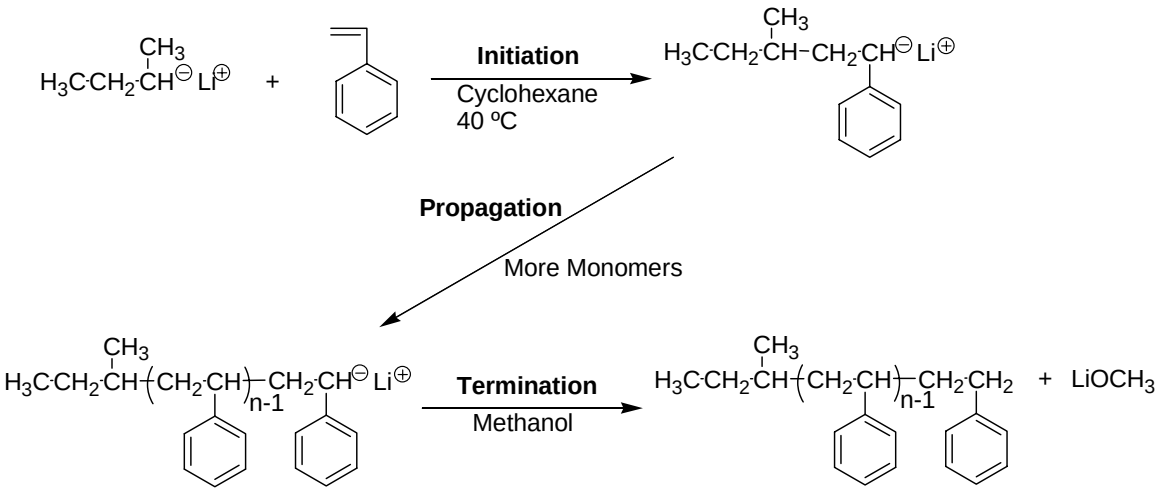


**Scheme 2.1** Living anionic polymerization of styrene

Anionic polymerization reaction is solely based on carbanion chemistry. The carbanion structure, stability, and reactivity control the kinetic and mechanism of anionic polymerization.[7] As an alkyl carbanion initiator, alkyllithium is typically used for anionic polymerization due to their various unique characteristics. The unique characteristics stem from the uniqueness of lithium. Among alkali metals, lithium

possesses the highest electron affinity, electron negativity, and an ionization potential, coupled with the smallest covalent and ionic radius in the group.[7] Alkyllithium exhibits properties of both covalent and ionic compounds.[14] Additionally, alkyllithium compounds are readily soluble in various organic solvents and form aggregates in hydrocarbon solution. Table 2.1 shows aggregation states of organolithium compounds in hydrocarbon solution. In hydrocarbon solutions, alkyllithium compounds associate into dimmer, tetramers, and hexamers. Unhindered straight-chain alkyllithium compounds such as $C_2H_5Li$, *n*-$C_4H_9Li$, *n*-$C_5H_{11}Li$, and *n*-$C_8H_{17}Li$ are associated into hexamers in hydrocarbon solution, whereas alkyllithium compounds with bulky group such as *i*-$C_3H_7Li$, *sec*-$C_4H_9Li$, and *t*-$C_4H_9Li$ associate into tetramers. The increase of bulky substituted alkyl groups in alkyllithium compounds decreases the average degree of association. Furthermore, the aggregation behavior of alkyllithium influences the initiation kinetics of anionic polymerization.

**Table 2.1** Aggregation states of organolithium compounds in hydrocarbon solution

| Compound | Solvent | Degree of association | Reference |
|---|---|---|---|
| $C_2H_5Li$ | Benzene | 6 | 15, 16 |
| | Cyclohexane | 6 | 15, 16 |
| *n*-$C_4H_9Li$ | Benzene | 6 | 15-17 |
| | Cyclohexane | 6 | 17 |
| *n*-$C_5H_{11}Li$ | Benzene | 6 | 18 |
| *n*-$C_8H_{17}Li$ | Benzene | 6 | 18 |
| *i*-$C_3H_7Li$ | Benzene | 4 | 16 |
| | Cyclohexane | 4 | 16 |
| *sec*-$C_4H_9Li$ | Benzene | 4 | 19 |
| | Cyclohexane | 4 | 19 |
| *t*-$C_4H_9Li$ | Benzene | 4 | 20 |
| | Cyclohexane | 4 | 20 |
| $CH_3Li$ | Benzene | 2 | 21 |
| | Cyclohexane | 2 | 21 |

The relative reactivity of alkyllithium initiators for styrene polymerization and diene polymerization in hydrocarbon solution is summarized from greatest to least reactivity as:[7, 8] styrene polymerization: $CH_3Li$ > *sec*-$C_4H_9Li$ > *i*-$C_3H_7Li$ > *i*-$C_4H_9Li$ > *n*-$C_4H_9Li$ > *t*-$C_4H_9Li$, and diene polymerization: $CH_3Li$ > *sec*-$C_4H_9Li$ > *i*-$C_3H_7Li$ > *t*-$C_4H_9Li$ > *i*-$C_4H_9Li$ > *n*-$C_4H_9Li$. The reactivity of alkyllithium initiators are linked to the degree of association in hydrocarbon solution. The less associated alkyllithium is more reactive as an initiator for anionic polymerization.

Rapid initiation in hydrocarbon solution is achieved with the less associated alkyllithium. In styrene and diene polymerization in cyclohexane, *sec*-BuLi is often used as an initiator, which provides a rapid initiation. The rapid initiation relative to propagation enables achievement of narrow molecular weight distribution, which is characteristic of living polymerization. Living anionic polymerization of styrene, isoprene, or 1,3-butadiene, with a reaction condition described in Scheme 2.1, provides a molecular weight distribution of 1.00 – 1.02. *n*-BuLi is also often used as an initiator; however, *n*-BuLi-initiated polymerization regularly requires an elevated temperature (> 50 ºC) to increase the rate of initiation relative to propagation, which result in polymers with narrow molecular weight distributions.[22] Decomposition rates of *sec*-BuLi and *n*-BuLi hydrocarbon solution are 0.06%/month and 1.4 %/month at 20 ºC[23], respectively, which also implies the reactivity of the initiators as well as the stability upon storage.

Although styrene and diene anionic polymerization has been discussed so far, anionic polymerization is widely applicable to various monomers. Suitable monomers for anionic polymerization are mainly diene, vinyl, and cyclic monomers. Monomers for anionic polymerization regularly require substituents on the double bond that can

stabilize the negative charge. The substituents also need to be stable to the reactive anionic chain ends, thus acidic proton-donating groups or strongly electrophilic functional groups that react with bases and nucleophiles are not suitable substituents or those substituents must be protected.[24] Substituents that produce anionic delocalization to stabilize negative charge in the reaction intermediate generally work for anionic polymerization. Such substituents include aromatic rings, double bonds, carbonyl, ester, cyano, sulfoxide sulfone, and nitro groups.[7] Therefore, the polymerizable monomers via anionic polymerization include styrenes, dienes, methacrylates, epoxides, episulfides, cyclic siloxanes and lactones.[25]

### 2.2.3 Effect of Polar Additives in Living Anionic Polymerization

The environment of carbanion species affects the kinetics and mechanism of anionic polymerization. A schematic representation of polar additive effect to anionic polymerization is shown in Figure 2.2. If the carbon-lithium bond is replaced with carbon-carbon bond as a covalent bond, no active species remain for polymerization. Lithium carbanions form a tight ion-pair with lithium in a hydrocarbon solvent. The addition of polar additives such as tetrahydrofuran (THF) or N, N, N', N'-tetramethylethylenediamine (TMEDA) disrupts the alkyllithium aggregates and produces loose ion-pairs. An ion-pair of lithium carbanion in THF (polar solvent) becomes a free ion. The disruption of lithium carbanion association dramatically increases the reaction kinetics.

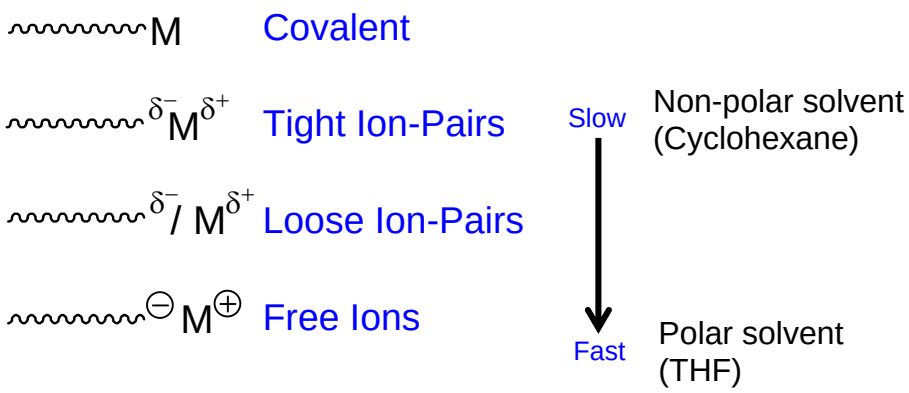


**Figure 2.2** Polar additive effect to anionic polymerization

The kinetics of anionic polymerization in hydrocarbon solvent exhibits a first-order dependence on monomer concentration and a one-sixth order or one-fourth order on initiator concentration, as shown in equation 2-2.

$$R_p = k_{obs}[M][I]^{1/N} \quad (2\text{-}2)$$

where $R_p$ is the rate of polymerization, $k_{obs}$ is the rate constant, M is the monomer concentration, I is the initiator concentration, and N is either 4 or 6. On the other hand, the value of N becomes close to 1 for anionic polymerization in polar solvent due to disruption of lithium carbanion associations.

**Table 2.2** Effect of polar solvent in microstructures of polybutadienes[8]

| Solvent System | THF/*sec*BuLi | cis-1,4 | trans-1,4 | 1,2 |
|---|---|---|---|---|
| *n*-hexanes | 0 | 35 | 57 | 8 |
| *n*-hexanes/THF | 1.0 | 25 | 40 | 35 |
| *n*-hexanes/THF | 8.2 | 21 | 31 | 45 |
| *n*-hexanes/THF | 17 | 14 | 28 | 58 |
| *n*-hexanes/THF | 53 | 7 | 10 | 85 |

Reaction temperature: 30 ˚C, Initiator: *sec*-BuLi

The change of reaction kinetics and environment of lithium carbanion association through polar additives also affects the resulting polymer composition. The microstructure of polybutadienes is tuned through addition of polar additives. Effect of

polar solvent in 1,3-butadiene polymerization with *sec*-BuLi is shown in Table 2-2.[8] As the amount of THF addition increases, the content of 1,2-polybutadienes in polybutadienes increases. Anionic polymerization of 1,3-butadiene in hydrocarbon solution, 1,2-polybutadiene ranges less than 10%, while that in THF results in approximately 90 % 1,2-polybutadiene.[26] Polydienyl anions provide less chain end association in polar media compared to hydrocarbon. The charge distribution of the allylic anions and the distribution of various kinds of ion pairs also differ in polar media against hydrocarbon. Bywater and Worsfold reported the charge distribution in asymmetrical allylic carbanions as a function of solvent and temperature.[27] They calculated the charge distribution for neopentylallyllithium (5,5-dimethylhexen-2-yllithium, Figure 2-3 (A)) and neopentylmethylallyllithium (2,5,5-trimethylhexen-2-yllithium, Figure 2-3 (B)), and as shown in Table 2-3. In polar media, there is less charges on α carbon and more charges on γ carbon in comparison to charges in benzene. The presence of more charge on γ carbon in polar media elucidates the increase of 1,2-microstructure in polybutadiene synthesis. In addition, Bywater postulated that solvated lithium cations locate close to α position and blocks the position. This favors the reaction at the less hindered γ carbon, resulting in 1,2-addition.[28]

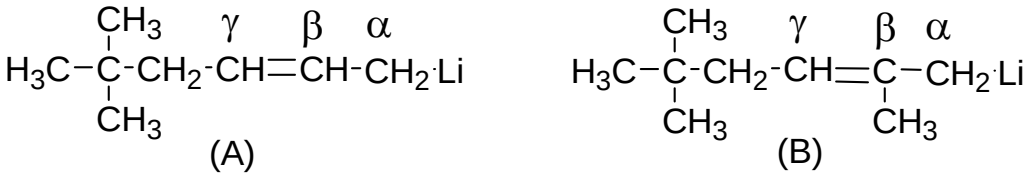


**Figure 2.3** Neopentylallyllithium (A) and neopentylmethylallyllithium (B)

**Table 2-3** Calculated charges of neopentylallyllithium (A) and neopentylmethylallyllithium (B)

| | | Calculated Charges on Allylic Carbon Atoms | | |
|---|---|---|---|---|
| | Solvent | α | β | γ |
| Neopentylallyllithium (A) | Benzene | 0.79 | -0.13 | 0.22 |
| | Diethylether | 0.69 | -0.13 | 0.35 |
| | THF | 0.69 | -0.15 | 0.40 |
| Neopentylmethylallyllithium (B) | Benzene | 0.80 | -0.14 | 0.19 |
| | Diethylether | 0.72 | -0.15 | 0.30 |
| | THF | 0.73 | -0.15 | 0.34 |

The above described microstructure of polybutadiene affects the subsequent polybutadiene properties. Approximate glass transition temperature ($T_g$) and melting temperature ($T_m$) of each polybutadiene microstructure are summarized in Figure 2.4.[7] Figure 2.5 shows a linear relationship of the glass transition temperature with the percentage of 1,2 configuration content in polybutadiene.[29] The linear relationship is described as equation 2-3.

$$T_g = 1.0\ x - 106.6\ (^{o}C) \qquad (2\text{-}3)$$

where x is the percentage of 1,2 configuration. Equation 2-3 and Figure 2.5 describe that 1 mol% increase in 1,2-microostructure raises $T_g$ 1 ºC. $T_g$ is related to many properties. Low $T_g$ rubbers such as high 1,4-polybutadienes possess good abrasion resistance and good tread wear but show inadequate road holding and wet skid deficiencies. Thus, commercial tire rubbers always have compositions which are result of a compromise of wear and traction properties, and the $T_g$ of rubber blends used in tires generally ranges – 50 to – 75 ºC.[29] SBR falls in this $T_g$ range as well as polybudiene with medium vinyl contents, 35 – 55 mol%. The detail property description of polybutadiene microstructure is summarized well in earlier literature.[30] In addition, controlled synthesis of 60% 1,2-polybutadiene will be described in Chapter 3.

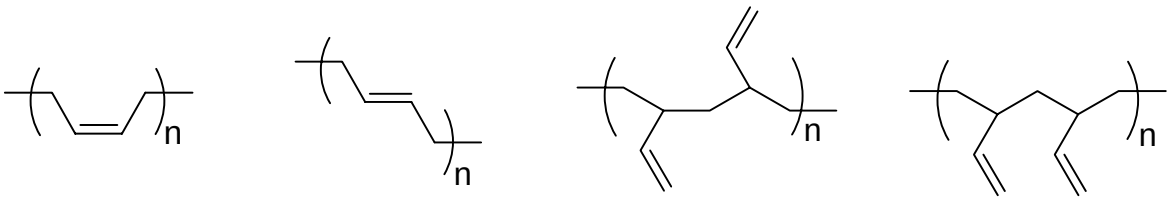

cis 1,4-PB
$T_g$ ~ - 100 ºC
$T_m$ ~ 0 ºC

Trans 1,4-PB
$T_g$ ~ - 80 ºC
$T_m$ ~ 140 ºC

Syndiotactic 1,2-PB
$T_m$ ~ 156 ºC

Isotactic 1,2-PB
$T_m$ ~ 125 ºC

Atactic 1,2-PB $T_g$ ~ 0 ºC

**Figure 2.4** Polybutadiene microstructure and their property

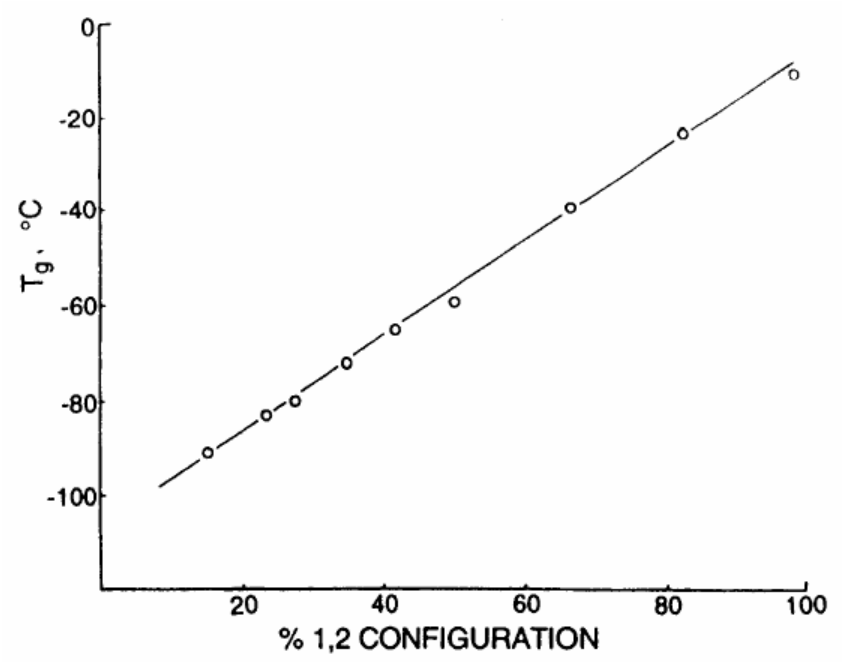


**Figure 2.5** Relationship of the glass transition temperature with the percentage 1,2 configuration content in polybutadiene[29]

### 2.2.4 Functional Termination, Star and Block Copolymer Synthesis

The carbanion end in living anionic polymerization can react with functional groups or a monomer to produce star and block copolymer rather than terminating with a proton typically from methanol. The approach for end-functionalization utilizes the reaction with electrophiles. Typical end-functionalization in living anionic polymerization includes carbonation with carbon dioxide, hydroxylation with ethylene

oxide, amination with protected imine such as *N*-(benzylidene)-trimethylsilylamine, sulfonation with sultone, aldehyde functionalization with 4-morpholinecarboxyaldehyde, and functionalization with silyl halides or substituted diphenyl ethylene.[7] Optimum conditions for these functionalizations depend on the chain-end structure, solvent, temperature, concentration, stoichiometry, and polar additives. One often needs to adjust the conditions to obtain the desired functional group.

Hydroxy-functionalized polymer readily reacts with methacryloyl chloride to form methacrylate macromonomers. The macromonomer polymerization with various combinations of monomers can produce branched polymers. The details of graft copolymer synthesis will be discussed in Chapter 6 and 7. End-functionalization with silylhalides and divinylbenzene also lead to form star copolymers.

Similar to end-group functionalization, sequential addition of monomers results in block copolymers. For example, an addition of distilled isoprene after styrene consumption and a subsequent addition of distilled styrene after isoprene consumption form a triblock copolymer thermoplastic elastomer of polystyrene-*b*-polyisoprene-*b*-polystyrene.

## 2.3 Microphase Separation of Block Copolymers

Preparation of well-defined polymer via living anionic polymerization was discussed and the living nature of anionic polymerization enables to synthesize various multiphase block copolymers. Block copolymers with immiscible blocks result in microphase separation and the microphase separation of block copolymer leads to nano-scale ordered morphology. The nanoscale morphology of block copolymer impacts the

subsequent property saliently. This section will describe the theory and characteristic of block copolymer phase separation.

AB diblock copolymer is shown in Figure 2.6 and the phase-behavior of the AB diblock copolymer will be discussed in this section. The phase behavior of a block copolymer is generally represented with a morphology diagram as a function of $\chi N$ and $f$, where $\chi$ is the Flory-Huggins interaction parameter, $N$ is the total degree of polymerization, and $f$ is the volume fraction of one block (e.g. block A in Figure 2.6). $\chi$ reflects the interaction energy between different segments and the configurational entropy contribution to the Gibbs energy is proportional to $N$.[31] Figure 2.6 shows the phase diagram of AB diblock copolymer and the subsequent morphology. The possible morphological structures include spheres (S, S', bcc (body-centered cubic) spheres), gyroid (G, G', bicontinuous Ia3d gyroid) where gyroid is not depicted in Figure 2.6, cylinder (C, C', hexagonally-packed cylinders), and lamellar (L).[32] The boundary line of the phase diagram (outer line of S and S') in Figure 2.6 represents order-disorder transition (ODT).

When $\chi N$ exceeds a critical value ($\chi N_{ODT}$), the block copolymer forms a microphase separated ordered structure. For symmetric diblock copolymers, $\chi N_{ODT}$ = 10.495.[31] The extent of phase separation of block copolymers depends on the magnitude of $\chi N$. Block copolymers weakly phase separate at low $\chi N$. The weak segregation limit is close to the ODT, which is about $\chi N$ = 12 for symmetric diblock copolymers.[31] The block copolymers are strongly segregated at larger $\chi N$ with a narrow interphase. The value of $\chi N > \sim 100$ is called the strong-segregation limit.[31]

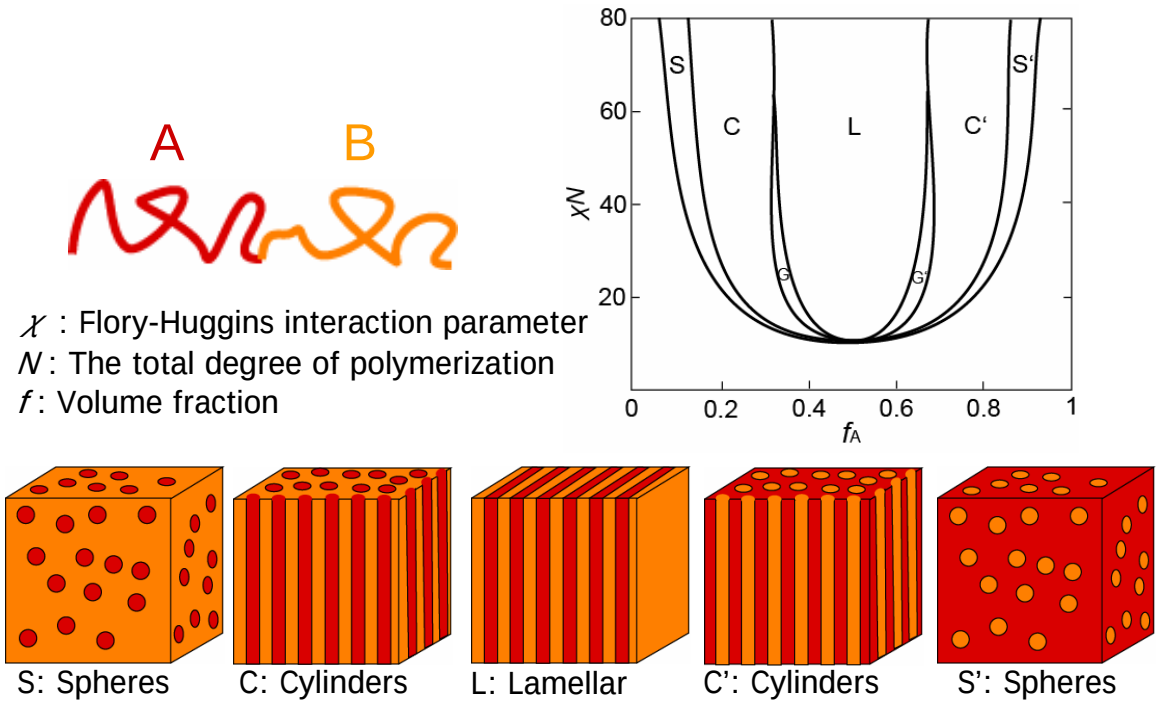


**Figure 2.6** Phase-behavior of AB diblock copolymer: Modified from a reference[33]

The Flory-Huggins parameter χ can be determined using scattering techniques.[34] The values of χ are also readily estimated from the molar volumes and the polymer solubility parameters via equation 2-4:

$$\chi_{12} = \frac{V_0(\delta_2 - \delta_1)^2}{RT} \tag{2-4}$$

where $V_0$ is the molar volume, $\delta_1$ and $\delta_2$ are the solubility parameters of the respective polymer components, $R$ is the gas constant, and $T$ is the temperature. $V_0$ was calculated from $V_0 = (V_1 V_2)^{1/2}$ where $V_1$ and $V_2$ are the molar volumes of the respective components.[35] The detailed derivation for equations 2-4 was well-described in Colby's and Rubinsteins' book, "Polymer Physics".[34] It should be noted that equations 2-4 are very useful method to estimate the Flory-Huggins parameter χ; however, this theory is based on the several assumptions. The Flory-Huggins theory is based on the assumption

of no volume change on mixing. In real polymer blends, the volume per monomer mostly changes upon mixing. In addition, the equations 2-4 work reasonably well for non-polar interactions, which is van der Waals forces between blocks, and do not work well in mixtures with strong polar or specific interactions, such as hydrogen-bonding.[34]

The main analytical techniques for block copolymer morphology include transmission electron microscopy (TEM), atomic force microscopy (AFM), and small angle x-ray (or neutron) scattering (SAXS). TEM and AFM give direct images of the structure from a small piece of a sample. TEM provides bulk morphology of a sample. Although the tedious sample preparation, such as microtoming and staining, challenges one to obtain clear images. AFM characterizes surface morphology of a sample and AFM images depict the contrast of hard and soft domain of the sample.

SAXS is a useful technique for studying polymer morphologies. SAXS is sensitive to the differences in electron density within a polymer and is able to resolve density fluctuations within polymeric materials. It is a powerful tool in determining the long-range structure within polymeric systems.[36] The Bragg's law describes the conditions of x-ray diffraction and is usually expressed as:

$$n\lambda = 2d\sin\theta \qquad (2\text{-}5)$$

where $\lambda$ is the wavelength of the x-radiation, $\theta$ is half the angle between incident beam and the diffracted beam, $d$ is the distance between neighboring domains, $n$ is the order of reflection. The equation 2-5 of the Bragg's law clearly states there is specific value of $\theta$ for every $d$, namely each diffracted beam is originated from a different plane.[37]

In SAXS analysis in polymeric system, the intensity is often measured as a function of scattering vector $q$,[38] which is

$$q = 4\pi\lambda^{-1} \sin\theta \tag{2-6}$$

Combining (2-5) and (2-6) gives

$$d = 2\pi / q \tag{2-7}$$

Since $\theta$ is small (small-angle), $d$ results in a large value in comparison to the case of a wide angle measurement. The typical $\theta$, $d$, and $q$ values in SAXS are $\theta < 3°$, $d >$ 20-40 Å ($d$ = 20 Å – 1μm), and $10^{-3} < q < 10^{-1}$ Å$^{-1}$, respectively.[38] In contrast, wide-angle X-ray scattering (WAXS) determines polymer crystal structure since the $d$ range is $d <$ 20-40 Å. Because of large measuring distance $d$, SAXS is mainly used for morphological study of polymers rather than studying molecular structure of polymers. SAXS intensity depends on location of the electron density in polymers. The electron density contrast describes the long-range structure existence in the polymeric systems.

The position of $q$ values from the equation 2-6 in SAXS is conventionally used to describe the morphology of polymeric system. As shown in the equations, $q$ is related to $d$. Thus, patterns of the $q$ peak values can describe polymeric morphologies. For lamellar morphology, the $q$ positions of the peaks appear at $q^*$, $2q^*$, $3q^*$,····, for hexagonally-packed cylinders $q^*$, $\sqrt{3}\,q^*$, $\sqrt{4}\,q^*$,····, for bicontinuous Ia3d gyroid $q^*$, $\sqrt{8}\sqrt{3}\,q^*$,····, for bcc spheres $q^*$, $\sqrt{2}\,q^*$, $\sqrt{3}\,q^*$,····, where $q^*$ = the primary Braggs reflection.[36] Appearance of multiple peaks of $q$ maxima is evidence of long-range phase separation and the sharp peaks represent formation of well-ordered morphology. Analyzing SAXS data via $q$ maximum positions is a well-used powerful method; however, some of the peaks could be missing or hidden due to the resolution or disordered morphology. To resolve this issue and to confirm the morphological

structures of polymers, microscopy techniques such as TEM and AFM are generally used to provide an image of the morphologies.

## 2.4 Non-covalent Interactions in Polymer Matrix

Non-covalent interactions in a polymer matrix control the subsequent properties as seen in morphological discussion for block copolymers. Schematic images of non-covalent interactions that might occur in a polymer matrix are shown in Figure 2.7. Covalent bonding consists of individual macromolecules, while non-covalent interactions could build nano-scale organization. For example, van der Waals interaction governs the phase separation behavior, which was discussed in section 2.3.

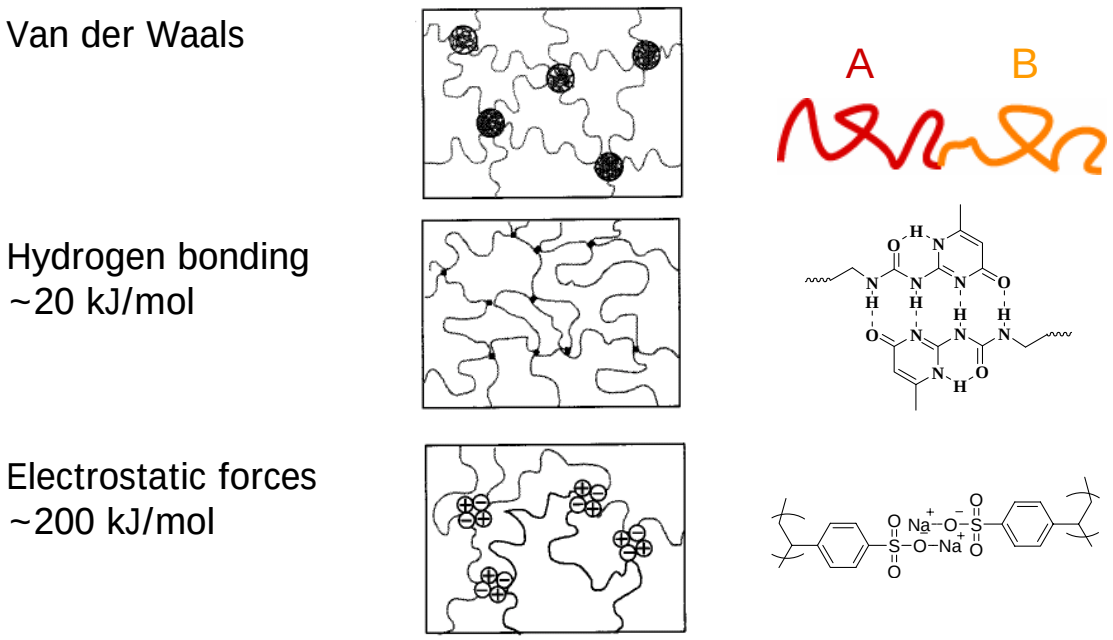


**Figure 2.7** Schematic images of non-covalent interactions in a polymer matrix
A portion of images was taken from the reference[34]

### 2.4.1 Hydrogen-bonding in Polymer Matrix

The strength of individual hydrogen bonds ranges 4 – 40 kJ/mol and the medium strength of hydrogen bonding such as urethane hydrogen bonding ranges approximately

20 kJ/mol (Figure 2.7).[39] As a comparison, the strength of a typical covalent bond ranges 300 – 450 kJ/mol. The hydrogen bonds dissociate and rearrange responding to their environment such as heat and solvent whereas covalent bonds are not easily broken. Introducing hydrogen-bonding within a polymer matrix regularly enhances the mechanical performance and aids the self-assembly.

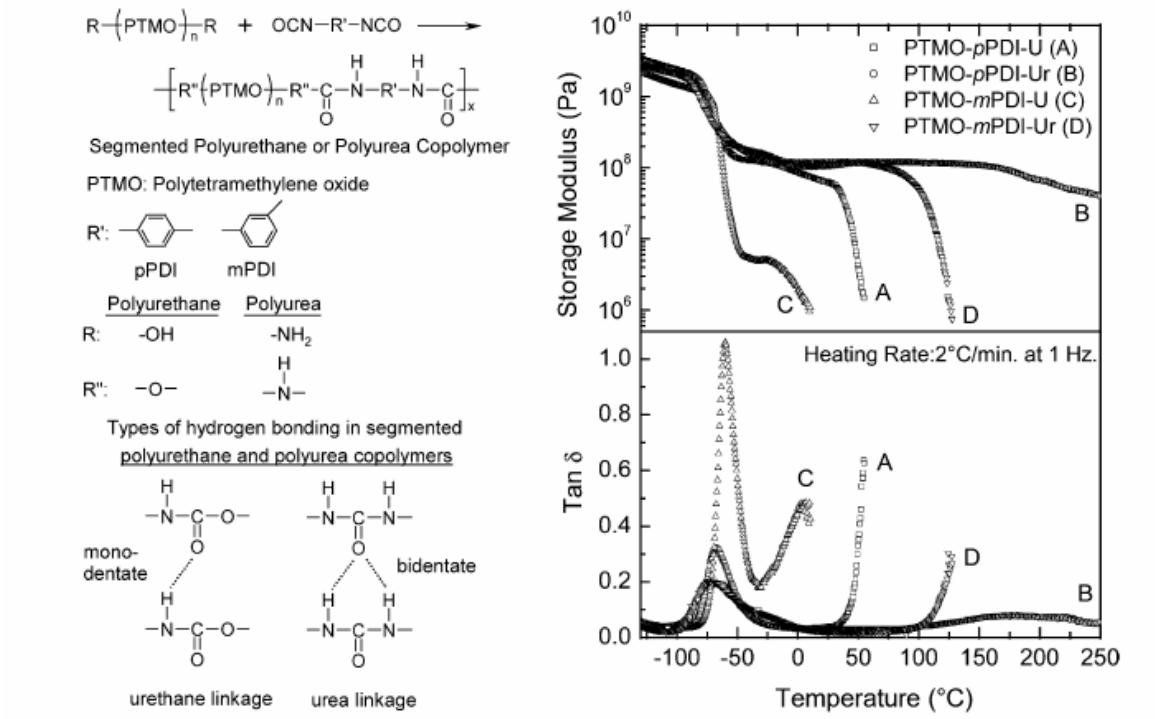


**Figure 2.8** Structures and DMA analysis of PTMO-based polyurethane and polyurea[40]

Schematic drawing, synthetic scheme and dynamic mechanical analysis (DMA) data for PTMO-based polyurethane and polyurea are shown in Figure 2.8.[40] Polyurethane possesses monodentate hydrogen-bonding, while polyurea possesses bidentate hydrogen-bonding. The bidentate hydrogen-bonding in polyurea enhanced the mechanical performance as shown in DMA curve in Figure 2.8. In addition, geometrical stacking influenced the mechanical strength. The kinked structure, mPDI segmented

copolymer, showed much lower flow temperature in comparison to pPDI copolymer. This work demonstrated role of chain symmetry and hydrogen bonding in segmented copolymers.

Quadruple hydrogen bonding systems demonstrated supramolecular structures with properties resembling covalent polymers, due to approaching the strength of the hydrogen bonding interaction to the strength of a covalent bond. Meijer investigated the supramolecular polymers with quadruple hydrogen bonding of 2-ureido-4[*1H*]-pyrimidone (UPy) units.[41-45] Schematic drawing of telechelic polymers functionalized with quadruple hydrogen-bonded ureidopyrimidone units is shown in Figure 2.9[45] and UPy association is also shown in Figure 2.7. The self-complementary association of UPy groups possesses association constants of $6\times10^7$ $M^{-1}$ in chloroform with solution lifetime of approximately 170 ms.[42, 46]

UPy linkages in polymer result in supramolecular polymer with thermoreversible character. For example, telechelic poly(ethylene-*co*-butylene) with UPy units (UPy-PEB-UPy) (Figure 2.9) formed a ductile film whereas the precursor hydroxyl-functionalized poly(ethylene-*co*-butylene) (HO-PEB-OH) was liquid.[45] The pictures of UPy-PEB-UPy and HO-PEB-OH are shown in Figure 2.10. The use of UPy-containing supramolecular polymers was also shown to form thermoreversible aggregates, which typically dissociate over 80-95 °C.[45, 47-50] Quadruple hydrogen bonding in polymer matrix will be further discussed in Chapter 4 and 5.

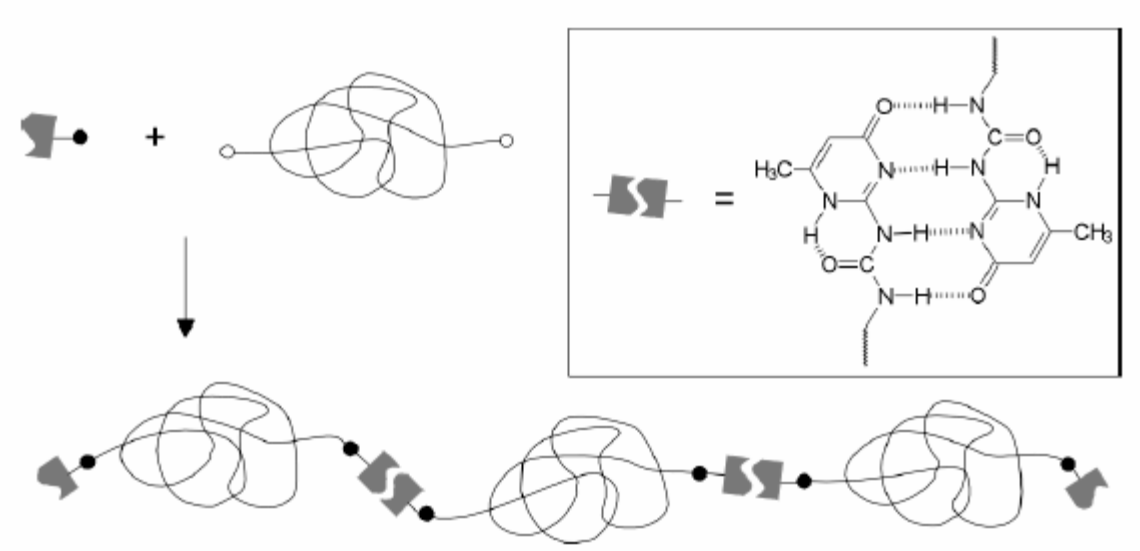

**Figure 2.9** Schematic drawing of functionalization of telechelic polymers with quadruple hydrogen-bonded ureidopyrimidone units[45]

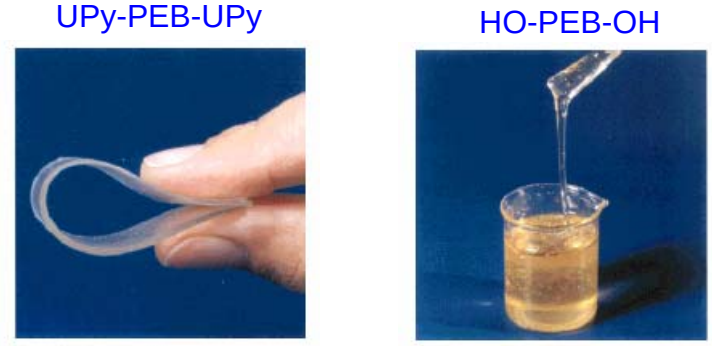


**Figure 2.10** Ductile film UPy-PEB-UPy and liquid HO-PEB-OH[45]

### 2.4.2 Ionic Interaction and General Aspects of Ionomers

The theory by Pearson et al[51] describes the relationship in which hard acids tend to bind to hard bases and soft acids tend to bind to soft bases. A dominant interaction between hard acids and hard bases is a Coulombic interaction whereas a dominant interaction in soft acids – soft bases is covalent bonding. As the hardness of acids and bases increases, the bonding increases toward ionic or dipole-dipole interactions. The ionic interaction ranges approximately 200 kJ/mol[52] (Figure 2.7) and the interactions

occur in non-directional way. Polymers that contain less than 15 mol% ionic groups are called ionomers. General aspects of ionomers will be discussed in this section.

Eisenberg made significant contributions to fundamental aspects of ionomers. In 1970, Eisenberg reported the first theoretical study of ionomers.[53] The report considered the association of ions in media of low dielectric constant. Eisenberg called associated ions as pairs, triplets, quartets, etc. as multiplets. Since his publication, researchers have used the term multiplets to describe the ionic association in macromolecular systems. Although their report well-described ion-clustering in organic polymers, the theory included only the specific condition such as no steric factors in the multiplet formation. Later in 1990, Eisenberg et al. reported more precise multiplet-cluster model for ionomers, known as Eisenberg-Hird-Moore Model (EHM model).[54] EHM model is the most accepted model of theoretical description of ionomers.

Ionic aggregates in ionomers consist of several ion pairs containing only ionic materials. The strength of the electrostatic (Coulombic) interactions between the ion pairs is the most important ionic parameter that affects multiplet formation. If the electrostatic interactions are too weak to overcome the elastic forces of polymer chains, multiplets cannot form. In addition, the electrostatic interactions determine the sizes of the ions and the ionic bond. For example, small highly polar ion pairs interact more strongly and tend to be held firmly.

The other factors for multiplet formation include the ion content of the ionomer and the characteristics of the host polymer. If the ion pairs are dilute, significant electrostatic interactions do not exist and aggregation does not occur. Low dielectric constant and low glass transition temperature ($T_g$) of the host polymer favor ionic

aggregation whereas high dielectric constant and high $T_g$ of the host polymer tend to inhibit multiplet formation.[54]

Indirect methods approximate the size of multiplets since the dimensions of ionic groups are not easily accessible. The densities and the formula weights of common inorganic compounds that resemble multiplet composition provide an average size per atom. The values are summarized in Table 2.4.[52] The average volume per atom of sodium hydroxide, sodium formate, sodium bicarbonate, sodium carbonate, sodium acetate, and sodium oxalate remains as constant, which is $(1.13 \pm 0.05) \times 10^{-2}$ nm$^3$. For example, the volume of sodium carboxylate ion pair can be calculated using this average. Since sodium carboxylate has four atoms, the volume becomes approximately $4.5 \times 10^{-2}$ nm$^3$. The same calculation method applies to the calculation of the volume of sodium sulfonate group, which suggests the volume as approximately $6.5 \times 10^{-2}$ nm$^3$ because the mean volume per atom in a sodium sulfonate ion pair is $(1.30 \pm 0.04) \times 10^{-2}$ nm$^3$. These indirect methods can provide an idea of the effective sizes of multiplets.

**Table 2.4** Volume per atom of various salts[52]

| Salt | Formula Weight | Density (g/cm$^3$) | Number of Atoms per Equivalent | Volume per Atom $\times 10^{-2}$ (nm$^3$) |
|---|---|---|---|---|
| Sodium hydroxide | 40.0 | 2.13 | 3 | 1.04 |
| Sodium formate | 68.0 | 1.92 | 5 | 1.18 |
| Sodium bicarbonate | 84.0 | 2.16 | 6 | 1.08 |
| Sodium carbonate | 106.0 | 2.53 | 6 | 1.16 |
| Sodium acetate | 82.0 | 1.53 | 8 | 1.11 |
| Sodium oxalate | 134.0 | 2.34 | 8 | 1.19 |
| *Mean* | | | | 1.13 ± 0.05 |
| Sodium sulfite | 126.0 | 2.63 | 6 | 1.33 |
| Sodium sulfate | 142.0 | 2.68 | 7 | 1.26 |
| *Mean* | | | | 1.30 ± 0.04 |

The schematic diagram of poly(styrene-*co*-sodium methacrylate) ionomer is shown in Figure 2.11 (1).[54] The polymer chains anchored to multiplets reduce the overall polymer mobility. Each multiplet produces a region of restricted mobility, although, no definite boundaries exist between the region of restricted mobility and the rest of the polymers. Therefore, the mobility of the polymer chain increases as the distance from the multiplet increases. Additionally, the flexibility of the polymer backbone also affects the thickness of the region of restricted mobility. A more flexible polymer backbone reduces the thickness. Increasing multiplet rigidity with strong electrostatic interaction decreases mobility. The higher numbers of multiplets would produce less mobility. Multiplets act similar to crosslinking so that the $T_g$ of the polymer increases as the number of multiplets increases.

The average distance between multiplets decreases as the ion content increases. When overlap of multiplets occurs frequently, large contiguous regions of restricted mobility should form. These continuous regions result in its own $T_g$, indicating the formation of clusters. Ionomers with ionic clusters cause a new $T_g$. The qualitative illustration is shown in Figure 2.11 (2). Figure 2.11 (2) schematically compares the chain mobility in the vicinity of isolated multiplets and in the region of clustered multiplets.

Small regions of restricted mobility effectively act as crosslinks and thus raise the $T_g$ of the material (Figure 2.11 (2A)). However, when a sufficient number of multiplets are close enough together to form a contiguous region of restricted mobility greater than 50-100 Å in dimension (Figure 2.11 (2B)), the region constitutes a cluster and exhibits its own separate $T_g$. The large regions of restricted mobility indicate the presence of clusters.[54]

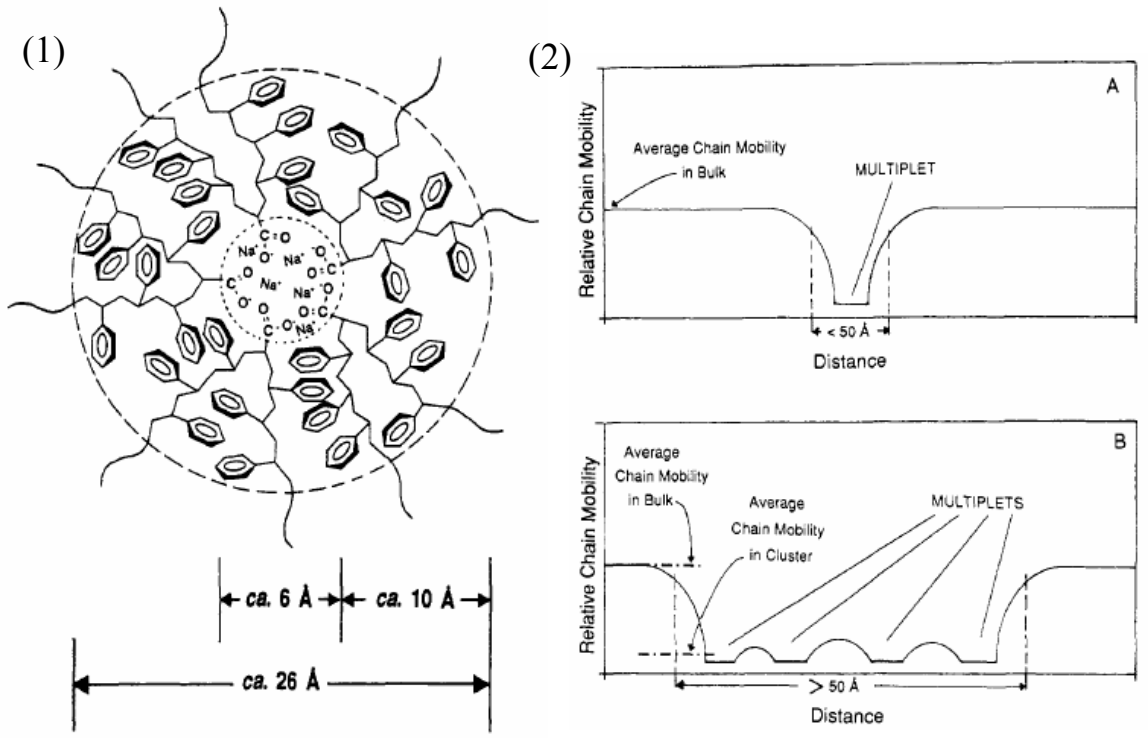


**Figure 2.11** (1) Schematic diagram of the region of restricted mobility surrounding a multiplet in a poly(styrene-co-sodium methacrylate) ionomer, (2) Schematic representation of chain mobility: (A) in the vicinity of an isolated multiplet; (B) in the region of clustered multiplets[54]

## 2.5 Sulfonated Multiphase Block Copolymers

In this section, recent advance of sulfonated multiphase block copolymers will be summarized. Sulfonated polymers are utilized in various industrial and domestic applications. Due to interesting chemical and mechanical properties, sulfonated polymers enable a number of advanced applications such as proton exchange membrane fuel cells (PEMFC), ion exchange materials, reverse osmosis and ultrafiltration membranes, and plasticizers.[55] Currently, most synthetic methods forming sulfonated-group-containing materials such as proton exchange membranes result in random or statistical placement of sulfonic acid units along the copolymer chain. The distribution of sulfonated groups

along the chain as well as the acid strength and the linkage to the polymer backbone strongly affects the morphology and the properties.[56]

The development of PEMFC has drawn significant attention among various applications of sulfonated polymers. Nafion®, pefluorosulfonic acid membrane produced by DuPont, has been a platform for PEMFC application. Nafion® is composed of a perfluorinated backbone with pendant vinyl ether side chains with sulfonic acid end group. Nafion® provides excellent selectivity and proton transport property. Extensive studies investigated the structure-property relationships of Nafion®.

The drawbacks of Nafion® include the high cost, the limitation of the operation temperature, and the difficulty of the synthesis and process. Thus, current research efforts are focused on searching for the alternative proton exchange membrane (PEM) materials that provide less cost, higher system performance, and better operational flexibility than Nafion®. Sulfonated block and graft copolymers may provide such alternative PEM since sulfonated block and graft copolymers control the placement of sulfonic acid groups and enhance the PEM performance.

Block copolymers, graft copolymers, and ionomers often exhibit microphase separation. Occurrence of microphase separation depends on compositional dissimilarity ($\chi$ parameter), molecular weight, and crystallizability.[57] Morphological trends by microphase separation direct the physical properties of the polymer. The microphase separation alters the placement of ionic domains, where sulfonic acid group connectivity in morphology enhances the PEM performance (Figure 2.12). Therefore, the precise location of sulfonated blocks in sulfonated block and graft copolymers introduce a

designed micorphase separation and control the physical properties of the resulting polymer.

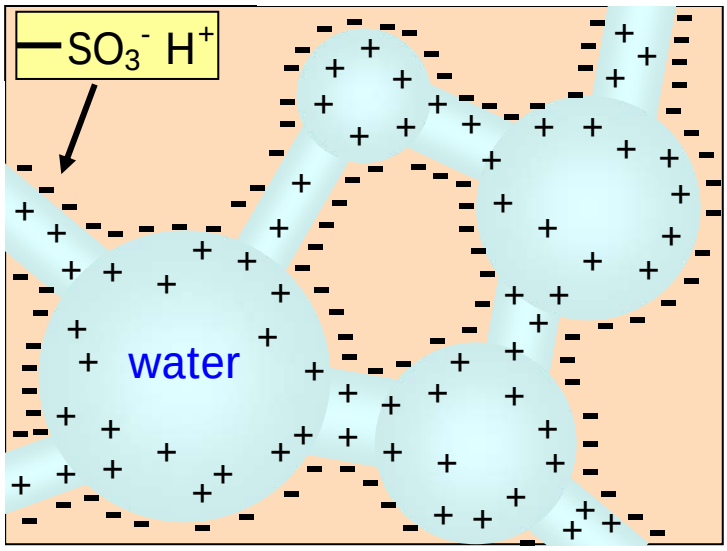


**Figure 2.12** Representation of the swollen sulfonic acid ionomer membrane

### 2.5.1 Synthesis of Sulfonated Block Copolymers

Post sulfonation of block copolymers has been the main strategy to prepare sulfonated block copolymers. A-B-A triblock copolymer, partially sulfonated polystyrene-*b*-poly(ethylene-*r*-butylene)-*b*-polystyrene (SSEBS), is a well known sulfonated block copolymer due to its commercial availability. The typical synthetic methods to prepare such sulfonated block copolymers utilize a living anionic polymerization, hydrogenation of butadiene block and a subsequent sulfonation with acetyl sulfate.[58-65] SEBS synthesis follows the sequential addition of monomers via living anionic polymerization, which was described in section 2.2. s*ec*-Butyl lithium or *n*-butyllithium initiates styrene (the first block monomer). Upon completion of the first block reaction, butadiene (the second monomer) is added, and then styrene (the third

block monomer) is charged after completion of butadiene monomer consumption. A proton from methanol typically terminates the reaction. The butadiene block is then hydrogenated with nickel octoate catalyst or platinum on carbon catalyst under hydrogen pressure. The sulfonation of the styrene blocks in the synthesized SEBS occurs with acetyl sulfate solution or similar analogues. Exchanging polybutadiene block to polyisoprene block in the block copolymer synthesis also prepares sulfonated polystyrene-*b*-poly(ethylene-*co*-propylene)-*b*-polystyrene (SSEPS).

Willis et al. reported sulfonated block copolymers having the general configuration A-B-A, A-B-A-B-A, (A-B-A)nX, or (A-B)nX, where n is an integer from 2 to about 30, and X is coupling agent residue.[66] Each A block is a polymer block resistant to sulfonation and each B block is a polymer block susceptible to sulfonation. Block A comprised the segments from polymerized (1) *para*-substituted styrene monomers, (2) ethylene, (3) alpha olefins of 3 to 18 carbon atoms; (4) 1,3-cyclodiene monomers, (5) monomers of conjugated dienes, (6) acrylic esters, and (7) methacrylic esters. B block is a copolymer block of at least one conjugated diene and at least one mono alkenyl arene selected from (1) unsubstituted styrene monomers, (2) ortho-substituted styrene monomers, (3) meta-substituted styrene monomers, (4) alpha-methylstyrene, (5) 1,1-diphenylethylene, and (6) 1,2-diphenylethylene. Each A block possessed a number average molecular weight ($M_n$) between 1,000 and 60,000 and each B block possessed $M_n$ between 10,000 and 300,000.

Some of the block copolymers required a post coupling polymerization. For example, the anionically-synthesized block copolymers were coupled with a coupling agent, resulting in (A-B-A)nX, or (A-B)nX. In addition, any A segments containing

polymerized 1,3-cyclodiene or conjugated dienes were hydrogenated prior to sulfonation step since unsaturated alkenyl chains would be sulfonated with acetyl sulfate. Thus, acetyl sulfate selectively sulfonate B blocks of the block copolymer precursors.

Sulfonated poly(styrene-*b*-isobutylene-*b*-styrene (S-SIBS) is another common sulfonated block copolymer.[67-71] The synthetic method to prepare S-SIBS includes a living cationic polymerization and a subsequent sulfonation with acetyl sulfate.[67, 68] For SIBS polymerization, 1,2-di(2-chloro-2-propyl)-5-*tert*-butylbenzene/$TiCl_4$ initiates IB monomer with pyridine. The difunctional PIB is first synthesized and then styrene is added to form the triblock copolymer, SIBS. The sulfonation step is generally same as the strategy for SEBS. Most of chain growth polymerization methods to prepare sulfonated block copolymers follow the strategy of sequential addition of monomers via living polymerization and post-functionalization of a polymer block susceptible to sulfonation.

Another strategy to prepare sulfonated block copolymers uses a condensation and a coupling reaction of sulfonated blocks and unsulfonated blocks. Segmented sulfonated polyimide was first reported in 1969[72] for the use of cation exchange membranes. Recently, the same approach has been taken to prepare segmented sulfonated polyimide for PEMFC application.[73-77] Synthesis of block segmented sulfonated polyimide involved two step polycondensation (Scheme 2.2). A diamine endcapped sulfonated oligomer was first obtained by the condensation of the dianhydrides with the sulfonated diamines. Then, adding the unsulfonated diamines and dianhydride to the condensation reaction results in the formation of segmented sulfonated polyimides.

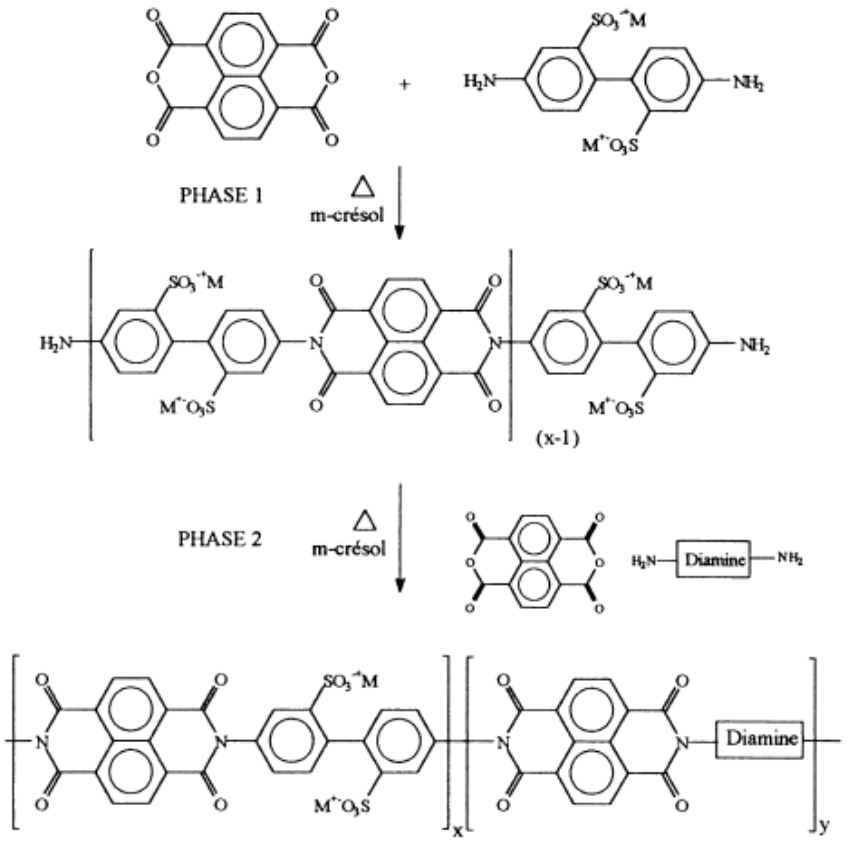


**Scheme 2.2** Synthesis of segmented sulfonated naphthalenic polyimide copolymer[73]

McGrath et al. employed the same strategy and reported segmented sulfonated poly(arylene ether sulfone)-*b*-polyimide (BPSH-*b*-PI) copolymers,[78, 79] segmented sulfonated poly(arylene ether sulfone),[80, 81] and segmented fluorinated, sulfonated poly(arylene ether sulfone),[82-84] for PEMFC application. Synthesis of segmented BPSH-*b*-PI[78, 79] is shown in Scheme 2.3. Amine terminated sulfonated poly (arylene ether sulfone) oligomers (Scheme 2.3 (1)) and anhydride terminated naphthalene based polyimide oligomers (Scheme 2.3 (2)) were synthesized using step growth polymerization. Synthesis of the segmented multiblock copolymers was achieved by an imidization coupling reaction of hydrophilic and hydrophobic oligomers in a m-cresol/NMP mixed solvent (Scheme 2.3 (3)).

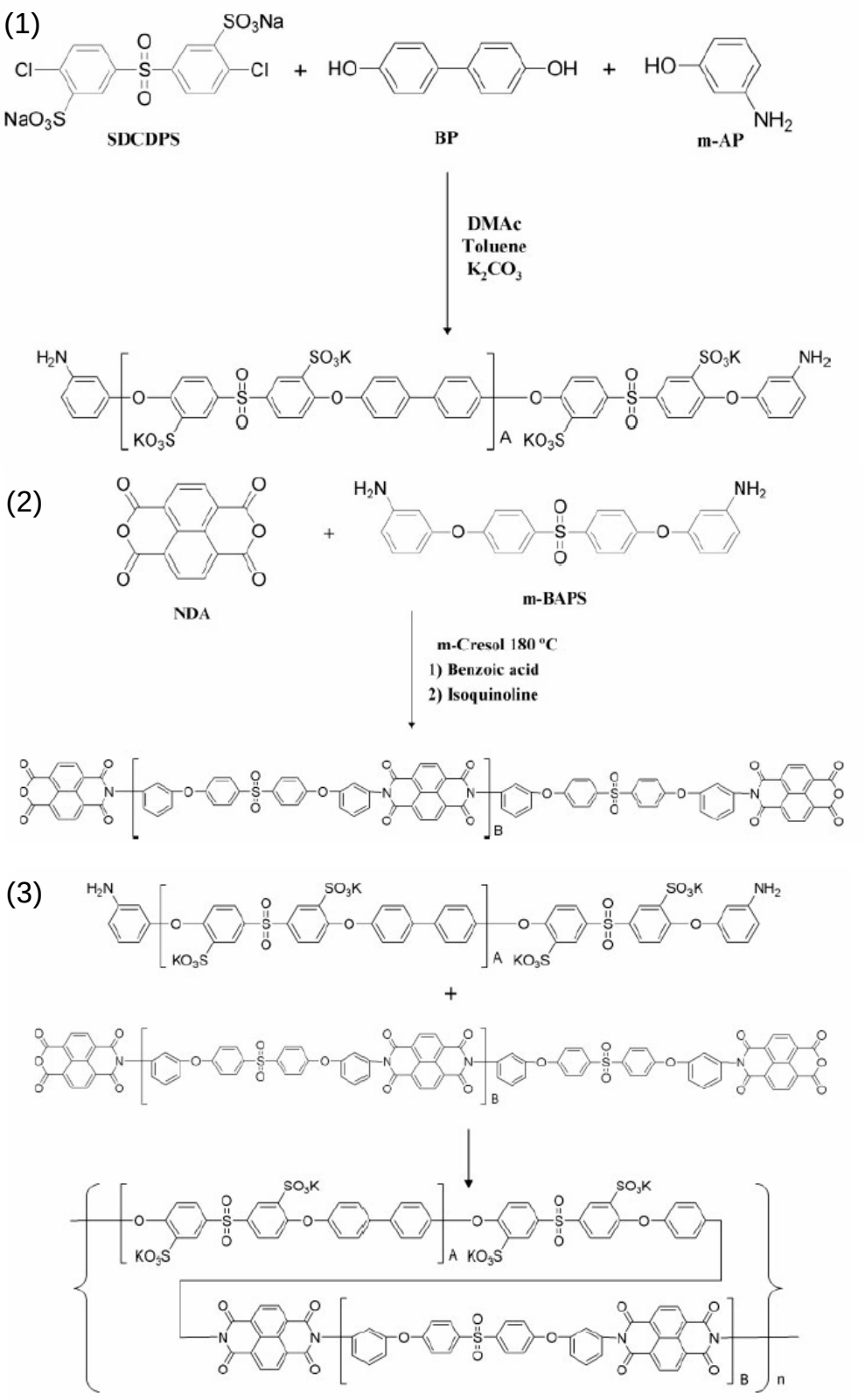


**Scheme 2.3** Synthesis of segmented sulfonated poly(arylene ether sulfone)-*b*-polyimide copolymers[78, 79]

### 2.5.2 Morphological Characterization of Sulfonated Block Copolymers using SAXS

Weiss et al. investigated the block microstructure of a block copolymer ionomer, lightly sulfonated poly(styrene-*b*-(ethylene-*co*-butylene)-*b*-styrene) (S-SEBS) using SAXS.[85] Sulfonation level was varied from 0 to 12 mol % of the polystyrene blocks and the sulfonic acid and Na and Zn salts were studied. SAXS profiles of four compression molded samples are shown in Figure 2.13: SEBS, 12H-S-SEBS, 12Zn-S-SEBS, and 12Na-S-SEBS (12 refers to 12 mol% sulfonation.). All the materials exhibited only a single intensity maximum. The counter ion of the sulfonated PS block affected the intensity and the position of the scattering peak. The most notable change in Figure 2.13 was a stronger and broader scattering peak for the block copolymer ionomer compared with that for the unmodified SEBS. The higher intensity of the scattering peak for the ionomers is due to an enhancement of the electron density contrast between the rubber and the sulfonated PS phases. The observed variation of the peak intensity with the counterion was $Zn^{2+} > Na^{+} > H^{+}$, which is consistent with the atomic weights of the counterions. Although, there is not so much significant difference between $Na^{+}$ and $H^{+}$ form of polystyrene. If the microstructures of the ionomers were equivalent, the intensity of the peak in the different materials should increase as the atomic number of the cation was increased, $Zn^{2+} > Na^{+} > H^{+}$.

Weiss's work raised two possible reasons for the peak broadening: (1) the ionic aggregates produce additional electron density fluctuations within the polystyrene block microdomains, (2) the hindrance of the block microphase separation due to longer relaxation times arising from the ionic aggregation may result in a broader distribution of

the center to center distance between neighboring microdomains and a more diffuse interphase boundary.

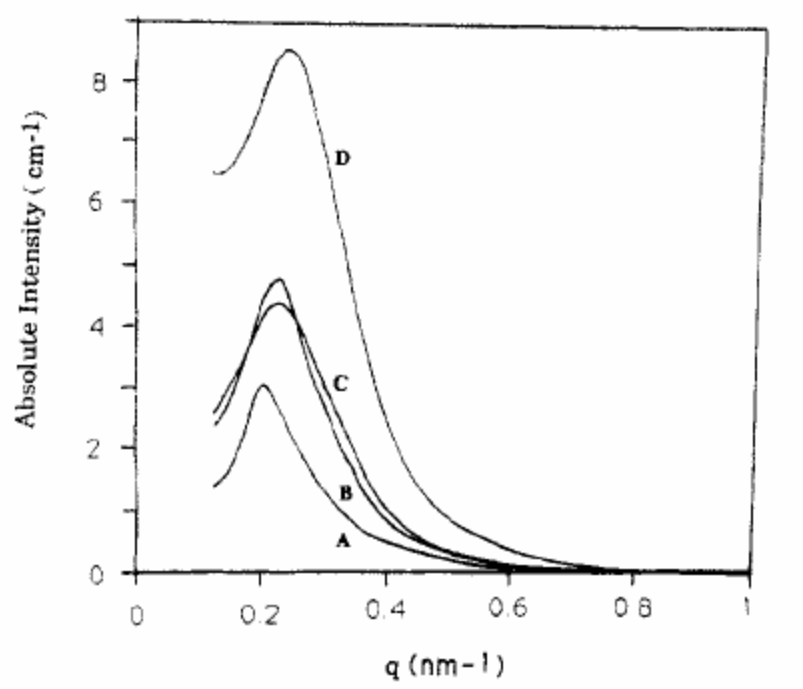


**Figure 2.13** Effect of the counterion on the SAXS profiles for compression molded block copolymer ionomers: (A) SEBS; (B)12H-S-SEBS; (C) 12Na-S-SEBS; (D) 12Zn-S-SEBS[85]

Weiss et al. also compared the influence of the sulfonation level of S-SEBS in SAXS.[85, 86] The comparison of scattering peak of Zn-S-SEBS is shown in Figure 2.14. The intensity of the maximum increased with increasing sulfonation level due to an enhancement of the electron density contrast between the rubbery backbone and the sulfonated PS phases.

The SAXS patterns for 5Zn-S-SEBS and 12Zn-S-SEBS cast from toluene/DMF solutions is shown in Figure 2.15. The increased molecular mobility of the block copolymer ionomer in solution allowed the formation of a microstructure closer to equilibrium. Much more details are seen in the scattering pattern compared with the corresponding molded samples, which indicated more long-range order in spatial

arrangement of the microdomains. The $q$ positions of the four scattering maxima corresponded to a ratio of $q/q^* = 1, 2, 3, 4$, where $q^* = q_1$. The ratio indicates a formation of a lamellar microstructure.

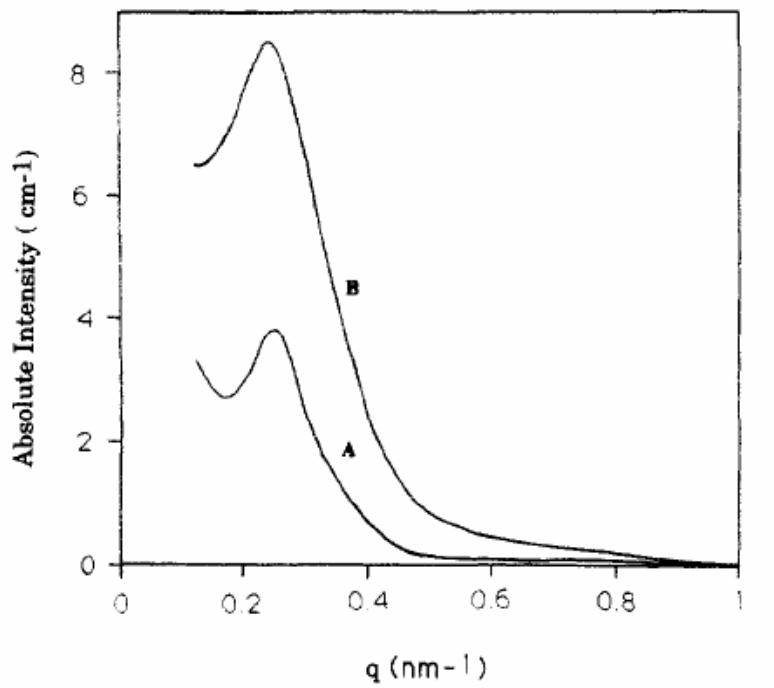


**Figure 2.14** SAXS curves for compression molded block copolymer ionomers: (A) 5Zn-S-SEBS; (B) 12Zn-S-SEBS[85]

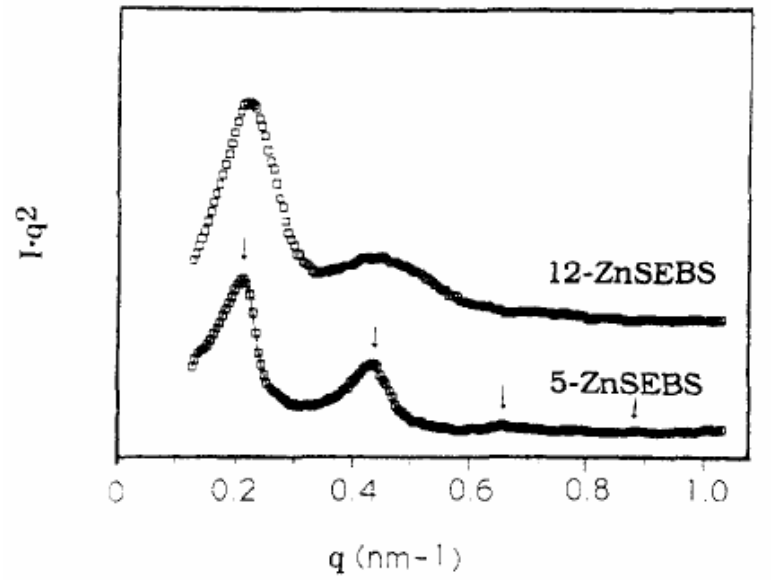


**Figure 2.15** SAXS curves for solution-cast Zn-S-SEBS **as** a function of sulfonation level: (a) 5Zn-S-SEBS; (b) 12Zn-S-SEBS[85]

Weiss et al. also reported microstructure of ionomers based on sulfonated diblock copolymer poly(ethylene-*alt*-propylene-*b*-styrene) (SEP) and triblock copolymer, poly(styrene-*b*-ethylene-*alt*-propylene-*b*-styrene) (SEPS) using SAXS.[87] SEP and SEPS was synthesized via living anionic polymerization, subsequent hydrogenation and postsulfonation. Sodium and zinc salts were prepared by fully neutralizing the free-acid derivatives. The samples were cast from 10% (w/v) solutions of the block copolymer ionomer in toluene/methanol (9/1 v/v). The samples were denoted by *s*M-SEPS*x*, where "*s*" and "M" represented the sulfonation level in mole percent of sulfonated styrene and the cation (H, Na, or Zn) and "*x*" is the weight percent of PS block.

Figure 2.16 shows the SAXS curves for the *s*M-SEPS21 triblock ionomers, *s*1.9-SEP35 and 2.0M-SEP50 diblock copolymers. Positions of peak maxima in the SAXS curves for *s*M-SEPS21 corresponded with $q/q^* = 1, \sqrt{3}, 2, ....$, indicative of formation of hcp cylinders. The values for $q/q^* = 1, 2, 3, 4....$ in SAXS curves for *s*1.9-SEP35 and 2.0M-SEP50 diblock copolymers corresponded with formation of lamellar morphology. Sodium and zinc sulfonate showed poor resolution of SAXS peak maxima, which indicated the degree of disorder for the sodium and zinc sulfonate was greater than sulfonic acid form or block copolymer precursor. The degree of disorder followed the order of the melt viscosity, which was $Na^+ > Zn^{2+} > H^+ >$ block copolymer.

The increased degree of disorder upon neutralization stemmed from the process of the forming films. The ionic associations within the PS domains decrease mobility of the molecules and therefore hinder the self-assembly of the block microphase separation. The degree of disorder of the sulfonated block copolymers depends on the strength of the

electrostatic interactions since the relaxation behavior of the ionic interactions dictates the local viscosity of the medium.

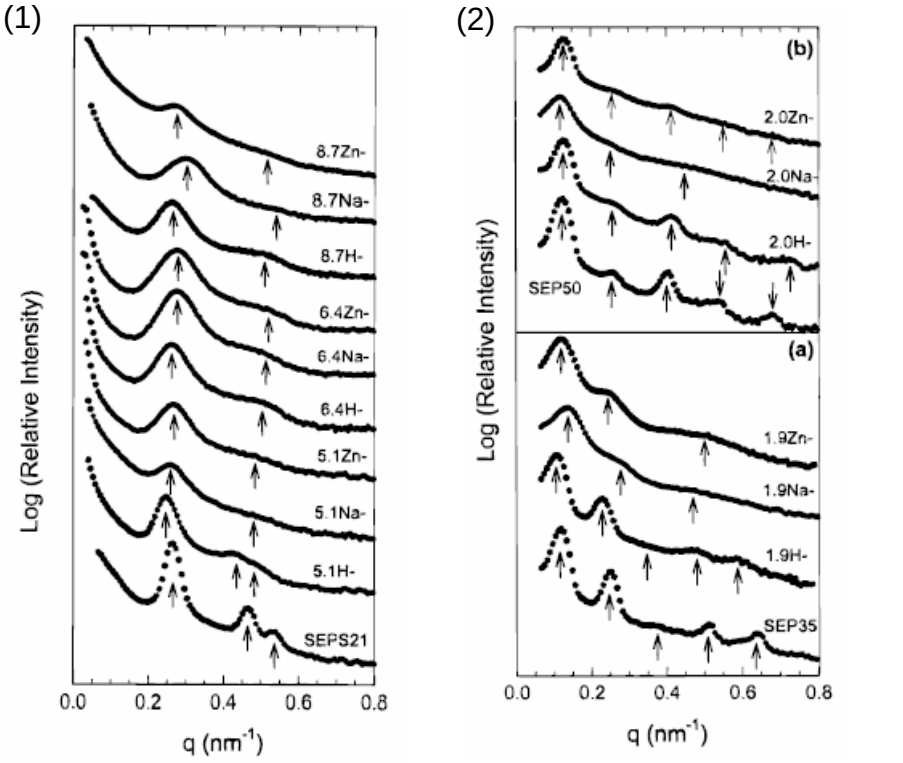


**Figure 2.16** SAXS curves for the block copolymer for (1) SEPS21 and *s*M-SEPS21 ionomers, (2-a) SEP35 and *s*1.9-SEP35 ionomers and (2-b) SEP50 and 2.0M-SEP50 ionomers[87]
Vertical arrows indicate maxima of the structure factor

### 2.5.3 Morphology and Proton Conductivity of Sulfonated Block Copolymers

#### 2.5.3.1 Suflonated Triblock Copolymers

Elabd et al. reported sulfonated poly(styrene-*b*-isobutylene-*b*-styrene) at high ion-exchange capacities (IEC).[69-71] They prepared various degree of sulfonated poly(styrene-*b*-isobutylene-*b*-styrene) (S-SIBS) and polystyrene (S-PS) and cast them from 85/15 (w/w) mixture of toluene/hexanol. The properties of S-PS and S-SIBS are summarized in Table 2.5. Figure 2.17 also shows proton conductivity as a function of IEC. The proton conductivity of S-SIBS was comparable to the proton conductivity of Nafion. The

conductivity values between S-SIBS and S-PS showed one order of magnitude difference. This suggested that the difference in architecture (block copolymer, S-SIBS) and (random copolymer, S-PS) resulted in different morphology, leading to enhanced proton transport property in S-SIBS.

**Table 2.5** Polymer membranes (Nafion 117, sulfonated polystyrene (S-PS), sulfonated poly(styrene-*b*-isobutylene-*b*-styrene (S-SIBS)) as a function of ion content[70]

| sample name | sulfonation level (mol %) | IEC (mequiv/g) | sample name | sulfonation level (mol %) | IEC (mequiv/g) |
|---|---|---|---|---|---|
| Nafion 117 | NA | 0.91 | S-SIBS-25 | 25.26 | 0.71 |
| S-PS-0[a] | 0 | 0 | S-SIBS-29 | 29.23 | 0.81 |
| S-PS-6[a] | 5.68 | 0.52 | S-SIBS-34 | 34.33 | 0.94 |
| S-PS-14 | 14.18 | 1.23 | S-SIBS-36 | 35.63 | 0.97 |
| S-PS-15 | 15.13 | 1.30 | S-SIBS-42 | 41.95 | 1.13 |
| S-PS-24 | 23.70 | 1.92 | S-SIBS-48 | 48.16 | 1.28 |
| S-SIBS-0[a] | 0 | 0 | S-SIBS-54 | 53.68 | 1.41 |
| S-SIBS-13[a] | 12.50 | 0.36 | S-SIBS-70 | 70.14 | 1.78 |
| S-SIBS-13 | 12.50 | 0.36 | S-SIBS-79 | 79.05 | 1.97 |
| S-SIBS-17 | 16.60 | 0.47 | S-SIBS-82 | 82.41 | 2.04 |
| S-SIBS-22 | 22.49 | 0.63 | | | |

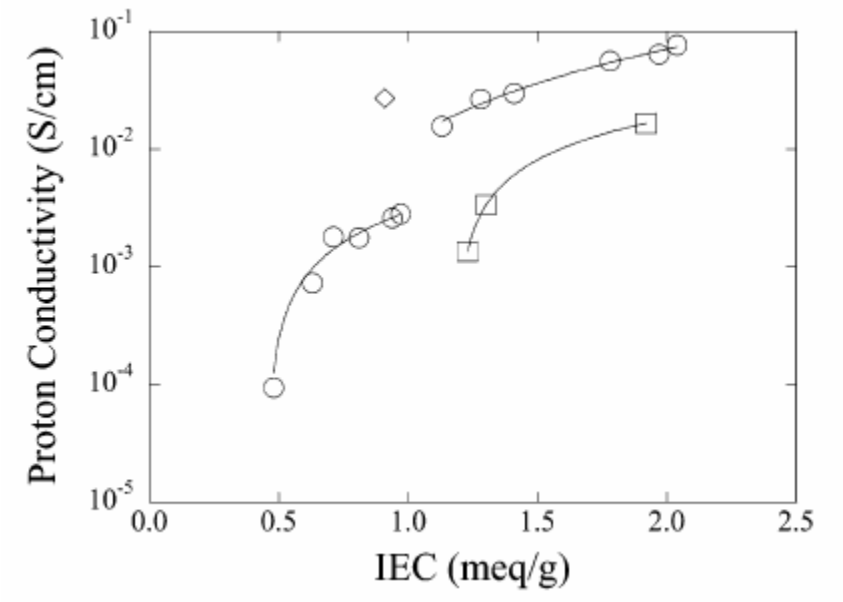


**Figure 2.17** Proton conductivity vs. IEC for Nafion 117 (◊), S-SIBS (O), and S-PS (□) membranes[70] The solid lines are trend lines.

They performed SAXS measurement for each sample. A scattering pattern with peak maxima for both S-SIBS-0 and S-SIBS-13 cast from toluene resulted in $q/q^* = 1, \sqrt{3}, 2, \sqrt{7}$ ...., indicative of formation of hcp cylinder morphology, while 85/15 (w/w) mixture of toluene/hexanol cast S-SIBS-13 to S-SIBS-82 displayed the intensity maxima located at $q/q^* = 1, 2, 3, 4$...., which corresponded to a lamellar morphology. As ion content increases in S-SIBS membranes, the SAXS peaks were broadened and the long-range order was disrupted. The Bragg's spacing *d* also increased with increasing ion content (0-2.0 mequiv/g) from 23.3 to 41.9 nm. This increased *d* spacing suggested that increasing ion content resulted in larger ion clusters.

Elabd et al. also studied the morphology and transport property as a function of casting solvent. The SAXS analysis for S-SIBS-29 (0.81 meq/g) cast from different solvents is shown in Figure 2.18 and their proton conductivity and *d* spacing of S-SIBS-29 membranes are summarized in Table 2.6. THF cast film showed the intensity maxima located at $q/q^* = 1, 2, 3, 4$...., which indicated the ordered lamellar structure, while the films from other casting solvent did not exhibit high level of long range order. The ordered lamellar morphology for THF cast S-SIBS-29 resulted in the highest proton conductivity among those solvents as shown in Table 2.6.

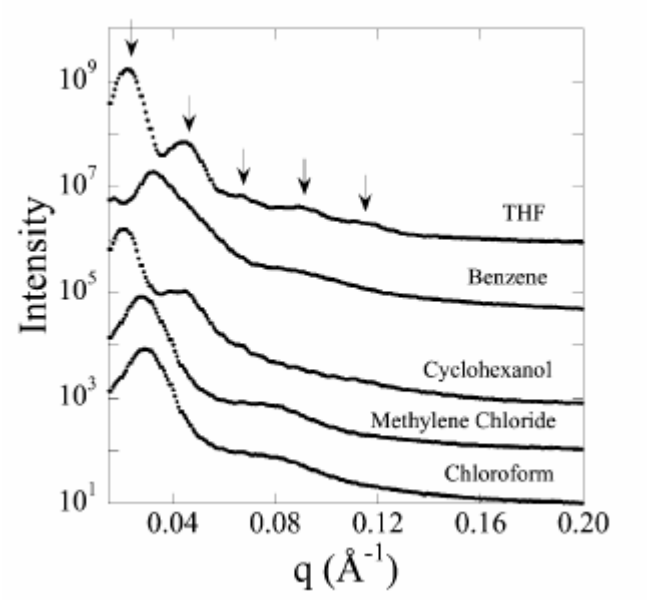


**Figure 2.18** Small-angle X-ray scattering intensities as a function of scattering vector for S-SIBS-29 (0.81 meq/g) cast form different solvents[70]

**Table 2.6** Proton conductivity and Bragg spacing of S-SIBS-29 membranes as a function of casting solvent at a constant ion content (0.81 meq/g)[70]

| casting solvent | proton conductivity (S/cm) ($\times 10^2$) | $d_1$ (nm) |
|---|---|---|
| chloroform | 0.0229 | 20.4 |
| cyclohexanone | 0.0277 | |
| methylene chloride | 0.125 | 25.4 |
| cyclohexanol | 0.166 | 28.4 |
| benzene | 0.291 | 18.8 |
| tetrahydrofuran | 0.522 | 26.3 |

Kim et al. reported effect of casting solvent on morphology and physical properties of partially sulfonated poly(styrene-*b*-(ethylene-*r*-butylene)-*b*-styrene) (SSEBS).[88-91] They prepared SSEBS with the degree of sulfonation of 8 (8SSEBS), 27 (27SSEBS), and 42 (42SSEBS) mol%. The films were cast from THF, THF/MeOH mixture (95/5, 90/10, 85/15, 80/20). TEM images for 27SSEBS membranes (a) cast with THF, and (b) cast with the mixed solvent of MeOH/THF (20/80 v/v) are shown in Figure 2.19. The THF cast 27SSEBS showed ordered lamellar morphology, whereas

MeOH/THF (20/80 v/v) cast 27SSEBS showed disordered lamellar type morphology. Kim et al. explained that this morphological transition caused from the residual solvent during the membrane formation. When the block copolymer membrane starts to phase-separate at a high concentration after a period time from casting, the concentration of methanol in the mixed solvent increases because of the difference of the vapor pressures between THF (160.0 mmHg at 25 ºC) and methanol (129.2 mmHg at 25 ºC).[92] Therefore, a high fraction of methanol is selectively trapped to SPS and the domain of SPS is swollen by methanol. Owing to the selective swelling to SPS domains, the volume ratio of SPS domains to EB domains increases due to the trapped methanol. The residual methanol behaves like a plasticizer only to the domain of SPS at the end of solvent evaporation.

Both SAXS profiles for THF cast film and THF/MeOH cast film exhibited the long range order formation and the positions of the scattering maxima confirmed the formation of lamellar morphology for both samples. SAXS profiles suggested that the increase of the degree of sulfonation and the increase of amount of methanol in the casting solvent increased the degree of disorder in the lamellar morphology. The SPS domains were interconnected in the three dimensions in the matrix of the EB domain. The well ordered lamellar morphology was transformed into an interconnected and disordered morphology as the concentration of methanol increased. Therefore, the interconnection of sulfonic acid groups resulted in the increase of the proton conductivity with the addition of methanol as shown in Figure 2.20.

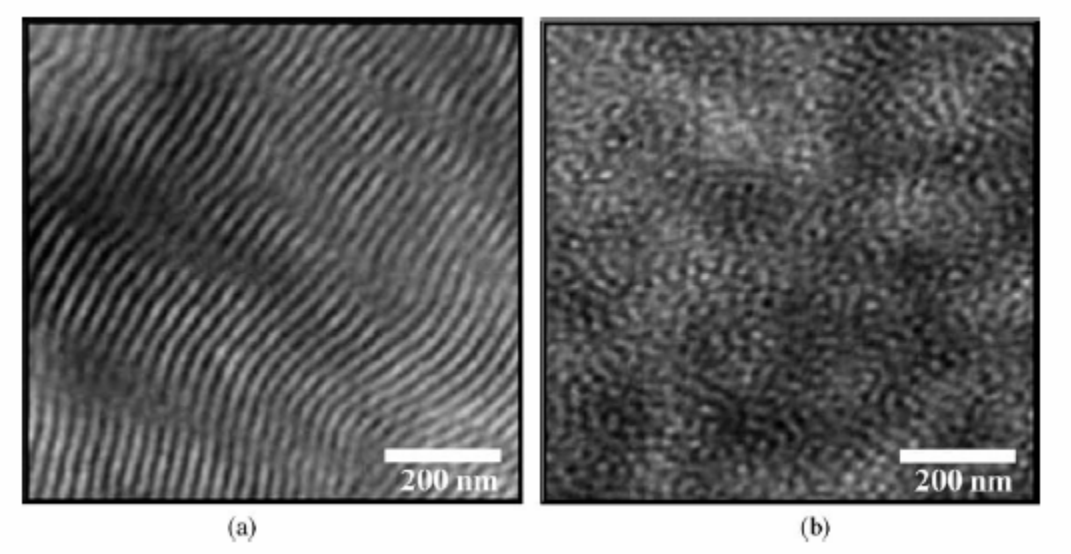


**Figure 2.19** Cross-sectional images of TEM for 27SSEBS membranes (a) cast with THF, and (b) cast with MeOH/THF (20/80 v/v)[89]

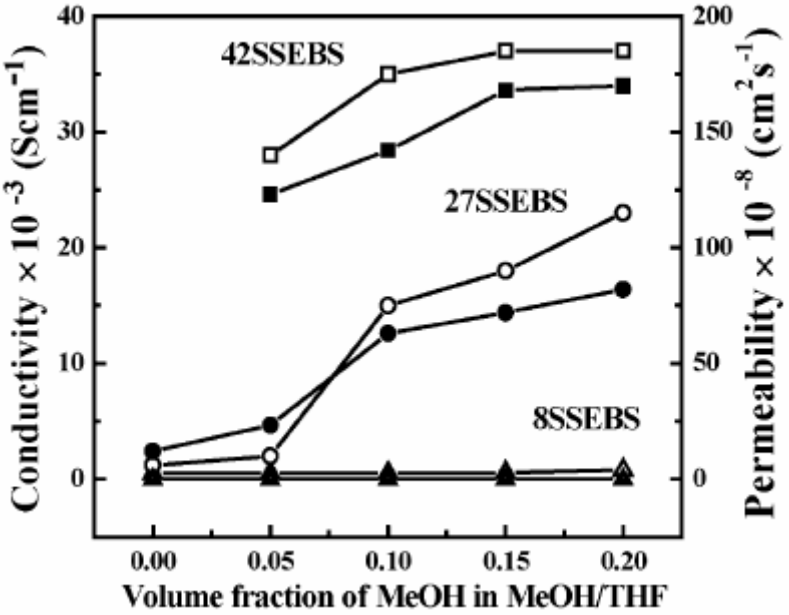


**Figure 2.20** Proton conductivity and methanol permeability of 8, 27, and 42SSEBS membranes prepared from MeOH/THF mixtures as a function of solvent composition. The unfilled and the filled symbols denote proton conductivity and methanol permeability, respectively[89]

### 2.5.3.2 Segmented Sulfonated Copolymers

McGrath et al. presented the formation of lamellar morphology from BPSH-*b*-PI segmented block copolymer. The synthetic procedure of BPSH-*b*-PI was described in

section 2.5.1 and the chemical structure is shown in Scheme 2.3. AFM images of BPSH-*b*-PI are shown in Figure 2.21. As the increase of the block length, brighter nonionic domains increased in size from small round domains to continuous lamellar structure. 15000 g/mol BISH-*b*-15000 g/mol PI exhibited the formation of lamellar morphology and continuous connection of sulfonic acid domain. We believe that this is the first published clear AFM image of lamellar morphology formation from segmented sulfonic acid block copolymers to the best of our knowledge. BPSH-*b*-PI also showed thermally stable over 300 ºC and proton conductivity approximately 0.1 S $cm^{-1}$.

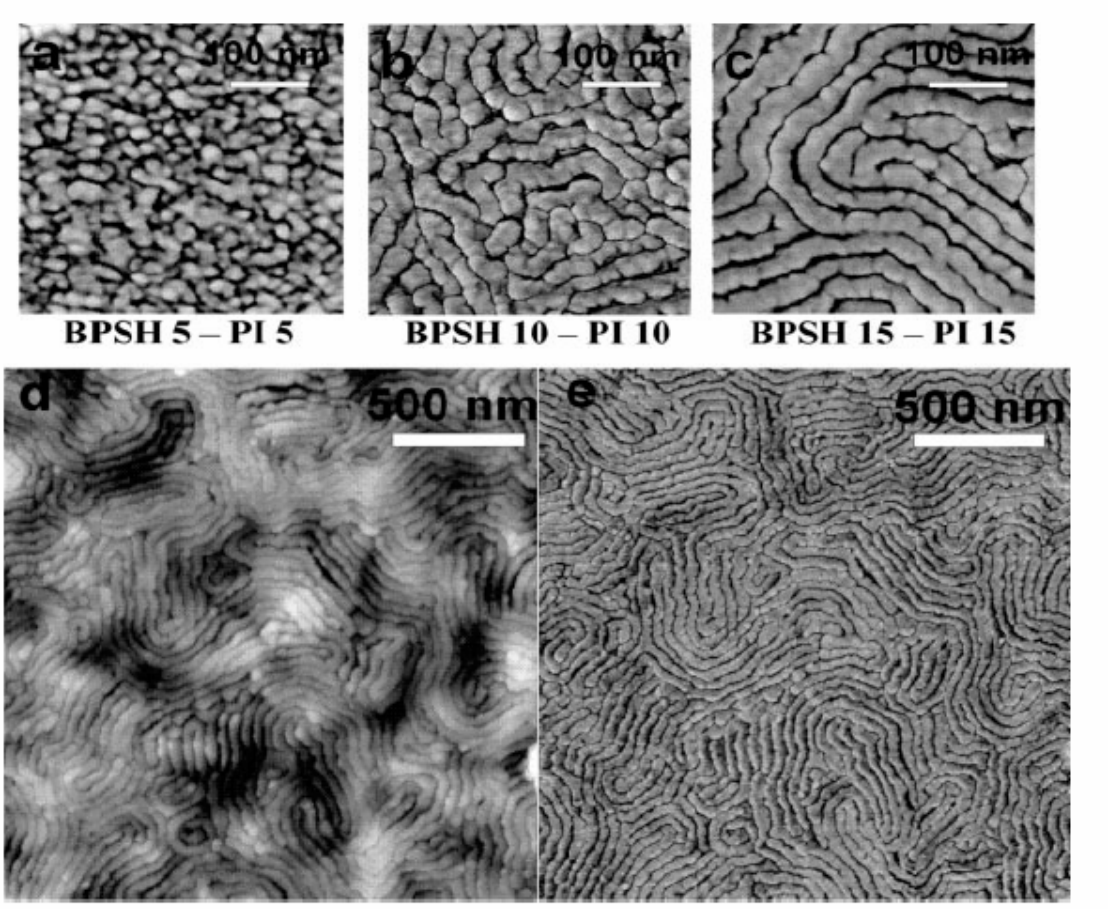


**Figure 2.21** (a)–(c) Tapping mode AFM phase images of BPSH-PI multiblock copolymers with different block lengths, (d) height image, and (e) phase image of BPSH15-PI15 demonstrating long-range order

### 2.5.3.3 Sulfonated Graft Copolymers

Holdcroft et al. synthesized graft copolymers containing ionic polymer grafts (polystyrene sulfonic acid graft chains) attached to a hydrophobic backbone.[93-96] Preparation of poly(styrene-*g*-*mac*PSSNa) graft polymers is shown in Scheme 2.4. They employed macromonomer strategy to prepare PS-*g*-*mac*PSSNa. The macromonomer synthesis involved pseudo-living free radical polymerization of sodium styrenesulfonate (SSNa) and termination with divinylbenzene (DVB). The macromonomer, *mac*PSSNa, served as both the comonomer and emulsifier in the emulsion copolymerization with styrene. They also synthesized poly(acrylonitrile-*g*-*mac*PSSNa) exchanging styrene monomer to acrylonitrile and poly(vinylidene fluoride-*g*-*mac*PSSNa) using radiation induced graft polymerization.[93, 97] Their macromonomer strategy resulted in uniform graft chain length of the poly(styrene sulfonic acid) branches.

Figure 2.22 compares the proton conductivity of PS-g-macPSSA and PS-*r*-PSSA membranes as a function of ion content. A graft copolymer exhibited much higher conductivity, while degree of sulfonation for both polymers ranged 16 - 17 mol%. The conductivity of the graft copolymer showed 13 times higher even though its water content is 60% lower.

TEM images (Figure 2.23) supported this high proton conductivity of the sulfonated graft copolymers. These TEM images gave phase-separated morphology for the graft polymers. The ionic domains of the graft copolymer were interconnected, whereas PS-*r*-PSSA did not provide any significant microphase separation. The density of the ionic pathways also increased with ionic content as seen in Figure 2.23 (a) – (c).

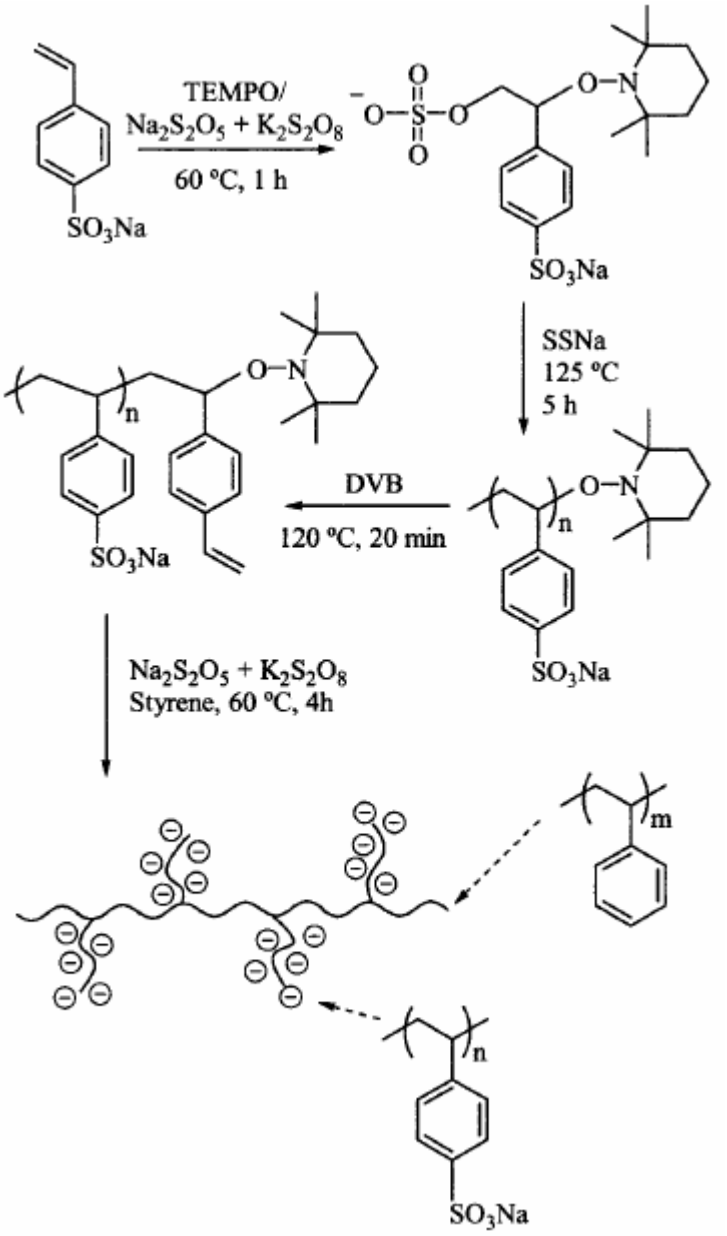


**Scheme 2.4** Preparation of PS-*g*-*mac*PSSNa graft polymers[96]

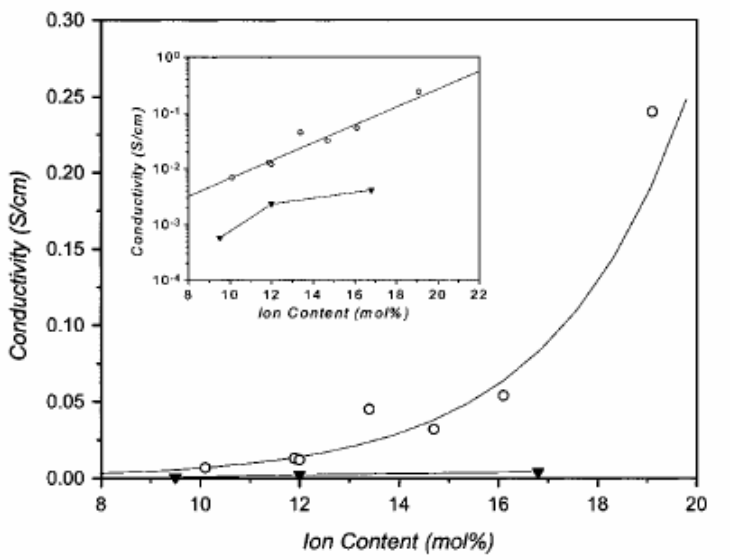


**Figure 2.22** Comparison of proton conductivity of PS-*r*-PSSA (triangle) and PS-*g*-*mac*PSSA (circle) copolymer membranes as a function of ion content. Inset: log scale plot[96]

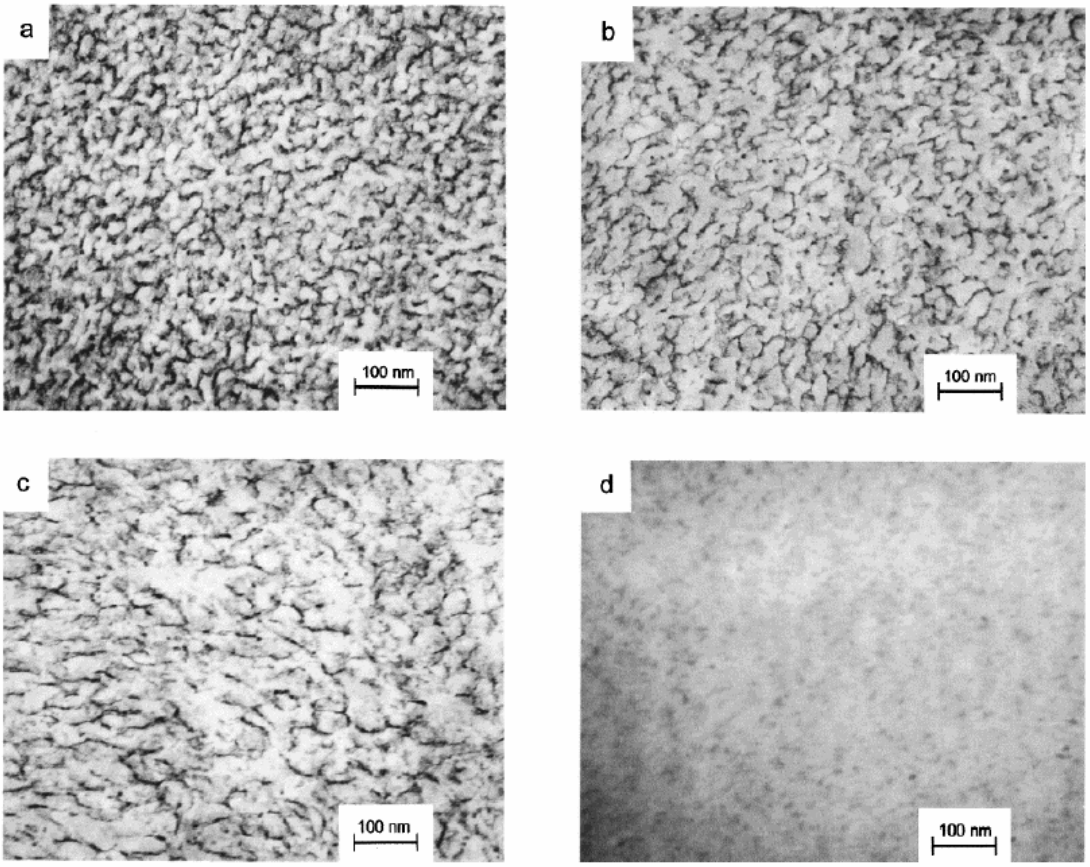


**Figure 2.23** TEM micrographs of $Pb^{2+}$-stained PS-*g*-*mac*PSSA graft polymer membranes possessing ion contents: 19.1 mol % (a), 11.9 mol % (b), and 8.1 mol % (c) and of a random copolymer membrane (PS-*r*-PSSA), ion content 12.0 mol % (d)[96]

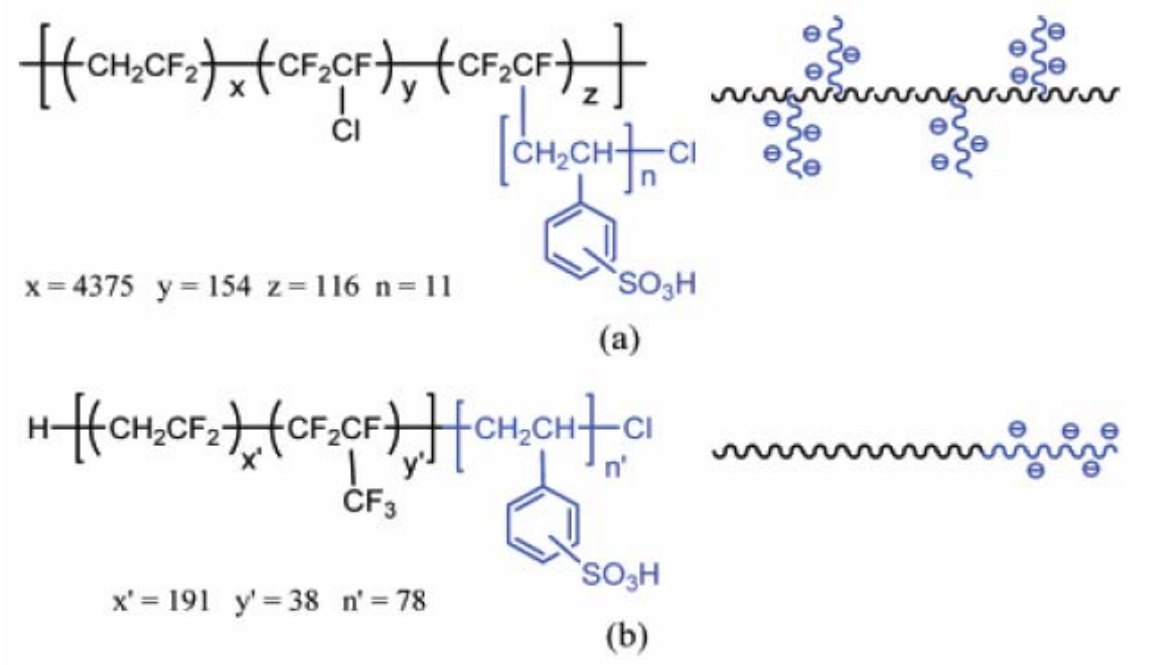


**Figure 2.24** Chemical structures of (a) P(VDF-*co*-CTFE)-*g*-SPS graft and (b) P(VDF-*co*-HFP)-*b*-SPS diblock copolymers[98]

Holdcroft et al. also reported the comparison between sulfonated graft copolymer and sulfonated diblock copolymer.[98] They prepared partially sulfonated poly([vinylidene difluoride-*co*-chlorotrifluoroethylene]-*g*-styrene [P(VDF-*co*-CTFE)-*g*-SPS] and partially sulfonated poly([vinylidene difluoride-*co*-hexafluoropropylene]-*b*-styrene) [P(VDF-*co*-HFP)-*b*-SPS] and the chemical structures are shown in Figure 2.24. Both P(VDF-*co*-CTFE)-*g*-SPS and [P(VDF-*co*-HFP)-*b*-SPS] were prepared using ATRP and subsequent postsulfonation.

The graft copolymers tolerated much higher ionic contents without excessive swelling, whereas diblock membranes exhibited a substantial increase in water content with increasing IEC (Figure 2.25 (a)), which resulted in poor mechanical properties with high water content. The graft copolymers demonstrated sufficient proton conductivity at high IEC (Figure 2.25 (b)). In contrast, the diblock copolymers exhibited a higher degree

of long-range order, which was also confirmed by TEM image. However, this characteristic ironically led to membranes to swell excessively at low IEC, and diluted the proton concentration (Figure 2.25 (c)). Their work raised another design parameter for novel block copolymer membranes for PEMFC application.

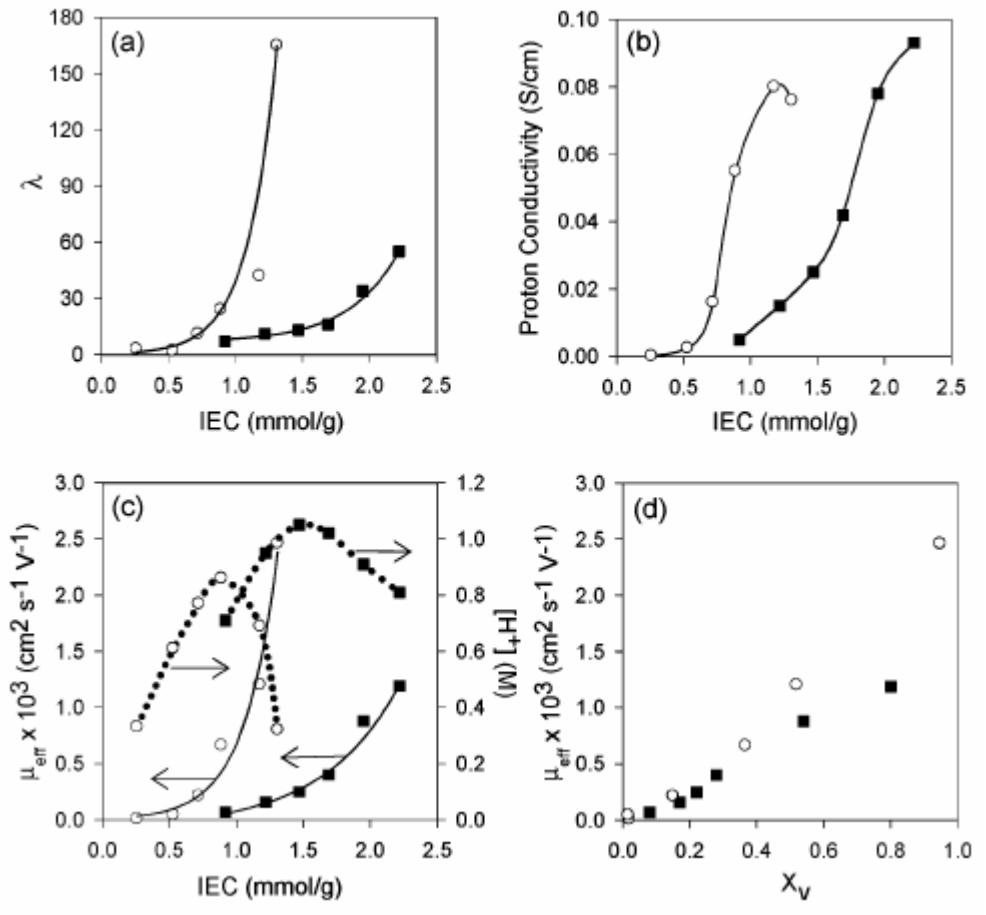


**Figure 2.25** Plots of (a) water content (λ) vs. IEC, (b) *in-plane* proton conductivity vs. IEC, (c) effective proton mobility ($\mu_{eff}$) (solid line) and analytical [H+] (dotted line) vs. IEC, (d) $\mu_{eff}$ vs. volume fraction of water (Xv) of P(VDF-*co*-CTFE)-*g*-SPS (■) and P(VDF-*co*-HFP)-*b*-SPS (O) membranes[98]

## 2.6 References


1. Grubbs, R. H.; Tumas, W., Polymer synthesis and organotransition metal chemistry. *Science* **1989,** 243, (4893), 907-915.
2. Webster, O. W., Living polymerization methods. *Science* **1991,** 251, (4996), 887-893.

3. Hadjichristidis, N.; Iatrou, H.; Pispas, S.; Pitsikalis, M., Anionic polymerization: high vacuum techniques. *Journal of Polymer Science, Part A: Polymer Chemistry* **2000,** 38, (18), 3211-3234.
4. Hadjichristidis, N.; Iatrou, H.; Pitsikalis, M.; Mays, J., Macromolecular architectures by living and controlled/living polymerizations. *Progress in Polymer Science* **2006,** 31, (12), 1068-1132.
5. Hadjichristidis, N.; Pitsikalis, M.; Iatrou, H., Synthesis of block copolymers. *Advances in Polymer Science* **2005,** 189, (Block Copolymers I), 1-124.
6. Hadjichristidis, N.; Pitsikalis, M.; Pispas, S.; Iatrou, H., Polymers with complex architecture by living anionic polymerization. *Chemical Reviews (Washington, D. C.)* **2001,** 101, (12), 3747-3792.
7. Hsieh, H. L.; Quirk, R. P., *Anionic Polymerization*. Marcel Dekker, Inc.: New York, Basel, Hong Kong, 1996.
8. Morton, M.; Fetters, L. J., Anionic polymerization of vinyl monomers. *Rubber Chemistry and Technology* **1975,** 48, (3), 359-409.
9. Szwarc, M., "Living" polymers. *Nature (London, United Kingdom)* **1956,** 178, 1168-9.
10. Szwarc, M.; Levy, M.; Milkovich, R., Polymerization initiated by electron transfer to monomer. A new method of formation of block polymers. *Journal of the American Chemical Society* **1956,** 78, 2656-7.
11. Odian, G., *Principles of polymerization*. Fourth ed.; John Wiley & Sons, Inc.: Hoboken, New Jersey, 2004.
12. Ziegler, K.; Jakob, L.; Wollthan, H.; Wenz, A., Alkali organic compounds. XIII. The first reaction products of alkali metals upon butadiene. *Ann.* **1934,** 511, 64-88.
13. Ziegler, K.; Colonius, H.; Schafer, O., Alkali organic compounds. II. Study of Schlenk's addition of alkali metals to unsaturated hydrocarbons. *Ann.* **1929,** 473, 36-56.
14. Lambert, C.; Schleyer, P. V., Are polar organometallic compounds carbanions-The gegenion effect on structure and energies of alkali-metal compounds. *Angewandte Chemie-International Edition in English* **1994,** 33, (11), 1129-1140.
15. Brown, T. L., Nuclear magnetic resonance studies of organometallic exchange processes. *Acc. Chem. Res. FIELD Full Journal Title:Accounts of Chemical Research* **1968,** 1, (1), 23-32.
16. Lewis, H. L.; Brown, T. L., Association of alkyllithium compounds in hydrocarbon media. Alkyllithium-base interactions. *Journal of the American Chemical Society* **1970,** 92, (15), 4664-70.
17. Margerison, D.; Newport, J. P., Degree of association of butyllithium in hydrocarbon media. *Transactions of the Faraday Society* **1963,** 59;Pt 9, (489), 2058-63.
18. Margerison, D.; Pont, J. D., Degrees of association of n-pentyllithium and n-octyllithium in benzene. *Transactions of the Faraday Society* **1971,** 67, (Pt. 2), 353-9.
19. Bywater, S.; Worsfold, D. J., Alkyllithium anionic polymerization initiators in hydrocarbon solvents. *Journal of Organometallic Chemistry* **1967,** 10, (1), 1-6.
20. Weiner, M.; Vogel, G.; West, R., Physical properties and structure of tert-butyllithium. *Inorganic Chemistry* **1962,** 1, 654-8.
21. Glaze, W. H.; Freeman, C. H., Cyclohexylmetal compounds. IV. The effect of aggregate size on the reactivity of alkyllithium compounds. *Journal of the American Chemical Society* **1969,** 91, (25), 7198-9.
22. Hsieh, H. L.; McKinney, O. F., Relation between the heterogeneity index and the kinetic ratio of anionically polymerized polymers. *Journal of Polymer Science, Polymer Letters Edition* **1966,** 4, (11), 843-7.
23. Bauer, R. J., *Ullman's Encyclopedia of Industrial Chemistry*. 5th ed.; VCH Verlagsgesellschaft: Weinheim, Germany, 1990; Vol. A15.
24. Nakahama, S.; Hirao, A., Protection and polymerization of functional monomers -Anionic living polymerization of protected monomers. *Progress in Polymer Science* **1990,** 15, (2), 299-335.
25. Rempp, P.; Franta, E.; Herz, J. E., Macromolecular engineering by anionic methods. *Advances in Polymer Science* **1988,** 86, 145-173.
26. Bywater, S.; Firat, Y.; Black, P. E., Microstructures of polybutadienes prepared by anionic polymerization in polar-solvents-Ion-pari and solvent effects. *Journal of Polymer Science Part a-Polymer Chemistry* **1984,** 22, (3), 669-672.
27. Bywater, S.; Worsfold, D. J., Charge-distribution in substituted allyl-alkali metal-compounds by C-13 NMR. *Journal of Organometallic Chemistry* **1978,** 159, (3), 229-235.

28. Bywater, S., Relationship of anion pair structure to stereospecificity of polymerization. In *ACS Symposium Series, Anionic Polymerization, Kinetics, Mechanisms, and Synthesis*, McGrath, J. E., Ed. American Chemical Society: Washington D.C., 1981; pp 71-77.
29. Duck, E. W.; Locke, J. M., Chapter 4 Polydiens by Anionic Catalyst. In *The stereo Rubbers*, Saltman, W. M., Ed. John Wiley & Sons: New York, London, Sydney, Toronto, 1977; pp 139-213.
30. Short, J. N.; Kraus, G.; Zelinski, R. P.; Naylor, F. E., Polybutadienes of controlled cis, trans, and vinyl structures. *Rubber Chemistry and Technology* **1959,** 32, 614-627.
31. Hamley, I. W., Introduction to Block Copolymers. In *Developments in Block Copolymer Science and Technology*, Hamley, I. W., Ed. john Wiley & Sons, Ltd: Chichester, New York, Weinheim, Brisbane, Toronto, Singapore, 2004; pp 1-29.
32. Fredrickson, G. H.; Bates, F. S., Dynamics of block copolymers: Theory and experiment. *Annual Review of Materials Science* **1996,** 26, 501-550.
33. Bates, F. S.; Fredrickson, G. H., Block copolymers-designer soft materials. *Physics Today* **1999,** 52, (Feb Issue), 32-38.
34. Colby, R. H.; Rubinstein, M., *Polymer Physics*. Oxford University Press: 2003.
35. Maynard, H. D.; Lyu, S. P.; Fredrickson, G. H.; Wudl, F.; Chmelka, B. F., Syntheses of nanophase-segregated poly(vinyl acetate)-poly(dimethylsiloxane) and poly(vinyl acetate)-poly(styrene) graft copolymers. *Polymer* **2001,** 42, (18), 7567-7574.
36. Fairclough, J. P. A.; Hamley, I. W.; Terrill, N. J., X-ray scattering in polymers and micelles. *Radiation Physics and Chemistry* **1999,** 56, (1-2), 159-173.
37. Dyson, D. J., *X-ray and electron diffraction studies in materials science* Maney: London, 2004.
38. Wignall, G. D., Neutron and X-ray Scattering. In *Physical Properties of polymers Handbook*, Mark, J. E., Ed. American Institute of Physics Press: Woodbury, New York, 1996.
39. Coleman, M. M.; Graf, J. F.; Painter, P. C., *Specific Interactions and the Miscibility of Polymer Blends*. Technomic Publishing Company, Inc.: Lancaster, Pennsylvania, 1991.
40. Sheth, J. P.; Klinedinst, D. B.; Wilkes, G. L.; Yilgor, I.; Yilgor, E., Role of chain symmetry and hydrogen bonding in segmented copolymers with monodisperse hard segments. *Polymer* **2005,** 46, (18), 7317-7322.
41. Lange, R. F. M.; Van Gurp, M.; Meijer, E. W., Hydrogen-bonded supramolecular polymer networks. *Journal of Polymer Science Part a-Polymer Chemistry* **1999,** 37, (19), 3657-3670.
42. Beijer, F. H.; Sijbesma, R. P.; Kooijman, H.; Spek, A. L.; Meijer, E. W., Strong dimerization of ureidopyrimidones via quadruple hydrogen bonding. *Journal of the American Chemical Society* **1998,** 120, (27), 6761-6769.
43. Beijer, F. H.; Kooijman, H.; Spek, A. L.; Sijbesma, R. P.; Meijer, E. W., Self-complementarity achieved through quadruple hydrogen bonding. *Angewandte Chemie-International Edition* **1998,** 37, (1-2), 75-78.
44. Sijbesma, R. P.; Beijer, F. H.; Brunsveld, L.; Folmer, B. J. B.; Hirschberg, J.; Lange, R. F. M.; Lowe, J. K. L.; Meijer, E. W., Reversible polymers formed from self-complementary monomers using quadruple hydrogen bonding. *Science* **1997,** 278, (5343), 1601-1604.
45. Folmer, B. J. B.; Sijbesma, R. P.; Versteegen, R. M.; van der Rijt, J. A. J.; Meijer, E. W., Supramolecular polymer materials: Chain extension of telechelic polymers using a reactive hydrogen-bonding synthon. *Advanced Materials* **2000,** 12, (12), 874-878.
46. Sontjens, S. H. M.; Sijbesma, R. P.; van Genderen, M. H. P.; Meijer, E. W., Stability and lifetime of quadruply hydrogen bonded 2-ureido-4[1H]-pyrimidinone dimers. *Journal of the American Chemical Society* **2000,** 122, (31), 7487-7493.
47. Elkins, C. L.; Viswanathan, K.; Long, T. E., Synthesis and characterization of star-shaped poly(ethylene-co-propylene) polymers bearing terminal self-complementary multiple hydrogen-bonding sites. *Macromolecules* **2006,** 39, (9), 3132-3139.
48. Yamauchi, K.; Kanomata, A.; Inoue, T.; Long, T. E., Thermoreversible polyesters consisting of multiple hydrogen bonding (MHB). *Macromolecules* **2004,** 37, (10), 3519-3522.
49. Yamauchi, K.; Lizotte, J. R.; Hercules, D. M.; Vergne, M. J.; Long, T. E., Combinations of microphase separation and terminal multiple hydrogen bonding in novel macromolecules. *Journal of the American Chemical Society* **2002,** 124, (29), 8599-8604.
50. Yamauchi, K.; Lizotte, J. R.; Long, T. E., Thermoreversible poly(alkyl acrylates) consisting of self-complementary multiple hydrogen bonding. *Macromolecules* **2003,** 36, (4), 1083-1088.

51. Pearson, R. G., Hard and soft acids and bases. *Journal of the American Chemical Society* **1963,** 85, (22), 3533-9.
52. Eisenberg, A.; Kim, J.-S., *Introduction to Ionomers*. John Wiley & Sons, Inc: 1998.
53. Eisenberg, A., Clustering of Ions in Organic Polymers. A Theoretical Approach. *Macromolecules* **1970,** 3, 147-154.
54. Eisenberg, A.; Hird, B.; Moore, R. B., A new multiplet-cluster model for the morphology of random ionomers. *Macromolecules* **1990,** 23, (18), 4098-4107.
55. Kucera, F.; Jancar, J., Homogeneous and heterogeneous sulfonation of polymers: A review. *Polymer Engineering and Science* **1998,** 38, (5), 783-792.
56. Hickner, M. A.; Ghassemi, H.; Kim, Y. S.; Einsla, B. R.; McGrath, J. E., Alternative polymer systems for proton exchange membranes (PEMs). *Chemical Reviews* **2004,** 104, (10), 4587-4611.
57. Yang, Y.; Holdcroft, S., Synthetic strategies for controlling the morphology of proton conducting polymer membranes. *Fuel Cells* **2005,** 5, (2), 171-186.
58. Makowski, H. S.; Lundberg, R. D.; Agarwal, P. K. Amine-terminated poly(alkylene oxide)-neutralized sulfonated thermoplastic polymers. 82-302463, 66970, 19820514., 1982.
59. Klein, R. R.; Makowski, H. S. Sulfonating EPDM. 81-301399, 37283, 19810331., 1981.
60. Makowski, H. S.; Lundberg, R. D.; Westerman, L.; Bock, J., Synthesis and properties of sulfonated EPDM. *Advances in Chemistry Series* **1980,** 187, (Ions Polym.), 3-19.
61. Makowski, H. S.; Lundberg, R. D.; Bock, J. Sulfonation of an elastomeric polymer. 78-951394, 4184988, 19781016., 1980.
62. Makowski, H. S.; Bock, J.; Lundberg, R. D. Forming a polymer that contains metalsulfonate. 78-300684, 2353, 19781128., 1979.
63. Makowski, H. S.; Lundberg, R. D.; Bock, J. Sulfonating elastomeric polymers. 78-300685, 2354, 19781128., 1979.
64. Makowski, H. S.; Lundberg, R. D.; Bock, J. Bulk neutralization of sulfonated elastomeric polymers and compositions thereof. 78-300686, 2355, 19781128., 1979.
65. Makowski, H. S.; Lundberg, R. D.; Singhal, G. H. Flexible plastic masses. 73-2348842, 2348842, 19730928., 1974.
66. Willis, C. L.; Handlin, D. L., Jr.; Trenor, S. R.; Mather, B. D. Sulfonated block copolymers, method for their preparation, and their. 2006-EP64513, 2007010039, 20060721., 2007.
67. Storey, R. F.; Baugh, D. W., III, Poly(styrene-b-isobutylene-b-styrene) block copolymers and ionomers therefrom: morphology as determined by small-angle X-ray scattering and transmission electron microscopy. *Polymer* **2000,** 41, (9), 3205-3211.
68. Storey, R. F.; Baugh, D. W.; Choate, K. R., Poly(styrene-b-isobutylene-b-styrene) block copolymers produced by living cationic polymerization - I. Compositional analysis. *Polymer* **1999,** 40, (11), 3083-3090.
69. Elabd, Y. A.; Napadensky, E., Sulfonation and characterization of poly(styrene-isobutylene-styrene) triblock copolymers at high ion-exchange capacities. *Polymer* **2004,** 45, (9), 3037-3043.
70. Elabd, Y. A.; Napadensky, E.; Walker, C. W.; Winey, K. I., Transport properties of sulfonated poly(styrene-b-isobutylene-b-styrene) triblock copolymers at high Ion-exchange capacities. *Macromolecules* **2006,** 39, (1), 399-407.
71. Elabd, Y. A.; Walker, C. W.; Beyer, F. L., Triblock copolymer ionomer membranes. Part II. Structure characterization and its effects on transport properties and direct methanol fuel cell performance. *Journal of Membrane Science* **2004,** 231, (1-2), 181-188.
72. Sauviat, M.; Salle, R.; Sillion, B. Sulfonated polyimides useful as cation exchangers. 69-23249, 2050251, 19690708., 1971.
73. Genies, C.; Mercier, R.; Sillion, B.; Cornet, N.; Gebel, G.; Pineri, M., Soluble sulfonated naphthalenic polyimides as materials for proton exchange membranes. *Polymer FIELD Full Journal Title:Polymer* **2001,** 42, (2), 359-373.
74. Meyer, G.; Perrot, C.; Gebel, G.; Gonon, L.; Morlat, S.; Gardette, J.-L., Ex situ hydrolytic degradation of sulfonated polyimide membranes for fuel cells. *Polymer* **2006,** 47, (14), 5003-5011.
75. Perrot, C.; Meyer, G.; Gonon, L.; Gebel, G., Aging mechanisms of proton exchange membrane used in fuel cell applications. *Fuel Cells (Weinheim, Germany)* **2006,** 6, (1), 10-15.
76. Rollet, A. L.; Blachot, J. F.; Delville, A.; Diat, O.; Guillermo, A.; Porion, P.; Rubatat, L.; Gebel, G., Characterization of porous structure through the dynamical properties of ions confined in

sulfonated polyimide ionomers films. *European Physical Journal E: Soft Matter* **2003,** 12, (Suppl. 1), S131-S134.
77. Blachot, J. F.; Diat, O.; Putaux, J.-L.; Rollet, A.-L.; Rubatat, L.; Vallois, C.; Muller, M.; Gebel, G., Anisotropy of structure and transport properties in sulfonated polyimide membranes. *J. Membr. Sci. FIELD Full Journal Title:Journal of Membrane Science* **2003,** 214, (1), 31-42.
78. Lee, H. S.; Badami, A. S.; Roy, A.; McGrath, J. E., Segmented sulfonated poly(arylene ether sulfone)-b-polyimide copolymers for proton exchange membrane fuel cells. i. copolymer synthesis and fundamental properties. *Journal of Polymer Science Part a-Polymer Chemistry* **2007,** 45, (21), 4879-4890.
79. Lee, H. S.; Roy, A.; Badami, A. S.; McGrath, J. E., Synthesis and characterization of sulfonated poly(arylene ether) polyimide multiblock copolymers for proton exchange membranes. *Macromolecular Research* **2007,** 15, (2), 160-166.
80. Wang, H.; Badami, A. S.; Roy, A.; McGrath, J. E., Multiblock copolymers of poly(2,5-benzophenone) and disulfonated poly(arylene ether sulfone) for proton-exchange membranes. I. Synthesis and characterization. *Journal of Polymer Science Part a-Polymer Chemistry* **2007,** 45, (2), 284-294.
81. Lee, H. S.; Roy, A.; Lane, O.; Dunn, S.; McGrath, J. E., Hydrophilic-hydrophobic multiblock copolymers based on poly(arylene ether sulfone) via low-temperature coupling reactions for proton exhange membrane fuel cells. *Polymer* **2008,** 49, 715-723.
82. Li, Y. X.; Roy, A.; Badami, A. S.; Hill, M.; Yang, J.; Dunn, S.; McGrath, J. E., Synthesis and characterization of partially fluorinated hydrophobic-hydrophilic multiblock copolymers containing sulfonate groups for proton exchange membrane. *Journal of Power Sources* **2007,** 172, (1), 30-38.
83. Ghassemi, H.; McGrath, J. E.; Zawodzinski, T. A., Multiblock sulfonated-fluorinated poly(arylene ether)s for a proton exchange membrane fuel cell. *Polymer* **2006,** 47, (11), 4132-4139.
84. Yu, X.; Roy, A.; Dunn, S.; Yang, J.; McGrath, J. E., Synthesis and characterization of sulfonated-fluorinated, hydrophilic-hydrophobic multiblock copolymers for proton exhange membranes. *Macromolecular Symposia* **2006,** 245-246, 439-449.
85. Lu, X. Y.; Steckle, W. P.; Weiss, R. A., Morphological-studies of a triblock copolymer ionomer by small-angle x-ray-scattering. *Macromolecules* **1993,** 26, (24), 6525-6530.
86. Lu, X. Y.; Steckle, W. P.; Weiss, R. A., Ionic aggregation in a block-copolymer ionomer. *Macromolecules* **1993,** 26, (22), 5876-5884.
87. Mani, S.; Weiss, R. A.; Williams, C. E.; Hahn, S. F., Microstructure of ionomers based on sulfonated block copolymers of polystyrene and poly(ethylene-alt-propylene). *Macromolecules* **1999,** 32, (11), 3663-3670.
88. Kim, B.; Kim, J.; Cha, B. J.; Jung, B., Effect of selective swelling on protons and methanol transport properties through partially sulfonated block copolymer membranes. *Journal of Membrane Science* **2006,** 280, (1+2), 270-277.
89. Kim, B.; Kim, J.; Jung, B., Morphology and transport properties of protons and methanol through partially sulfonated block copolymers. *Journal of Membrane Science* **2005,** 250, (1-2), 175-182.
90. Kim, J.; Kim, B.; Jung, B., Proton conductivity and methanol permeability of membranes made from partially sulfonated polystyrene-block-poly(ethylene-ran-butylene)-block-polystyrene copolymers. *Journal of Membrane Science* **2002,** 207, (1), 129-137.
91. Kim, J.; Kim, B.; Jung, B.; Kang, Y. S.; Ha, H. Y.; Oh, I.-H.; Ihn, K. J., Effect of casting solvent on morphology and physical properties of partially sulfonated polystyrene-block-poly(ethylene-ran-butylene)-block-polystyrene copolymers. *Macromolecular Rapid Communications* **2002,** 23, (13), 753-756.
92. David, R. L., *Handbook of Chemistry and Physics*. 61st ed.; CRC Press: Florida, 1993.
93. Chuy, C.; Ding, J.; Swanson, E.; Holdcroft, S.; Horsfall, J.; Lovell, K. V., Conductivity and electrochemical ORR mass transport properties of solid polymer electrolytes containing poly(styrene sulfonic acid) graft chains. *Journal of the Electrochemical Society* **2003,** 150, (5), E271-E279.
94. Ding, J.; Chuy, C.; Holdcroft, S., Solid polymer electrolytes based on ionic graft polymers: effect of graft chain length on nano-structured, ionic networks. *Advanced Functional Materials* **2002,** 12, (5), 389-394.

95. Ding, J.; Chuy, C.; Holdcroft, S., A self-organized network of nanochannels enhances ion conductivity through polymer films. *Chemistry of Materials* **2001,** 13, (7), 2231-2233.
96. Ding, J. F.; Chuy, C.; Holdcroft, S., Enhanced conductivity in morphologically controlled proton exchange membranes: Synthesis of macromonomers by SFRP and their incorporation into graft polymers. *Macromolecules* **2002,** 35, (4), 1348-1355.
97. Siu, A.; Pivovar, B.; Horsfall, J.; Lovell, K. V.; Holdcroft, S., Dependence of methanol permeability on the nature of water and the morphology of graft copolymer proton exchange membranes. *Journal of Polymer Science, Part B: Polymer Physics* **2006,** 44, (16), 2240-2252.
98. Tsang, E. M. W.; Zhang, Z.; Shi, Z.; Soboleva, T.; Holdcroft, S., Considerations of macromolecular structure in the design of proton conducting polymer membranes: Graft versus diblock polyelectrolytes. *Journal of the American Chemical Society* **2007,** 129, (49), 15106-15107.

# Chapter 3: Pseudo-living Anionic Telomerization of 1,3-Butadiene

**Take from:**
Tomonori Saito, Kim C. Harich, and Timothy E. Long, **"**Pseudo-living Anionic Telomerization of 1,3-Butadiene,**"** submitted to *Macromolecular Chemistry and Physics*

## 3.1 Abstract

This report describes the synthesis and characterization of liquid polybutadienes via anionic telomerization. The influence of the initiation procedures, reaction temperature, and scale of reaction on the various telomerization processes were studied and compared to the properties of liquid polybutadiene synthesized using conventional anionic polymerization. Low molecular weight liquid polybutadienes (1000 – 2000 g/mol) consisting of 60 mol% 1,2-polybutadiene repeating units were synthesized via anionic telomerization. We determined that maintaining the initiation and reaction temperature less than 70 °C minimized chain transfer and enabled the polymerization to occur in a living fashion, which resulted in well-controlled molecular weights and narrow polydispersity indices. MALDI-TOF mass spectrometry confirmed that the end group of liquid polybutadienes synthesized via anionic telomerization contained one benzyl end and one protonated end. In comparison, the end group of liquid polybutadienes synthesized via living anionic polymerization contained one *sec*-butyl or *n*-butyl end and one protonated end.

## 3.2 Introduction

Liquid polybutadienes (PB), which typically range from 1000 to 10000 g/mol, are highly versatile oligomers that have received attention for many decades due to their industrial importance in the field of microelectronics, coatings, and adhesives. The main characteristics that enable potential applications for liquid PBs are their low bulk and solution viscosity and their high level of unsaturation, which facilitates subsequent chemical modifications.[1, 2] As described in the earlier literature, liquid PBs are prepared via anionic, coordination, cationic or free radical polymerization.[1, 2] Among these various polymerization mechanisms, anionic polymerization is the most common strategy for preparing liquid PBs with controlled molecular weight and well-defined microstructure.

The production of low molecular weight liquid PBs, especially in the 1000 – 5000 g/mol range, is typically achieved via the anionic telomerization process. Anionic telomerization involves the addition of a chain transfer agent (telogen), which possesses an acidic hydrogen that protonates an initiating or propagating anion.[1] Toluene is one of the common telogens, reported in the earlier literatures.[2-7] Use of an organolithium initiator in a telomerization process with toluene as telogen requires the presence of a polar promoter such as N, N, N', N'-tetramethylethylenediamine (TMEDA) to obtain a sufficient rate of transmetallation. Moreover, the addition of a polar promoter controls the final microstructure of the resulting liquid PB, which inevitably impacts the polymer's final properties. Because the ratio of propagation to the rate of transmetallation governs the molecular weight of anionic telomerization, the molecular weight distribution of a telomer is approximately 2.0, which corresponds to the statistical nature of a chain termination reaction.[1, 2]

The term "telomerization" refers to the process where a low molar mass molecule TH (telogen) forms oligomers known as telomers having the formula $T(A)_nH$.[8] When a fragment of a chain-transfer agent (telogen) is attached to the terminus of a polymer product, it impacts the properties of the resulting telomer. This is especially true for a low molecular weight oligomer, which an anionic telomerization typically produces. For example, in the case of toluene, the attachment of a terminal benzyl group to a telomer results in different optical and chemical properties compared to the attachment of a *sec*-butyl or *n*-butyl group via conventional anionic polymerization.

Matrix-assisted laser desorption/ionization time-of-flight mass spectrometry (MALDI-TOF MS) enables determination of repeating units and end group composition. MALDI-TOF MS measures an absolute molecular weight in the absence of fragmentation.[9, 10] Proper matrices for MALDI-TOF MS measurement are required, although it is often a challenge to identify an appropriate matrix for a novel polymer.[6-8] While a variety of matrices are reported in the literature, most synthetic polymers have been analyzed using 1,8,9-trihydroxyanthracene (dithranol), 2,5-dihydroxybenzoic acid (DHB), 2-(4-hydroxyphenyl-azo)-benzoic acid (HABA), trans-3-indoleacrylic acid (IAA), and 2,4,6-trihydroxyacetophenone (THAP).[10] The determination of polymer end groups using MALDI-TOF MS is generally accepted and reported widely in the earlier literature,[11-23] however, the analysis of liquid PBs, as described herein, remains unprecedented.

In this study, liquid PBs were synthesized via both anionic telomerization and conventional anionic polymerization of 1,3-butadiene, and the results were compared. We studied the influence of the reaction procedures, reaction temperature and reaction

scale on the telomerization process. The end groups of the liquid PBs were analyzed using MALDI-TOF MS to better understand the various processes associated with anionic telomerization. In addition, the properties of liquid PBs derived from anionic telomerization were compared with those from conventional anionic polymerization methods. The molecular weights of liquid PBs were targeted at 1000 – 2000 g/mol and their microstructures were synthesized to approximately 60 mol% 1,2-vinyl microstructures.

## 3.3 Experimental

### 3.3.1 Materials and Chemicals

1,3-Butadiene (99.5%, Matheson Tri-Gas Inc.), 10.0 M *n*-butyllithium solution in hexanes (*n*BuLi, Aldrich), 1.4 M *sec*-butyllithium solution in hexanes (*sec*BuLi, Aldrich), Irganox 1076 antioxidant (Ciba-Geigy Corp.), silver tetrafluoroacetate (99.99+%, Aldrich), 1,8,9-trihydroxyanthracene (97+%, Alfa Aesar), methanol (Fisher Scientific) and deuterated chloroform ($CDCl_3$, Cambridge Isotope Laboratories) were used as received. N, N, N', N'-Tetramethylethylenediamine (TMEDA, 99.5%, Aldrich) was treated with *sec*-butyllithium (Aldrich, 0.1 mM) and distilled under vacuum. Toluene (Fisher Scientific) and tetrahydrofuran (THF, Fisher Scientific) were passed through PURE SOLV MD-3 SOLVENT PURIFICATION SYSTEM (Innovative Technology Inc.) immediately prior to use.

### 3.3.2 Synthesis of Liquid 60 mol% 1,2-Polybutadienes via Living Anionic Polymerization in Cyclohexane

Synthesis of liquid 60 mol% 1,2-polybutadienes was performed in a glass anionic reactor, consisting of a 600 mL glass bowl, a stainless steel top plate, and stainless steel magnetically coupled mechanical stirrer. In addition, a heat-exchange coil, a thermocouple, a septum sealed port, various stainless steel transfer lines to introduce solvent (cyclohexane), and inlet/vent for purified nitrogen were equipped to the anionic reactor.[24, 25] The anionic reactor system was maintained at a constant nitrogen pressure (40 psi). The 600 mL-capacity anionic polymerization reactor was filled with cyclohexane (300 mL). THF (7.5 mL, 2.5 vol%) was added to the cyclohexane. 1,3-Butadiene (104 mL, 68 g) was collected in a round-bottomed flask at -78 °C and transferred to the cyclohexane/THF solution via a cannula. *sec*BuLi (48.6 mL, 68 mmol) (A) or *n*BuLi (6.8 mL, 68 mmol) (B) was injected to the reaction solution via a syringe. The reaction mixture was stirred for 3 h at 30 °C. The reaction was terminated with nitrogen-degassed methanol. 0.1 wt% Irganox 1076 was added to the reaction mixture and the polymer solution was passed through a filter to remove lithium salts. The polymer solution was precipitated into methanol and dried at reduced pressure and room temperature for 48 h. $^1$H NMR (400 MHz, $CDCl_3$, δ): 0.6 – 0.8 ppm (br, $CH_3CH_2CH(CH_3)$- or $CH_3CH_2CH_2CH_2$-), 1.0 – 1.8 ppm (br, -$CH_2$CH- in 1,2-polybutadiene), 1.9 – 2.2 ppm (br, -$CH_2$- in 1,4-polybutadiene, -$CH_2CH$- in 1,2-polybutadiene), 4.7 – 5.1 ppm (br, -CH=$CH_2$ in 1,2-polybutadiene and vinyl cyclopentane), 5.1 – 5.5 ppm (br, -CH=CH- in 1,4-polybutadiene), 5.5 – 5.7 ppm (br, -CH=$CH_2$ in 1,2-polybutadiene), 5.7 – 5.9 ppm (br, -CH=$CH_2$ in vinyl cyclopentane).

### 3.3.3 Synthesis of Liquid 60 mol% 1,2-Polybutadienes via Anionic Telomerization at 5 g Scale

Toluene (36 mL) was transferred to a flame-dried 100 mL round-bottomed flask equipped with a magnetic stirrer. *n*BuLi (0.25 mL, 2.5 mmol) was added to the toluene solution and TMEDA (0.76 mL, 5.0 mmol) was subsequently added. The *n*BuLi/TMEDA mixture in toluene was stirred at 25 ºC for 2 h and 75 °C for 2 h (C) or at 25 ºC for 10 min (D). (C) 1,3-Butadiene (7.7 mL, 5 g) was collected in a round-bottomed flask at -78 °C and transferred to the *n*BuLi/TMEDA toluene solution at -78 °C via a cannula. After 30 sec in a dry ice bath, the reaction flask was removed and allowed to stand at ambient temperature. After initiation, the reaction temperature was held at 25 °C for 2 h. (D) 1,3-Butadiene (7.7 mL, 5 g) was collected in a round-bottomed flask at -78 °C and transferred to the *n*BuLi/TMEDA toluene solution at 0 ºC via a cannula. After initiation, the reaction temperature was held at 25 ºC. A portion of the reaction mixture was removed using a cannula in 15 min (D-1). The reaction was performed at 25 ºC for 6 h (D-2). Both of the reactions ((C) and (D)) were terminated with nitrogen-degassed methanol. 0.1 wt% Irganox 1076 was added to the reaction mixture and the polymer solution was passed through a filter to remove lithium salts. The polymer solution was precipitated into methanol and dried at reduced pressure at room temperature for 48 h. $^1$H NMR (400 MHz, $CDCl_3$, δ): 0.6 – 1.8 ppm (br, -C*H*$_2$CH- in 1,2-polybutadiene and vinyl cyclopentane), 1.9 – 2.2 ppm (br, -C*H*$_2$- in 1,4-polybutadiene, -CH$_2$C*H*- in 1,2-polybutadiene), 2.2 – 2.6 ppm (br, -C*H*$_2$CH$_2$C$_6$H$_5$), 2.6 – 2.7 ppm (br, -C*H*$_2$C$_6$H$_5$), 4.7 – 5.1 ppm (br, -CH=C*H*$_2$ in 1,2-polybutadiene and vinyl cyclopentane), 5.1 – 5.5 ppm (br, -C*H*=C*H*- in 1,4-polybutadiene), 5.5 – 5.7 ppm (br, -C*H*=CH$_2$ in 1,2-polybutadiene), 5.7 – 5.9 ppm (br, -C*H*=CH$_2$ in vinyl cyclopentane), 6.9– 7.3 ppm (br, -C$_6$*H*$_5$).

### 3.3.4 Synthesis of Liquid 60 mol% 1,2-Polybutadienes via Anionic Telomerization at 80 g Scale

The 600 mL-capacity anionic polymerization reactor was filled with toluene (400 mL). *n*BuLi (8.0 mL, 80 mmol) was added to the toluene solution and TMEDA (12.1 mL, 80 mmol) was subsequently added. The *n*BuLi/TMEDA mixture in toluene was stirred at 50 ºC for 15 min. 1,3-Butadiene (123 mL, 80 g) was collected in a round-bottomed flask at -78 °C and transferred to the *n*BuLi/TMEDA toluene solution via a cannula with 1.7 mL/min (E) and 2.2 mL/min (F). During the addition of 1,3-butadiene, the temperature was maintained at 45 – 50 ºC (E) and 66 – 69 ºC (F) due to the exothermic reaction. After complete addition of 1,3-butadiene, the reaction mixture was stirred for an additional 30 min at 30 ºC. The reaction was terminated with nitrogen-degassed methanol. 0.1 wt% Irganox 1076 was added to the reaction mixture and the polymer solution was passed through a filter to remove lithium salts. The polymer solution was precipitated into methanol and dried at reduced pressure and room temperature for 48 h. $^1$H NMR (400 MHz, $CDCl_3$, δ): 0.6 – 1.8 ppm (br, -C*H*$_2$CH- in 1,2-polybutadiene and vinyl cyclopentane), 1.9 – 2.2 ppm (br, -C*H*$_2$- in 1,4-polybutadiene, -CH$_2$C*H*- in 1,2-polybutadiene), 2.2 – 2.6 ppm (br, -C*H*$_2$CH$_2$C$_6$H$_5$), 2.6 – 2.7 ppm (br, -C*H*$_2$C$_6$H$_5$), 4.7 – 5.1 ppm (br, -CH=C*H*$_2$ in 1,2-polybutadiene and vinyl cyclopentane), 5.1 – 5.5 ppm (br, -C*H*=C*H*- in 1,4-polybutadiene), 5.5 – 5.7 ppm (br, -C*H*=CH$_2$ in 1,2-polybutadiene), 5.7 – 5.9 ppm (br, -C*H*=CH$_2$ in vinyl cyclopentane), 6.9– 7.3 ppm (br, -C$_6$*H*$_5$).

### 3.3.5 Polymer Characterization

$^1$H NMR spectra of the polymers were obtained on a Varian Unity spectrometer operating at 400 MHz at ambient temperature. $CDCl_3$ was used as the solvent. Size

exclusion chromatography (SEC) measurements were performed in THF at 40 °C at flow rate 1 mL/min using a Waters size exclusion chromatograph equipped with an autosampler, three 5-mm PLgel Mixed-C columns, a Waters 410 refractive index (RI) detector operating at 880 nm, and a miniDAWN multiangle laser light scattering (MALLS) detector operating at 690 nm which was calibrated with narrow polydispersity polystyrene standards. The RI increment (*dn*/*dc*) was calculated online. Fourier-transfer Infrared (FT-IR) spectroscopy was performed using Spectrum One Perkin Elmer FT-IR spectrometer. Glass transition temperatures were determined using a differential scanning calorimeter (DSC) Q100 (TA instruments) at a heating rate of 10 °C/min under helium. Glass transition temperatures are reported as the transition midpoint during the second heat.

### 3.3.6 MALDI-TOF Mass Spectrometry Characterization

Liquid PB samples were analyzed via MALDI-TOF mass spectrometry on a Kratos Kompact SEQ instrument equipped with the standard 337.1 nm nitrogen laser. The sample slide was treated with 0.2 uL of a solution of silver tetrafluoroacetate (Ag TFA) in toluene (1 mg/mL) followed by 0.2 uL of a solution of 1,8,9-trihydroxyanthracene (dithranol) matrix compound in chloroform (2 mg/mL). Approximately 0.5 uL of each polymer was dissolved in 0.5 mL of chloroform and 0.2 uL of this preparation was applied to the matrix. Mass analysis was in the positive ion mode, and the laser power was set at an average of 160 (arbitrary relative units; range 0 - 180). Mass calibration was performed using an endohedral metalofullerene reference compound mixture.

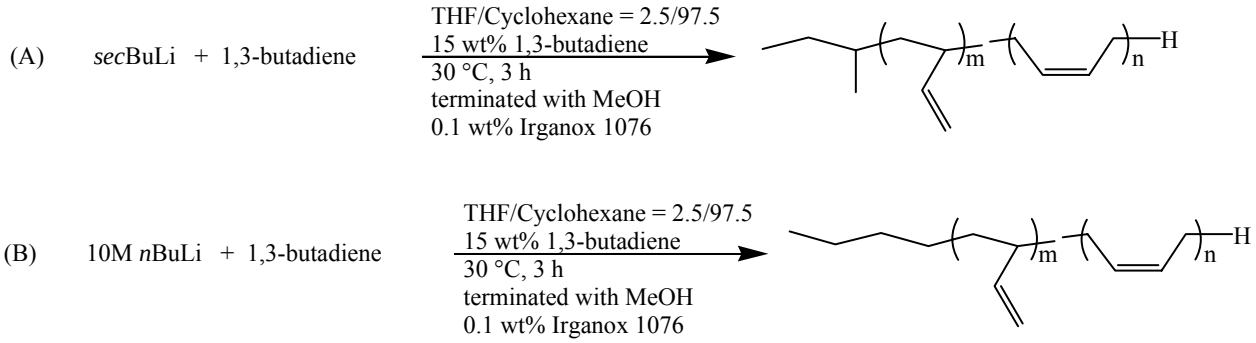


**Scheme 3.1** Synthesis of 60 mol% 1,2-polybutadienes via living anionic polymerization

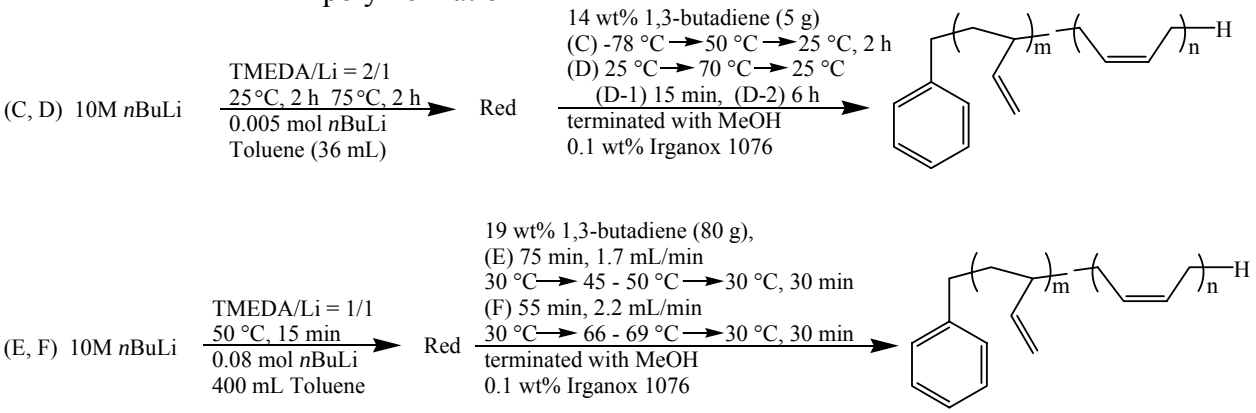


**Scheme 3.2** Synthesis of 60 mol% 1,2-polybutadienes via anionic telomerization

## 3.4 Results and Discussion

### 3.4.1 Synthesis of 60% 1,2-Polybutadiene via Conventional Anionic Polymerization of 1,3-Butadiene

Synthesis of 60% 1,2-polybutadiene in a 600 mL anionic reactor via conventional living anionic polymerization was performed. The results were then compared to those obtained from anionic telomerization. Following well-established synthetic procedures,[7, 26, 27] repetitive preliminary experiments of polybutadiene synthesis were performed. The results from the preliminary experiments determined that the addition of 2.5 vol% of THF to the cyclohexane solution resulted in 60% 1,2-polybutadiene repeating units. As shown in Scheme 1, the initiation was performed either with *sec*BuLi (A) or *n*BuLi (B).

The microstructure and molecular weights of the resulting liquid PBs are summarized in Table 1. $^{1}$H NMR analysis of the polybutadiene product (A) is shown in Figure 3.1. The integration of the $^{1}$H NMR resonances for two methyl groups in the s*ec*-butyl group (A), or for one methyl group in the *n*-butyl group (B) at 0.6 - 0.8 ppm, was used to calculate number-average molecular weight. The microstructure of the liquid PBs were calculated using the integration for -CH=C*H*$_2$ in 1,2-polybutadiene at 4.7 – 5.1 ppm and for -C*H*=C*H*- in 1,4-polybutadiene at 5.1 – 5.5 ppm. Predicted 1,2-polybutadiene microstructures (59 mol% and 51 mol%, respectively) and molecular weights (approximately 1200 - 1400 g/mol) were achieved. FT-IR spectroscopy determined cis-1,4 and tran-1,4 components of the obtained liquid PBs with assignments of 724 cm$^{-1}$ for cis-1,4 and 967 cm$^{-1}$ for trans-1,4[28], and the microstructures are shown in Table 3.1. The cis-1,4/trans-1,4 ratio was consistent with the earlier literature[26] for anionic polymerization of 1,3-butadiene at 30 or 60 °C with addition of THF for preparing high 1,2-polybutadiene. The narrow polydispersity index for both (A) and (B) ($M_w/M_n$ = 1.04), and the monodisperse SEC curves were demonstrated.

**Table 3.1** Molecular weights and microstructure of liquid PBs

| | | | | Microstructure | | |
|---|---|---|---|---|---|---|
| | $M_n$[a] | $M_n$[b] | $M_w/M_n$[b] | 1,2 [mol%][a] | Cyclic [mol%][a] | cis-1,4/trans-1,4[c] |
| A | 1320 | 1370 | 1.04 | 59 | 5 | 30/70 |
| B | 1050 | 1220 | 1.04 | 51 | 4 | 34/64 |
| C | 1960 | 1900 | 1.09 | 63 | 11 | 60/40 |
| D | 2710 | 2000 | 1.05 | 64 | 9 | 42/58 |
| E | 800 | 840 | 1.24 | 65 | 29 | 40/60 |
| F | 910 | 790 | 1.09 | 64 | 35 | 40/60 |

*1,2 microstructure contains cyclic units

[a] $^{1}$H NMR conditions; Varian Unity 400 MHz, $CDCl_3$

[b] Determined using SEC at 40 °C in THF with a MALLS detector

[c] Determined using FT-IR spectroscopy, cis-1,4: 724 cm$^{-1}$, trans-1,4: 967 cm$^{-1}$

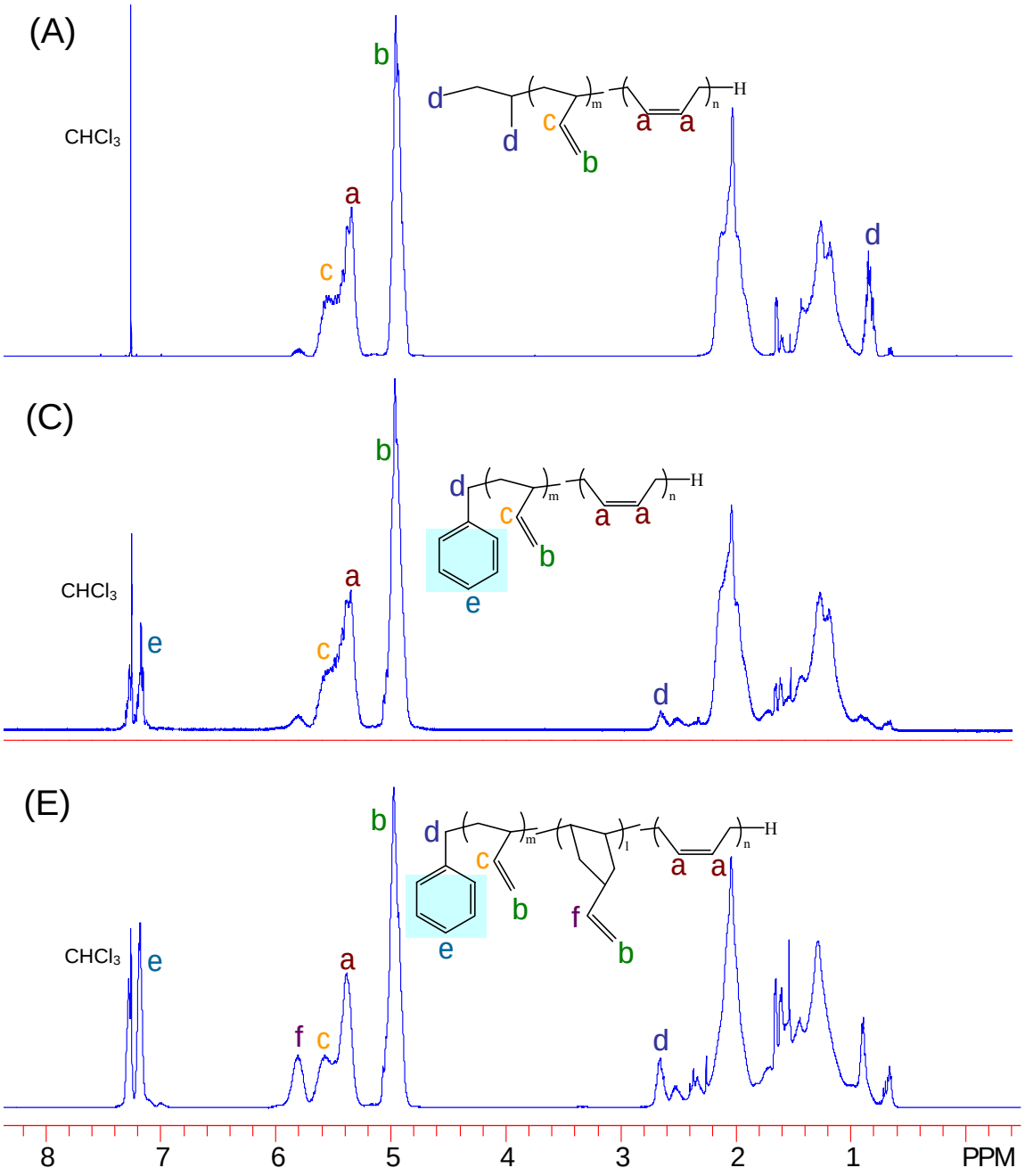


**Figure 3.1** $^{1}$H NMR comparison of 60 mol% 1,2-polybutadienes synthesized via living anionic polymerization (A) and anionic telomerization (C), (E) $^{1}$H NMR conditions; Varian Unity 400 MHz, $CDCl_3$

### 3.4.2 The Influence of Anionic Telomerization Reaction Temperature

Young et al.[6] reported the anionic telomerization of 1,3-butadiene with toluene using different ratios of TMEDA/*n*BuLi. They also studied the influence of the TMEDA/*n*BuLi ratio with respect to polybutadiene microstructure. The polydispersity indices of the reported liquid PBs were approximately 2.0 at reaction temperature 75°C. When the TMEDA:*n*BuLi ratio was higher than 1:2, it afforded approximately 60 mol% of the 1,2-vinyl microstructure. We modified these reaction conditions to obtain a narrower polydispersity, as shown in Schemes 2. Specifically, at polymerization temperatures lower than 75°C, we synthesized 60 mol% 1,2-polybutadienes with 1,3-butadiene addition at the onset of reaction in a round-bottomed flask (Scheme 1 (C, D)), and 60 mol% 1,2-polybutadienes with 1,3-butadiene constant addition in a large-scale customized anionic reactor to investigate the influence of reaction conditions on polydispersity indices and microstructures.

The influence of the modified initiation procedures and reduced temperature was examined for the reaction (C) and (D). When TMEDA was added to a *n*BuLi toluene solution, a red color immediately appeared, suggesting the formation of benzyl anions. For reaction (C), the *n*BuLi/TMEDA mixture in toluene was stirred at 25 ºC for 2 h and then at 75 °C for 2 h to ensure quantitative conversion of the *n*BuLi initiator to benzyllithium anions. The initiation of the 1,3-butadiene polymerization was performed at -78 °C. The collected 1,3-butadiene was transferred at once via a cannula to the *n*BuLi/TMEDA toluene solution at -78 °C and then the reaction flask was allowed to stand at ambient temperature. Due to an exothermic reaction, the reaction temperature immediately increased to 50 °C (C). Once the temperature returned to 25 ºC, the reaction

was allowed to proceed for another 2 h. For reaction (D), the *n*BuLi/TMEDA mixture in toluene was stirred at 25 ºC for 10 min. 1,3-Butadiene was transferred to the *n*BuLi/TMEDA toluene solution at 0 ºC via a cannula to initiate the polymerization. After initiation, the reaction temperature increased to 80 ºC and then returned to 25 ºC. A portion of the reaction mixture was removed using a cannula in 15 min (D-1). The reaction was held at 25 ºC for 6 h (D-2).

$^1$H NMR spectra and SEC determined the microstructure and molecular weights of the liquid PBs, as summarized in Table 3.1. The $^1$H NMR spectrum of the liquid PB from the telomerization reaction (C) is shown in Figure 3.1. The microstructure of the liquid PBs were calculated using the integration for -CH=C*H*$_2$ in 1,2-polybutadiene at 4.7 – 5.1 ppm and for -C*H*=C*H*- in 1,4-polybutadiene at 5.1 – 5.5 ppm. The methylene adjacent to the benzyl group (2H, -C*H*$_2$C$_6$H$_5$) at 2.6 – 2.7 ppm was used to calculate $M_n$. Well-controlled 1,2-polybutadiene microstructures (63 – 64 mol%) and number-average molecular weights (approximately 2000 g/mol) were obtained. Quantitative isolated yield were achieved in all polymerizations. Cis-1,4 and trans-1,4 microstructure were analyzed using FT-IR spectroscopy. Cis-1,4 microstructure of the PB samples from the reaction (C) resulted in higher ratio than trans-1,4 microstructure, whereas the PB sample from the reaction (D) resulted in higher trans-1,4 microstructure than cis-1,4 microstructure. The initiation temperature of the reaction (C) was – 78 ºC, while the initiation temperature of the reaction (D) was 0 °C. The low initiation temperature of (C) presumably resulted in the higher contents of cis-1,4 microstructure, which was consistent with previous reports[26, 29, 30] of higher cis-1,4 microstructure than trans-1,4 microstructure in low temperature anionic polymerization of 1,3-butadiene.

The microstructure of polybutadiene in an anionic telomerization of 1,3-butadiene with TMEDA is known to possess a substituted cyclopentane.[5, 6, 30] While cyclic contents were dominant in the polybutadiene microstructure associated with Young's studies,[6] this study minimized the presence of the substituted cyclopentane. The monomer concentration and reaction temperature may explain the reduction of the vinyl cyclopentane rings. Moreover, intramolecular cyclization requires a higher energy of activation than the propagation step, while lower monomer concentration and higher temperature favor the cyclization reaction.[5] In the present study, all of the monomer was present at the onset of the reaction and the reaction temperature was moderate for both reactions (C) and (D). In addition to reducing cyclic contents in the 1,2 microstructure, SEC curves were monodisperse. The molecular weight distribution of the liquid PBs was shown to be less than 1.1, indicating rapid initiation relative to propagation. To the best of our knowledge, such a narrow polydispersity index in polybutadiene telomerization has not been reported earlier. Fetters et al.[5] and Hay et al.[31] reported that the polymerization of 1,3-butadiene with TMEDA in *n*-haxanes occurred via the living anionic addition mechanism at reaction temperatures lower than 60 °C. These results suggest, therefore, that lower initiation and reaction temperatures resulted in a narrow polydispersity index and minimized the occurrence of telomer chain transfer.

As a component of this study, a portion of the reaction mixture was removed after 15 min (D-1) to determine the reaction completion. The molecular weight and the microstructure of D-2 (6 h reaction) did not show significant changes from the D-1 sample (15 min reaction). A quantitative isolated yield for D-2 was also obtained. Our results supported that 15 min was sufficient for complete monomer consumption at the

conditions described above. Kanbara et al.[3, 4] reported that the rate constants involving the propagation $k_p$ of benzyl-(butadiene)$_n$- for an anionic telomerization of butadiene was about ten times as large as the $k_p$ for -(butadiene)$_n$-. The reaction kinetics observed for this study were consistent with these earlier reports.

### 3.4.3 Anionic Telomerization Reaction at a Constant 1,3-Butadiene Addition

An 80 g scale of 60% 1,2-polybutadiene synthesis in a 600 mL anionic reactor was performed using the following conditions. 1,3-Butadiene (123 mL, 80 g) was transferred to an *n*BuLi/TMEDA toluene solution via a cannula at a rate of 1.7 mL/min (E) and 2.2 mL/min (F). During the addition of 1,3-butadiene (75 min (E) and 55 min (F), respectively), the temperature remained at 45 – 50 ºC (E) and 66 – 69 ºC (F) due to the exothermic reaction. The $^1$H NMR spectrum of the liquid PB from the telomerization reaction (E) is shown in Figure 3.1. The microstructure and molecular weights of the obtained liquid PBs were analyzed using $^1$H NMR spectra and SEC, as described earlier (Table 1). The microstructures of the obtained liquid PBs using FT-IR spectroscopy are also tabulated in Table 3.1. Well-controlled 1,2-polybutadiene microstructures (64 – 65 mol%) and molecular weights (approximately 1000 g/mol) were achieved. The obtained cis-1,4 and trans-1,4 microstructures were consistent with the 5 g scale reaction (D), which indicated that a 1,3-butadiene telomerization in the moderate temperature range would result in the cis-1,4/trans-1,4 ratio, 40/60. The increase of $^1$H NMR resonance 5.7 – 5.9 ppm (-C*H*=$CH_2$ in vinyl cyclopentane) revealed the cyclic contents increased compared to the small scale synthesis ((C) and (D)) as described above. It should be noted that the low monomer concentration via the continuous addition of 1,3-butadiene may have accounted for the increase in vinyl cyclopentane in the present study, since it

had been previously shown to enhance the formation of vinyl cyclopentane.[5] SEC curves confirmed the monodisperse molecular weight distribution of the liquid PBs, indicative of rapid initiation relative to propagation. In addition, the occurrence of the narrow polydispersity index implied that a chain transfer reaction to the propagation chain end rarely occurred, regardless of whether the 1,3-butadiene monomer was added slowly (75 min) or more rapidly (55 min). Thus, a pseudo-living polymerization process was achieved during an 80 g scale involving the anionic telomerization of 1,3-butadiene at reaction temperatures of lower than 70 °C. In addition, the glass transition temperature ($T_g$) of liquid PBs (E) and (F) showed higher values than liquid PBs (A) and (B) from the conventional anionic polymerization. For example, $T_g$ of (F) was – 45 °C, whereas $T_g$ of (A) was – 63 °C. This was mainly due to the increase of the cyclic contents in the microstructure of (E) and (F).

### 3.4.4 End-group Analysis via MALDI-TOF Mass Spectrometry

MALDI-TOF MS is a powerful technique for determination of end groups and the absolute mass of polymers. For example, an anionically synthesized polystyrene was analyzed using MALDI-TOF MS and reported in the earlier literature.[10] As expected, each peak in the spectrum represented a different degree of polymerization. The peak-to-peak distance showed 104.15, reflecting the mass of a polystyrene repeating unit. The polystyrene mass was composed of *n* repeating units and the masses of the two end groups. The mass of two end groups were readily calculated by "mass from MALDI-TOF MS – $104.15 \times n$ – 108 (F.W. Ag)", giving 57.7 m/z. With the knowledge of initiation and termination of anionically polymerized styrene, this number leads to the identification of end groups i.e., a butyl group and a hydrogen atom.

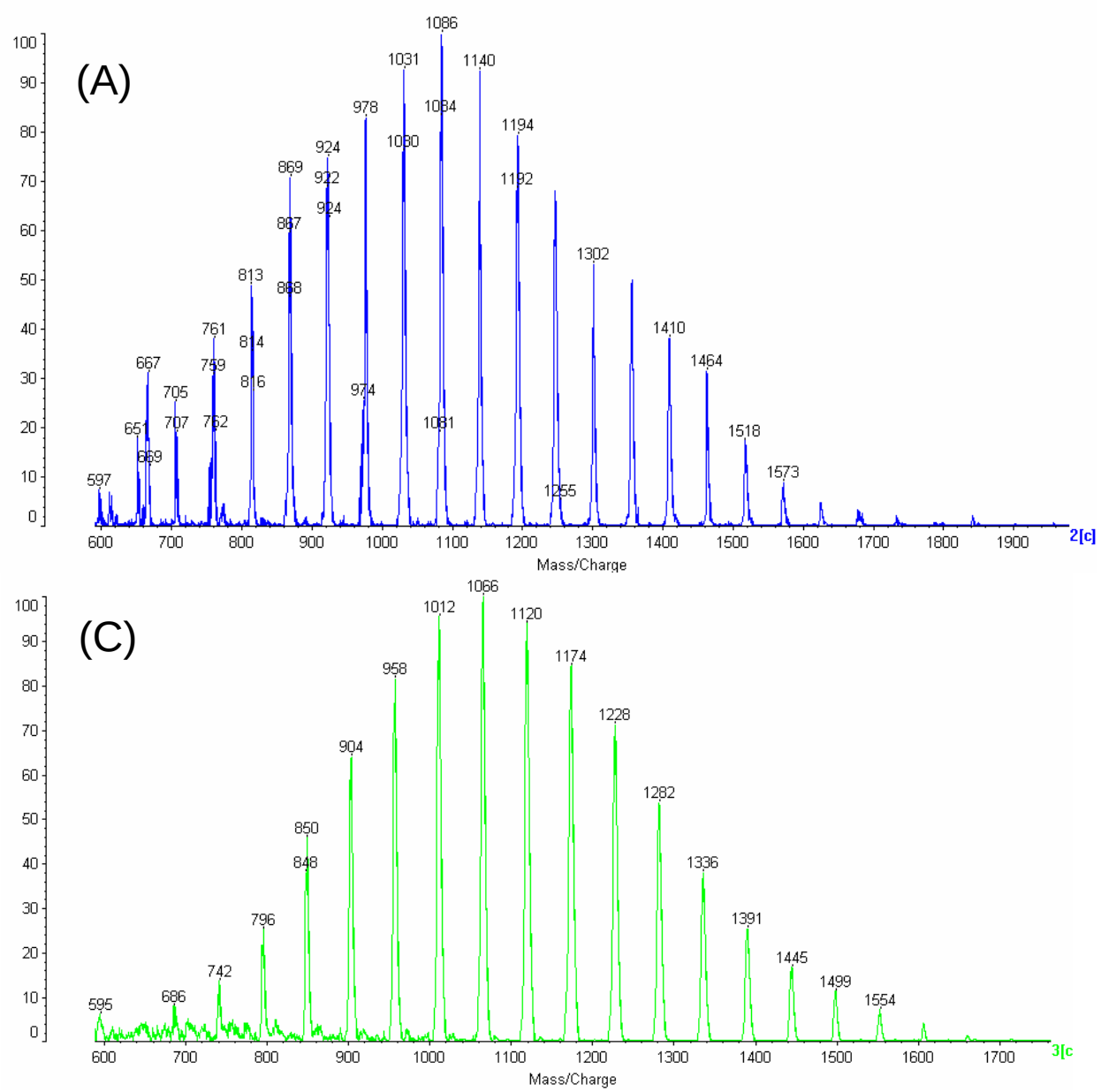


**Figure 3.2** MALDI-TOF spectra of 60 mol% 1,2-polybutadienes synthesized via living anionic polymerization (A) and anionic telomerization (C) MALDI-TOF MS condition: Kratos Kompact SEQ instrument, 337.1 nm nitrogen laser, AgTFA/dithranol

In a similar fashion to the above example for anionically synthesized polystyrene, MALDI-TOF MS was used for end group analysis of the synthesized liquid PB samples. The sample slide was treated with a solution of AgTFA in toluene followed by a solution

of dithranol matrix compound in chloroform. The representative MALDI-TOF spectra are shown in Figure 3.2. The peak-to-peak distance in the MALDI-TOF spectrum for the reaction (A) in Figure 3.2 (A) amounted to 54 m/z, reflecting the mass of polybutadiene repeating unit 54.09. The end group mass of liquid PB sample from the reaction (A) was calculated by 1086 m/z = 54.09 m/z × 17 (repeat units) + 108 (F.W. Ag) + 58 m/z (mass of end groups). The monomer, 1,3-butadiene, in the reaction (A) was initiated with *sec*BuLi and terminated with a proton from methanol. The formula weight of *sec*Bu + H, 58.12, corresponded well with the mass of end groups from MALDI-TOF MS, 58, indicating that the liquid PB from the reaction (A) possessed a *sec*-butyl end and a proton end. The MALDI-TOF MS for the liquid PB sample from the reaction (B) showed the same trend as reaction (A). The peak-to-peak distance in the MALDI-TOF spectrum for reaction (B) amounted to 54 m/z and the end group mass was determined to be 58 m/z. The determined end group mass, 58, was a good agreement with the formula weight of *n*Bu + H, 58.12. Considering that *n*BuLi initiated the reaction and a proton from methanol terminated the reaction, the end groups of liquid PB from the reaction (B) were confirmed to be a *n*-butyl group and a proton.

The MALDI-TOF spectrum for the liquid PB sample from reaction (C) is shown in Figure 3.2 (C). Each peak represents a 54 m/z difference (e.g. peaks at 1012, 1066, 1120 m/z in Figure 3.2 (C)), which corresponds to the repeat units of polybutadiene (54.09). Since dividing the peak by the repeat unit determines the mass of end groups, we verified that the end group mass of liquid PB samples from reactions (C), (D), (E) and (F) ranged from 91-93 m/z. For instance in reaction (C) in Figure 3.2 (C), the end group calculation showed 1066 m/z = 54.09 m/z × 16 (repeat units) + 108 (F.W. Ag) + 92 m/z

(mass of end groups). The end group mass determined in this study was consistent with the formula weight of benzyl + H, 92.14. These results indicated that all of the liquid PBs obtained via telomerization possessed one benzyl end and one proton end. End group analysis for telomerized polybutadiene using NMR spectroscopy was reported in the earlier literature,[32] however, we believe that this study is the first report to determine the polybutadiene telomer end groups as one benzyl end and one proton end using MALDI-TOF MS.

Results using MALDI-TOF MS demonstrated that stirring a *n*BuLi/TMEDA mixture in toluene quantitatively converted *n*BuLi initiator to benzyllithium anions. Moreover, the synthetic conditions associated with reaction (D) confirmed that (1) mixing *n*BuLi/TMEDA at 25 ºC for 10 min was sufficient to convert *n*BuLi to benzyllithium initiators, and (2) benzyllithium was sufficient to serve as an initiator as indicated by the narrow polydispersity indices. The presence of one benzyl end group in the synthesized PB samples was consistent with the agreement of $^{1}$H NMR molecular weights and SEC molecular weights.

## 3.5 Conclusions

The synthesis of low molecular weight PBs using different reaction conditions was performed. By maintaining both the initiation and reaction temperatures at lower than 70 °C, we were able to synthesize well-controlled molecular weight PBs displaying narrow polydispersity indices. Pseudo-living anionic telomerization has not been reported earlier due to the chain transfer characteristic of a telomer. However, this study demonstrated that lower reaction temperatures minimized chain transfer, thereby

enabling the polymerization to occur in a living fashion. The continuous addition of 1,3-butadiene was required to maintain the temperature lower than 70 °C in the large scale synthesis, which may have increased the formation of cyclic pentane rings. The end groups of liquid PB samples were determined via MALDI-TOF MS. This study verified that liquid PBs synthesized from anionic telomerization possessed one benzyl and one proton end group. Importantly, we also established that we could prepare a monodisperse, low molecular weight polybutadiene with one benzyl end. The attachment of a benzyl group to a telomer may alter various properties, including UV stability and subsequent reactivity. Subsequent chemical modifications will also be altered in comparison with the attachment of *sec*-butyl or *n*-butyl groups via conventional anionic polymerization. In summary, the synthesis and characterization of well-defined liquid polybutadienes will be important for many commercial applications involving microelectronics and coating applications.

## 3.6 Acknowledgements

The authors of this paper would like to thank the IBM Corporation for financial support of this research.

## 3.7 References

1. Hsieh, H. L.; Quirk, R. P., *Anionic Polymerization*. Marcel Dekker, Inc.: New York, Basel, Hong Kong, 1996.
2. Luxton, A. R., The preparation, modification and applications of nonfunctional liquid polybutadienes. *Rubber Chemistry and Technology* **1981,** 54, (3), 596-626.
3. Kume, S.; Akisawa, K.; Takahashi, A.; Nishikawa, G.; Hatano, M.; Kambara, S., Anionic telomerization of butadidne with aromatic hydrocarbons II. Solvents effects on rate constants. *Die Makromolekulare Chemie* **1965,** 34, 147-155.
4. Kume, S.; Takahashi, A.; Nishikawa, G.; Hatano, M.; Kambara, S., Anionic telomerization of butadidne with aromatic hydrocarbons. *Die Makromolekulare Chemie* **1965,** 34, 137-146.

5. Luxton, A. R.; Burrage, M. E.; Quack, G.; Fetters, L. J., Observations on the preparation of polybutadiene containing vinyl cyclopentane units. *Polymer* **1981,** 22, (3), 382-386.
6. Milner, R.; Young, R. N.; Luxton, A. R., Anionic telomerization of butadiene with toluene and diphenylmethane - Microstructure and molecular-weight. *Polymer* **1985,** 26, (8), 1265-1267.
7. Morton, M.; Fetters, L. J., *Rubber Chemistry and Technology* **1975,** 48, 359-409.
8. Gordon, B., III; Loftus, J. E., *Telomerization*. 1989; Vol. 16, p 533-54.
9. Montaudo, G.; Samperi, F.; Montaudo, M. S., Characterization of synthetic polymers by MALDI-MS. *Progress in Polymer Science* **2006,** 31, (3), 277-357.
10. Rader, H. J.; Schrepp, W., MALDI-TOF mass spectrometry in the analysis of synthetic polymers. *Acta Polymerica* **1998,** 49, (6), 272-293.
11. Pasch, H.; Schrepp, W., *MALDI-TOF mass spectrometry of synthetic polymers*. Springer-Verlag: Berlin, Heidelberg, New York, 2003.
12. Chang, C.; Lipian, J.; Barnes, D. A.; Seger, L.; Burns, C.; Bennett, B.; Bonney, L.; Rhodes, L. F.; Benedikt, G. M.; Lattimer, R.; Huang, S. S.; Day, V. W., The effect of end group modification on the transparency of vinyl addition norbornene polymers at 193 nm. *Macromolecular Chemistry and Physics* **2005,** 206, (19), 1988-2000.
13. Choi, J.; Kim, I. K.; Kwak, S. Y., Synthesis and characterization of a series of star-branched poly (epsilon-caprolactone)s with the variation in arm numbers and lengths. *Polymer* **2005,** 46, (23), 9725-9735.
14. Datta, H.; Bhowmick, A. K.; Singha, N. K., Tailor-made poly(ethyl acrylate) by atom transfer radical polymerization. *Journal of Polymer Science Part a-Polymer Chemistry* **2007,** 45, (9), 1661-1669.
15. Guttman, C. M.; Wetzel, S. J.; Flynn, K. M.; Fanconi, B. M.; VanderHart, D. L.; Wallace, W. E., Matrix-assisted laser desorption/ionization time-of-flight mass spectrometry interlaboratory comparison of mixtures of polystyrene with different end groups: Statistical analysis of mass fractions and mass moments. *Analytical Chemistry* **2005,** 77, (14), 4539-4548.
16. Ihara, E.; Omura, N.; Itoh, T.; Inoue, K., Anionic polymerization of methyl methacrylate and tert-butyl acrylate initiated with the YCl3/lithium amide/nBuLi systems. *Journal of Organometallic Chemistry* **2007,** 692, (1-3), 698-704.
17. Jeffries-El, M.; Sauve, G.; McCullough, R. D., Facile synthesis of end-functionalized regioregular poly(3-alkylthiophene)s via modified Grignard metathesis reaction. *Macromolecules* **2005,** 38, (25), 10346-10352.
18. Ji, H. N.; Farmer, B. S.; Nonidez, W. K.; Advincula, R. C.; Smith, G. D.; Kilbey, S. M.; Dadmun, M. D.; Mays, J. W., Anionic synthesis of epoxy end-capped polymers. *Macromolecular Chemistry and Physics* **2007,** 208, (8), 807-814.
19. Katayama, H.; Nagao, M.; Nishimura, T.; Matsui, Y.; Fukuse, Y.; Wakioka, M.; Ozawa, F., Stereocontrolled synthesis and characterization of cis-poly(arylenevinylene)s. *Macromolecules* **2006,** 39, (6), 2039-2048.
20. Kowalski, A.; Libiszowski, J.; Biela, T.; Cypryk, M.; Duda, A.; Penczek, S., Kinetics and mechanism of cyclic esters polymerization initiated with tin(II) octoate. Polymerization of epsilon-caprolactone and L,L-lactide co-initiated with primary amines. *Macromolecules* **2005,** 38, (20), 8170-8176.
21. Nagai, D.; Sato, M.; Ochiai, B.; Endo, T., Matrix-assisted laser desorption/ionization time-of-flight mass spectroscopic analysis of telechelic polythiourethanes obtained by the cationic ring-opening polymerization of six-membered cyclic thiourethane. *Journal of Polymer Science Part a-Polymer Chemistry* **2006,** 44, (14), 4281-4289.
22. Opsteen, J. A.; Van Hest, J. C. M., Modular synthesis of ABC type block copolymers by "click" chemistry. *Journal of Polymer Science Part a-Polymer Chemistry* **2007,** 45, (14), 2913-2924.
23. Ray, B.; Kotani, M.; Yamago, S., Highly controlled synthesis of poly(N-vinylpyrrolidone) and its block copolymers by organostibine-mediated living radical polymerization. *Macromolecules* **2006,** 39, (16), 5259-5265.
24. Elkins, C. L.; Viswanathan, K.; Long, T. E., Synthesis and characterization of star-shaped poly(ethylene-co-propylene) polymers bearing terminal self-complementary multiple hydrogen-bonding sites. *Macromolecules* **2006,** 39, (9), 3132-3139.

25. McGrath, J. E.; Wilkes, G. L.; Ward, T. C.; Broske, A. D.; Lee, B.; Yilgor, I.; Bradley, D. J.; Hoover, J. M.; Long, T. E., *New Elastomer Synthesis for High Performance Applications*. Noyes Data Corporation Parkridge, New Jersey, 1988; p 118.
26. Elgert, K.-F.; Quack, G.; Stutzel, B., *Polymer* **1975,** 16, 154-156.
27. Santee, E. R. J.; Malotky, L. O.; Morton, M., *Rubber Chemistry and Technology* **1973,** 46, 1156-1165.
28. Hampton, R. R., Infrared analysis of low temperature polymers. *Analytical Chemistry* **1949,** 21, (8), 923-926.
29. Bywater, S.; Worsfold, D. J.; Hollingworth, G., Structure of oligomeric polybutadienyllithium and polybutadiene. *Macromolecules* **1972,** 5, 389-393.
30. Quack, G.; Fetters, L. J., Nuclear magnetic-resonance characterization of a cyclic structure in anionically prepared polybutadiene. *Macromolecules* **1978,** 11, (2), 369-373.
31. Hay, J. N.; McCabe, J. F.; Robb, J. C., Kinetic of reaction of metal alkyls with alkens. *Faraday Trans* **1972,** 1, 1-9.
32. Proni, A.; Corno, C.; Roggero, A.; Santi, G.; Gandini, A., Anionic-polymerization of butadiene with organo-sodium soluble catalysts and structure of the resulting polymers. *Polymer* **1979,** 20, (1), 116-121.

# Chapter 4: Ureido Pyrimidone Functionalized Telechelic Hydrogenated Polyisoprenes Containing Ureido Pyrimidone Functionalized Carbon Nanotubes

Taken from:
Tomonori Saito, Akshay Kokil, Casey L. Elkins, Sharlene R. Williams, Renlong Gao, and Timothy E. Long, "Ureido Pyrimidone Functionalized Telechelic Hydrogenated Polyisoprenes Containing Ureido Pyrimidone Functionalized Carbon Nanotubes", *Chemistry of Materials*, manuscript in preparation

## 4.1 Abstract

Composites of telechelic 2-ureido-4[*1H*]-pyrimidone (UPy) quadruple hydrogen-bonding functionalized poly(ethylene-*co*-propylene) ($M_n$ = 19100 g/mol, $M_w/M_n$ = 1.27) with 5 wt% multiwalled carbon nanotubes (MWCNTs) or 5 wt% UPy-functionalized multiwall carbon nanotubes (UPy-MWCNTs) were prepared. Thermal and mechanical performances of the composites were characterized, and the presence of UPy sites and CNTs in the composites was further confirmed using thermogravimetric analysis. Association of UPy sites on the CNTs to UPy groups on the functionalized telechelic polymers affected the thermal degradation behavior. Addition of MWCNTs or UPy-MWCNTs to UPy-PEP-UPy polymer increased Young's modulus from 2.3 MPa to 3.6 MPa and increased tensile strength at break approximately 30% at room temperature. An increase in the rubbery plateau storage modulus at 25 ºC for both the MWCNT composites and UPy-MWCNT composites (4.5 – 4.7 MPa) in dynamic mechanical analysis relative to the matrix polymer (2.9 MPa) was consistent with tensile data. The matrix polymer elongated $243 \pm 12$%, whereas MWCNT and UPy-MWCNT composites elongated $75 \pm 3$% and $158 \pm 3$%, respectively. The lower decrease in elongation at break for the UPy-MWCNT composites compared to MWCNT composites was attributed to

the UPy-UPy association between the matrix polymer and UPy-MWCNTs. Complex viscosity as a function of temperature confirmed dissociation at similar temperatures to the matrix polymer upon addition of MWCNTs or UPy-MWCNTs, which indicated that the matrix UPy telechelic polymer was reinforced with MWCNTs or UPy-MWCNTs without sacrificing processability.

## 4.2 Introduction

Carbon nanotubes (CNTs) have attracted researcher's attention since Iijima's report on detail characteristic of CNTs in 1991.[1] CNTs possess remarkable mechanical and electrical properties.[2, 3] For example, Treacy et al.[4] measured the Young's modulus of individual CNTs to be 0.4 – 3.7 TPa. CNTs' unique properties stem from their special combination of high aspect ratio, structure, and topology.[5-7] Due to the unique properties and potentials of CNTs, many researchers have investigated CNTs as nano-scale reinforcing fillers to prepare polymer nanocomposites.[8-12]

Reinforcement of polymers with nano-scale fillers possesses several advantages, relative to conventional fillers with size scales on the order of several microns. Good dispersion of nano-scale fillers results in large interfacial areas between the nano-filler and matrix polymer, and the interface behavior significantly affects the resulting mechanical properties of the nanocomposites.[8, 13] CNTs as nano-fillers also are lighter in weight than conventional fillers such as silica particles, making CNTs an attractive candidate for polymer composite fillers.

The incorporation of CNTs in polymer matrices generally improves the moduli and ultimate strength of the matrix polymer. However, achievement of such mechanical

reinforcement generally requires a homogeneous dispersion of CNTs in matrices. CNTs have a propensity to bundle together due to their large surface areas and strong van der Waals interactions, and either high-shear mixing or ultrasonication is typically required to obtain good dispersion of CNTs in polymer composites. Chemical modification of CNTs also improves the CNT nano-dispersion. One of the common strategies to prepare functionalized CNTs is through an oxidation process with concentrated acid, resulting in carboxylic acid functionalities on CNTs. The carboxylic acid is readily reacted with various functional groups, making carboxylic acid functionalized CNTs versatile precursors for advanced materials.[14, 15] In fact, this work utilized this initial strategy for carboxylic acid functionalized CNTs as a reactive precursor for UPy introduction.

We have recently reported the synthesis of 2-ureido-4[*1H*]-pyrimidone (UPy) (self-complementary hydrogen bonding (SCMHB) units associating via quadruple hydrogen bonds) functionalized MWCNTs (UPy-MWCNTs),[16] which were subsequently functionalized starting from carboxylic acid functionalized MWCNTs. We reported composites with SCMHB random copolymers, (poly(2-ethylhexyl methacrylate-*co*-2-ureido-4[*1H*]-pyrimidone methacrylate), PEHMA-*co*-UPyMA).[17-19] Mechanical testing of PEHMA-*co*-UPyMA (5 mol% UPy copolymer and 1 mol % UPy copolymer) composites with 5 wt% UPy-functionalized MWCNTs (UPy-MWCNTs) was performed. The 5 mol% UPy-containing PEHMA-*co*-UPyMA composite showed significant enhancement of mechanical performance, whereas the 1 mol% UPy-containing PEHMA-*co*-UPyMA composite displayed mechanical properties similar to a viscous liquid. The enhanced mechanical performance was attributed to an increase in physical crosslinks in the UPy-MWCNT composites.

In this chapter, we selected telechelic UPy-functionalized poly(ethylene-*co*-propylene) (UPy-PEP-UPy) as a matrix polymer for nanocomposites. Telechelic UPy-functionalized polymers contained UPy groups at both termini, resulting in the formation of a supramolecular polymer (Figure 1). Telechelic UPy-functionalized polymers showed improved mechanical properties as an elastic film at room temperature and a low melt viscosity at elevated temperature.[20-23] UPy groups dissociate and the viscosity decreases typically at temperatures greater than 80 ºC, making the UPy-containing polymer melt processable.[21, 24-27] We dispersed pristine MWCNTs and the previously synthesized UPy-MWCNTs in UPy-PEP-UPy to form composites, i.e., UPy-PEP-UPy/MWCNTs and UPy-PEP-UPy/UPy-MWCNTs. Schematic depictions of UPy-PEP-UPy, UPy-PEP-UPy/MWCNTs, and UPy-PEP-UPy/UPy-MWCNTs composites are shown in Figure 4.1. We examined the thermal and mechanical properties of the composites, since association of UPy sites in the composites was propposed to alter the properties of UPy-PEP-UPy/UPy-CNTs composites.

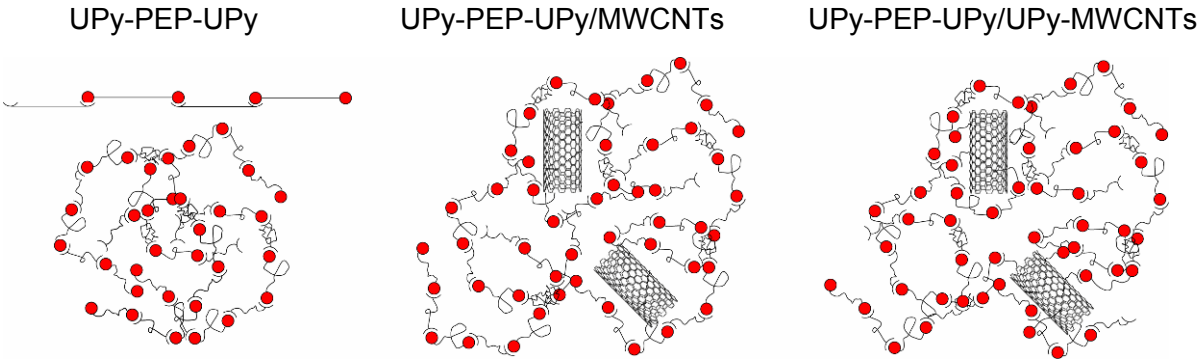


**Figure 4.1** Schematic images of UPy-PEP-UPy, UPy-PEP-UPy/MWCNTs, and UPy-PEP-UPy/UPy-MWCNTs composites

## 4.3 Experimental

### 4.3.1 Materials and Chemicals

Nickel 2-ethyl hexanoate (nickel octoate, Alfa Aesar), 1.0 M triethylaluminum in hexanes (TEA, Aldrich), citric acid (Aldrich, 98%), 3-(*tert*-butyldimethylsilyloxy)-1-propyllithium (TBDMSPrLi, FMC Corp. Lithium Division, 0.4 M in cyclohexane), ethylene oxide (Aldrich, 99.9%), dimethyl sulfoxide (DMSO, Aldrich, anhydrous), isophorone diisocyanate (IPDI, Aldrich, 98%), concentrated sulfuric acid (VWR International), concentrated nitric acid (VWR International), and deuterated chloroform ($CDCl_3$, Cambridge Isotope Laboratories) were used as received. Isoprene (Aldrich, 99%) and cyclohexane (EM Science, ACS grade) were passed through an alumina column and a molecular sieves column immediately prior to use. Tetrahydrofuran (THF, EM Science, HPLC grade) was distilled from sodium/benzophenone immediately prior to use. Dibutyl tin dilaurate (DBTDL) (Aldrich, 99%) was dissolved in THF as a 1 wt % solution. 6-Methylisocytosine (MIC, Aldrich, 98%) was dried at 100 °C under a reduced pressure overnight to remove moisture impurity. MWCNTs with outer diameters of 20 – 40 nm and lengths of 10 – 30 μm were purchased from Cheap Tubes Inc. (112 Merucry Drive, Brattleboro, VT 05301 USA) and were used as obtained.

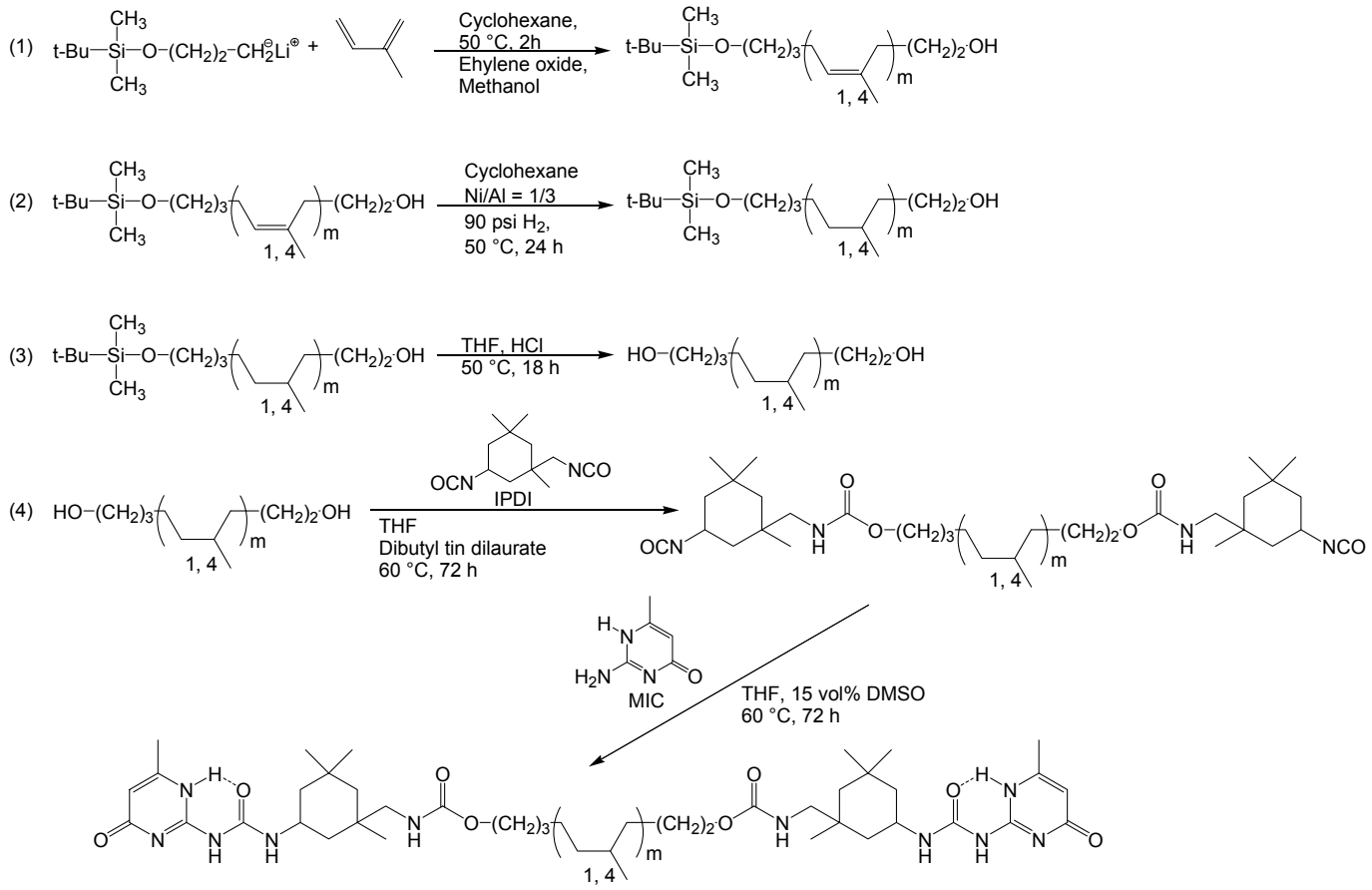


**Scheme 4.1** Synthesis of UPy functionalized telechelic poly(ethylene-*co*-propylene)
* Only the 1,4-microstructure is shown for simplicity, although the polymer product contained both 1,4- and 3,4-enchainment.

### 4.3.2 Synthesis of UPy-functionalized Telechelic Poly(ethylene-*co*-propylene)

Isoprene in a 600 mL reaction vessel with cyclohexane was initiated with TBDMSPrLi. After 2 h reaction, an excess of ethylene oxide was bubbled through the polymerization solution and nitrogen-degassed methanol was added to terminate the polymerization (Reaction (1) in Scheme 4.1). A polyisoprene polymer was dissolved in cyclohexane and a preformed nickel catalyst (nickel octoate/TEA (1/3) in cyclohexane solution) was added to a 600 mL reactor. The reactor was pressurized with hydrogen (90 psi) and heated to 50 °C for 24 h (Reaction (2) in Scheme 4.1). The nickel catalyst was

removed from the polymer solution with citric acid solution washes. Then, the poly(ethylene-*co*-propylene) was dissolved in THF, and deprotection of the primary hydroxyl chain ends was achieved using concentrated hydrochloric acid (Reaction (3) in Scheme 4.1). Lastly, the telechelic hydroxyl ends in poly(ethylene-*co*-propylene) were reacted with IPDI with DBTDL catalyst in THF at 60 ºC for 72 h. Then, MIC and 15 vol% of anhydrous DMSO were added and the reaction was allowed to proceed at 60 °C for 72 h (Reaction (4) in Scheme 4.1). The detailed synthetic procedures, results and discussion were reported in previous publication.[21]

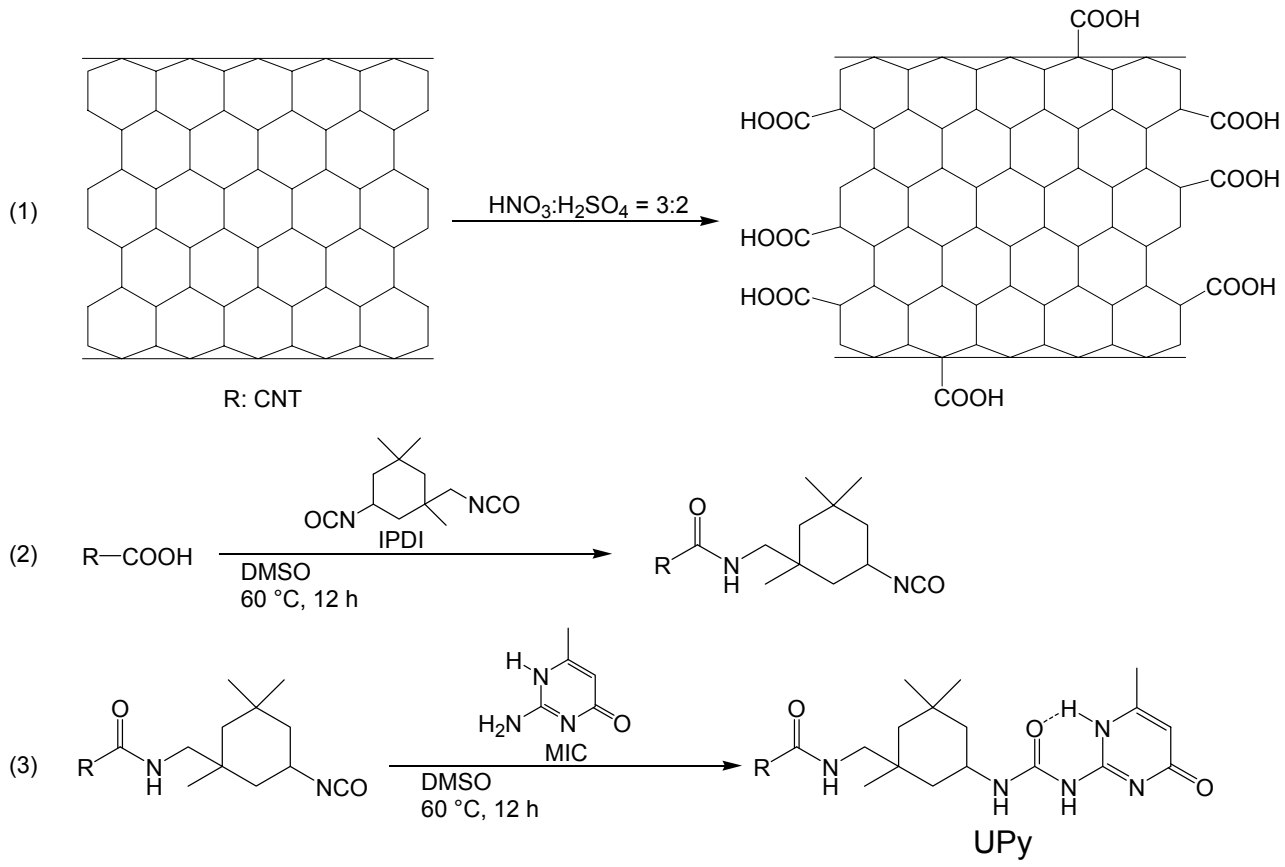


**Scheme 4.2** Synthesis of UPy functionalized MWCNTs

### 4.3.3 Synthesis of UPy-functionalized MWCNTs

The MWCNTs were first functionalized with carboxylic acid groups (Reaction (1) in Scheme 4.2). The MWCNTs in a round-bottomed flask with 3:2 mixture of

$HNO_3$:$H_2SO_4$ for 6 h were sonicated in VWR Ultrasonic Cleaners 50T (VWR International) at 38.5 – 40.5 kHz, 117V, 50W. The obtained carboxylic acid functionalized MWCNTs were subsequently washed with DI water until the eluent had a neutral pH. In the second step (Reaction (2) in Scheme 4.2), the carboxylic acid-functionalized MWCNTs were reacted with three-fold excess of IPDI in anhydrous DMSO at 60 °C for 12 h. The resulting MWCNTs were filtered and washed with toluene to remove any excess of IPDI. In the third step (Reaction (3) in Scheme 4.2), the isocyanate-functionalized MWCNTs were dispersed in anhydrous DMSO. Three-fold excess of MIC was added and the reaction was allowed to stir at 60°C for 6 h. The UPy-functionalized MWCNTs were filtered, washed with chloroform. The resulting cake was dried overnight under a reduced pressure at 25 ºC. The detail of synthetic procedures and results were described in another paper.[16]

### 4.3.4 Polymer Composites Preparation

Telechelic UPy-functionalized poly(ethylene-*co*-propylene) (UPy-PEP-UPy) (1.5 g) was dissolved in THF (45 mL) and the solution was allowed to sit for 24 h. THF (2 mL) was charged to each vial of three. Pristine MWCNTs (0.025 g, 5 wt % compared to a polymer content) and UPy-MWCNTs (0.025 g, 5 wt % compared to a polymer content), respectively, were charged into 2 mL of the THF-containing vials and were sonicated for 30 min at room temperature in in VWR Ultrasonic Cleaners 50T (VWR International) at 38.5 – 40.5 kHz, 117V, 50W. UPy-PEP-UPy solution (15 mL) was added to each vial. Each vial was sonicated for 30 min and then the contents of each vial were cast into Teflon™ molds under ambient conditions. The Teflon™ molds were covered with a glass cover and film formation occurred over 3 days. Each film was removed from the

Teflon™ mold and melt-pressed at 120 °C for 40 s using a PHI pneumatic press GS-21. The resulting films were approximately 0.4 mm thick.

### 4.3.5 Characterization

$^1$H NMR spectra of the polymers were collected in $CDCl_3$ with a Varian Unity spectrometer operating at 400 MHz at ambient temperature. Size exclusion chromatography (SEC) measurements were performed in THF at 40 °C at flow rate 1 mL/min using a Waters size exclusion chromatograph equipped with an autosampler, three in-line 5 μm PLgel Mixed-C columns, a Waters 410 refractive index (RI) detector operating at 880 nm, and a miniDAWN multiangle laser light scattering (MALLS) detector operating at 690 nm which was calibrated with narrow polydispersity polystyrene standards. The RI increment (d*n*/d*c*) was calculated online. All reported weight-average molecular weights are absolute molecular weights, which were obtained using the MALLS detector. Thermogravimetric analysis (TGA) measurements were performed on a TA Instruments Hi-Res TGA 2950 thermogravimetric analyzer under nitrogen at a heating rate of 3 °C/min or 10 °C/min. Glass transition temperatures were determined using a Perkin-Elmer Pyris 1 cryogenic differential scanning calorimeter (DSC) at a heating rate of 20 °C/min under nitrogen, which was calibrated using indium (mp = 156.60 °C) and zinc (mp = 419.47 °C). Glass transition temperatures are reported as the transition midpoints of the heat capacity change during the second heating cycle. Complex viscosities of the UPy-PEP-UPy, UPy-PEP-UPy/MWCNTs composite, and UPy-PEP-UPy/UPy-MWCNTs composite were measured using TA Instruments AR G2 rheometer. A 25 mm parallel plate geometry was used, and rheological analysis was performed at a 5% strain amplitude at 1 Hz with a 1000 μm gap. Dynamic mechanical

analysis (DMA) was performed with a TA Instruments Q800 dynamic mechanical analyzer in tension mode at 15 μm amplitude and at a frequency of 1 Hz with a heating rate of 3 °C/min. Stress-strain experiments were performed using dogbone-shaped film samples ($n$ = 4) cut using a die according to ASTM D3368. The tensile tests were performed under ambient conditions on a 5500R Instron universal testing machine at a crosshead displacement rate of 10 mm/min. Stress-strain profiles were recorded and analyzed using Bluehill 2 software. Pneumatic grips were used, and no slippage was observed.

**Table 4.1** Molecular weight and its molecular weight distribution of the telechelic polyisoprene and degree of UPy functionalization

| Precursor polymer $M_n$ ($M_w/M_n$)[a] | UPy-functionalized polymer $M_n$ ($M_w/M_n$)[a] | % End-capping[b] | UPy-groups (mol/g} |
|---|---|---|---|
| 24300 (1.08) | 19100 (1.27) | 100 | $1.05 \times 10^{-4}$ |

[a] Determined using SEC at 40 °C in THF with a MALLS detector
[b] $^1$H NMR conditions; Varian Unity 400 MHz, $CDCl_3$

## 4.4 Results and Discussion

### 4.4.1 Preparation of Self-Complementary Multiple Hydrogen-Bonding Containing Polymer Composites

The synthetic scheme of UPy-functionalized telechelic poly(ethylene-*co*-propylene) is shown in Scheme 4.1. Synthesis of well-defined linear telechelic polyisoprene via living anionic polymerization was accomplished with a protected hydroxyl functional initiator, TBDMSPrLi (Reaction (1) in Scheme 4.1). The microstructure of polyisoprene resulted in approximately 92% 1,4-enchainment and 8% 3,4-enchainment. Subsequently, quantitative hydrogenation of polyisoprene blocks (Reaction (2) in Scheme 4.1), quantitative deprotection of the hydroxyl group (Reaction

(3) in Scheme 4.1), and quantitative UPy-functionalization (Reaction (4) in Scheme 4.1) were successfully achieved.[21] The molecular weight and degree of UPy-functionalization are summarized in Table 4.1. Quantitative conversion of telechelic ends to UPy groups led to the formation of a supramolecular polymer, which was evidently shown as the transformation from a liquid-like sample to a ductile film at room temperature.

A three step reaction strategy was employed for UPy-functionalization of MWCNTs.[28] The synthetic scheme of UPy-functionalized MWCNTs is shown in Scheme 4.2. The first step of the reaction was the oxidation of MWCNTs in a concentrated acid mixture (Reaction (1) in Scheme 4.2). The degree of functionalization for the oxidized CNTs was determined as $7.3 \times 10^{-4}$ mol/g. The second step involved isocyanate functionalization of the oxidized MWCNTs (Reaction (2) in Scheme 4.2). In the third step of the reaction, the isocyanate groups on the CNTs reacted with MIC to produce UPy functionalized MWCNTs as the final product (Reaction (3) in Scheme 4.2). TGA measurement estimated the degree of functionalization for the UPy-MWCNTs as $6.1 \times 10^{-4}$ mol/g. SEM and TEM performed on the UPy-MWCNTs demonstrated no significant structural degradation (Figure 4.2).[28]

UPy-PEP-UPy, UPy-PEP-UPy/MWCNTs, and UPy-PEP-UPy/UPy-MWCNTs composite films were prepared from solution-casting and subsequent melt pressing at 120 °C. Uniform and elastic films were obtained. MWCNTs and UPy-MWCNTs (5 wt%) were dispersed in UPy-PEP-UPy/MWCNTs and UPy-PEP-UPy/UPy-MWCNTs, respectively. The molar ratio of UPy groups on polymers to UPy groups on UPy-MWCNTs was readily calculated to be 3/1 based on wt% of the components and the degree of UPy-functionalization in UPy-PEP-UPy (Table 4.1) and UPy-MWCNTs. This

ratio implied both association between UPy sites on polymers and UPy sites on UPy-MWCNTs.

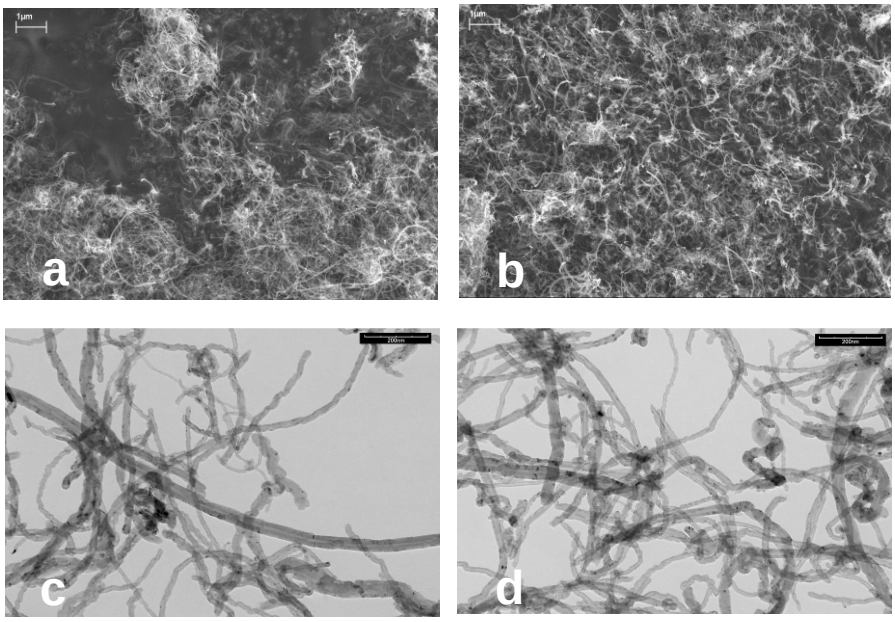


**Figure 4.2** SEM (top) and TEM (bottom) images of pristine MWCNT (a, c) and UPy-MWCNTs (b, d)

### 4.4.2 Thermal Stability of UPy-functionalized Polymer Composites

Thermal stability of UPy-PEP-UPy, UPy-PEP-UPy/MWCNTs, and UPy-PEP-UPy/UPy-MWCNTs composite films were evaluated using TGA at heating rate of 10 °C/min under nitrogen (Figure 4.3). The weight loss at 280 °C, the residue at 550 °C, and the derivative TGA curve peak ($T_{max}$) are reported in Table 4.2. In UPy-containing polymers, the initial degradation step from 200 ºC corresponds to the elimination of the UPy groups upon reversal of the urethane linkage and the initial weight loss of polymer is consistent with weight fraction of the UPy groups in the polymer composition.[10, 11] TGA curves in Figure 4.3 exhibited an onset of decomposition around 200 ºC and initial thermal degradation up to approximately 280 ºC. The measured weight loss of UPy-PEP-UPy at 280 °C, 4.6 wt% in Table 4.2, corresponds to approximate wt% of UPy groups in

the polymer, which is 4 wt%. The weight loss of UPy-PEP-UPy/MWCNTs at 280 °C showed less than those of UPy-PEP-UPy due to the addition of 5 wt% MWCNTs into the polymer. The weight losses of UPy-PEP-UPy/UPy-MWCNTs at 280 °C were 5.4 wt%, as shown in Table 4.2. The trend of these weight losses was consistent with the amount of UPy groups in the composite films. The residual weight at 550 °C also supported the components of these composite films. Most of UPy-PEP-UPy polymers were degraded at 550 °C whereas MWCNTs are thermally stable at 550 °C. CNTs were the main components of the residue in UPy-PEP-UPy/MWCNTs and UPy-PEP-UPy/UPy-MWCNTs at 550 °C. Due to 5 wt% addition of MWCNTs or UPy-MWCNTs, the residual weight of UPy-PEP-UPy/MWCNTs and UPy-PEP-UPy/UPy-MWCNTs was 4 – 9 wt%. UPy-PEP-UPy/MWCNTs gave higher residue than UPy-PEP-UPy/UPy-MWCNTs due to lack of UPy groups on MWCNTs.

Different thermal degradation behavior between UPy-PEP-UPy/MWCNTs and UPy-PEP-UPy/UPy-MWCNTs were reflected in TGA curves and $T_{max}$ values. Thermal degradation behavior of UPy-PEP-UPy/UPy-MWCNTs was similar to that of UPy-PEP-UPy, whereas the thermal degradation curve of UPy-PEP-UPy/MWCNTs shifted toward higher temperatures. Significant delay in weight loss for polymer degradation by addition of MWCNTs to polymers has been reported in earlier literatures.[5, 29, 30] This delay of polymer thermal degradation was attributed to a barrier labyrinth effect of fillers in nanocomposites, which slowed down the diffusion of degradation products from the bulk of the polymer to the gas phase.[30] This effect contributed to the larger values of $T_{max}$ in UPy-PEP-UPy/MWCNTs. However, polymer degradation in UPy-PEP-UPy/UPy-MWCNTs did not show significant degradation delay. Little thermal

degradation delay in UPy-PEP-UPy/UPy-MWCNTs was attributed to the interaction between UPy-PEP-UPy and UPy-MWCNTs. Although UPy groups decomposed in the range of 200 – 300 °C, the association between UPy-PEP-UPy and UPy-MWCNTs presumably affected the dispersion of MWCNTs and altered the barrier labyrinth effect of fillers.

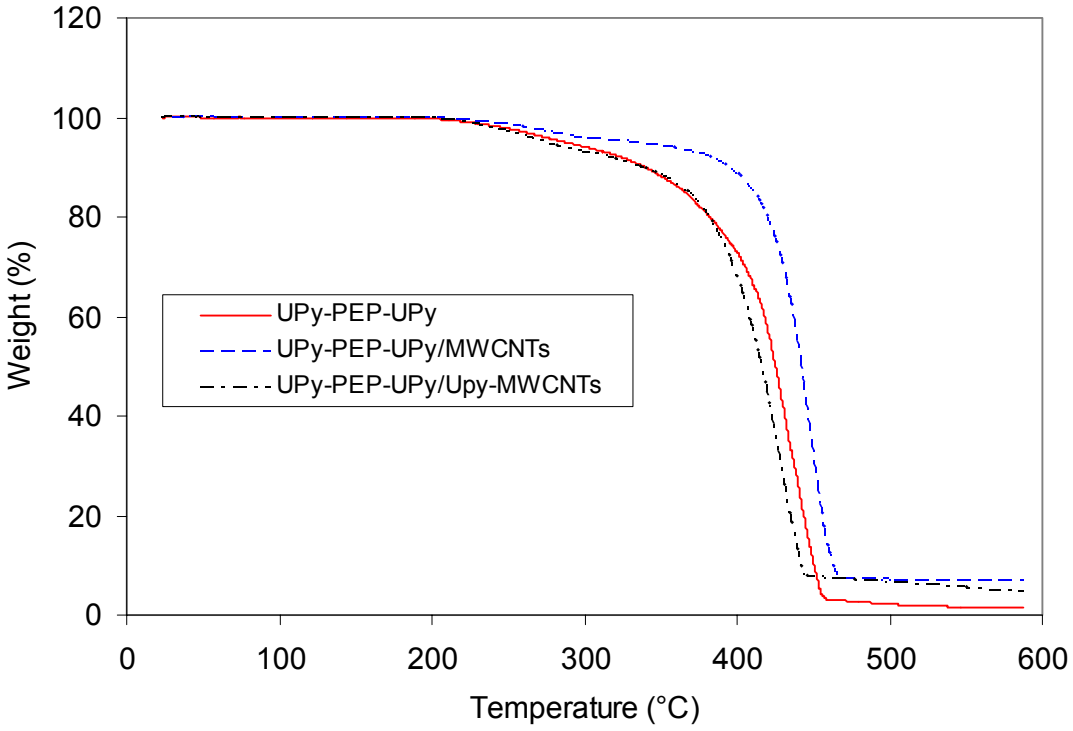


**Figure 4.3** Thermal degradation on UPy-PEP-UPy, UPy-PEP-UPy/MWCNTs, and UPy-PEP-UPy/UPy-MWCNTs composite films under nitrogen flow at 10 °C/min

**Table 4.2** Thermogravimetric Analysis on UPy-PEP-UPy, UPy-PEP-UPy/MWCNTs, and UPy-PEP-UPy/UPy-MWCNTs Composite Films under Nitrogen Flow at 10 °C/min

| | Weight loss at 280 °C (wt %) | Residue at 550 °C (wt %) | $T_{max}$(°C) |
|---|---|---|---|
| UPy-PEP-UPy | 4.6 ± 1.2 | 2.0 ± 0.4 | 432.2 ± 1.1 |
| UPy-PEP-UPy/MWCNTs | 3.5 ± 0.4 | 8.3 ± 1.3 | 445.6 ± 3.6 |
| UPy-PEP-UPy/UPy-MWCNTs | 5.4 ± 0.2 | 4.8 ± 0.7 | 429.9 ± 2.9 |

### 4.4.3 Mechanical Performance of UPy-containing Polymer Composites

Mechanical performance of UPy-PEP-UPy, UPy-PEP-UPy/MWCNTs, and UPy-PEP-UPy/UPy-MWCNTs composite films were studied using tensile testing and DMA. Stress-strain profiles for UPy-PEP-UPy, UPy-PEP-UPy/MWCNTs, and UPy-PEP-UPy/UPy-MWCNTs are shown in Figure 4.4, and the resulting data are summarized in Table 4.3. The addition of MWCNTs or UPy-MWCNTs to UPy-PEP-UPy polymer increased Young's modulus from 2.3 MPa to 3.6 MPa and increased tensile strength at break approximately 30%. The increase of Young's modulus and tensile strength with a MWCNT addition to the polymer matrix has been reported and our results were consistent with previous literature.[9, 31-35]

Tensile strain of the composites showed significantly different results. UPy-PEP-UPy elongated 243 ± 12% whereas UPy-PEP-UPy/MWCNTs and UPy-PEP-UPy/UPy-MWCNTs elongated 75 ± 3% and 158 ± 3%, respectively. The macromolecular architecture of UPy-PEP-UPy was a supramolecular linear polymer connected with UPy groups (Figure 4.1). The supramolecular linear architecture provided the resulting elongation at break 243 ± 12%. However, the addition of CNTs in UPy-PEP-UPy/MWCNTs resulted in the decreased elongation at break (75 ± 3%). Brittleness of CNT fillers decreased the tensile elongation, which was consistent with other nanocomposite works.[9, 31, 33] The elongation at break in UPy-PEP-UPy/UPy-MWCNTs (158 ± 3%) was higher than UPy-PEP-UPy/MWCNTs. This was attributed to the UPy-UPy association occurrence between UPy-PEP-UPy and UPy-MWCNTs. As described in the above discussion, the ratio of UPy groups on UPy-MWCNTs to UPy groups on UPy-PEP-UPy was 1/3, and some degree of UPy-UPy association between UPy-PEP-

UPy and UPy-MWCNTs was expected to occur, which resulted in higher elongation than that of UPy-PEP-UPy/MWCNTs. UPy-MWCNTs served as crosslinkers between UPy-PEP-UPy. Unlike previous work,[28] UPy-PEP-UPy/UPy-MWCNTs did not show a higher storage modulus than UPy-PEP-UPy/MWCNTs, but rather showed higher elongation. This is due to the functionality of the polymer matrix, where UPy-PEP-UPy possesses only two UPy groups per chain.

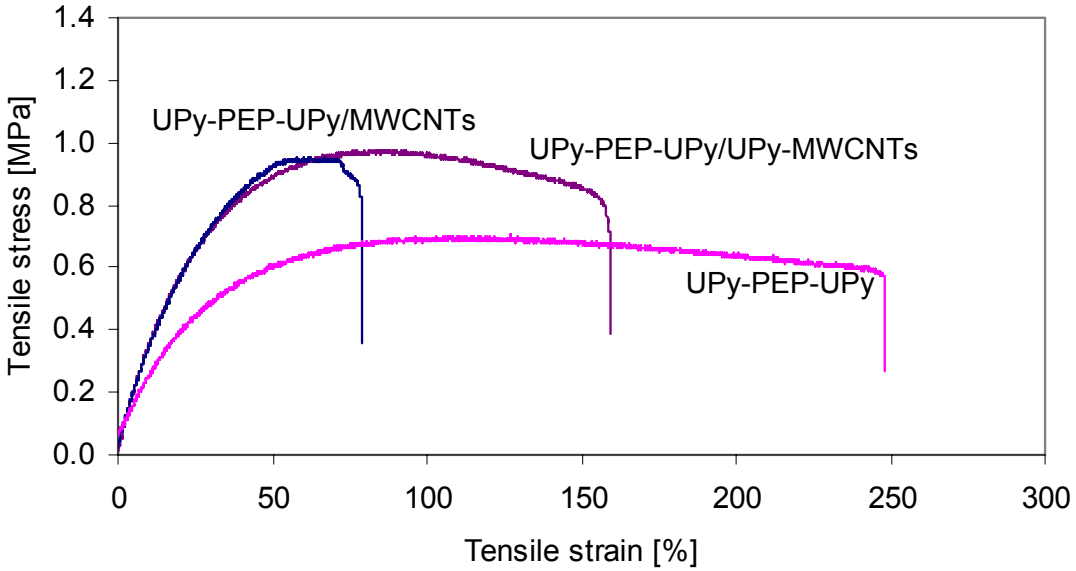


**Figure 4.4** Stress-strain experiments of UPy-PEP-UPy, UPy-PEP-UPy/MWCNTs, and UPy-PEP-UPy/UPy-MWCNTs composite films Tensile test condition: 5500R Instron universal testing machine at a crosshead displacement rate of 10 mm/min

**Table 4.3** Summary of tensile data for UPy-PEP-UPy, UPy-PEP-UPy/MWCNTs, and UPy-PEP-UPy/UPy-MWCNTs Composite

| | Tensile stress at break (MPa) | Tensile strain at break (%) | Young's Modulus (MPa) |
|---|---|---|---|
| UPy-PEP-UPy | $0.573 \pm 0.011$ | $243 \pm 12$ | $2.28 \pm 0.22$ |
| UPy-PEP-UPy/MWCNTs | $0.745 \pm 0.069$ | $75 \pm 3$ | $3.58 \pm 0.07$ |
| UPy-PEP-UPy/UPy-MWCNTs | $0.725 \pm 0.027$ | $158 \pm 3$ | $3.62 \pm 0.31$ |

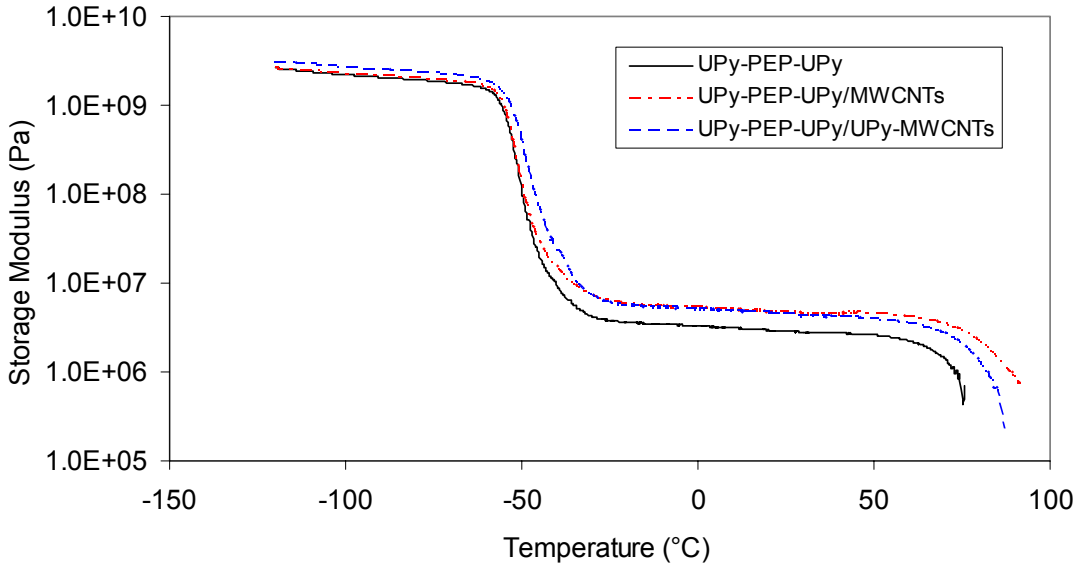


**Figure 4.5** Dynamic mechanical analysis of UPy-PEP-UPy, UPy-PEP-UPy/MWCNTs, and UPy-PEP-UPy/UPy-MWCNTs composite films DMA condition: tension mode at 15 μm amplitude at a frequency of 1 Hz at a heating rate of 3 °C/min

**Table 4.4** Transition temperatures and rubbery-plateau for UPy-PEP-UPy, UPy-PEP-UPy/MWCNTs, and UPy-PEP-UPy/UPy-MWCNTs composite films

| | $T_g$ (°C) | $T_{flow}$ (°C) | Modulus at Rubbery-Plateau (Storage Modulus at 25 °C) (MPa) |
|---|---|---|---|
| UPy-PEP-UPy | -54 | 69 | 2.9 |
| UPy-PEP-UPy/MWCNTs | -54 | 77 | 4.7 |
| UPy-PEP-UPy/UPy-MWCNTs | -52 | 76 | 4.5 |

*$T_{flow}$: flow temperature

DMA curves of UPy-PEP-UPy, UPy-PEP-UPy/MWCNTs, and UPy-PEP-UPy/UPy-MWCNTs composite films are shown in Figure 4.5 and the resulting data are summarized in Table 4.4. The glass transition temperature ($T_g$) was determined using the loss modulus curves. $T_g$ values of the composite films ranged -52 to -54 °C, which was consistent with the DSC measured $T_g$ of UPy-PEP-UPy (- 62 °C). UPy-PEP-UPy/MWCNTs, and UPy-PEP-UPy/UPy-MWCNTs composite films exhibited a slightly longer rubbery plateau compared to UPy-PEP-UPy rubbery plateau due to the increase of

the flow temperature ($T_{flow}$). The increased modulus of MWCNTs or UPy-MWCNTs reinforcement resulted in requiring more thermal energy for the composites to flow. The obtained flow temperatures agreed well with the dissociation temperature of multiple hydrogen-bonding, which was reported earlier.[21, 24, 26, 27] The rubbery plateau storage modulus at 25 °C of UPy-PEP-UPy/MWCNTs and UPy-PEP-UPy/UPy-MWCNTs (4.5 – 4.7 MPa) significantly increased compared to UPy-PEP-UPy (~ 2.9 MPa), which was consistent with the above results from tensile testing. With the results obtained from mechanical analysis of the composite films, one can conclude that the modulus of samples increased by the addition of fillers (CNTs), and the elongation of the samples depended on the interactions of UPy groups. UPy-UPy association between UPy-PEP-UPy and UPy-MWCNTs prevented the decrease of the elongation.

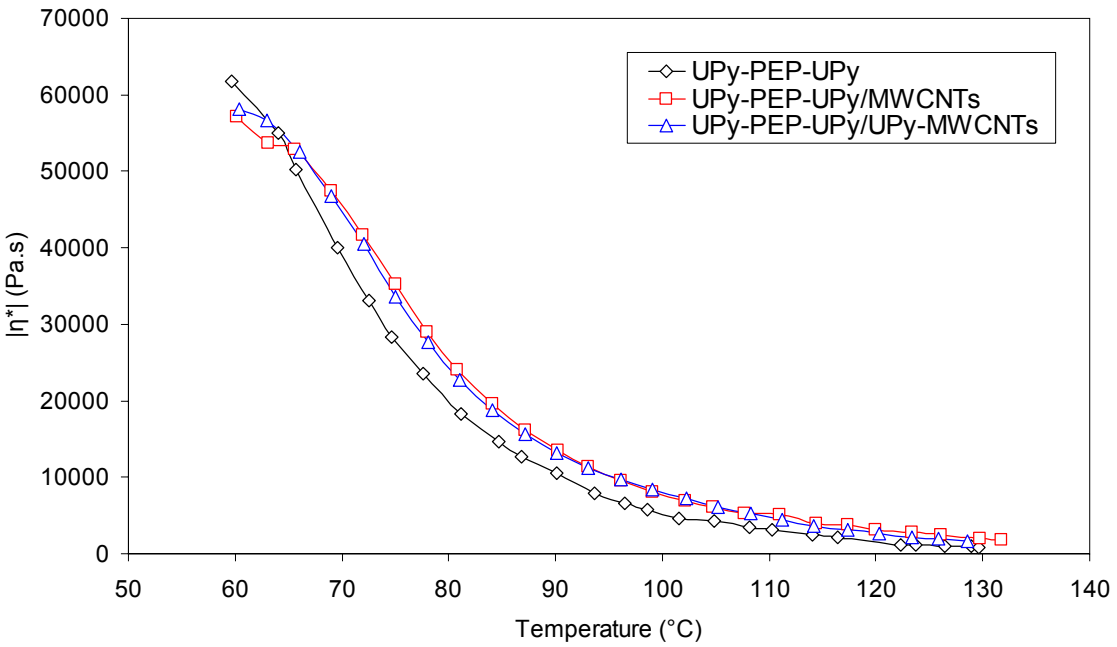


**Figure 4.6** Dependence of complex viscosity on temperature for UPy-PEP-UPy, UPy-PEP-UPy/MWCNTs, and UPy-PEP-UPy/UPy-MWCNTs composite films
ARG2 rheometer condition: 1 mm parallel plate at 5% strain amplitude at 1 Hz

### 4.4.3 Melt Rheological Characterization

Melt rheological characterization of UPy-PEP-UPy, UPy-PEP-UPy/MWCNTs, and UPy-PEP-UPy/UPy-MWCNTs composite films was performed and viscosity vs. temperature profiles of the composites are shown in Figure 4.6. UPy-PEP-UPy/MWCNTs, and UPy-PEP-UPy/UPy-MWCNTs composite films exhibited a slightly higher viscosity than UPy-PEP-UPy. The addition of MWCNTs resulted in the slight increase of viscosity due to the increased modulus. On the other hand, little change of viscosity by addition of MWCNTs or UPy-MWCNTs revealed good processability of these composites at similar processing temperature to UPy-PEP-UPy. Reinforced or modified polymers often result in the increase of melt viscosity, which make the polymer difficult to melt process.[36] Maintaining processability is crucial for composite materials. The reinforced UPy-PEP-UPy composites with CNTs and UPy-MWCNTs were prepared without sacrificing the processability.

## 4.5 Conclusions

Telechelic UPy functionalized poly(ethylene-*co*-propylene) (UPy-PEP-UPy) and composites with CNTs (UPy-PEP-UPy/MWCNTs) and UPy-MWCNTs (UPy-PEP-UPy/UPy-MWCNTs) were prepared. Thermal and mechanical performance of the composites was evaluated. In TGA measurements, the initial degradations gave a good agreement with the amount of incorporated UPy groups in each composite, and the residues were consistent with the CNT content in the polymer composites. Derivative weight loss, $T_{max}$ indicated thermal degradation delayed by addition of MWCNTs to polymer in UPy-PEP-UPy/MWCNTs. This was due to a barrier labyrinth effect of fillers,

which slowed down the diffusion of degradation products from the bulk of the polymer to the gas phase. However, UPy-PEP-UPy/UPy-MWCNTs did not show significant thermal degradation delay. This was presumably due to good dispersion of UPy-MWCNTs through association of UPy groups on UPy-MWCNTs to UPy groups on a polymer.

The addition of MWCNTs to polymer increased the modulus of composites in tensile testing and DMA. However, no significant difference appeared in modulus between CNT filler composite and UPy-MWCNT filler composite. When a polymer contains abundant UPy groups, they act as physical crosslinks and enhance the mechanical rigidity.[16] UPy-PEP-UPy possesses only two UPy groups on each end, not enough for significant crosslinking to occur. On the other hand, the effect of UPy functionalization to MWCNTs altered the elongation of the composite. The elongation of UPy-PEP-UPy/UPy-MWCNTs sample in tensile testing resulted in a higher value than that of UPy-PEP-UPy/MWCNTs. The interactions of UPy groups between UPy-PEP-UPy and UPy-MWCNTs prevented the decrease of elongation at break, whereas pristine MWCNTs resulted in significant decrease of elongation at break. Melt rheological experiment confirmed addition of MWCNTs or UPy-MWCNTs to UPy-PEP-UPy did not change melt viscosity compared to UPy-PEP-UPy, indicating that UPy-PEP-UPy was reinforced with MWCNTs or UPy-MWCNTs without sacrificing the processability. This work showed the association between UPy groups on MWCNTs and UPy groups on polymer termini had significant influence to the subsequent properties.

## 4.6 References


1. Iijima, S., Helical Microtubules of Graphitic Carbon. *Nature* **1991,** 354, (6348), 56-58.
2. Ishikawa, H.; Fudetani, S.; Hirohashi, M., Mechanical properties of thin films measured by nanoindenters. *Applied Surface Science* **2001,** 178, (1-4), 56-62.

3. Kracke, B.; Damaschke, B., Measurement of nanohardness and nanoelasticity of thin gold films with scanning force microscope. *Applied Physics Letters* **2000,** 77, (3), 361-363.
4. Treacy, M. M. J.; Ebbesen, T. W.; Gibson, J. M., Exceptionally high Young's modulus observed for individual carbon nanotubes. *Nature* **1996,** 381, (6584), 678-680.
5. Peeterbroeck, S.; Laoutid, F.; Taulemesse, J. M.; Monteverde, T.; Lopez-Cuesta, J. M.; Nagy, J. B.; Alexandre, M.; Dubois, P., Mechanical properties and flame-retardant behavior of ethylene vinyl acetate/high-density polyethylene coated carbon nanotube nanocomposites. *Advanced Functional Materials* **2007,** 17, (15), 2787-2791.
6. Popov, V. N., Carbon nanotubes: properties and application. *Materials Science & Engineering R-Reports* **2004,** 43, (3), 61-102.
7. Tasis, D.; Tagmatarchis, N.; Bianco, A.; Prato, M., Chemistry of carbon nanotubes. *Chemical Reviews* **2006,** 106, (3), 1105-1136.
8. Bal, S.; Samal, S. S., Carbon nanotube reinforced polymer composites - A state of the art. *Bulletin of Materials Science* **2007,** 30, (4), 379-386.
9. Bokobza, L., Multiwall carbon nanotube elastomeric composites: A review. *Polymer* **2007,** 48, (17), 4907-4920.
10. Coleman, J. N.; Khan, U.; Blau, W. J.; Gun'ko, Y. K., Small but strong: A review of the mechanical properties of carbon nanotube-polymer composites. *Carbon* **2006,** 44, (9), 1624-1652.
11. Coleman, J. N.; Khan, U.; Gun'ko, Y. K., Mechanical reinforcement of polymers using carbon nanotubes. *Advanced Materials* **2006,** 18, (6), 689-706.
12. Moniruzzaman, M.; Winey, K. I., Polymer nanocomposites containing carbon nanotubes. *Macromolecules* **2006,** 39, (16), 5194-5205.
13. Tan, H.; Jiang, L. Y.; Huang, Y.; Liu, B.; Hwang, K. C., The effect of van der Waals-based interface cohesive law on carbon nanotube-reinforced composite materials. *Composites Science and Technology* **2007,** 67, (14), 2941-2946.
14. Lin, Y.; Meziani, M. J.; Sun, Y.-P., Functionalized carbon nanotubes for polymeric nanocomposites. *Journal of Materials Chemistry* **2007,** 17, (12), 1143-1148.
15. Xie, X.-L.; Mai, Y.-W.; Zhou, X.-P., Dispersion and alignment of carbon nanotubes in polymer matrix: A review. *Materials Science & Engineering, R: Reports* **2005,** R49, (4), 89-112.
16. Kokil, A.; Saito, T.; DePolo, W.; Elkins, C. L.; Wilkes, G. L.; Long, T. E., Multiple hydrogen bonding functionalized carbon nanotubes and their composites. *Chemistry of Materials* **2008,** in progress.
17. Beijer, F. H.; Kooijman, H.; Spek, A. L.; Sijbesma, R. P.; Meijer, E. W., Self-complementarity achieved through quadruple hydrogen bonding. *Angewandte Chemie-International Edition* **1998,** 37, (1-2), 75-78.
18. Beijer, F. H.; Sijbesma, R. P.; Kooijman, H.; Spek, A. L.; Meijer, E. W., Strong dimerization of ureidopyrimidones via quadruple hydrogen bonding. *Journal of the American Chemical Society* **1998,** 120, (27), 6761-6769.
19. Sijbesma, R. P.; Beijer, F. H.; Brunsveld, L.; Folmer, B. J. B.; Hirschberg, J.; Lange, R. F. M.; Lowe, J. K. L.; Meijer, E. W., Reversible polymers formed from self-complementary monomers using quadruple hydrogen bonding. *Science* **1997,** 278, (5343), 1601-1604.
20. Dankers, P. Y. W.; Zhang, Z.; Wisse, E.; Grijpma, D. W.; Sijbesma, R. P.; Feijen, J.; Meijer, E. W., Oligo(trimethylene carbonate)-based supramolecular biomaterials. *Macromolecules* **2006,** 39, (25), 8763-8771.
21. Elkins, C. L.; Viswanathan, K.; Long, T. E., Synthesis and characterization of star-shaped poly(ethylene-co-propylene) polymers bearing terminal self-complementary multiple hydrogen-bonding sites. *Macromolecules* **2006,** 39, (9), 3132-3139.
22. Folmer, B. J. B.; Sijbesma, R. P.; Versteegen, R. M.; van der Rijt, J. A. J.; Meijer, E. W., Supramolecular polymer materials: Chain extension of telechelic polymers using a reactive hydrogen-bonding synthon. *Advanced Materials* **2000,** 12, (12), 874-878.
23. Kautz, H.; van Beek, D. J. M.; Sijbesma, R. P.; Meijer, E. W., Cooperative end-to-end and lateral hydrogen-bonding motifs in supramolecular thermoplastic elastomers. *Macromolecules* **2006,** 39, (13), 4265-4267.
24. Elkins, C. L.; Park, T.; McKee, M. G.; Long, T. E., Synthesis and characterization of poly(2-ethylhexyl methacrylate) copolymers containing pendant, self-complementary multiple-hydrogen-bonding sites. *Journal of Polymer Science Part a-Polymer Chemistry* **2005,** 43, (19), 4618-4631.

25. McKee, M. G.; Elkins, C. L.; Park, T.; Long, T. E., Influence of random branching on multiple hydrogen bonding in poly(alkyl methacrylate)s. *Macromolecules* **2005,** 38, (14), 6015-6023.
26. Yamauchi, K.; Lizotte, J. R.; Hercules, D. M.; Vergne, M. J.; Long, T. E., Combinations of microphase separation and terminal multiple hydrogen bonding in novel macromolecules. *Journal of the American Chemical Society* **2002,** 124, (29), 8599-8604.
27. Yamauchi, K.; Lizotte, J. R.; Long, T. E., Thermoreversible poly(alkyl acrylates) consisting of self-complementary multiple hydrogen bonding. *Macromolecules* **2003,** 36, (4), 1083-1088.
28. Kokil, A.; Saito, T.; DePolo, W.; Elkins, C. L.; Wilkes, G. L.; Long, T. E., Multiple hydrogen bonding functionalized carbon nanotubes and their composites. *Materials of Chemistry* **2008,** Submitted.
29. Bocchini, S.; Frache, A.; Camino, G.; Claes, M., Polyethylene thermal oxidative stabilisation in carbon nanotubes based nanocomposites. *European Polymer Journal* **2007,** 43, (8), 3222-3235.
30. Kashiwagi, T.; Grulke, E.; Hilding, J.; Harris, R.; Awad, W.; Douglas, J., Thermal degradation and flammability properties of poly(propylene)/carbon nanotube composites. *Macromolecular Rapid Communications* **2002,** 23, (13), 761-765.
31. Deng, F.; Ogasawara, T.; Takeda, N., Tensile properties at different temperature and observation of micro deformation of carbon nanotubes-poly(ether ether ketone) composites. *Composites Science and Technology* **2007,** 67, (14), 2959-2964.
32. Knauert, S. T.; Douglas, J. F.; Starr, F. W., The effect of nanoparticle shape on polymer-nanocomposite rheology and tensile strength. *Journal of Polymer Science Part B-Polymer Physics* **2007,** 45, (14), 1882-1897.
33. Ryan, K. P.; Cadek, M.; Nicolosi, V.; Blond, D.; Ruether, M.; Armstrong, G.; Swan, H.; Fonseca, A.; Nagy, J. B.; Maser, W. K.; Blau, W. J.; Coleman, J. N., Carbon nanotubes for reinforcement of plastics? A case study with poly(vinyl alcohol). *Composites Science and Technology* **2007,** 67, (7-8), 1640-1649.
34. Wang, Z.; Ciselli, P.; Peijs, T., The extraordinary reinforcing efficiency of single-walled carbon nanotubes in oriented poly(vinyl alcohol) tapes. *Nanotechnology* **2007,** 18, (45).
35. Xiong, J. W.; Zheng, Z.; Qin, X. M.; Li, M.; Li, H. Q.; Wang, X. L., The thermal and mechanical properties of a polyurethane/multi-walled carbon nanotube composite. *Carbon* **2006,** 44, (13), 2701-2707.
36. Zhou, X.; Zhu, Y.; Liang, J., Effects of the vulcanizing reagent addition on the properties of CNTs/SBR powder composites. *Journal of Applied Polymer Science* **2007,** 106, (3), 1836-1841.

# Chapter 5: Self-Complementary Multiple Hydrogen Bonding in Styrene-Butadiene Rubber

## 5.1 Abstract

The chemical modification of rubbers alters their properties and produces new polymeric materials. This report describes the modification of styrene-butadiene rubbers (SBRs) and their subsequent characterization. SBRs were first reacted with 3-chloroperoxybenzoic acid (MCPBA) to epoxidize the butadiene repeat units. These epoxidized butadiene repeat units were subsequently reduced with lithium aluminum hydride ($LiAlH_4$) to give the hydroxyl-functionalized SBR (SBR-OH). The SBR-OH was reacted with 2-ureido-4[*1H*]-pyrimidone (UPy) containing monoisocyanate (IPDI-MIC), consisting of self-complementary multiple hydrogen bonding (SCMHB). The UPy contents in UPy-SBRs were controlled to 1 - 3 mol%. Initial weight loss as determined by TGA was consistent with the weight fraction of the incorporated UPy groups in UPy-SBRs. Introducing SCMHB to SBRs drastically changed the physical properties of these materials. Specifically, the SCMHB networks served as mechanically effective crosslinks, which raised $T_g$ and enhanced the mechanical performance of the SBRs.

## 5.2 Introduction

Scientists have known for many years that chemically modifying rubbers can result in new polymeric materials with attractive mechanical properties. Because of the high reactivity of the double bond in polyisoprene or polybutadiene repeat units, various functional groups can be added to the rubbery backbone. Among the various options for chemically modifying rubbers, introducing hydrogen bonding groups to the rubber repeat

unit is known to be an effective strategy for producing thermoplastic elastomers. Hydrogen-bonding serves as physical crosslinks whereas vulcanized rubbers result in having covalent crosslinks. The physical crosslinks reinforce the low $T_g$ backbone, thereby producing a thermoplastic elastomer. One of the advantages of a thermoplastic elastomer as compared to a thermoset crosslinked rubber is that it can be processed at elevated temperatures.

In the 1980s and 90s, Stadler et al. reported the introduction of hydrogen bonding groups to polyisoprenes, polybutadienes and styrene butadiene rubbers to form thermoreversible elastomers.[1-15] Their synthetic strategy involved the rapid ene reaction of 4-pheny-3,5-dioxo-1,2,4-triazoline (PTD) with allylic systems. The PTD reaction achieved quantitative conversion at room temperature, which resulted in a controlled degree of incorporation of phenylurazole groups (1-polydienyl-4-phenyl-3,5-dioxo-1,2,4-triazolidine) (PU) or similar analogues into polydienes. The PTD reaction followed pseudo-first order kinetics, with the 1,4 repeat unit in the polydienes reacting faster than the analogous 1,2 repeat unit. They investigated the synthetic strategy, mechanical performance, and hydrogen-bonding interaction mechanisms for PU-functionalized rubber.

Abetz et al. described thermoreversible crosslinking rubber comprising sulfonyl urethane groups.[16] Their reaction strategy followed a three-step reaction. The first step involved the epoxidation of the polybutadiene repeat unit. In second step, the epoxides were hydrochlorinated with hydrochloric acid to produce hydroxyl functionalized polybutadienes. In third step, the hydroxyl groups were reacted with sulfonyl isocyanate to form sulfonyl urethane groups on the polybutadiene backbone. $^1$H NMR demonstrated

quantitative modification of the sulfonyl urethane groups. However, even though Abetz et al. verified the crosslinking behavior via dynamic mechanical analysis (DMA), they could not provide any evidence for the thermoreversibility of the sulfonyl urethane polybutadienes.

The epoxidation reaction strategy typically used to modify polybutadienes is both simple and versatile. Starting with the epoxidation of SBR (styrene-butadiene rubber), we modified SBR with 2-ureido-4-[*1H*]-pyrimidone (UPy) quadruple hydrogen-bonding groups, which is shown in Figure 5.1. The strong association of the self-complementary multiple hydrogen bonding (SCMHB) acts as a physical crosslinking mechanism, which results in a supramolecular elastic polymer. Stadler's work introduced urea linkages into polydiene backbones, and Abetz's work incorporated urethane linkages to polybutadiene backbones. Unfortunately, the two techniques are not interchangeable. However, in comparison studies involving polyureas and polyurethanes, a number of researchers have shown that the use of bidentate urea linkages was superior to the use of monodentate urethane linkages in improving the properties of these materials.[17-22] Thus, when one considers the increase in hydrogen-bonding interactions, the use of UPy quadruple hydrogen bonding groups is expected to significantly impact physical crosslinking behaviors in SBR. Indeed, previous work has shown that introducing UPy groups to polymer end-groups or polymer repeat units dramatically alters mechanical, rheological, and thermal properties.[23-29] Moreover, the use of self-complementary multiple hydrogen bonding (SCMHB) units in polymers was also shown to form thermoreversible aggregates, which typically dissociate at 80-95 °C.

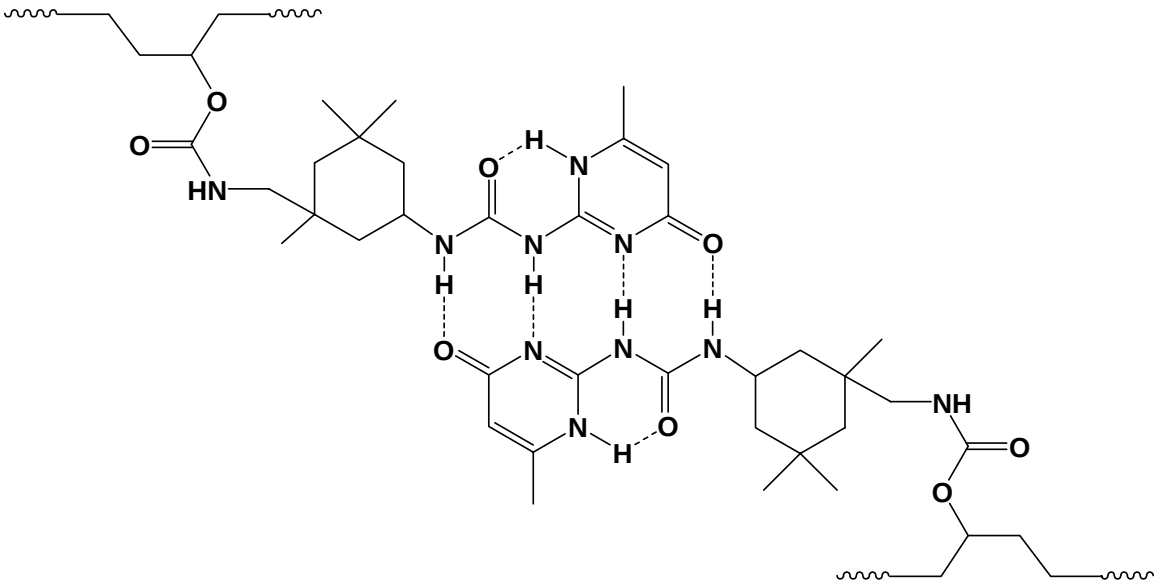


**Figure 5.1** Schematic representation of self-complementary multiple hydrogen bonding associations in SBRs

We have developed a synthetic methodology for preparing novel UPy-containing SBRs. The first step involves the epoxidation of the 1,4 repeat unit in a polybutadiene. As described above, the epoxidation is a straightforward process (unlike the hydroboration of 1,2 repeat unit)[30] to introduce hydroxyl groups. The epoxides on the polybutadiene are subsequently reduced with lithium aluminum hydride ($LiAlH_4$) to convert to hydroxyl groups, which are then reacted with novel synthesized UPy isocyanate. Thermal and mechanical analyses of the obtained UPy-functionalized SBRs were conducted in order to determine the influence of SCMHB on resulting properties. In addition, reinforcement studies of the synthesized UPy-functionalized SBRs and UPy-functionalized CNTs, described in Chapter 4, were conducted and a schematic image is shown in Figure 5.2. The filler-matrix interactions due to SCMHB were expected to enhance mechanical performance.

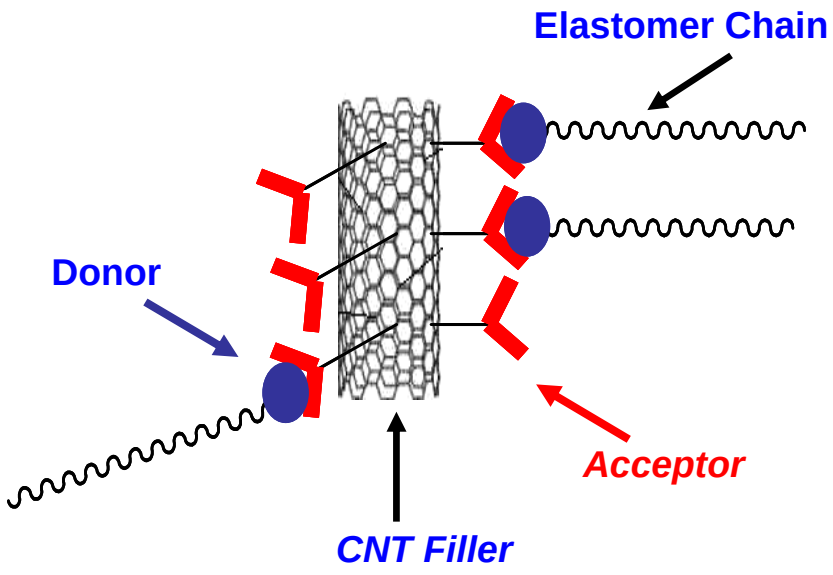


**Figure 5.2** General schematic of complementary hydrogen bonding interactions between the elastomeric matrix and the filler particle

## 5.3 Experimental

### 5.3.1 Materials and Chemicals

Low vinyl SBR (styrene-butadiene rubber) was provided by the Goodyear Tire & Rubber Company and the composition was verified using $^{1}$H NMR and size exclusion chromatography (SEC). The low vinyl SBR was soluble in chloroform ($CHCl_3$), tetrahydrofuran (THF), NMP, hexanes, and toluene. $^{1}$H NMR spectroscopy (Figure 4.1) revealed that the composition of the low vinyl SBR was polystyrene (PS) : 1,4-polybutadiene (1,4-PB) : 1,2-polybutadiene (1,2-PB) = 0.083 : 0.809 : 0.108 (molar ratio). SEC analysis for the same SBR (PS : PB wt fraction of 0.149 : 0.851) indicated $M_n$ 133,000, $M_w$ 221,000, and PDI of 1.66. 3-chloroperoxybenzoic acid (MCPBA, 70-75% Across Chemicals), potassium carbonate (EM Science), 1.0 M lithium aluminum hydride ($LiAlH_4$) solution in THF (Aldrich), isophorone diisocyanate (IPDI, 98%,

Aldrich), 6-methylisocytosine (MIC, 98%, Aldrich), dibutyl tin dilaurate (DBTDL, 95%, Aldrich), chloroform ($CHCl_3$, Fisher Scientific), dimethyl sulfoxide (DMSO, anhydrous, 99.9+%, Aldrich), and methanol (Fisher Scientific) were used as received. Tetrahydrofuran (THF, Fisher Scientific) was passed through PURE SOLV MD-3 SOLVENT PURIFICATION SYSTEM (Innovative Technology Inc.) immediately prior to use. $^1$H NMR for low vinyl SBR (400 MHz, $CDCl_3$, δ): 1.0 – 1.8 ppm (br, -C*H*$_2$CH- in 1,2-polybutadiene and polystyrene), 1.9 – 2.2 ppm (br, -C*H*$_2$- in 1,4-polybutadiene, -CH$_2$C*H*- in 1,2-polybutadiene and polystyrene), 2.3 – 2.7 ppm (br, -C*H*$_2$CH$_2$C$_6$H$_5$, -C*H*$_2$C$_6$H$_5$), 4.7 – 5.1 ppm (br, -CH=C*H*$_2$ in 1,2-polybutadiene and vinyl cyclopentane), 5.1 – 5.5 ppm (br, -C*H*=C*H*- in 1,4-polybutadiene), 5.5 – 5.7 ppm (br, -C*H*=CH$_2$ in 1,2-polybutadiene), 6.4 – 7.3 ppm (br, aromatic protons in polystyrene)

### 5.3.2 Synthesis of Epoxidized SBR (SBR-E)

An epoxidation reaction of the SBR was performed following literature procedures (Reaction 1 in Scheme 5.1).[16, 31] For this study, a 2.0 mol% modification of the SBR is described as a typical example. SBR (160 g, 2.517 mol of butadiene repeating unit) was first dissolved in 4 L $CHCl_3$ in a 4 L beaker with a magnetic stirrer. A solution of 11.5 g of MCPBA (0.050 mol) in 100 mL $CHCl_3$ was added at once to the SBR solution at 0 ºC. The reaction mixture was then stirred at 0 ºC for 3 h. Water (200 mL) was subsequently added with potassium carbonate and stirred for 1 h. The water was exchanged twice to remove salts. Finally, the water was removed and the polymer was precipitated into methanol/water mixture. The polymer was re-dissolved in either $CHCl_3$ or THF and the precipitation was repeated at least three times to remove salts. The isolated polymer was dried at room temperature under reduced pressure for 3 days. $^1$H

NMR (400 MHz, $CDCl_3$, δ): 1.0 – 1.8 ppm (br, -C*H*$_2$CH- in 1,2-polybutadiene, polystyrene and next to epoxy ring), 1.9 – 2.2 ppm (br, -C*H*$_2$- in 1,4-polybutadiene, -$CH_2$C*H*- in 1,2-polybutadiene and polystyrene), 2.3 – 2.6 ppm (br, -C*H*$_2$$CH_2C_6H_5$, -C*H*$_2$$C_6H_5$), 2.6 – 3.0 ppm (br, -C*H*$_2$OC*H*$_2$-), 4.7 – 5.1 ppm (br, -CH=C*H*$_2$ in 1,2-polybutadiene and vinyl cyclopentane), 5.1 – 5.5 ppm (br, -C*H*=C*H*- in 1,4-polybutadiene), 5.5 – 5.7 ppm (br, -C*H*=$CH_2$ in 1,2-polybutadiene), 6.4 – 7.3 ppm (br, aromatic protons in polystyrene)

### 5.3.3 Synthesis of Hydroxyl-functionalized SBR (SBR-OH)

A reduction of epoxides in SBR-E was performed (Reaction 2 in Scheme 5.1). SBR-E (55.5 g, 0.021 mol epoxide) was dissolved in 1800 mL THF in a 2L one-neck round-bottomed flask equipped with a magnetic stirrer under nitrogen ($N_2$). 1M $LiAlH_4$ solution (42 mL, 0.042 mol $LiAlH_4$) was then added drop-wise to 0 ºC SBR-E solution using a syringe. The reaction mixture was slowly warmed to room temperature. In 2-3 h after the addition of the 1M $LiAlH_4$ solution, the reaction mixture formed a gel, indicating that the lithium alkoxide intermediate had linked the SBR-Es. The reaction gel remained under nitrogen for 5 days to ensure a quantitative reduction. Water (10 mL) was then added slowly over a period of 1 day. The addition of water disrupted the gel and resulted in a homogeneous solution. The polymer was isolated by precipitation into a methanol/water mixture, re-dissolved in $CHCl_3$, washed over water, and re-precipitated into a methanol/water mixture. This separation step was repeated several times to remove the lithium and aluminum salts. The isolated polymer was dried at room temperature under reduced pressure for 3 days. $^1$H NMR (400 MHz, $CDCl_3$, δ): 1.0 – 1.8 ppm (br, -C*H*$_2$CH-, in 1,2-polybutadiene, polystyrene, and hydroxyl unit), 1.9 – 2.2 ppm

(br, -C*H*$_2$- in 1,4-polybutadiene, -CH$_2$C*H*- in 1,2-polybutadiene and polystyrene), 2.3 – 2.6 ppm (br, -C*H*$_2$CH$_2$C$_6$H$_5$, -C*H*$_2$C$_6$H$_5$), 3.4 – 3.6 ppm (br, -C*H*$_2$OH), 4.7 – 5.1 ppm (br, -CH=C*H*$_2$ in 1,2-polybutadiene and vinyl cyclopentane), 5.1 – 5.5 ppm (br, -C*H*=C*H*- in 1,4-polybutadiene), 5.5 – 5.7 ppm (br, -C*H*=CH$_2$ in 1,2-polybutadiene), 6.4 – 7.3 ppm (br, aromatic protons in polystyrene)

### 5.3.4 Synthesis of UPy Isocyanate (MIC- IPDI and MIC-HDI)

The reaction of MIC with IPDI (Reaction 3 in Scheme 5.1) was performed using modifed literature procedures.[23] MIC (25.6 g, 0.205 mol) was reacted with a 3-fold excess of IPDI (130 mL, 0.614 mol) at 100 ºC for 24 h in a bulk condition under $N_2$. The product was precipitated in heptane, washed with heptane, and filtered. The filtered product was re-dissolved in $CHCl_3$ and the precipitation step was repeated. The isolated compound was dried at 80 ºC under reduced pressure for 20 h. The reaction of MIC with HDI (Reaction (3') in Scheme 4.1) was also attempted following literature procedures.[23, 28] MIC (12.4 g, 99.17 mmol) was reacted with a 6-fold excess of HDI (100 g, 595 mmol) at 100 ºC for 24 h in a bulk condition. The product was precipitated in *n*-hexanes and washed with *n*-hexanes several times, filtered, and dried under reduced pressure at 80 ºC (yield: 99 %). $^1$H NMR for MIC-IPDI (400 MHz, $CDCl_3$, δ): 13.2 ppm (m, 1H, -N*H*C(CH$_3$)=), 11.9 ppm (m, 1H, -N*H*CONHCH$_2$-), 10.1 ppm (m, 1H, -NHCON*H*CH$_2$-), 5.9 ppm (s, 1H, -C*H*=C(CH$_3$)), 3.9 ppm (br, 1H, >C*H*NH- CONH-), 3.6 ppm (br, 1H, >C*H*NCO), 3.0 ppm (s, 2H, -NHCONHC*H*$_2$-, -C*H*NCO), 2.2 ppm (s, 3H, -NHC(C*H*$_3$)=CH-CO-), 1.3-2.0 ppm (m, 6H, >C(CH$_3$)C*H*$_2$C(CH$_3$)$_2$-, -CH(NCO)C*H*$_2$C(CH$_3$)$_2$-, -CH(NH)C*H*$_2$C(CH$_3$)$_2$-, >C(CH$_3$)C*H*$_2$CH(NH)-, >C(CH$_3$)C*H*$_2$CH(NCO)-), 1.0 ppm (m, 9H, –C(C*H*$_3$)$_2$-, >C(C*H*$_3$)CH$_2$(NCO),

>C(C*H*$_3$)CH$_2$NH-). MIC-IPDI was soluble in chloroform and DMSO. $^1$H NMR for MIC-HDI (400 MHz, $CDCl_3$, δ): 13.2 ppm (s, 1H, -N*H*C(CH$_3$)=), 11.8 ppm (s, 1H, -N*H*CONHCH$_2$-), 10.5 ppm (s, 1H, -NHCON*H*CH$_2$-), 5.8 ppm (s, 1H, -C*H*=C(CH$_3$)), 3.3ppm (s, 4H, -NHCONHC*H*$_2$-, -C*H*$_2$NCO), 2.2 ppm (s, 3H, -NHC(C*H*$_3$)=CHCO-), 1.3-1.7 ppm (s, 8H, -(C*H*$_2$)$_4$-). MIC-HDI was partially soluble in chloroform and DMSO.

### 5.3.5 Synthesis of UPy-SBR

The introduction of UPy groups to SBRs was conducted through the reaction of SBR-OH with IPDI-MIC (Reaction 4 in Scheme 5.1). SBR-OH (49 g, (0.019 mol hydroxyl)) was first dissolved in 1 L $CHCl_3$ in a 2 L one-neck round-bottomed flask equipped with a magnetic stirrer. Nitrogen gas was bubbled through the SBR-OH solution for 20 min and 110 mL anhydrous DMSO was added. Then, 2 mL of DBTDL and MIC-IPDI (25.7 g, 0.074 mol) were added. The reaction was allowed to stir at 60 °C for 72 h. The polymer was precipitated into methanol. The polymer was re-dissolved in THF and precipitated into methanol. The isolated polymer was dried at room temperature under reduced pressure for 3 days. $^1$H NMR (400 MHz, $CDCl_3$, δ): 0.8 – 1.1 ppm (br, –C(C*H*$_3$)$_2$-, >C(C*H*$_3$)CH$_2$(NCO), >C(C*H*$_3$)CH$_2$-NH-), 1.0 – 1.8 ppm (br, -C*H*$_2$-, in 1,2-polybutadiene, polystyrene, and hydroxyl unit), 1.9 – 2.2 ppm (br, -C*H*$_2$- in 1,4-polybutadiene, >C*H*- in 1,2-polybutadiene and polystyrene), 2.3 – 2.6 ppm (br, -C*H*$_2$CH$_2$C$_6$H$_5$, -C*H*$_2$C$_6$H$_5$), 4.7 – 5.1 ppm (br, -CH=C*H*$_2$ in 1,2-polybutadiene and vinyl cyclopentane), 5.1 – 5.5 ppm (br, -C*H*=C*H*- in 1,4-polybutadiene), 5.5 – 5.7 ppm (br, -C*H*=CH$_2$ in 1,2-polybutadiene), 6.4 – 7.3 ppm (br, aromatic protons in polystyrene).

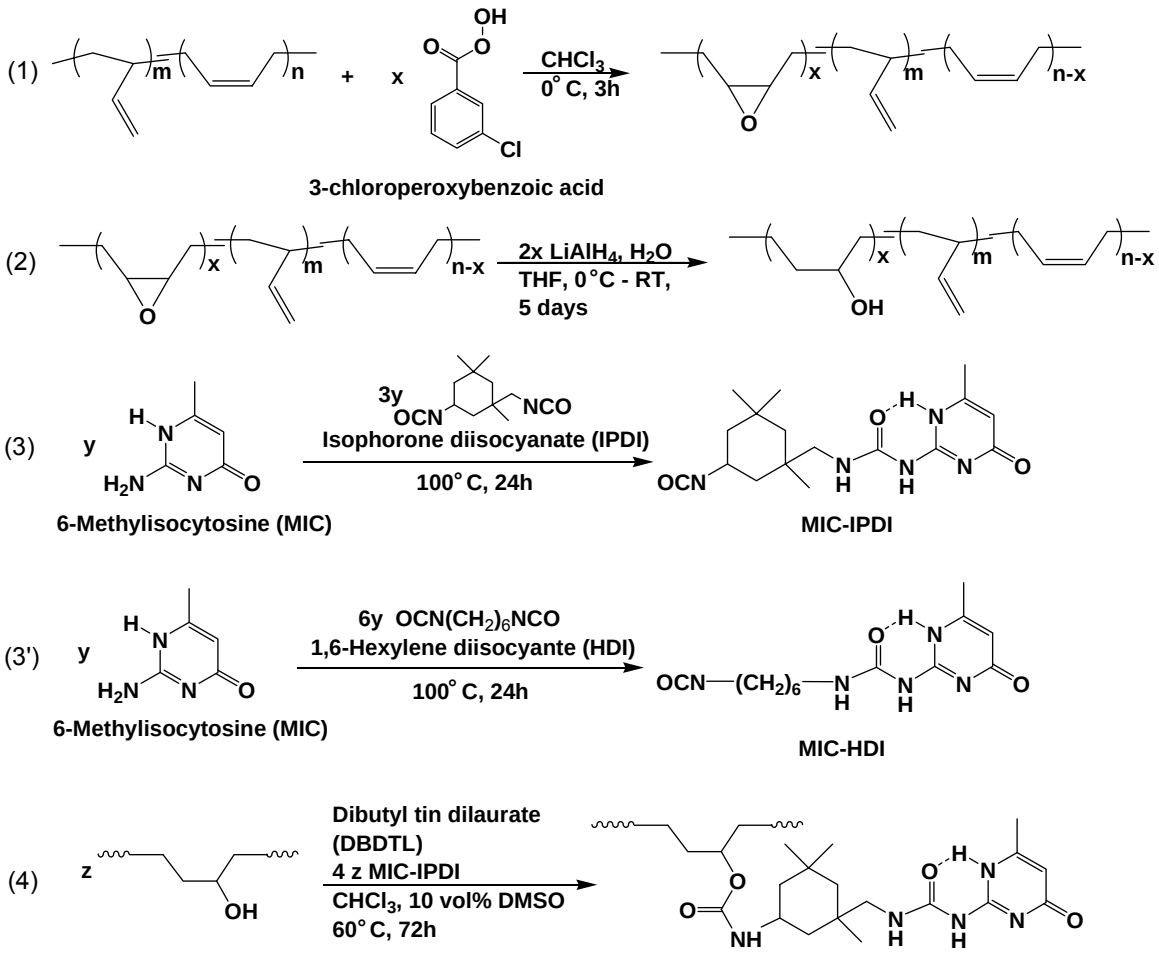


**Scheme 5.1** Synthesis of UPy-containing SBRs

### 5.3.6 Polymer Characterization

$^1$H NMR spectra of the polymers were obtained on a Varian Unity spectrometer operating at 400 MHz at ambient temperature. $CDCl_3$ (Cambridge Isotope Laboratories) was used as the solvent. SEC measurements were performed in THF at 40 °C at a flow rate of 1 mL/min using a Waters size exclusion chromatograph equipped with an autosampler, three 5-mm PLgel Mixed-C columns, a Waters 2410 refractive index (RI) detector operating at 880 nm, and a miniDAWN multiangle laser light scattering (MALLS) detector operating at 690 nm, which was calibrated with narrow polydispersity

polystyrene standards. The RI increment (dn/dc) was calculated online. Thermogravimetric analysis (TGA) measurements were obtained using a TA Instruments Hi-Res TGA 2950 thermogravimetric analyzer under $N_2$ at a heating rate of 10 ºC per minute. The films were prepared using a PHI pneumatic press GS-21 at 150 °C for 2 min. Dynamic mechanical analysis (DMA) measurements were performed on a TA Instruments Q 800 at a heating rate of 3 ºC per minute. Stress-strain experiments were performed using dogbone-shaped film samples ($n$ = 5) cut using a die according to ASTM D3368. The tensile tests were performed under ambient conditions on a 5500R Instron universal testing machine at a crosshead displacement rate of 100 mm/min. Stress-strain profiles were recorded and analyzed using Bluehill 2 software. Pneumatic grips were used, and no slippage was observed. Complex viscosities of the films were measured using TA Instruments AR G2 rheometer. A 25 mm parallel plate geometry was used, and rheological analysis was performed at a 1% strain amplitude at 1 rad/s with a 1000 μm gap under nitrogen atmosphere.

1.6 mol % UPy-functionalized SBR was first dissolved in THF at a concentration of 41 mg/ml. The solution was sonicated for 2 h for complete dissolution of the functionalized SBR prior to the processing step. Both pristine and functionalized MWCNTs (5 wt%) were then added to the solution and the mixture was sonicated for 2 h. The composite films were then cast in Teflon™ molds under ambient conditions. The films were then further dried overnight in a vacuum oven. Mini dog bone samples ($n$ = 3) were cut using a die according to ASTM D3368. Tensile tests were performed under ambient conditions on a 5500R Instron universal testing machine at a crosshead displacement rate of 500 mm/min.

## 5.4 Results and Discussion

### 5.4.1 Synthesis of UPy-containing SBRs

Reaction strategies used to synthesize the UPy-containing SBRs are illustrated in Scheme 5.1. SBRs were first reacted with MCPBA to epoxidize the butadiene repeat units (Reaction 1 in Scheme 5.1). The target epoxidation levels were 2 and 4 mol%. The epoxidized butadiene repeat units were subsequently reduced with $LiAlH_4$ to afford the hydroxyl-functionalized SBR (SBR-OH). The characterization data for these products are summarized in Table 5.1. The degree of epoxidation was readily calculated based on C = C bond conversion. The epoxidation was quantitative and well-controlled. $^1$H NMR (Figure 5.3) confirmed that only 1,4-poly(butadiene) repeat units were epoxidized, while epoxidation was not observed for 1,2-poly(butadiene) repeat units under the same reaction conditions. This follows the well-established trend for epoxidation, which is $CH_2{=}CH_2$ < $RCH{=}CH_2$ < $RCH{=}CHR$ ~ $R_2C{=}CH_2$ < $R_2C{=}CHR$ < $R_2C{=}CR_2$ = 1 < 24 < 500 ~ 500 < 6500 < very fast.[32] The subsequent change in $^1$H NMR results, from 2.6 – 3.0 ppm (epoxide) to 3.6 ppm (methylene adjacent to hydroxyl), demonstrated that the epoxides were quantitatively reduced to hydroxyl groups with $LiAlH_4$, which is shown in Figure 5.3. The hydroxy functionalization was quantitative and reproducibly achieved. SEC results of 2.0 mol% epoxidized and hydroxy-functionalized SBRs are summarized in Table 5.2, and the SEC trace for the 2.0 mol% hydroxy-functionalized SBR is shown in Figure 5.4. The SEC results for the SBR-E and SBR-OH samples ensured a monomodel product. Moreover, no significant change in molecular weight from that of SBR precursor was observed. This revealed that neither branching nor crosslinking had occurred during either derivatization step.

Although the hydroxyl functionalization was successful using these reaction conditions, there were a few issues associated with the derivatization step that we had to address. As described in the experimental section, the reaction mixture formed a gel after 2-3 h once the 1M $LiAlH_4$ solution had been added. We attributed this to lithium ion linking with the lithium alkoxide intermediates, which formed a gelled SBR network. The diffusion of $LiAlH_4$ limited the rate of reduction, which required a long reaction time (5 days) to complete. The quantitative reduction was not achieved for 1 to 2 day reaction time. The presence of residual epoxides would lead to crosslinking during the additional derivatization step, during which the hydroxyl groups would react with the epoxides and the DBTDL catalyst. After reacting for 5 days, an addition of water quantitatively converted the lithium alkoxides to hydroxyl groups. In addition, removing lithium salts from the polymer solution required multiple precipitations, although we were unable to obtain a perfectly clear solution free from lithium salts even with multiple precipitations. We could not use typical filtration strategies for the separation step due to the high solution viscosity of the SBRs. In fact, alternative strategies for conducting a ring-opening reaction involving epoxides generally requires an acid-catalyzed reaction, which results in crosslinked polybutadiene repeat units in SBRs. For example, the hydrochlorination of an epoxidized SBR was attempted following literature procedures.[16] Although hydrochlorination was quantitatively achieved, crosslinking was observed in the subsequent derivatization step. We attributed this to the chlorine leaving groups initiating the crosslinking with the hydroxyl groups. We also conducted a ring-opening reaction of epoxidized SBRs with sodium methoxide. This resulted in very little

conversion unless we used an acid catalyst, which was unsuitable for this derivatization step.

**Table 5.1** Hydroxyl-functionalized and UPy-functionalized SBRs

| SBR-OH [mol%-OH] | UPy conversion [%] | UPy [mol%] | UPy [wt%] |
|---|---|---|---|
| 2.0 | 84 | 1.6 | 11 |
| 3.6 | 74 | 2.6 | 18 |

$^1$H NMR conditions; Varian Unity 400 MHz, $CDCl_3$

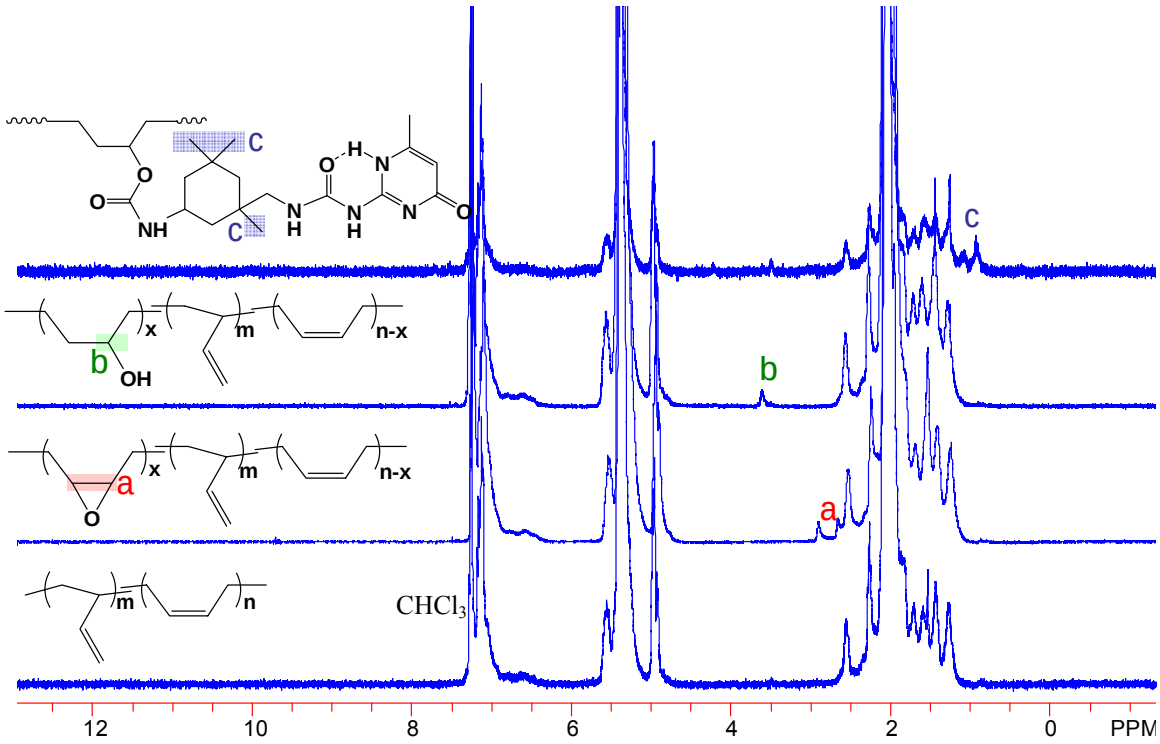


**Figure 5.3** $^1$H NMR spectra of SBR with 2.0 mol% degree of modification

**Table 5.2** Molecular weights of 2.0 mol% epoxidized and hydroxy-functionalized SBRs

| | $M_n$ | $M_w$ | $M_w/M_n$ |
|---|---|---|---|
| 2.0 mol% SBR-OH | 146000 | 251000 | 1.72 |
| 2.0 mol% SBR-E | 150000 | 257000 | 1.72 |
| SBR precursor | 133000 | 221000 | 1.66 |

Determined using SEC at 40 °C in THF with a MALLS detector

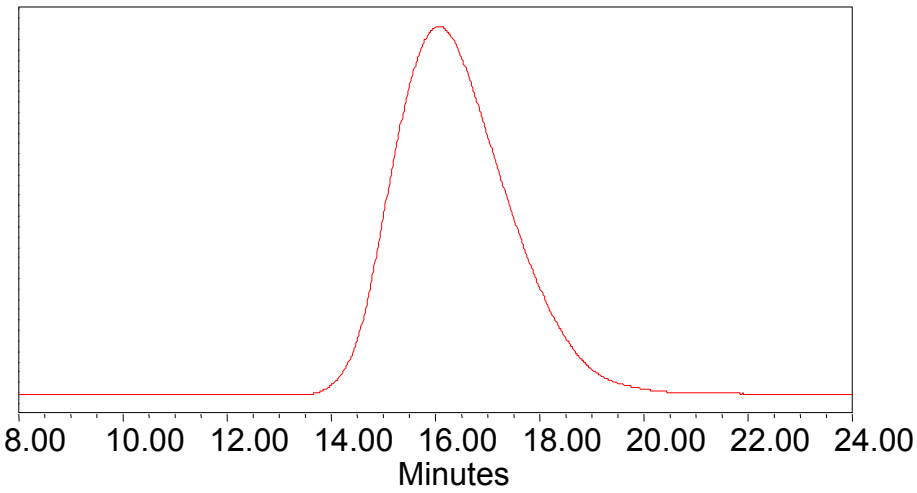


**Figure 5.4** SEC curve of 2.0 mol% hydroxy-functionalized SBR.

The third synthetic step involved the reaction of 6-methylisocytosine (MIC) with either an IPDI or an HDI diisocyanate in a bulk reaction at 100 °C. Yamauchi et al.[23] synthesized monoisocyanato methylisocytosine (MIC-HDI, reaction (3') in Scheme 5.1), and used this reagent to introduce UPy end-groups to telechelic polyesters. Following reported procedures, the reaction of MIC with HDI was attempted. All of the resonances as shown by $^{1}$H NMR for the MIC-HDI were quantitatively assigned (Figure 5.5). The mass obtained using FAB-MS spectrometry was 294.1566, which corresponds well with the theoretical mass of 294.1565. Repeated yields from this reaction were consistently greater than 95%. Although, MIC-HDI was partially soluble in both $CHCl_3$ and DMSO, low solubility became an issue during the additional derivatization step. Thus, the synthesis of the alternative compound was attempted. Specifically, MIC was reacted with IPDI in a bulk reaction at 100 °C to prepare a novel compound MIC-IPDI (Reaction (3) in Scheme 5.1). All of the $^{1}$H NMR resonances for the MIC-IPDI were quantitatively assigned, as shown in Figure 5.6. The literature has shown that a primary isocyanate possesses higher reactivity than a secondary isocyanate in IPDI.[24, 27] However, the $^{1}$H NMR resonance shown in Figure 5.6 revealed no significant selectivity between a

primary and a secondary isocyanate upon functionalization, which resulted in approximately 50/50 isomers. This was presumably due to the high reaction temperature of 100 °C, which provided enough thermal energy for the MIC to react with either isocyanate. Because either isomer can serve as the UPy isocyanate, no separation step was required. FAB-MS spectrometry was performed for the isolated product. The resulting molecular weight was 348.2038, which was in good agreement with the theoretical mass of 348.2036. Our initial reaction resulted in a 40% isolated yield after the product was washed with hexane several times. After the precipitation and washing solvent was changed to heptanes, the isolated yield from the reaction was approximately 70%. This yield increase implies that the solubility of the final product inhibited our ability to obtain a quantitative yield. MIC-IPDI is a white solid, which was found to be highly soluble in both $CHCl_3$ and DMSO—especially in comparison to the MIC-HDI. FT-IR spectroscopy confirmed the presence of isocyanate groups in the MIC-IPDI. In addition, the reaction of MIC with IPDI at both 80 °C and 120 °C was attempted. While the reaction at 80 °C resulted in very little conversion to MIC-IPD, the reaction at 120 °C resulted in a yellow compound which produced by-products as a number of extra peaks seen in $^1$H NMR. Moreover, the 80 °C reaction did not provide enough thermal energy for IPDI to react with MIC; while a higher reaction temperature (120 °C) initiated undesired side reactions. Therefore, 100 °C appeared sufficient for the reaction of MIC with IPDI.

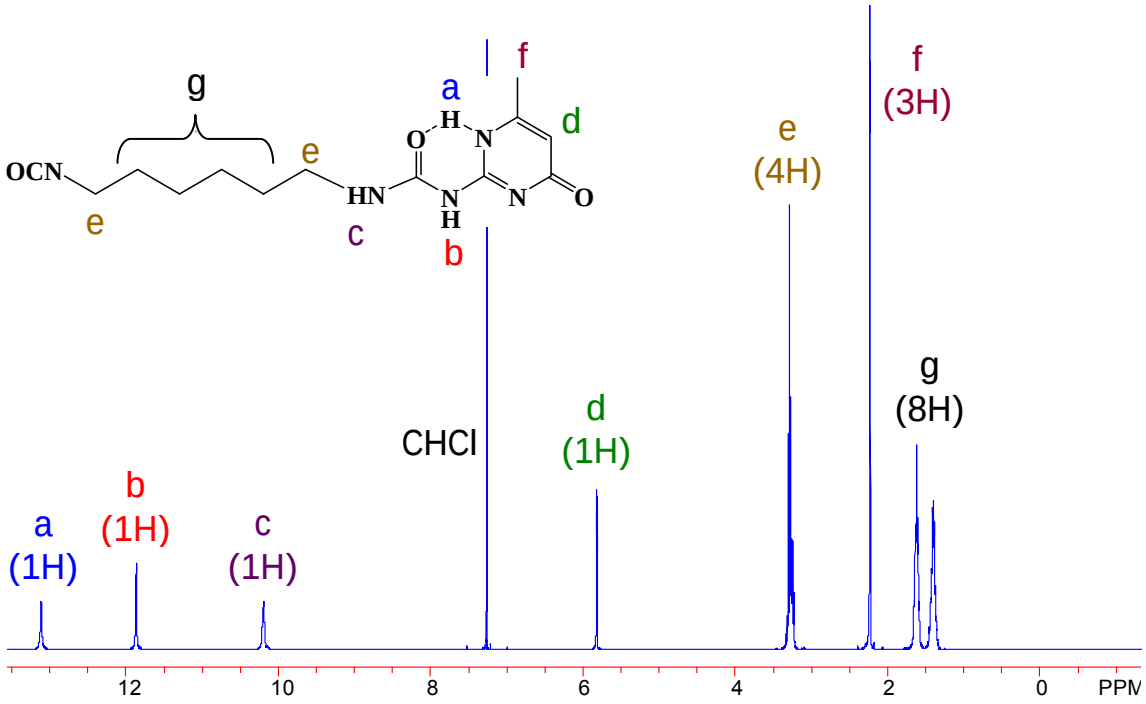


**Figure 5.5** $^{1}$H NMR of MIC-HDI
$^{1}$H NMR conditions; Varian Unity 400 MHz, $CDCl_3$

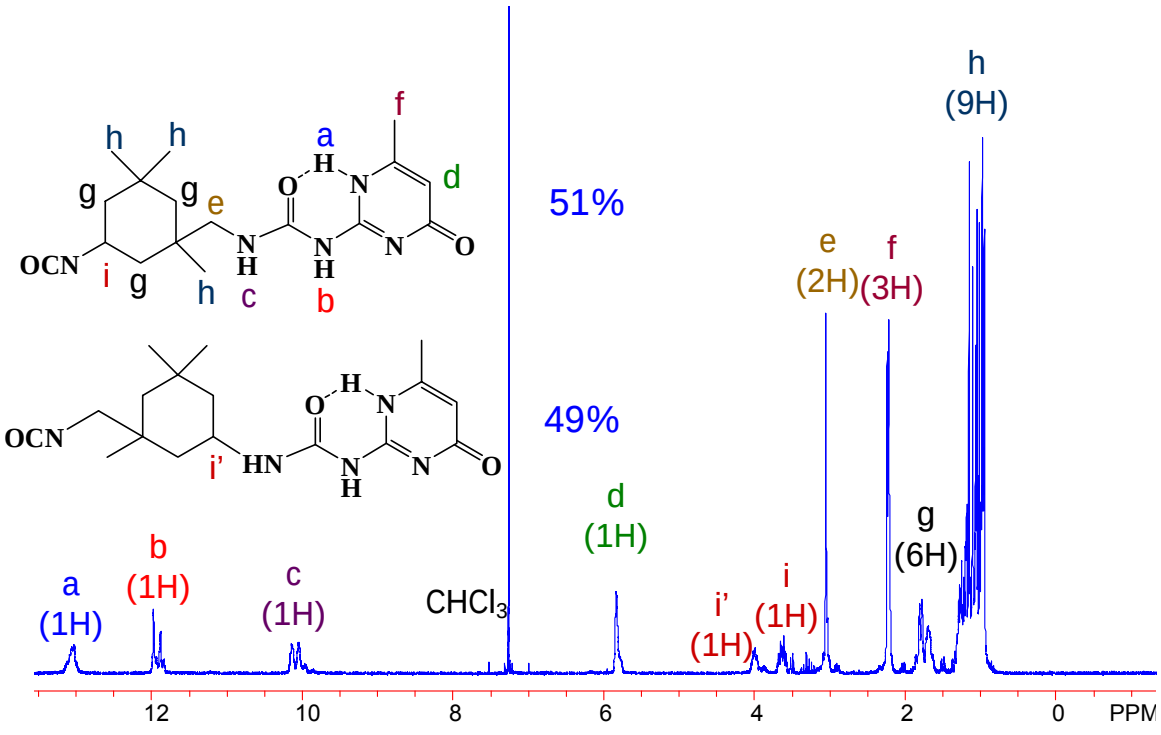


**Figure 5.6** $^{1}$H NMR of MIC-IPDI
$^{1}$H NMR conditions; Varian Unity 400 MHz, $CDCl_3$

The fourth step of synthesis (Reaction 4 in Scheme 5.1) involved reacting a 4-fold molar excess of MIC-IPDI with SBR-OH in the presence of a catalytic amount of DBTDL. $^1$H NMR spectra of the SBR-OH and UPy-SBR are shown in Figure 5.3. Over 75% UPy conversion was achieved as evidenced by the peaks at 0.8 – 1.1 ppm (three methyl groups in IPDI) as shown by $^1$H NMR. Our calculations from the UPy conversion showed that 1.6 mol% (11 wt%) and 2.6 mol% (19 wt%) UPy-functionalized SBR (UPy-SBR) had been obtained. These UPy functionalization results are summarized in Table 5.1. We observed increased viscosity during the course of this reaction, which implies that the MIC-IPDI was prevented from reacting with all of hydroxyl groups in the SBR-OH. The UPy-SBR was soluble in both $CHCl_3$ and THF as long as it was solvated in methanol. Once dried, however, UPy-SBR was no longer soluble in any solvents, which we attributed to the strong hydrogen-bonding association that occurred under dry conditions. Therefore, isolated UPy-SBR was stored in methanol. For our $^1$H NMR studies, the UPy-SBR was dissolved in $CDCl_3$, evaporated by half, and redissolved in $CDCl_3$. This procedure was repeated until no methanol was observed via $^1$H NMR. When a methanol-solvated 2.6 mol% functionalized UPy-SBR was dissolved in THF, precipitation occurred after 1 day. This indicates a stronger UPy-UPy association in highly functionalized UPy-SBR, which prevented the polymer from remaining soluble in THF.

### 5.4.2 Thermal and Mechanical Characterization of UPy-containing SBRs

TGA of 1.6 mol% UPy-SBR, 2.6 mol% UPy-SBR, and SBR were performed and the resulting curves are depicted in Figure 5.7. TGA data indicated that the UPy-SBR sample exhibited an onset of weight loss at 180-225 ºC, which is consistent with

literature values for UPy-functionalized polymers.[24, 25] These reports also linked the initial degradation step to the elimination of the UPy groups. Observed weight loss values, as shown in Figure 5.7, were consistent with the weight fractions of the UPy groups in the polymer (Table 5.3). The initial degradation step using 1.6 mol% UPy-SBR resulted in a 9 wt% weight loss at 350 °C, while the 2.6 mol% UPy-SBR sample showed 19 wt% weight loss at 350 °C. These reported initial weight losses are in a good agreement with incorporated weight fraction of the UPy groups, 11 wt% and 18 wt%, respectively, which are shown in Table 5.1. Significant residual weight was observed in the UPy-functionalized SBRs, whereas the SBR precursor showed no significant residual weight. This implies that thermal crosslinking occurred in the UPy-functionalized SBRs during the degradation step.

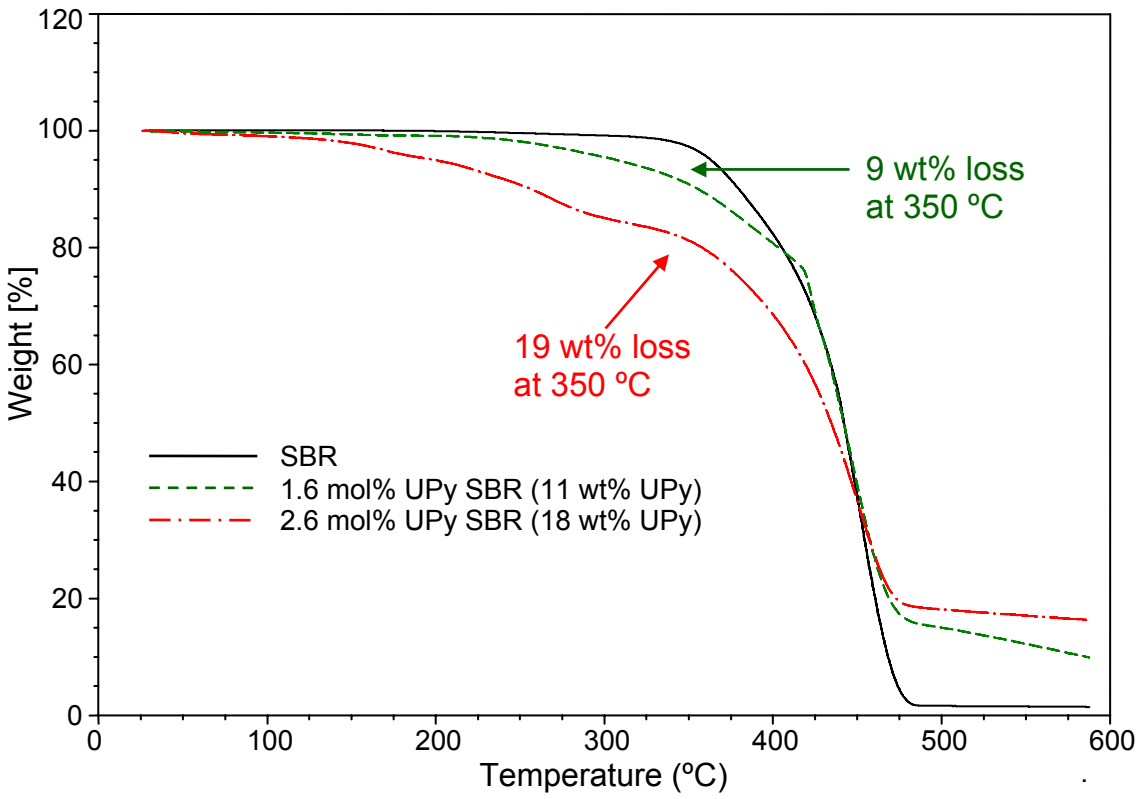


**Figure 5.7** TGA of 1.6 mol% UPy-SBR, 2.6 mol% UPy-SBR and SBR

DMA analysis was performed on the melt-pressed films of 1.6 mol% UPy-SBR, 2.6 mol% UPy-SBR, and SBR. The films were prepared using a PHI pneumatic press GS-21 at 150 °C for 2 min. A homogeneous film was obtained from 1.6 mol% UPy-SBR, whereas 2.6 mol% UPy-SBR resulted in a cloudy film. The resulting DMA curves are shown in Figure 4.8. The observed glass transition temperatures ($T_g$) were as follows: SBR -73 °C, 1.6 mol% UPy-SBR -67 °C, and 2.6 mol% UPy-SBR -64 °C. $T_g$ values for the SBRs increased with the increase in the amount of hydrogen bonding groups, which acted as physical crosslinks, thereby raising $T_g$ results. In addition, the storage modulus significantly increased with an increase in the number of hydrogen bonding groups in the SBR. SCMHB groups aided the formation of effective crosslinked networks, thereby enhancing mechanical performance. For comparative purposes, DMA experiments were conducted at temperatures up to 80 °C, following reported literature procedures[16]. In Abetz's work,[16] for example, sulfonyl urethane functionalized polybutadiene showed little modulus increase via DMA, except the 20 mol% functionalized sulfonyl urethane polybutadiene showed a significant increase in modulus. For our study, the UPy-functionalized SBR showed a modulus that was an order of magnitude higher than that of the 20 mol% functionalized sulfonyl urethane polybutadiene.

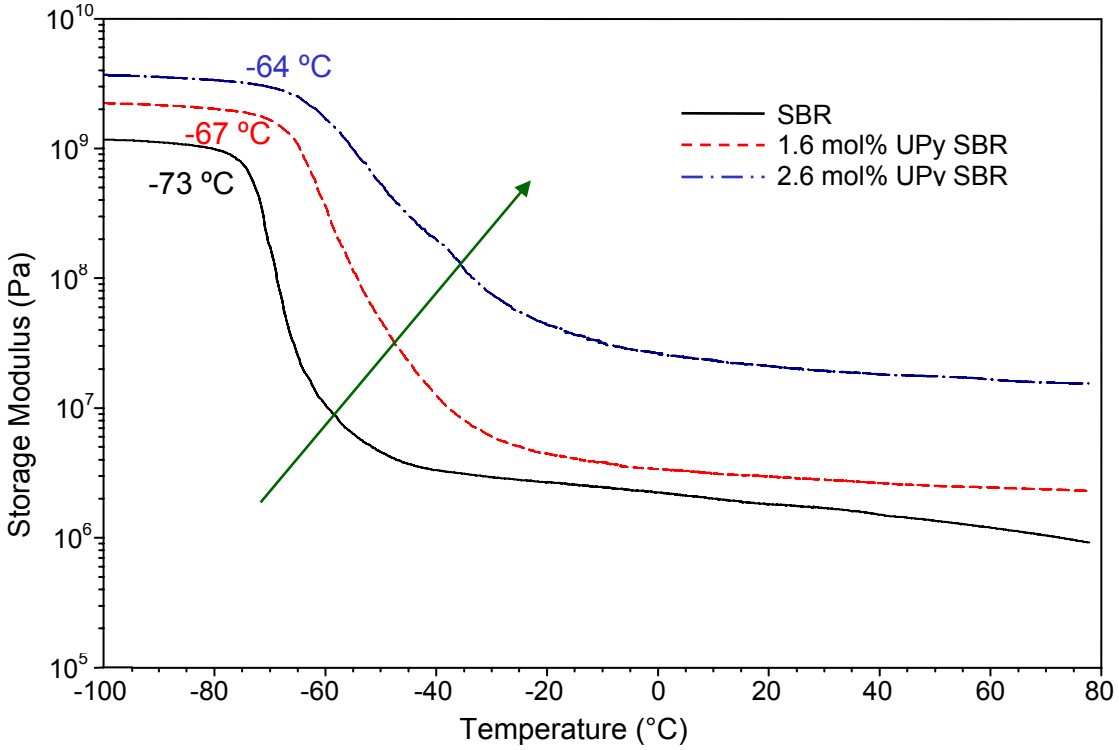


**Figure 5.8** DMA of 1.6 mol% UPy-SBR, 2.6 mol% UPy-SBR and SBR

Stress-strain experiments were performed using dogbone-shaped film samples (*n* = 5) under ambient conditions at a crosshead displacement rate of 100 mm/min. Stress-strain curves are shown in Figure 5.9 and the stress-strain data are summarized in Table 5.3. Both the Young's modulus and the stress-at-break results for the SBR significantly increased with an increase in the number of hydrogen bonding groups. The Young's modulus for the 1.6 mol% UPy-SBR film sample showed an increase of approximately 250% compared to SBR, while the Young's modulus for the 2.6 mol% UPy-SBR film sample showed an increase of approximately 1000% compared to SBR. With respect to stress-at-break results, the 1.6 mol% UPy-SBR film sample showed an increase of about 2500% compared to SBR, while the 2.6 mol% UPy-SBR film sample showed a 4900% increase in comparison to SBR. These trends are consistent with storage modulus increases observed via DMA experiments. The UPy groups formed crosslinked networks

with enhanced mechanical strength. A significant increase in elongation-at-break values was also observed for the 1.6 mol% UPy-SBR. The crosslinked network resulted in a supramolecular polymer matrix, which accounted for the higher elongation values. It should be noted, however, that the elongation-at-break values for the 2.6 mol% UPy-SBR decreased. We attributed this phenomenon to the increased crosslink junction points with increasing numbers of UPy groups.

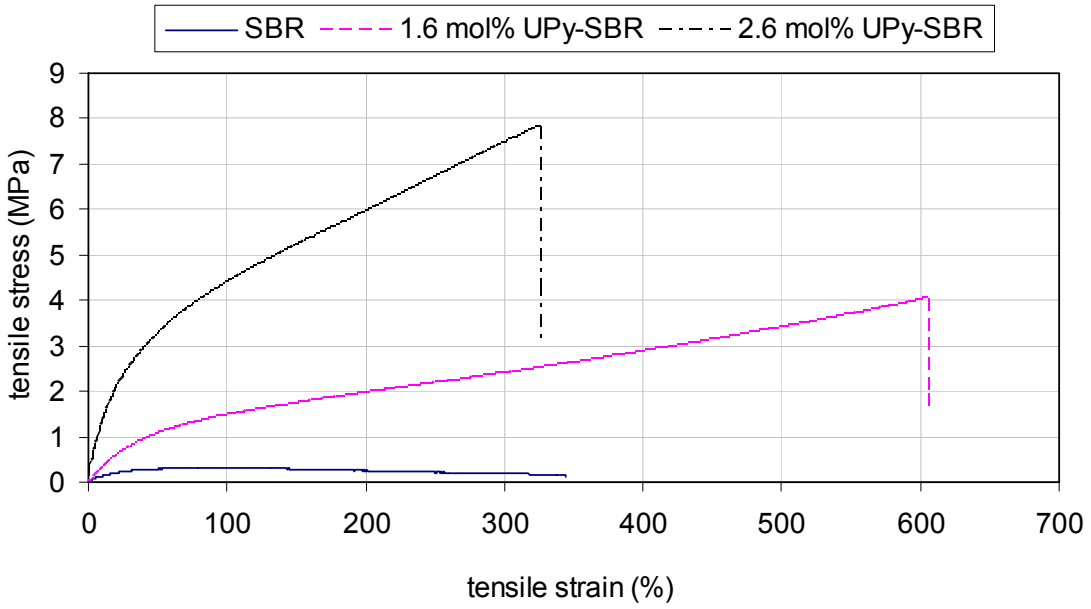


**Figure 5.9** Comparison of tensile testing of 1.6 mol% UPy-SBR, 2.6 mol% UPy-SBR and SBR

**Table 5.3** Tensile testing of 1.6 mol% UPy-SBR, 2.6 mol% UPy-SBR and SBR

| | SBR | 1.6 mol% UPy-SBR | 2.6 mol% UPy-SBR |
|---|---|---|---|
| Tensile strain at break (%) | 351 ± 38 | 595 ± 62 | 332 ± 7 |
| Tensile stress at break (MPa) | 0.16 ± 0.02 | 4.03 ± 0.27 | 7.75 ± 0.17 |
| Young's Modulus (MPa) | 0.995 ± 0.104 | 2.42 ± 0.17 | 10.2 ± 1.9 |

Instron 5500, 100 mm/min, film formation for a dog bone: melt press at 150 ºC

The Storage modulus of the 1.6 mol% UPy-SBR, the 2.0 mol% SBR-E, and SBR as a function of temperature were measured to verify the thermoreversible behavior of UPy-SBR (Figure 5.10). As shown in Figure 5.10, the 1.6 mol% UPy-SBR did not show

any decrease in melt viscosity at higher temperatures, whereas both the precursor SBR and the SBR-E showed a consistent decrease in melt viscosity with increasing temperature. Such thermo-irreversible behavior is often seen in covalently crosslinked polymers, which may imply the UPy-SBR was covalently crosslinked. However, the reaction scheme we used did not introduce any covalent crosslinks—although we cannot eliminate the possibility that this occurred during the derivatization steps. Strong quadruple hydrogen-bonding interactions between high molecular weight SBRs are thought to raise the dissociation or flow temperature. As reported in many polyurea studies,[17, 18, 21] strong hydrogen-bonding interactions prevent polyureas from flowing until a temperature of 200-250 °C has been reached. TGA experiments showed that UPy groups start degrading at 180-225 ºC. Similarly, the dissociation temperature for UPy-SBR polymers might be higher than the degradation temperature. And indeed, once the cleavage of UPy groups has occurred, covalent crosslinking seemed to follow, as evidenced by TGA results.

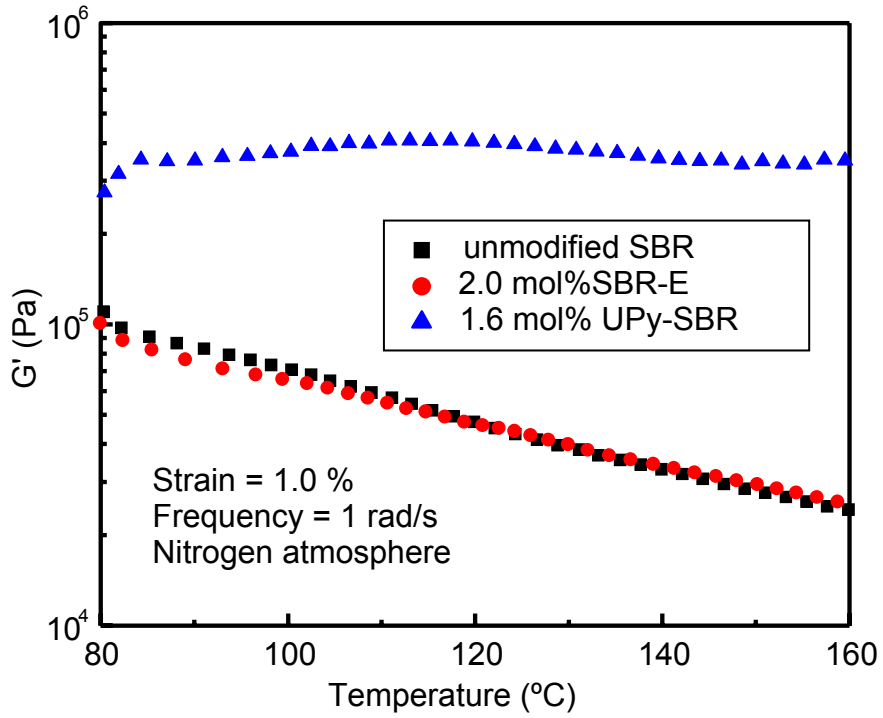


**Figure 5.10** Storage modulus as a function of temperature for unmodified and modified SBR

As a component of this study, we performed stress-strain experiments involving composites films of 1.6 mol % UPy-SBR with pristine CNTs and UPy-functionalized CNTs using dogbone-shaped film samples ($n$ = 3) under ambient conditions. The resulting non-uniform cast films and the difficulty in performing CNT and UPy-CNT dispersions in the SBR matrix using a high viscosity media prevented us from obtaining any consistent results. Therefore, we were unable to formulate any meaningful stress-strain assessments of these composite films.

## 5.5 Conclusions

The quantitative epoxidation and hydroxyl functionalization of SBRs were achieved and a novel UPy isocyanate compound, MIC-IPDI, was successfully synthesized. $^{1}$H NMR and FAB-MS of MIC-IPDI confirmed the proposed chemical

structure. Reactions of 2.0 mol% and 3.6 mol% SBR-OH with MIC-IPDI resulted in 1.6 mol% and 2.6 mol% UPy-functionalized SBRs, respectively. Initial weight losses in TGA were consistent with the weight fraction of the incorporated UPy groups in the UPy-SBRs. The SCMHB network served as a mechanically effective crosslinking network. The crosslinked networks raised the $T_g$ and significantly increased mechanical performance. However, melt viscosity measurements corroborated the thermo-irreversible behavior of these polymers. We attributed this to (1) an occurrence of covalent-crosslinking, or (2) the fact that too many UPy groups had been incorporated in the UPy-SBRs. This suggests that reducing the number of UPy groups in styrene-butadiene rubbers would be desirable. Another possible strategy might involve the use of UPy-methacrylate as one of monomers in a styrene, 1,3-butadiene polymerization. In so doing, the derivatization steps would not be required to synthesize UPy-SBR with similar chemical composition, as documented in this study.

## 5.7 Acknowledgements

The authors would like to thank US Navy RDT&E PE 0602236N Wartime Sustainment Applied Research, ONR's Long Range Navy and Marine Corps Science & Technology Programs and the Goodyear Tire & Rubber Company for financial support of this research.

## 5.8 References

1. Abetz, V.; Dardin, A.; Stadler, R.; Hellmann, J.; Samulski, E. T.; Spiess, H. W., Orientation of polybutadiene chains in a thermoplastic elastomer. *Colloid and Polymer Science* **1996,** 274, (8), 723-731.
2. Dardin, A.; Stadler, R.; Boeffel, C.; Spiess, H. W., Molecular-dynamics of new thermoplastic elastomers based on hydrogen-bonding complexes - A deuteron nuclear-magnetic-resonance

investigation. *Makromolekulare Chemie-Macromolecular Chemistry and Physics* **1993,** 194, (12), 3467-3477.

3. Freitas, L. D.; Auschra, C.; Abetz, V.; Stadler, R., Hydrogen-bonds in unipolar matrix-comparison of complexation in polymeric and low-molecular-weight systems. *Colloid and Polymer Science* **1991,** 269, (6), 566-575.
4. Freitas, L. D.; Burgert, J.; Stadler, R., Thermoplastic elastomers by hydrogen-bonding 5. Thermorheologically complex behavior by hydrogen-dond clustering. *Polymer Bulletin* **1987,** 17, (5), 431-438.
5. Freitas, L. D.; Jacobi, M. M.; Goncalves, G.; Stadler, R., Microphase separation induced by hydrogen bonding in a poly(1,4-butadiene)-block-poly(1,4-isoprene) diblock copolymer - An example of supramolecular organization via tandem interactions. *Macromolecules* **1998,** 31, (10), 3379-3382.
6. Freitas, L. D.; Stadler, R., Thermoplastic elastomers by hydrogen-donding 4. Influence of hydrogen-bonding on the temperature-dependence of the viscoelastic properties. *Colloid and Polymer Science* **1988,** 266, (12), 1095-1101.
7. Freitas, L. L. D.; Stadler, R., Thermoplastic elastomers by hydrogen-donding 3. Interrelations between molecular parameters and rheological properties. *Macromolecules* **1987,** 20, (10), 2478-2485.
8. Hilger, C.; Drager, M.; Stadler, R., Cooperative structure formation by combination of covalent and association chain polymers 6. Molecular-origin of supramolecular self-assembling in statistical copolymers. *Macromolecules* **1992,** 25, (9), 2498-2501.
9. Hilger, C.; Stadler, R., Cooperative structure formation by combination of covalent and Association chain polymers 3. Control of association polymer chain-length. *Makromolekulare Chemie-Macromolecular Chemistry and Physics* **1991,** 192, (4), 805-817.
10. Muller, M.; Kremer, F.; Stadler, R.; Fischer, E. W.; Seidel, U., The molecular-dynamics of thermoreversible networks as studied by broad-band dielectric-spectroscopy. *Colloid and Polymer Science* **1995,** 273, (1), 38-46.
11. Muller, M.; Seidel, U.; Stadler, R., Influence of hydrogen-bonding on the viscoelastic properties of thermoreversible networks - Analysis of the local complex dynamics *Polymer* **1995,** 36, (16), 3143-3150.
12. Petzhold, C.; Jacobi, M. M.; Stadler, R., Influence of hydrogen-bonding on the properties of elastomeric blends - Synergism in SBR-NBR blends. *Polymer Communications* **1989,** 30, (4), 111-114.
13. Stadler, R.; Burgert, J., Influence of hydrogen-bonding on the properties of elastomers and elastomeric blends *Makromolekulare Chemie-Macromolecular Chemistry and Physics* **1986,** 187, (7), 1681-1690.
14. Stadler, R.; Freitas, L. D., Thermoplastic elastomers by hydrogen-bonding 1. Rheological properties of modified polybutadiene *Colloid and Polymer Science* **1986,** 264, (9), 773-778.
15. Stadler, R.; Freitas, L. D., TThermoplastic elastomers by hydrogen-bonding 2. IR-spectoscopic characterization of the hydrogen-bonding. *Polymer Bulletin* **1986,** 15, (2), 173-179.
16. Peng, C. C.; Abetz, V., A simple pathway toward quantitative modification of polybutadiene: A new approach to thermoreversible cross-linking rubber comprising supramolecular hydrogen-bonding networks. *Macromolecules* **2005,** 38, (13), 5575-5580.
17. Das, S.; Yilgor, I.; Yilgor, E.; Wilkes, G. L., Probing the urea hard domain connectivity in segmented, non-chain extended polyureas using hydrogen-bond screening agents. *Polymer* **2008,** 49, (1), 174-179.
18. Das, S.; Cox, D. F.; Wilkes, G. L.; Klinedinst, D. B.; Yilgor, I.; Yilgor, E.; Beyer, F. L., Effect of symmetry and H-bond strength of hard segments on the structure-property relationships of segmented, nonchain extended polyurethanes and polyureas. *Journal of Macromolecular Science, Part B: Physics* **2007,** 46, (5), 853-875.
19. Klinedinst, D. B.; Yilgoer, E.; Yilgoer, I.; Beyer, F. L.; Wilkes, G. L., Structure-property behavior of segmented polyurethaneurea copolymers based on an ethylene-butylene soft segment. *Polymer* **2005,** 46, (23), 10191-10201.
20. Sheth, J. P.; Unal, S.; Yilgor, E.; Yilgor, I.; Beyer, F. L.; Long, T. E.; Wilkes, G. L., A comparative study of the structure-property behavior of highly branched segmented poly(urethane urea) copolymers and their linear analogs. *Polymer* **2005,** 46, (23), 10180-10190.

21. Sheth, J. P.; Klinedinst, D. B.; Wilkes, G. L.; Yilgor, I.; Yilgor, E., Role of chain symmetry and hydrogen bonding in segmented copolymers with monodisperse hard segments. *Polymer* **2005,** 46, (18), 7317-7322.
22. Sheth, J. P.; Wilkes, G. L.; Fornof, A. R.; Long, T. E.; Yilgor, I., Probing the hard segment phase connectivity and percolation in model segmented poly(urethane urea) copolymers. *Macromolecules* **2005,** 38, (13), 5681-5685.
23. Yamauchi, K.; Kanomata, A.; Inoue, T.; Long, T. E., Thermoreversible polyesters consisting of multiple hydrogen bonding (MHB). *Macromolecules* **2004,** 37, (10), 3519-3522.
24. Yamauchi, K.; Lizotte, J. R.; Hercules, D. M.; Vergne, M. J.; Long, T. E., Combinations of microphase separation and terminal multiple hydrogen bonding in novel macromolecules. *Journal of the American Chemical Society* **2002,** 124, (29), 8599-8604.
25. Yamauchi, K.; Lizotte, J. R.; Long, T. E., Thermoreversible poly(alkyl acrylates) consisting of self-complementary multiple hydrogen bonding. *Macromolecules* **2003,** 36, (4), 1083-1088.
26. Elkins, C. L.; Park, T.; McKee, M. G.; Long, T. E., Synthesis and characterization of poly(2-ethylhexyl methacrylate) copolymers containing pendant, self-complementary multiple-hydrogen-bonding sites. *Journal of Polymer Science Part a-Polymer Chemistry* **2005,** 43, (19), 4618-4631.
27. Elkins, C. L.; Viswanathan, K.; Long, T. E., Synthesis and characterization of star-shaped poly(ethylene-co-propylene) polymers bearing terminal self-complementary multiple hydrogen-bonding sites. *Macromolecules* **2006,** 39, (9), 3132-3139.
28. Folmer, B. J. B.; Sijbesma, R. P.; Versteegen, R. M.; van der Rijt, J. A. J.; Meijer, E. W., Supramolecular polymer materials: Chain extension of telechelic polymers using a reactive hydrogen-bonding synthon. *Advanced Materials* **2000,** 12, (12), 874-878.
29. Sijbesma, R. P.; Beijer, F. H.; Brunsveld, L.; Folmer, B. J. B.; Hirschberg, J.; Lange, R. F. M.; Lowe, J. K. L.; Meijer, E. W., Reversible polymers formed from self-complementary monomers using quadruple hydrogen bonding. *Science* **1997,** 278, (5343), 1601-1604.
30. Boker, A.; Reihs, K.; Wang, J. G.; Stadler, R.; Ober, C. K., Selectively thermally cleavable fluorinated side chain block copolymers: Surface chemistry and surface properties. *Macromolecules* **2000,** 33, (4), 1310-1320.
31. Williamson, D. T.; Mather, B. D.; Long, T. E., Oxidation and epoxidation of poly(1,3-cyclohexadiene). *Journal of Polymer Science Part a-Polymer Chemistry* **2003,** 41, (1), 84-93.
32. Vollhardt, K. P. C.; Schore, N. E., *Oragnic Chemistry, Structure and Function*. Third ed.; W. H. Freeman and Company: New York, 1999.

# Chapter 6: Influence of Site-Specific Sulfonation on Acrylic Graft Copolymer Morphology

Taken from:
Tomonori Saito, Brian D. Mather, Philip J. Costanzo, Frederick L. Beyer and Timothy E. Long', "Influence of Site-Specific Sulfonation on Acrylic Graft Copolymer Morphology", *Macromolecules*, ASAP

## 6.1 Abstract

Novel site-specifically sulfonated graft copolymers, poly(methyl methacrylate)-*g*-(poly(sulfonic acid styrene)-*b*-poly(*tert*-butyl styrene)), poly(methyl methacrylate)-*g*-(poly(*tert*-butyl styrene)-*b*-poly(sulfonic acid styrene)), and the corresponding sodium sulfonate salts were successfully synthesized. The weight average molecular weights ($M_w$) of the graft copolymers were approximately 200000 g/mol and the polydispersity ranged from 1.86 to 2.22. The graft copolymers contained approximately 9 – 10 branches on average and 4 wt% of sulfonic acid or sodium sulfonate blocks adjacent to the backbone or at the branch terminus. The mobility of the sulfonated blocks located at the branch terminus enabled the sulfonated blocks to more readily interact and form ionic aggregates. The glass transition temperatures of the sulfonated graft copolymer with sulfonated blocks at the branch terminus were higher than values for copolymers with sulfonated blocks adjacent to the backbone. This behavior was attributed to the sulfonated blocks at the branch terminus more easily forming ionic aggregates. In general, appearance of multiple scattering maxima in the small-angle X-ray scattering (SAXS) data indicated the formation of lamellar morphologies. More facile aggregation of sulfonated blocks at the branch terminus resulted in the appearance of ionomer peaks in SAXS whereas ionomer peaks were not observed in sulfonated graft copolymers with

sulfonated blocks adjacent to the backbone. Reasonable fits of the Yarusso-Cooper model to the SAXS data strongly supported the identification of the non-lamellar maxima as ionomer peaks. Strong ionic interactions with $Na^+$ counter-ions reduced the Bragg spacings, d, of the sodium sulfonate graft copolymers and increased the size of the ionic aggregates. The location of sulfonated blocks in both sulfonic acid and sodium sulfonate graft copolymers significantly affected thermal properties and morphologies.

## 6.2 Introduction

Graft copolymers enable a wide variety of emerging applications due to their unique macromolecular architecture. Understanding intra- and intermolecular interactions in graft copolymers is crucial for tuning the functionality and performance of graft copolymers. Well-defined synthesis and characterization of graft copolymers is necessary to understand their unique structure-property relationships.[1] A generally accepted strategy for obtaining more well-defined branched polymers involves copolymerization of macromonomers with backbone-forming monomers. A macromonomer is defined as a functional oligomer with a polymerizable end group.[2] The chain length of the macromonomer, which defines the length of branches in the graft copolymer, is predetermined and precisely controlled using living polymerization strategies. The choice of monomers and the order of monomer addition also control the composition of the branch and backbone upon subsequent copolymerization.[3]

Block copolymers, graft copolymers, and ionomers often exhibit microphase separation, and this morphological control dramatically influences the physical properties of the polymer. Occurrence of microphase separation depends on many factors,

including compositional dissimilarity, molecular weight, and crystallizability.[4] The Flory-Huggins binary segmental interaction parameter, $\chi$, describes the degree of the enthalpic interactions between components. The volume fraction of the component and $\chi N/\lambda$, where $N$ is the degree of polymerization, and $\lambda$ is the number of branches per graft copolymer, predict the phase behavior of graft copolymer systems.[5]

Gido and coworkers[6, 7] demonstrated the utility of the constituting block copolymer hypothesis in their studies on several graft copolymers. The graft copolymers possessed either regularly spaced tetrafunctional branch points[6] or randomly placed trifunctional and tetrafunctional branch points.[7] The morphological behavior of the regularly spaced graft copolymers supported the constituting block copolymer hypothesis, in which smaller architectural subunits of the graft copolymers dictated the morphological behavior of the large complex architectures of graft copolymers.[6] Graft copolymers with randomly placed branch points also followed the constituting block copolymer hypothesis, but exhibited less well-ordered morphologies than analogues with regularly spaced branch points.[7]

Holdcroft et al. synthesized graft copolymers containing ionic polymer grafts (polystyrene sulfonic acid graft chains) attached to a hydrophobic backbone.[8, 9] Their macromonomer strategy resulted in uniform graft chain length of the poly(styrene sulfonic acid) branches. They studied the thermal, morphological, and proton exchange properties. This study provided insight into the importance of a well-defined graft copolymer in determining and understanding the structure-property relationships. Although this class of ionomeric graft copolymers is suitable for studying structure-property relationships, due to the challenging synthesis of well-defined ionomers, the

relationship between structure and morphology of branched polymers remains as a challenge.

We are interested in the structure-property relationships of multiphase ionomers as a function of the relative location of sulfonated blocks. The location of sulfonated blocks in branched architecture is expected to affect various properties. Understanding this fundamental concept may provide important insight for macromolecular design and property tuning. Researchers have predicted that the distribution of sulfonated groups along the backbone, acid strength, and the relative location to the polymer backbone have a considerable effect on the final morphology and properties.[10] However, due to synthetic difficulties, most synthetic methods that are utilized to form acid- and ion-containing polymers such as proton exchange membranes have resulted in random or statistical placement of sulfonic acid units along the copolymer chain.[10, 11] Thus, a fundamental study of the structure-property relationships with well-defined branched sulfonated ionomers has only received sparse attention.

This chapter describes selectively sulfonated graft copolymers, which leads to the elucidation of structure-property relationships of sulfonated graft copolymers as a function of the relative location of sulfonated blocks. The structures and schematic representations of the site-specifically sulfonated graft copolymers are shown in Figure 6.1. The synthetic methodology that was utilized for controlled graft copolymer synthesis with precise location of sulfonated blocks involved preformed macromonomers.[12] Poly(*t*-butyl styrene)-*b*-polystyrene (P*t*BS-*b*-PS) diblock macromonomers were synthesized via living anionic polymerization. The diblock macromonomer contained 1000 g/mol polystyrene and 9000 g/mol poly(*t*-butyl styrene).

The macromonomer ensured controlled molecular weight and distribution of the graft. P*t*BS-*b*-PS diblock macromonomers were subsequently copolymerized with methyl methacrylate (MMA). Polystyrene blocks were selectively sulfonated as the *t*-butyl group hindered sulfonation of the poly(*t*-butyl styrene) blocks.[13-19] The sulfonated blocks were placed either adjacent to the backbone, which will be referred to as A, or at the branch terminus, which will be referred to as B. In this manuscript, we will discuss the synthesis of well-defined site-specifically sulfonated graft copolymers and thermal and morphological characterization of the sulfonated graft copolymers using differential scanning calorimetry (DSC), small angle X-ray scattering (SAXS), and transmission electron microscopy (TEM) as a function of relative location of sulfonated blocks.

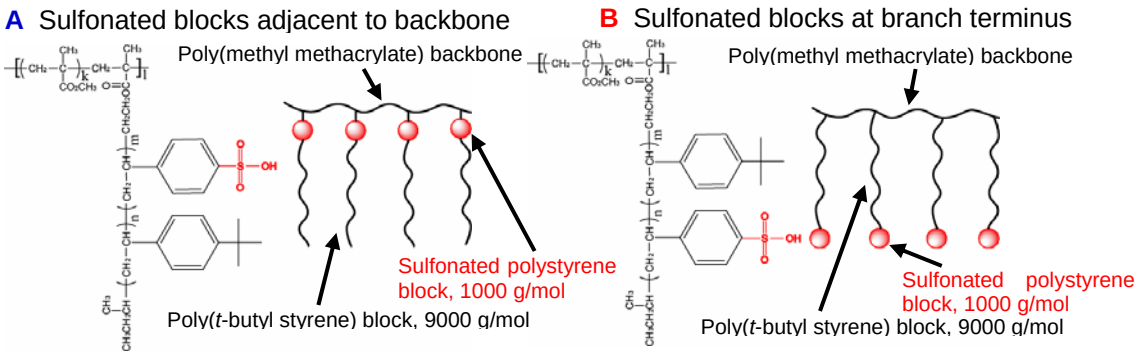


**Figure 6.1** Chemical structures and schematic images of the site-specifically sulfonated graft copolymers

## 6.3 Experimental

### 6.3.1 Materials and Chemicals

Styrene (Aldrich, 99%) and *tert*-butyl styrene (Scientific Polymer Products, 95%) were dried over calcium hydride (Aldrich, 95%) for 24 h and distilled under vacuum. The monomers were treated with an aliquot of dibutylmagnesium (Aldrich, 1.0 M) and distilled under vacuum prior to use. Cyclohexane (Burdick & Jackson, HPLC) and

tetrahydrofuran (THF, Fischer Scientific) were passed through an activated molecular sieve column (Aldrich, 60 Å mesh) and activated alumina column immediately prior to use. Methacryloyl chloride (Aldrich, 96%) was distilled under nitrogen. Triethylamine (Aldrich, 99%) was stirred over calcium hydride (Aldrich, 95%) and distilled under vacuum. Methyl methacrylate (MMA, 98%, Aldrich) was de-inhibited via passing through activated basic alumina column. *sec*-Butyllithium (Aldrich, 1.4 M), ethylene oxide (Aldrich, 99.98%), 2,2-azobisisobutyronitrile (AIBN, 99%, Aldrich,) dichloroethane (Aldrich, 99%), acetic anhydride (Aldrich, 98%) and sulfuric acid (Aldrich, 98%) were used as received.

### 6.3.2 Synthesis of Hydroxy-terminated Poly(*tert*-butyl styrene-*block*-styrene)

A 500 mL-capacity anionic polymerization reactor was filled with cyclohexane (350 mL) and the temperature was maintained at 50 °C. *tert*-Butyl styrene (44.12 mL, 39.00g) was syringed into the reactor. *sec*-Butyllithium (3.961 mL, 4.333 mmol) was then added to the solution to initiate anionic polymerization. As illustrated in Scheme 6.1 (1), the first reaction was allowed to proceed 1 h and the second monomer, styrene (4.767 mL, 4.333 g) was added. After 1 h of polymerization, ethylene oxide was bubbled through the reaction solvent for 2 min and then terminated by adding acidified methanol. The diblock copolymer was precipitated into methanol, and the recovered polymer was dried at 100 °C in vacuum for 24 h. Synthesis of γ-hydroxy-poly(styrene-*block*-*tert*-butyl styrene) was also performed by exchanging the order of first block (*tert*-butyl styrene) and the second block (styrene) addition. $^{1}$H NMR (400 MHz, $CDCl_3$, δ): 0.6 – 0.8 ppm (br, $CH_3CH_2CH(CH_3)$-), 0.9 – 2.5 ppm (br, -$CH_2$-, -$CH_2CH$-, -$C(CH_3)_3$ in polystyrene

and poly(*t*-butyl styrene) units), 3.2 – 3.4 ppm (br, -$CH_2CH_2OH$), 6.0 – 7.3 ppm (br, aromatic protons in polystyrene and poly(*t*-butyl styrene) units).

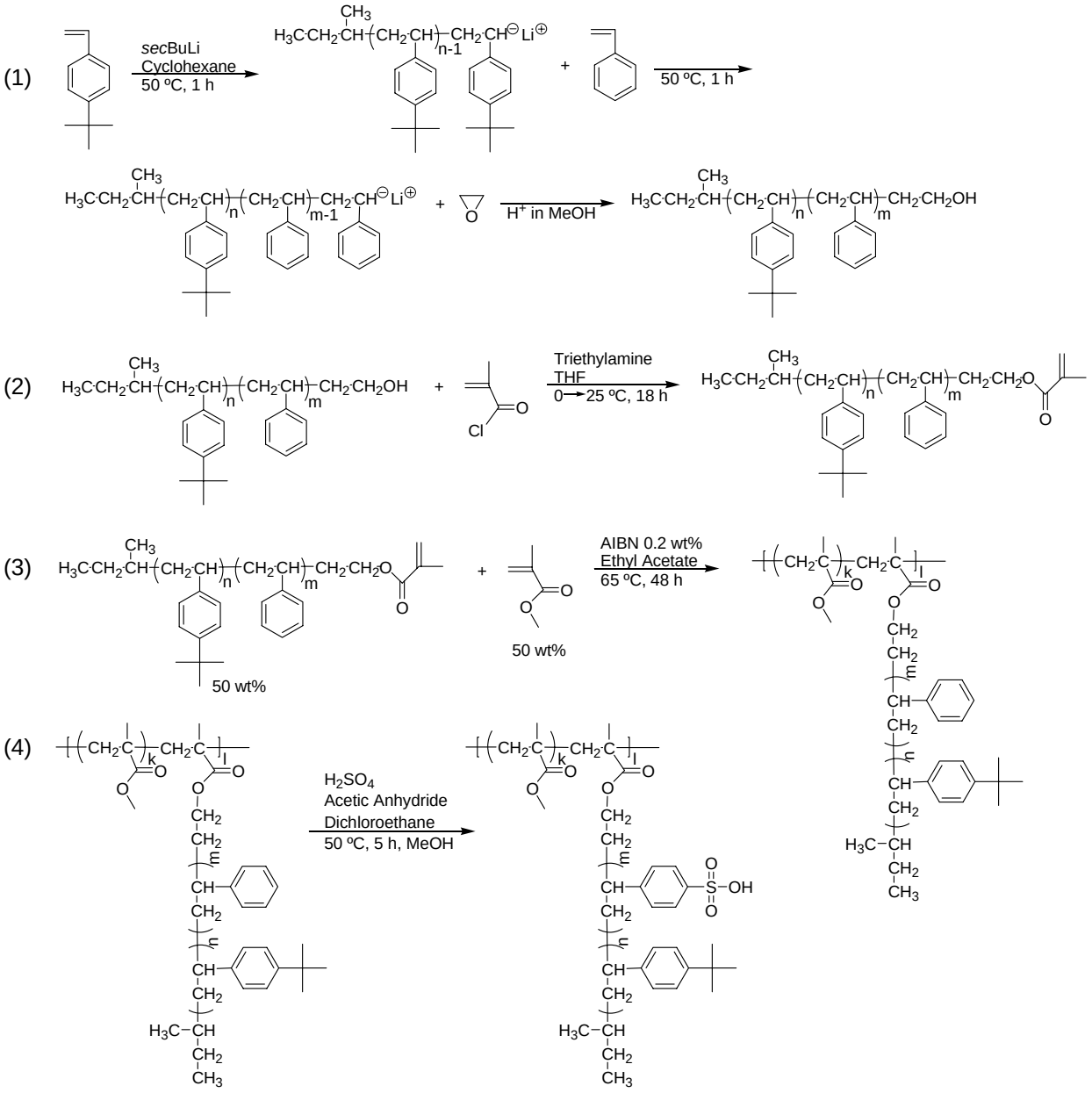


**Scheme 6.1** Synthesis of selectively-sulfonated graft copolymers, (1) synthesis of γ-hydroxy-poly(*tert*-butyl styrene-*b*-styrene (P*t*BS-*b*-PS-OH), (2) reaction of P*t*BS-*b*-PS-OH with methacryloyl chloride, (3) graft copolymerization of methyl methacrylate with the methacrylate macromonomer, (4) sulfonation of the graft copolymers

### 6.3.3 Functionalization of Hydroxy-terminated Diblock Copolymers to Methacrylate Macromonomers

γ-hydroxy-poly(*tert*-butyl styrene-*block*-styrene) (36.60 g) was dissolved in THF (350 mL). Triethylamine (3.014 mL, 18.94 mmol) was syringed into the reaction vessel. After cooling to 0 °C, methacryloyl chloride (1.683 mL, 17.22 mmol) in dry THF (10 mL) was added dropwise. The reaction proceeded for 18 h with warming to room temperature. The macromonomer was precipitated into isopropyl alcohol, and the recovered copolymer was dried at 50 °C in vacuum for 24 h (Scheme 6.1 (2)). $^1$H NMR (400 MHz, $CDCl_3$, δ): 0.6 – 0.8 ppm (br, C*H*$_3$CH$_2$CH(C*H*$_3$)-), 0.9 – 2.5 ppm (br, -C*H*$_2$-, -CH$_2$C*H*-, -C(C*H*$_3$)$_3$, CH$_2$=C(C*H*$_3$)-), 3.7 – 4.1 ppm (br, -CH$_2$C*H*$_2$OCO-), 5.5 ppm (d, $J$ = 17.2 Hz, CH*H*$_{trans}$=C(C*H*$_3$)-), 5.9 ppm (d, $J$ = 17.2 Hz, CH*H*$_{cis}$=C(C*H*$_3$)-), 6.0 – 7.3 ppm (br, aromatic protons in polystyrene and poly(*t*-butyl styrene) units).

### 6.3.4 Graft Copolymerization of Methacrylate Macromonomers with Methyl Methacrylate

Methacrylate macromonomer (10.1 g), methyl methacrylate (10.737 mL, 10.1 g) and AIBN (40.2 mg) were dissolved in ethyl acetate (90 mL). Nitrogen was bubbled through the solution for 10 min. The reaction proceeded for 48 h at 65 °C (Scheme 6.1 (3)). The graft copolymer was precipitated into methanol. The precipitated graft copolymer was filtered and dried at 100 °C in vacuum for 24 h. The graft copolymers, poly(methyl methacrylate)-*g*-(polystyrene-*b*-poly(*tert*-butyl styrene) (PMMA-*g*-PS-*b*-P*t*BS) and poly(methyl methacrylate)-*g*-(poly(*tert*-butyl styrene)-*b*-polystyrene) (PMMA-*g*-P*t*BS-*b*-PS), were separated from residual methacrylate macromonomer via cyclohexane extraction for 3 days. $^1$H NMR (400 MHz, $CDCl_3$, δ): 0.6 – 0.8 ppm (br, C*H*$_3$CH$_2$CH(C*H*$_3$)-), 0.9 – 2.5 ppm (br, -C*H*$_2$-, -CH$_2$C*H*-, -C(C*H*$_3$)$_3$, -C(C*H*$_3$)-), 3.4 – 3.9

ppm (br, -$CH_2CH_2OCO$-, $CH_3OCO$-), 6.0 – 7.3 ppm (br, aromatic protons in polystyrene and poly(*t*-butyl styrene) units).

### 6.3.5 Selective Sulfonation and $Na^+$ Neutralizaton of Graft Copolymers

2.5 M acetyl sulfate solution was generated via the sequential addition of sulfuric acid (9.3 mL, 0.175 mol) and acetic anhydride (18.9 mL, 0.200 mol) in dichloroethane (41.8 mL) at 0 °C.[20-27] PMMA-*g*-PS-*b*-P*t*BS (10.5 g) was dissolved in dichloroethane (75.0 mL). Nitrogen was bubbled through the solution for 10 min. The reaction scheme is shown in Scheme 6.1 (4). The reactor was maintained at 50 °C and the acetyl sulfate solution (27.1 mL, 2.5 M in dichloroethane) was slowly added. The reaction was allowed to proceed for 5 h at 50 °C until methanol was added to terminate the reaction. The poly(styrene sulfonic acid)-containing graft polymer was first precipitated in a 1:1 mixture of methanol and water, filtered, re-dissolved in THF, and then precipitated into water. The precipitation and recovery were repeated at least three times. The dried sulfonic acid-containing graft polymer was re-dissolved in THF and the acid groups were neutralized with one equivalent of NaOH solution (1 mol/L). The product polymer was isolated by precipitation into hot water.

### 6.3.6 Polymer Characterization

$^1$H NMR spectra of the polymers were obtained on a Varian Unity spectrometer operating at 400 MHz at ambient temperature. Deuterated chloroform (Cambridge Isotope Laboratories) was used as the solvent. Size exclusion chromatography (SEC) measurements were performed in THF at 40 °C at flow rate 1 mL/min using a Waters size exclusion chromatograph equipped with an autosampler, three in-line 5 μm PLgel Mixed-C columns, a Waters 410 refractive index (RI) detector operating at 880 nm, and a

miniDAWN multiangle laser light scattering (MALLS) detector operating at 690 nm which was calibrated with narrow polydispersity polystyrene standards. The RI increment (dn/dc) was calculated online. All reported weight-average molecular weights are absolute molecular weights, which were obtained using the MALLS detector. Glass transition temperatures were determined using a differential scanning calorimeter (DSC) Q200 (TA instruments) at a heating rate of 10 °C/min under nitrogen. Glass transition temperatures are reported as the onset and the transition midpoint during the second heat.

### 6.3.7 Morphological Characterization

Solvent cast films of the graft polymer precursors and the sulfonic acid graft copolymers were prepared from 5 wt% solutions of the polymer in toluene. The solutions were covered to slow solvent evaporation, and films formed over a period of 20 days. Solvent cast films of the sodium sulfonate graft copolymers were prepared from 5 wt% polymer MeOH/THF (50/50) solution, and film formation occurred over a period of 2 days. The sodium sulfonate graft copolymers are insoluble in THF and a polar protic solvent needed to be added. The highest solubility of sodium sulfonate graft copolymers were observed in MeOH/THF (50/50). Thin sections of the graft copolymer films (~ 50 nm) were prepared for TEM by embedding the bulk films in epoxy and ultramicrotoming using a Leica EM-FCS microtome at room temperature. Only the unsulfonated samples were able to be sectioned. The sections were then stained 4 h in $OsO_4$ vapor. TEM was performed using a JEOL 200CX TEM operated at an accelerating voltage of 120 kV. SAXS data were collected with a customized pinhole collimated 3 m camera. X-rays were generated with a Rigaku Ultrax18 rotating Cu anode generator operated at 45 kV and 100 mA, then filtered with Ni foil to select the $Cu_{K\alpha}$ doublet ($\lambda$ = 1.542 Å). Two-

dimensional data sets were collected using a Molecular Metrology multi-wire area detector, located approximately 150 cm from the sample. The raw data were corrected for absorption and background noise, then azimuthally averaged. The corrected data were placed on an absolute scale using a sample of type-2 glassy carbon previously calibrated at the Advanced Photon Source, Argonne National Laboratory.

All data reduction and analysis was performed using Igor Pro v5.04B from Wavemetrics, Inc. The features in the scattering data were analyzed by fitting a multivariate model to the data using the least squares analysis tool in Igor Pro. Bragg diffraction maxima were modeled as Lorentzian (Cauchy) distributions with three variables (amplitude, position, and width). Background functions were usually the sum of a constant (one variable) and a power law (two variables), although for determining peak positions of strong maxima, a linear background function may have been used. Ionomer scattering maxima were fit using the Yarusso-Cooper model with four independent variables, as discussed below. For complex combinations of functions, rather than letting all variables be minimized independently, sections of the data were fitted separately to obtain starting values for subsequent analyses. Where higher order Bragg diffraction maxima were present, the starting values for the distribution centers were taken as the corresponding multiple of the primary Bragg diffraction peak center.

## 6.4 Results and Discussion

### 6.4.1 Synthesis of Methacrylate Macromonomers

Hydroxy-terminated poly(*tert*-butyl styrene-*b*-styrene) (P*t*BS-*b*-PS-OH) and hydroxy-terminated poly(styrene-*b*-*tert*-butyl styrene) (PS-*b*-P*t*BS-OH), containing 1000

g/mol polystyrene block and 9000 g/mol poly(*tert*-butyl styrene) block were synthesized via living anionic polymerization and end-capping of the living styryl anions with ethylene oxide. The structural characterization of the diblock copolymers are summarized in Table 6.1. Molecular weights ($M_n$ from NMR and SEC) of the diblock copolymers ranged from 9500 - 10300 g/mol with narrow molecular weight distributions ($M_w/M_n$) 1.07 – 1.10. Based on the integration of the $^1$H NMR resonance for the methylene adjacent to the hydroxyl at 3.2 – 3.4 ppm to the integration of the $^1$H NMR resonance for the two methyls in the s*ec*-butyl fragment at 0.6 - 0.8 ppm, 100 % endcapping to the terminal hydroxyl group was obtained for all diblock copolymers. The hydroxyl end-groups of the diblock copolymers (P*t*BS-*b*-PS-OH and PS-*b*-P*t*BS-OH) were reacted with methacryloyl chloride to produce methacrylate macromonomers (P*t*BS-*b*-PS-methacrylate and PS-*b*-P*t*BS-methacrylate). Conversion of hydroxyl groups to methacrylate groups ranged from 80 – 87 % based on the analysis of the shift of the alcohol methylene resonance at 3.2 – 3.4 ppm to ester methylene resonance at 3.7 – 4.1 ppm. Thus, the functionality of the methacrylate macromonomers was 0.80 – 0.87.

**Table 6.1** Properties of hydroxy-terminated poly(*tert*-butyl styrene-*b*-styrene) and poly(styrene-*b*-*tert*-butyl styrene)

| | $M_n$[a] | $M_n$[b] | $M_n$ PS[a] | $M_n$ PS[b] | $M_w/M_n$[b] | EO-endcapping [%] |
|---|---|---|---|---|---|---|
| P*t*BS-*b*-PS-OH | 9740 | 9670 | 1020 | 1790 | 1.10 | 100 |
| PS-*b*-P*t*BS-OH | 10300 | 10200 | N/A | 915 | 1.07 | 100 |

[a] $^1$H NMR conditions; Varian Unity 400 MHz, $CDCl_3$
[b] Determined using SEC at 40 °C in THF with a MALLS detector

### 6.4.2 Graft Copolymerization of Methacrylate Macromonomer with MMA and Subsequent Sulfonation of Polystyrene Blocks

Graft copolymerization of methacrylate macromonomer with MMA via free radical copolymerization was performed. The results are summarized in Table 6.2.

Sample A has polystyrene blocks adjacent to the PMMA backbone, and sample B has polystyrene blocks at the branch terminus. The weight average molecular weights were approximately 200000 g/mol, and the polydispersity indices were near 2.0. Representative SEC traces of a graft copolymer and a macromonomer are shown in Figure 6.2. All SEC results showed a monomodel signal, indicating that the cyclohexane extraction quantitatively removed residual macromonomer. Isolated yields were 60 – 66 % and based on final composition, macromonomer conversion was 43 – 56 %. In the $^{1}$H NMR spectrum of the graft copolymers, integrations of the aromatic region (6.0 – 7.3 ppm) and methyl esters in PMMA (3.4 – 3.9 ppm) determined the molar ratio of PMMA to macromonomer. Based on the polymer composition from $^{1}$H NMR and molecular weight of the graft copolymers using SEC, an average number of branches ($\lambda$) of the graft copolymers were calculated and listed in Table 6.2. The graft copolymers contained 9 - 10 branches on average. The wt% and the volume fractions of polystyrene (PS) block in the graft copolymers were approximately 4 wt% and 0.04, respectively.

Site-specific sulfonation of PS blocks with acetyl sulfate solution was performed and the sulfonic acid content was determined via acid-base titration. All graft copolymers were 100 % sulfonated of the polystyrene block based on titration results. Thus, approximately 4 wt% of the graft copolymer was precisely sulfonated as shown in Figure 1. The sulfonic acid graft copolymers, poly(methyl methacrylate)-*g*-(sulfonated polystyrene-*b*-poly(*tert*-butyl styrene)) (PMMA-*g*-SPS-*b*-P*t*BS) and poly(methyl methacrylate)-*g*-(poly(*tert*-butyl styrene)-*b*-sulfonated polystyrene) (PMMA-*g*-P*t*BS-*b*-SPS), were successfully synthesized. Finally, a portion of the sulfonic acid graft copolymers, both PMMA-*g*-SPS-*b*-P*t*BS (A) and PMMA-*g*-P*t*BS-*b*-SPS (B) were

neutralized with NaOH to produce sodium sulfonate graft copolymers, poly(methyl methacrylate)-*g*-(sodium sulfonate polystyrene-*b*-poly(*tert*-butyl styrene) (PMMA-*g*-NaSPS-*b*-P*t*BS) and poly(methyl methacrylate)-*g*-(poly(*tert*-butyl styrene)-*b*-sodium sulfonate polystyrene) (PMMA-*g*-P*t*BS-*b*-NaSPS). The equivalent weight (EW) of PMMA-*g*-SPS-*b*-P*t*BS (A) and PMMA-*g*-P*t*BS-*b*-SPS (B), which is defined as the weight of polymer per mole of sulfonic acid groups, was estimated to be approximately 2200 g/mol (A) and 2700 g/mol (B), respectively, although the distribution of ionic species in these samples is not random and the EW measure is not very helpful in describing the salient characteristics of these block-specific sulfonated copolymers. Ion exchange capacity was determined as 0.36 meq/g (A) and 0.33 meq/g (B), respectively.

Non-sulfonated graft copolymers, sulfonic acid graft copolymers, and sodium sulfonate graft copolymers were characterized using DSC, SAXS, and TEM and the influence of relative location of sulfonated blocks in the graft copolymer architecture will be discussed. For simplicity, non-sulfonated graft copolymers A and B will be referred to $A_G$ and $B_G$, sulfonic acid graft copolymers will be referred to $A_H$ and $B_H$, and sodium sulfonate graft copolymers will be referred to $A_{Na}$ and $B_{Na}$.

**Table 6.2** Properties of graft copolymers

| | Number of branches λ | PMMA [wt%] | P*t*BS [wt%] | PS [wt%] | PMMA *f* | P*t*BS *f* | PS *f* | $M_w$ [a] | $M_w/M_n$ [a] |
|---|---|---|---|---|---|---|---|---|---|
| A | 9 | 58.0 | 37.9 | 4.1 | 0.53 | 0.43 | 0.04 | 176000 | 2.22 |
| B | 10 | 54.0 | 42.2 | 3.8 | 0.49 | 0.47 | 0.04 | 234000 | 1.86 |

*f*: volume fraction

[a] Determined using SEC at 40 °C in THF with a MALLS detector

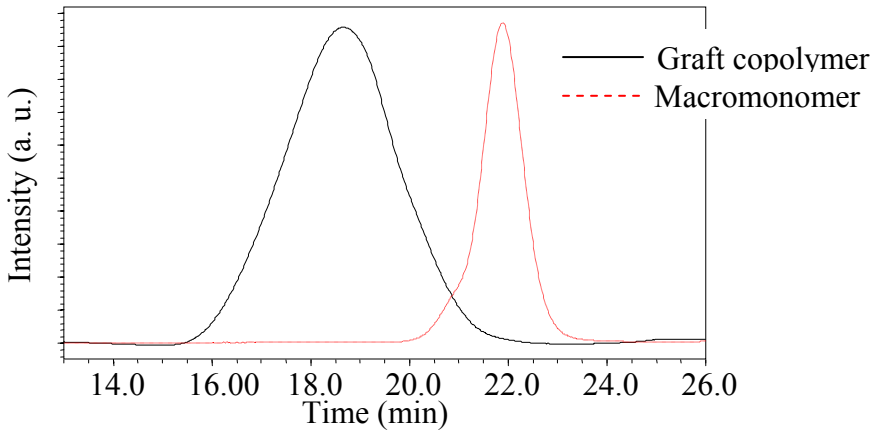


**Figure 6.2** SEC traces of a graft copolymer, PMMA-*g*-P*t*BS-*b*-PS and a macromonomer, PS-*b*-P*t*BS-methacrylate
SEC conditions: at 40 °C in THF with RI and MALLS detector

### 6.4.3 Thermal Characterization

Glass transition temperatures ($T_g$) of PMMA-*g*-PS-*b*-P*t*BS ($A_G$), PMMA-*g*-P*t*BS-*b*-PS ($B_G$), PMMA-*g*-SPS-*b*-P*t*BS ($A_H$), PMMA-*g*-P*t*BS-*b*-SPS ($B_H$), PMMA-*g*-NaSPS-*b*-P*t*BS ($A_{Na}$), and PMMA-*g*-P*t*BS-*b*-NaSPS ($B_{Na}$) are shown in Table 6.3. All the $T_g$s were determined from the second heating cycle at 10 °C/min. Some of the samples upon the first heating cycle provided two transitions, which were consistent with $T_g$s of PMMA and P*t*BS. All graft copolymers had a single $T_g$ in the second heating cycle. This suggested that the rapid cooling rate in DSC did not provide sufficient time for microphase separation to occur. Graft copolymers with immiscible blocks such as poly(vinyl acetate)-*g*-poly(dimethylsiloxane) and poly(vinyl acetate)-*g*-polystyrene[5] typically exhibit a $T_g$ for each block. However, the graft copolymers with low $\chi$ value blocks such as poly(*n*-butyl acrylate)-*g*-polystyrene have been reported to show a single $T_g$.[28]

The Gordon-Taylor equation (equation 6-1) was used to predict the $T_g$ of the graft copolymers. The reference $T_g$s of poly(methyl methacrylate), poly(*t-butyl* styrene) and

polystyrene were 120 °C, 145 °C, and 100 °C, respectively.[29] The $T_g$s and the weight fractions of each block in Table 2 were inserted into the Gordon-Taylor equation:

$$\frac{1}{T_g} = \frac{w_{PMMA}}{T_{g,PMMA}} + \frac{w_{PtBS}}{T_{g,PtBS}} + \frac{w_{PS}}{T_{g,PS}} \quad (6\text{-}1)$$

The calculated $T_g$s of $A_G$ and $B_G$ were 127 °C and 128 °C, respectively. These $T_g$s agreed with the experimentally determined $T_g$s of $A_G$ and $B_G$, reported in Table 6.3, suggesting that microphase separation did not occur, resulting in a single glass transition in the second heating cycle.

The $T_g$ values of the sulfonated graft copolymer with sulfonated blocks at the branch terminus ($B_H$ and $B_{Na}$) were higher than the $T_g$ values with sulfonated blocks adjacent to the backbone ($A_H$ and $A_{Na}$). The $T_g$ for the PS block in sulfonated polystyrene block copolymer generally increases with the increase of the degree of the sulfonation (DS).[30-32] For example, the $T_g$ of the sulfonated polystyrene segment of sulfonated poly(styrene-*b*-[ethylene-*co*-butylene]-*b*-styrene) was reported to increase from 82 to 92 °C when DS increased from 2.8 to 14.3%.[30] The $T_g$ of SPS block of sulfonated poly([vinylidene difluoride-*co*-hexafluoropropylene]-*b*-styrene) increased from 86 to 166 °C when DS increased from 0 to 40%.[32] The increase of $T_g$ is associated with ion content and the ionomeric effect. Small regions of restricted mobility are known to act as physical crosslinks and raise $T_g$.[31, 33] In this study, the relative location of the sulfonated block was presumed to affect $T_g$ values since the sulfonated graft copolymers possessed similar DS. The higher $T_g$ values of $B_H$ and $B_{Na}$ suggested that the sulfonated blocks at the branch terminus more easily formed ionic interactions. The mobility of the sulfonated blocks on the branch terminus of $B_H$ and $B_{Na}$ presumably enabled more sulfonated blocks to interact and produce ionic aggregates. The sulfonated blocks on the

graft branches of $A_H$ and $A_{Na}$ were presumed to be less mobile due to the adjacent backbone and P*t*BS segments, preventing dense ionic associations to occur.

**Table 6.3** Glass transition temperatures ($T_g$) of PMMA-*g*-PS-*b*-P*t*BS ($A_G$), PMMA-*g*-P*t*BS-*b*-PS ($B_G$), PMMA-*g*-SPS-*b*-P*t*BS ($A_H$), PMMA-*g*-P*t*BS-*b*-SPS ($B_H$), PMMA-*g*-NaSPS-*b*-P*t*BS ($A_{Na}$), and PMMA-*g*-P*t*BS-*b*-NaSPS ($B_{Na}$)

| | $T_g$ (onset) [°C] | $T_g$ (midpoint) [°C] |
|---|---|---|
| $A_G$ | 122 | 130 |
| $B_G$ | 123 | 130 |
| $A_H$ | 122 | 131 |
| $B_H$ | 128 | 136 |
| $A_{Na}$ | 129 | 142 |
| $B_{Na}$ | 135 | 151 |

DSC conditions; TA instrument Q 200, 10 °C/min second heat

### 6.4.4 Morphological Characterization

It has been reported that the constituting unit of a graft copolymer, rather than the entire polymer, controls the morphological behavior of graft copolymers[5-7, 34, 35] Phase behavior of graft copolymer systems depends on the volume fraction of the component and $\chi N/\lambda$, where $\chi$ is Flory-Huggins interaction parameter, $N$ is the total degree of polymerization, and $\lambda$ is the number of branches per graft copolymer.[5] As discussed in Chapter 2, The values of $\chi$ were estimated from the molar volumes and the polymer solubility parameters via equation 2-4:

$$\chi_{12} = \frac{V_0(\delta_2 - \delta_1)^2}{RT} \qquad (2\text{-}4)$$

where $V_0$ is the molar volume, $\delta_1$ and $\delta_2$ the solubility parameters of the respective polymer components, $R$ the gas constant, and $T$ the temperature. $V_0$ was calculated from $V_0 = (V_1 V_2)^{1/2}$ where $V_1$ and $V_2$ are the molar volumes of the respective components.[5] The molar volumes of PMMA, P*t*BS, PS, and SPS are 85.6 $cm^3$/mol, 168.7 $cm^3$/mol, 99.0 $cm^3$/mol,[36] and 129.1 $cm^3$/mol,[36] respectively, where the molar volume for SPS was

calculated using addition principle of the group contributions and the atomic contributions.[36] The solubility parameters of PMMA, P*t*BS, PS, and SPS are 18.27 $(J/cm^3)^{1/2}$,[29] 16.60 $(J/cm^3)^{1/2}$,[29] 18.66 $(J/cm^3)^{1/2}$,[29] and 33.96 $(J/cm^3)^{1/2}$,[37, 38] respectively, where the solubility parameter for P*t*BS was calculated using addition principle of the molar attraction constant.[29] The calculated $\chi$ values at $T$ = 298 K are summarized in Table 6.4. The large difference of the solubility parameters between SPS and the other components led to very large values of $\chi_{PMMA/SPS}$ and $\chi_{PtBS/SPS}$. This trend agreed well with the trend of $\chi_{PS/SPS}$ in the literature,[39, 40] although the calculation of $\chi$ value with ionic interaction may not represent the exact value of $\chi$. Beck Tan et al. reported $\chi_{PS/SPS}$ was at least 5.6[39] and Winey et al. concluded $\chi_{PS/SPS}$ was always greater than 25.[40] The calculated results for $\chi N/\lambda$ of the PMMA-*g*-PS-*b*-P*t*BS ($A_G$), PMMA-*g*-P*t*BS-*b*-PS ($B_G$), PMMA-*g*-SPS-*b*-P*t*BS ($A_H$), and PMMA-*g*-P*t*BS-*b*-SPS ($B_H$) at 298 K are tabulated in Table 6.5. In $A_G$ and $B_G$, PMMA/P*t*BS and P*t*BS/PS phases possess $\chi N/\lambda$ = 13.4 – 25.5, within the weak segregation limit, whereas the $\chi N/\lambda$ = 0.63 and 0.79 of PMMA/PS phase is too low to cause microphase separation. Disordered microphase separated morphologies were expected for $A_G$ and $B_G$ since PMMA and P*t*BS were the dominant components, with volume fraction PMMA 0.49 – 0.53 and P*t*BS 0.43 – 0.47 which are shown in Table 2. On the other hand, extremely large $\chi N/\lambda$ values of PMMA/SPS and P*t*BS/SPS phases in $A_H$ and $B_H$ suggested that introduction of sulfonic acid groups would lead to very strong phase separation. The extent of the microphase separation and the morphologies of these graft copolymers were characterized using SAXS and TEM.

**Table 6.4** $\chi$ values for the each components between PMMA, PS, P*t*BS and SPS at $T$ = 298 K

| $\chi_{PMMA/PS}$ | $\chi_{PMMA/PtBS}$ | $\chi_{PtBS/PS}$ | $\chi_{PMMA/SPS}$ | $\chi_{PtBS/SPS}$ |
|---|---|---|---|---|
| 0.00565 | 0.135 | 0.221 | 10.4 | 18.0 |

**Table 6.5** Estimation of $\chi N/\lambda$ values for the PMMA-*g*-PS-*b*-P*t*BS ($A_G$), PMMA-*g*-P*t*BS-*b*-PS ($B_G$), PMMA-*g*-SPS-*b*-P*t*BS ($A_H$), and PMMA-*g*-P*t*BS-*b*-SPS ($B_H$) at $T$ = 298 K

| | $\chi_{PMMA/PS}N/\lambda$ | $\chi_{PMMA/PtBS}N/\lambda$ | $\chi_{PtBS/PS}N/\lambda$ | $\chi_{PMMA/SPS}N/\lambda$ | $\chi_{PtBS/SPS}N/\lambda$ |
|---|---|---|---|---|---|
| A | 0.63 | 20.9 | 13.4 | 1173 | 1622 |
| B | 0.79 | 25.5 | 14.7 | 979 | 1193 |

SAXS is a powerful tool for determining the long-range structure within polymeric structures.[41, 42] Scattering of X-rays by ordered structures generates data in the form of a Fourier transform of the morphology of the sample, and while the loss of morphological information due to the squaring of the scattering amplitude function requires the collection of additional morphological information to draw definitive conclusions, the ability to examine a large sample volume makes SAXS an appealing technique for characterizing bulk morphology. SAXS is an appropriate characterization technique to observe the influence of relative location of sulfonated blocks with constant sulfonation level, 4 wt%, in the sulfonated graft copolymers.

SAXS data for graft copolymers ($A_G$ and $B_G$) that were prepared from 5 wt% solutions of the polymer in toluene are shown in Figure 6.3. Absolute scattering intensity was plotted versus the magnitude of the scattering vector, $q$, where $q = 2\pi \cdot \sin(\theta)/\lambda$, and $2\theta$ is the scattering angle. The Bragg spacings, d, were calculated from the primary Bragg maxima as $d = 2\pi/q$ and are listed in Table 6.6. The data for sample $A_G$ clearly show multiple Bragg reflections, evidence of long-range morphological order. For $A_G$, the ratio $q_1:q_2:q_3$ was approximately 1:2:3, consistent with the expected lamellar morphology. The SAXS data for $B_G$ exhibited a very weak increase in scattered intensity at $q \approx 2 \cdot q_1$ (as indicated by the red arrow in Figure 6.3), implying that a very poorly formed lamellar morphology might be present. It should be noted that these films were prepared with a very slow evaporation rate (20 days) to obtain morphologies more

equilibrium in character. The SAXS data for $A_G$ and $B_G$, which were cast quickly from THF, each showed only a single scattering maximum. The lack of higher order reflections from THF cast films proved that the slow film formation process promoted self-assembly.

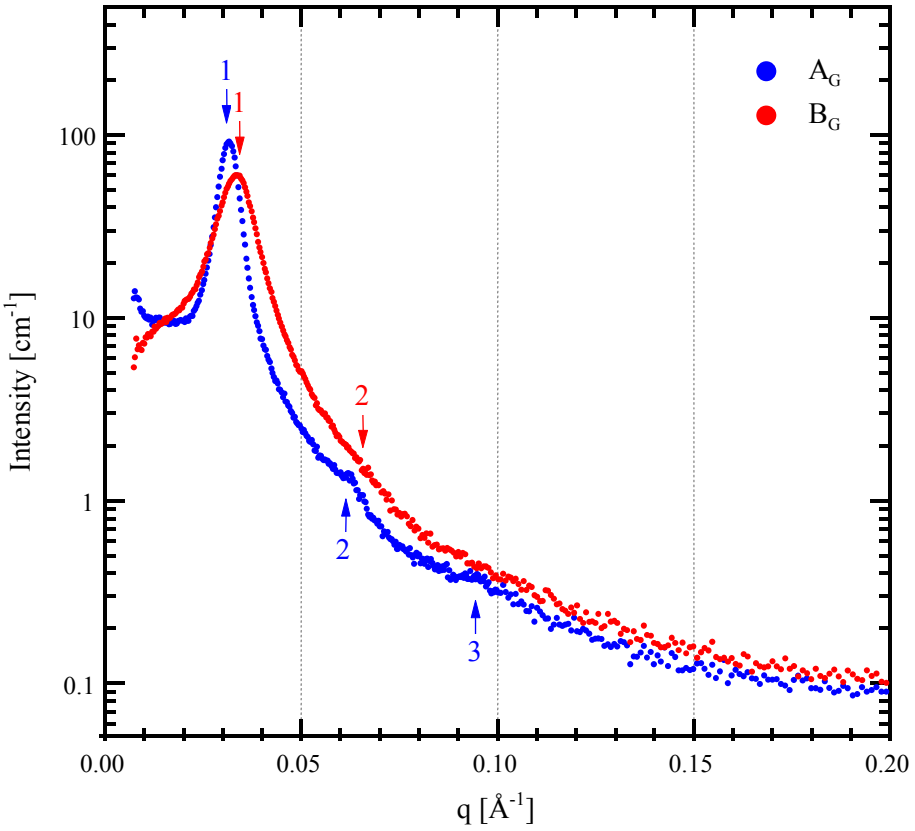


**Figure 6.3** SAXS profiles for PMMA-*g*-PS-*b*-P*t*BS ($A_G$) and PMMA-*g*-P*t*BS-*b*-PS ($B_G$)

**Table 6.6** Physical properties of graft copolymers, sulfonic acid and sodium sulfonated graft copolymers investigated in SAXS

| | $q_1$ maxima (= q*) [$Å^{-1}$] | q/q* | d [nm][a] | Morphology |
|---|---|---|---|---|
| $A_G$ | 0.0316 | 1,2,3 | 19.9 | Lamellar |
| $B_G$ | 0.0334 | 1,2 | 18.8 | Lamellar |
| $A_H$ | 0.0279 | 1,2 | 22.5 | Lamellar |
| $B_H$ | 0.0310 | 1,2 | 20.2 | Lamellar + Ionic Aggregates |
| $A_{Na}$ | 0.0413 | 1,2 | 15.2 | Lamellar |
| $B_{Na}$ | 0.0397 | 1 | 15.8 | Ionic Aggregates |

[a]Primary SAXS reflection, $d = 2\pi/q^*$

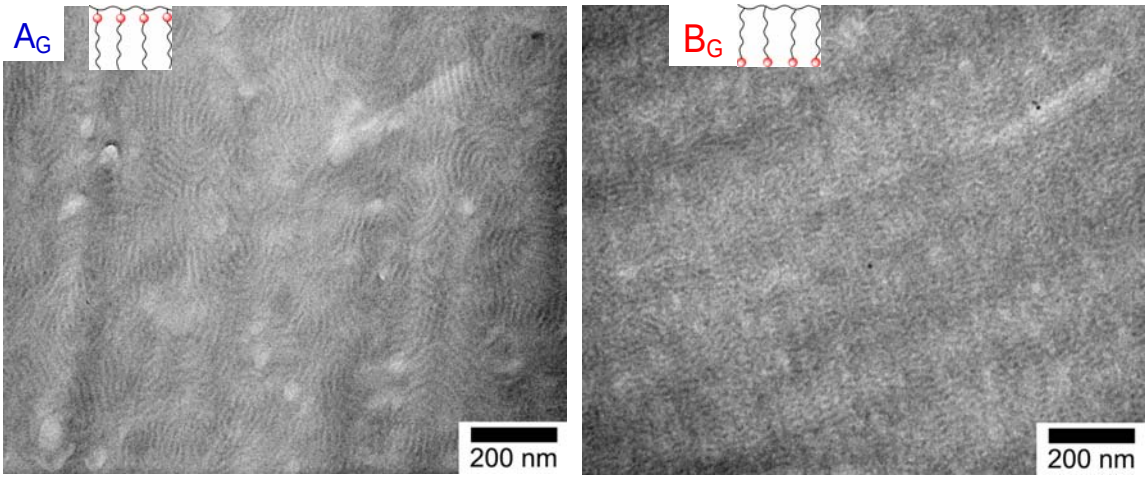


**Figure 6.4** TEM micrographs of PMMA-*g*-PS-*b*-P*t*BS ($A_G$) and PMMA-*g*-P*t*BS-*b*-PS ($B_G$)

Figure 6.4 shows TEM micrographs from samples $A_G$ and $B_G$. The micrograph of $A_G$ shows a lamellar morphology with both domains having approximately equal thicknesses. TEM micrograph of $B_G$ shows microphase separation into a poorly ordered morphology in which some regions appear to have a lamellar character. These observations from TEM are in agreement with the analysis of the SAXS data in Figure 6.3. The lamellar periods of $A_G$ and $B_G$ from TEM micrographs are approximately $17(\pm 2)$ and $16(\pm 2)$ nm, respectively. The lamellar spacings are in good agreement with the Bragg spacings, given in Table 6.6, as determined from the SAXS data. PMMA and P*t*BS blocks should have a dominant contribution to the morphology and the expected morphology would be lamellar based on the volume fraction of PMMA and P*t*BS, 0.43 – 0.53 in Table 3 and $\chi_{PMMA/PtBS}N/\lambda$, 20.9 or 25.5 in Table 6.5. $\chi_{PMMA/PtBS}N/\lambda$ = 20.9 or 25.5 large enough to possess distinctive microphase separation in comparison with the order-disorder transition boundary for comb copolymers with randomly placed graft junctions, approximately $\chi N/\lambda = 10$.[35]

The different morphological behaviors of $A_G$ and $B_G$ are determined by a balance between relatively weak driving forces for microphase separation and self-assembly. The main difference between $A_G$ and $B_G$ is the location of PS blocks, and because there is a significant difference between the $\chi$ values for the interactions between PS, PMMA, and P*t*BS, this difference in architecture has a critical effect. In the $A_G$ copolymer, because the PS blocks are located adjacent to the PMMA backbone and are nearly miscible with PMMA ($\chi_{PMMA/PS}$ = 0.00565), the strong repulsive forces between P*t*BS and both PS ($\chi_{PtBS/PS}$ = 0.221) and PMMA ($\chi_{PMMA/PtBS}$ = 0.135) combine to dominate the morphological behavior. These interactions push the morphological behavior into the weak segregation regime and a lamellar morphology is formed ($\chi_{PMMA/PtBS}N/\lambda = 20.9$ and $\chi_{PtBS/PS}N/\lambda = 13.4$). In the $B_G$ copolymer, however, the PS is located at the end of the grafts, away from the PMMA backbone, dramatically impeding the ability of the graft copolymer to microphase separate and form an ordered morphology. Although the P*t*BS blocks are strongly immiscible with the PMMA backbone, they are also strongly repelled by the PS blocks at the end of the grafts. Combined with the near miscibility of the PS and PMMA blocks, the formation of microphase separated domains containing both PS and P*t*BS is strongly inhibited. As a result, the morphology of $B_G$, as shown in Figure 6.4, is microphase separated, but with poorly ordered, frustrated lamellar domains.

Sulfonation of these complex graft copolymers further complicates their morphological behavior. SAXS profiles for sulfonic acid graft copolymers ($A_H$ and $B_H$) that were cast from 5 wt% solutions of the polymer in toluene are shown in Figure 6.5. Two Bragg reflections in the SAXS data for $A_H$ indicate that this material retains its lamellar morphology, although with a slight decrease in long-range order. The maxima

positions $q_1$ and $q_2$ and the Bragg spacings, d, are summarized in Table 6. The data for sample $B_H$ show two maxima, but the shape of the second maximum is unusually broad and was not fit well with a single Lorentzian or Gaussian distribution as would be the case for a Bragg reflection. If the angle at which the maximum intensity of the second scattering maximum for $B_H$ is taken as $q_2$, then $B_H$ also exhibits a 2:1 ratio of scattering maxima value, again consistent with the predicted lamellar morphology.

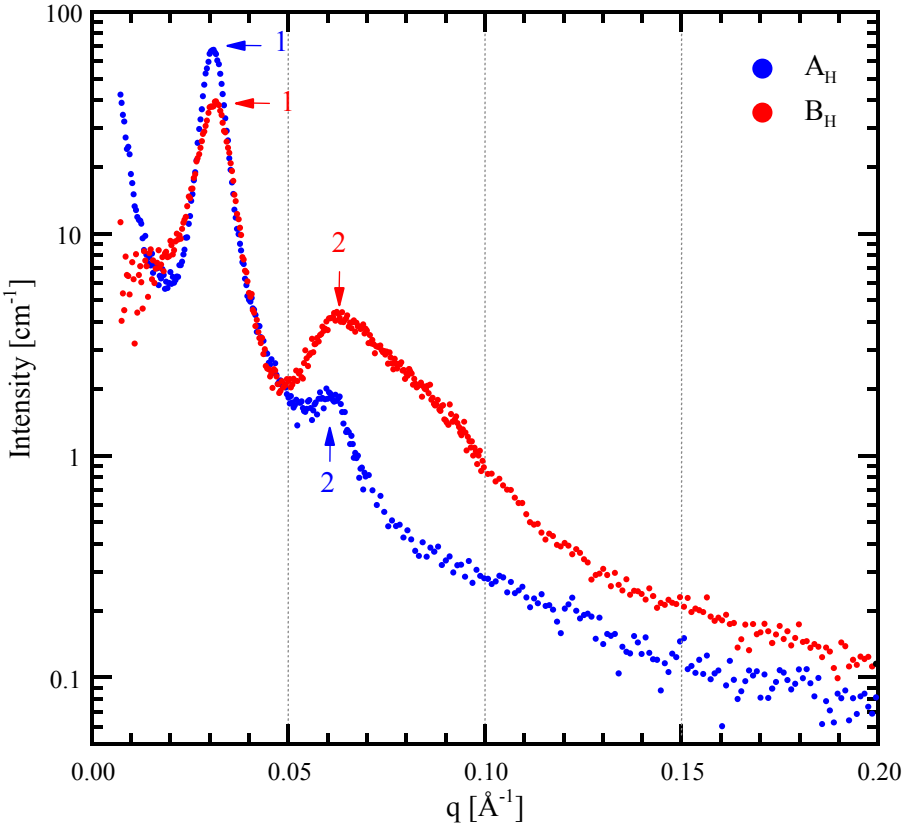


**Figure 6.5** SAXS profiles for sulfonic acid graft copolymers PMMA-*g*-SPS-*b*-P*t*BS ($A_H$) and PMMA-*g*-P*t*BS-*b*-SPS ($B_H$)

Due to the extremely brittle nature of sulfonated samples, TEM data were not obtained. However, for both $A_H$ and $B_H$, the SAXS data (Figure 6.5) show clear and noteworthy differences from that obtained for $A_G$ and $B_G$. In both $A_H$ and $B_H$, the polystyrene sulfonic acid (SPS) blocks comprise only 4 wt% of each graft copolymer,

but due to the strong enthalpic repulsion between the SPS and both PMMA and P*t*BS ($\chi_{PMMA/SPS}$ = 10.4 and $\chi_{PtBS/SPS}$ = 18.0), the morphological behavior as deduced from the SAXS data is significantly altered. First, quick casting from THF was sufficient to produce well-ordered lamellar microphase separation, a marked contrast from the behavior of the THF-cast $A_G$ and $B_G$. Second, for $A_H$, the location of the SPS block at the PMMA backbone has an effect similar to the location of the P*t*BS block at the backbone in $B_G$, creating a situation where the block grafted to the backbone is strongly driven to microphase separate both from the backbone and the end of the graft. In the case of $A_H$, the underlying lamellar morphology of the graft copolymer is only somewhat disrupted, with only two Bragg maxima observed in SAXS, rather than the three maxima observed for $A_G$ (Figure 6.3). Third, the lamellar period of $A_H$ (22.4 nm) is slightly larger than that for $A_G$ (19.6 nm), a natural result of the addition of bulky sulfonic acid groups to the PS block and possibly indicative of water uptake.

The effect of sulfonating the PS block is much more profound for the B architecture ($B_H$). Instead of the single SAXS maximum observed for $B_G$, a large, broad second maximum is observed. The unusual shape of the second maximum in sample $B_H$ was estimated to be a combination of a second-order Bragg reflection, located around $q \approx 2*q_1$, and a third feature in the scattering data. The molecular architecture of this sample, with sulfonated PS blocks at the end of the grafts, makes the formation of ionic aggregates such as those observed in ionomers very likely. SAXS data for such ionomers is characterized by a strong "ionomer peak", usually attributed to interparticle scattering between aggregates of ionic functional groups, and generally fit using the Yarusso-Cooper (YC) model.[43]

The YC model treats the ionic aggregates as spherical particles with an ionic core having radius $R_1$. The ionic aggregates are not allowed to come into contact with each other, using the approach of Guinier and Fournet to include liquid-like ordering of the aggregates in the sample.[42] A shell of restricted mobility with radius $R_{CA}$ defined from the center of each aggregate, where the closest approach distance between two aggregates is $2 \cdot R_{CA}$. The average sample volume per aggregate is defined as $V_p$. In this model, the X-ray scattering intensity is represented by

$$I(q) = I_e(q) V \frac{1}{V_p} V_1^2 \rho_1^2 \Phi^2(qR_1) \frac{1}{1 + \left( \frac{8 V_{CA}}{V_p} \right) \in \Phi(2qR_{CA})} \tag{6-2}$$

$$V_{CA} = \frac{4}{3} \pi R_{CA}^3 \tag{6-3}$$

$$V_1 = \frac{4}{3} \pi R_1^3 \tag{6-4}$$

$$\Phi(x) = 3 \frac{\sin x - x \cos x}{x^3} \tag{6-5}$$

where $I(q)$ is the observed intensity and $I_e(q)$ is the intensity scattered by a single electron under the experimental conditions, $V$ is the volume of the sample, $\rho_1$ is the electron density difference between the matrix and the ionic aggregate, and $\epsilon$ is a constant close to unity. Because $I_e(q)$ can be regarded as a constant, the term $I_e(q) V \rho_1^2$ can be viewed as a single adjustable parameter. Thus, the model has four fitting parameters: $R_1$, $R_{CA}$, $V_p$, and $I_e(q) V \rho_1^2$. By fitting calculated scattering data to the experimental data, one can determine a combination of the four most probable fitting parameters, describing the characteristics of ionic aggregates in the sample.[43-46]

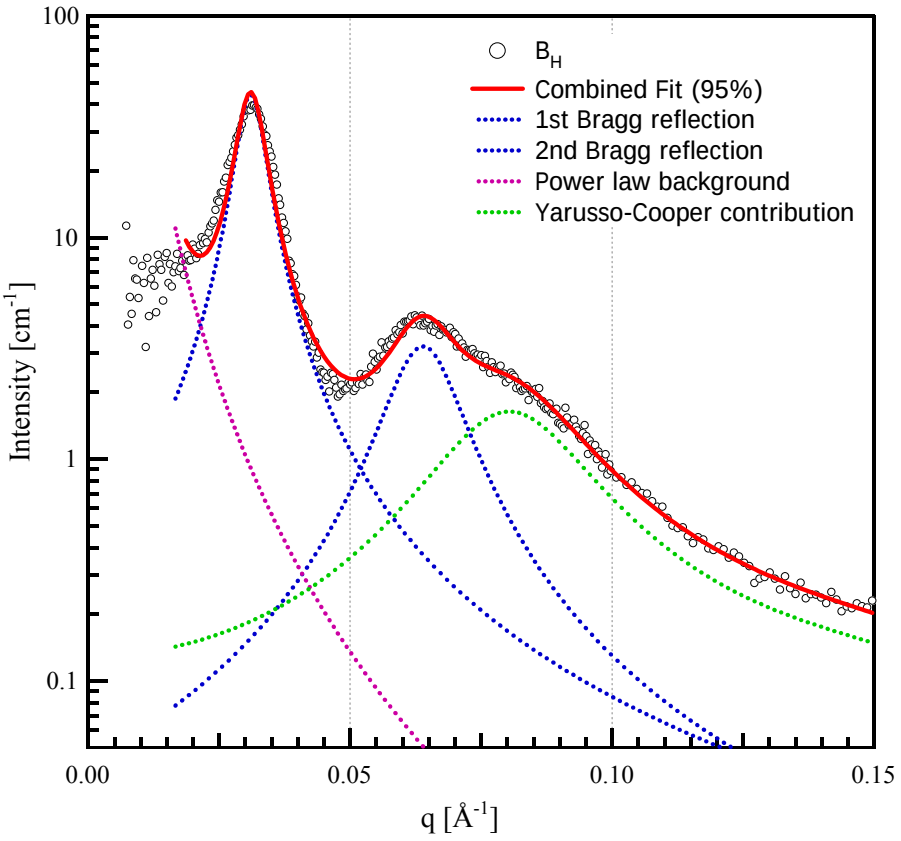


**Figure 6.6** Fitting SAXS ionomer peak of PMMA-*g*-P*t*BS-*b*-SPS($B_H$) to Yarusso-Cooper model

The result of fitting the YC model to the ionomer peak in the SAXS data for PMMA-*g*-P*t*BS-*b*-SPS ($B_H$) is shown in Figure 6.6. Lorentzian distributions were used for the primary Bragg maximum and for a secondary Bragg maximum centered at approximately $2 \cdot q_1$. The significantly diminished intensity of the second order reflection relative to the primary Bragg reflection, in addition to the increase in peak width, is consistent with typical scattering data from lamellar materials with moderate long-range order. The YC model was used to add a contribution from ionic aggregates to the second maximum in the data, which has a shape expanded beyond the second Lorentzian. This approach generated hypothetical scattering data that fit the main features of the SAXS data very well, particularly the slight dip in scattered intensity between $q_2 = 0.06$ Å$^{-1}$ and

q = 0.085 Å$^{-1}$, where the contributions from the second Bragg maximum and the ionomer peak overlap. The YC fitting parameters for the ionomer peak are summarized in Table 6.7.

**Table 6.7** Best-fit parameters of the Yarusso-Cooper model for the ionomer peak

| | $R_1$ (Å) | $R_{CA}$ (Å) | $V_p$ (Å$^3$) | $R_{CA}$ - $R_1$ (Å) | $V_1$ (Å$^3$) | $V_p^{-1}$ (Å$^{-3}$) | $V_1/V_p$ |
|---|---|---|---|---|---|---|---|
| $B_H$ | 19 | 35 | $2.0\times10^5$ | 16 | $2.9\times10^4$ | $4.9\times10^{-6}$ | 0.14 |
| $B_{Na}$ | 30 | 38 | $2.5\times10^5$ | 8 | $1.1\times10^5$ | $4.0\times10^{-6}$ | 0.45 |

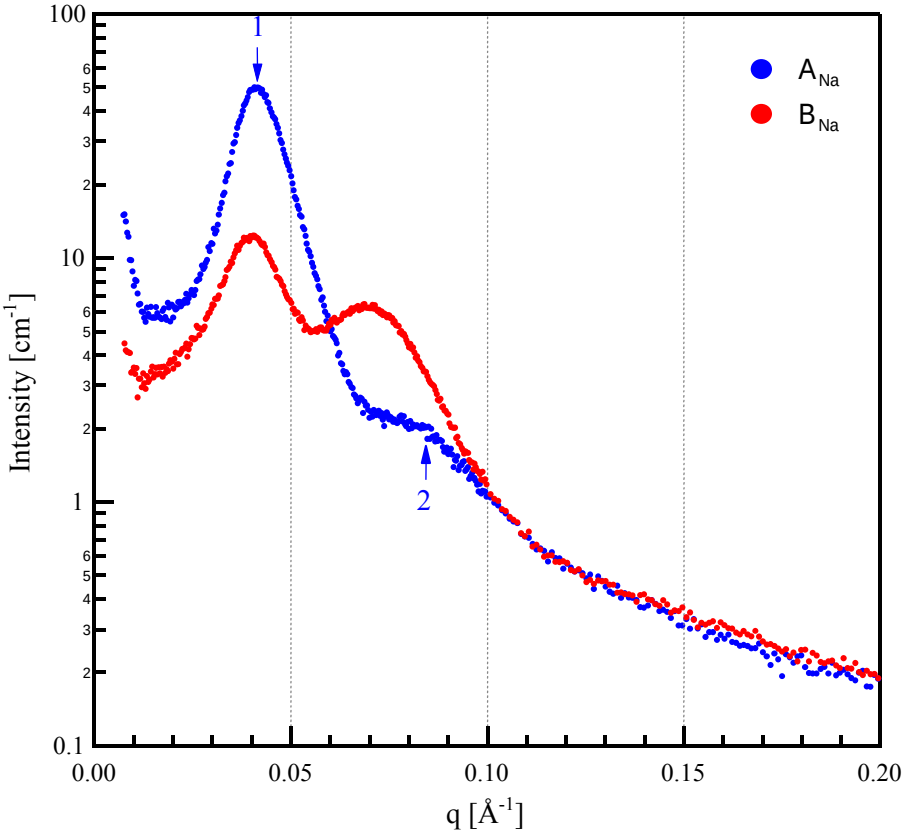


**Figure 6.7** SAXS profiles for sodium sulfonate graft copolymers PMMA-*g*-NaSPS-*b*-P*t*BS ($A_{Na}$) and PMMA-*g*-P*t*BS-*b*-NaSPS ($B_{Na}$) prepared from THF/MeOH

The SAXS data for the sodium sulfonate graft copolymers ($A_{Na}$ and $B_{Na}$), prepared from THF/MeOH solutions, are shown in Figure 6.7. For sample $A_{Na}$ they show multiple Bragg reflections for which the ratio of scattering angles follows $q_1$:$q_2$ = 1:2, indicating a lamellar morphology. When compared to the scattering data for $A_H$, the

peaks for $A_{Na}$ appear to have been broadened by neutralization of the copolymer with sodium, indicating the formation of a less well-ordered microstructure. This observation agrees with Weiss' findings that the SAXS reflections broadened as the ionic interactions increased (i.e., as the cation was changed from $H^+$ to $Zn^{2+}$ to $Na^+$, the morphology became less ordered).[47, 48] The degree of ordering of the block copolymer morphology should depend on the strength of the ion-dipole interactions since the relaxation behavior of the dipolar interactions dictates the local viscosity of the medium.[48] The lamellar periods, *d*, of the sodium sulfonate graft copolymers were only 15.2 nm for $A_{Na}$ and 15.8 nm for $B_{Na}$, significantly less than those measured for either $A_G$ and $B_G$ or the acid forms $A_H$ and $B_H$, confirming that the strong ionic interactions with the $Na^+$ counter ions have a dominant effect on morphology. The change of the Bragg spacings, d upon neutralization derived from shifting scattering maxima in SAXS profiles. The positions of the primary Bragg maxima were shifted to higher q value upon neutralization.

The scattering data for the second sodium neutralized copolymer, $B_{Na}$, does not present scattering data typical of lamellar microphase separated block copolymer morphologies. The second maximum is unusually strong and broad. In addition, a third order reflection is also absent, which would be expected given the intensity of the second order reflection. As was seen for $B_H$, the molecular architecture of this sample, with sulfonated PS blocks at the branch termini, appears to promote the formation of ionic aggregates. Therefore, the same approach used to model the scattering data for $B_{Na}$ was used for $B_H$, where the second maximum was modeled as an ionomer peak using the YC model.

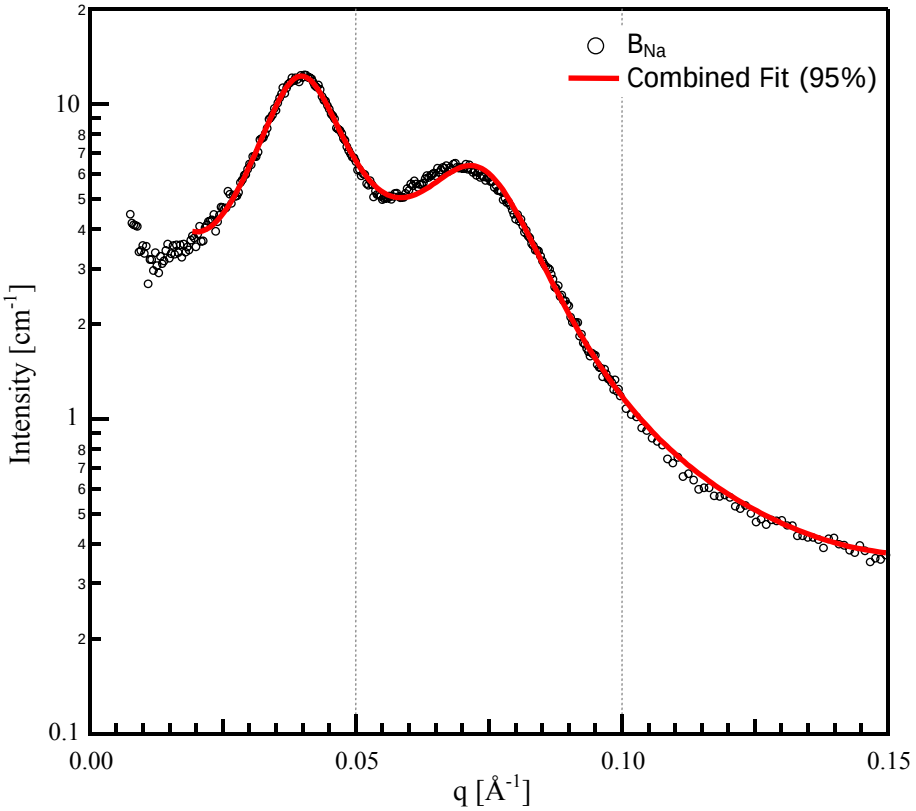


**Figure 6.8** Fitting SAXS ionomer peak of PMMA-*g*-P*t*BS-*b*-SNaPS($B_{Na}$) to Yarusso-Cooper model

The calculated scattering data fit to the SAXS data collected for PMMA-*g*-P*t*BS-*b*-NaSPS ($B_{Na}$) is shown in Figure 6.8. The second maxima (ionomer scattering maxima) were fitted using the YC model. A reasonable fit is obtained when the YC model is used to fit the second maximum while a Lorentzian is used for the primary scattering maximum, supporting the hypothesis that the second maximum is due primarily to the presence of ionic aggregates.

The fitting parameters for $B_{Na}$ from the YC model are summarized in Table 6.7. $R_1$ increases upon neutralization, while $R_{CA}$ remains constant. This leads to a decrease in the thickness of the restricted mobility layer $R_{CA}$ - $R_1$. $V_1$ increased due to the increase of $R_1$, indicating that the size of the ionic aggregates increased upon neutralization. The number density of scattering particles ($1/V_p$) was almost constant. The volume fraction of

aggregates in the sample, $V_I/V_p$ increased upon neutralization. A sodium counter ion is larger than a proton counter ion, which may lead to the increase of $V_I$ and $V_I/V_p$. The increase of the number of sodium sulfonate blocks (the increase of the number of sodium sulfonate graft copolymers) per an aggregate might also lead to the increase of $V_I$ and $V_I/V_p$.

## 6.5 Conclusions

Novel selectively-sulfonated graft copolymers, PMMA-*g*-(SPS-*b*-P*t*BS) and PMMA-*g*-(P*t*BS-*b*-SPS) were successfully synthesized and characterized via DSC, SAXS, and TEM. The graft copolymers contained approximately 9 – 10 branches on average and 4 wt% of sulfonic acid or sodium sulfonate blocks. The location of the sulfonated blocks, either adjacent to the backbone or at the branch termini, was determined from the molecular architecture of the starting graft copolymer. The thermal properties of the site-specific sulfonated graft copolymers were characterized using DSC and a single glass transition temperature was observed. The sulfonated graft copolymer with sulfonated blocks at the branch terminus ($B_H$ and $B_{Na}$) had higher $T_g$ values than those with sulfonated blocks adjacent to the backbone ($A_H$ and $A_{Na}$). The trend of higher $T_g$s indicated that sulfonated graft copolymer B enabled more sulfonated blocks to interact due to the mobility of the sulfonated blocks at the graft ends. SAXS data for the non-sulfonated graft copolymers ($A_G$ and $B_G$), sulfonic acid graft copolymers ($A_H$ and $B_H$), and sodium sulfonate graft copolymers ($A_{Na}$), showed the Braggs reflections indicative of lamellar morphologies. TEM confirmed the lamellar morphology of $A_G$ and lamellar-type morphology of $B_G$. Both $\chi$ and $\chi N/\lambda$ values were used to predict the phase

behavior of the ordered morphologies considering the location of each block. The expected morphologies from $\chi$ and $\chi N/\lambda$ values were consistent with the observed morphologies.

The SAXS data for the sulfonated graft copolymers with the B architecture revealed an ionomer peak whereas the sulfonated graft copolymers with the A architecture did not show evidence of ionic aggregates. The presence of ionomer peaks in the B samples was consistent with the observation of strong ionic interaction in $T_g$ analysis. The scattering from the ionic aggregates was characterized using the YC model. The best-fit parameters via the YC model suggested an increase of the size of the ionic aggregates and decrease of the restricted mobility layer upon neutralization.

The observation of resolved ionomer peaks in the scattering data for the samples with a B-type molecular architecture ($B_H$ and $B_{Na}$) illustrated that the balance between molecular architecture and microphase separation in these materials was not strictly dominated by large enthalpic repulsion of the SPS from the other blocks. Placing the sulfonated block at the branch terminus allowed the formation of ionic aggregates due to the mobility of the branch ends, while copolymers with the sulfonated blocks close to the polymer backbone exhibited little insignificant formation of ionic aggregates. Thus, while the calculated values of the Flory-Huggins parameter for SPS and the blocks are remarkable, it is clear from these experiments that molecular architecture plays a significant morphological role, and can be used as a design parameter for utilization of ionomers.

## 6.6 Acknowledgements

This material is based upon work funded by the U.S. Army Research Laboratory and the U.S. Army Research Office under grant number DAAD19-02-1-0275 Macromolecular Architecture for Performance (MAP) MURI. The authors acknowledge unrestricted complementary funding from Kraton Polymers LLC and insightful discussions with Dr. Carl Willis.

## 6.7 References

1. Jenkins, D. W.; Hudson, S. M., Review of vinyl graft copolymerization featuring recent advances toward controlled radical-based reactions and illustrated with chitin/chitosan trunk polymers. *Chemical Reviews* **2001,** 101, (11), 3245-3273.
2. Hadjichristidis, N.; Pitsikalis, M.; Iatrou, H.; Pispas, S., The strength of the macromonomer strategy for complex macromolecular architecture: Molecular characterization, properties and applications of polymacromonomers. *Macromolecular Rapid Communications* **2003,** 24, (17), 979-1013.
3. Ito, K., Polymeric design by macromonomer technique. *Progress in Polymer Science* **1998,** 23, (4), 581-620.
4. Yang, Y.; Holdcroft, S., Synthetic strategies for controlling the morphology of proton conducting polymer membranes. *Fuel Cells* **2005,** 5, (2), 171-186.
5. Maynard, H. D.; Lyu, S. P.; Fredrickson, G. H.; Wudl, F.; Chmelka, B. F., Syntheses of nanophase-segregated poly(vinyl acetate)-poly(dimethylsiloxane) and poly(vinyl acetate)-poly(styrene) graft copolymers. *Polymer* **2001,** 42, (18), 7567-7574.
6. Beyer, F. L.; Gido, S. P.; Buschl, C.; Iatrou, H.; Uhrig, D.; Mays, J. W.; Chang, M. Y.; Garetz, B. A.; Balsara, N. P.; Tan, N. B.; Hadjichristidis, N., Graft copolymers with regularly spaced, tetrafunctional branch points: Morphology and grain structure. *Macromolecules* **2000,** 33, (6), 2039-2048.
7. Xenidou, M.; Beyer, F. L.; Hadjichristidis, N.; Gido, S. P.; Tan, N. B., Morphology of model graft copolymers with randomly placed trifunctional and tetrafunctional branch points. *Macromolecules* **1998,** 31, (22), 7659-7667.
8. Chuy, C.; Ding, J. F.; Swanson, E.; Holdcroft, S.; Horsfall, J.; Lovell, K. V., Conductivity and electrochemical ORR mass transport properties of solid polymer electrolytes containing poly(styrene sulfonic acid) graft chains. *Journal of the Electrochemical Society* **2003,** 150, (5), E271-E279.
9. Ding, J. F.; Chuy, C.; Holdcroft, S., Enhanced conductivity in morphologically controlled proton exchange membranes: Synthesis of macromonomers by SFRP and their incorporation into graft polymers. *Macromolecules* **2002,** 35, (4), 1348-1355.
10. Hickner, M. A.; Ghassemi, H.; Kim, Y. S.; Einsla, B. R.; McGrath, J. E., Alternative polymer systems for proton exchange membranes (PEMs). *Chemical Reviews* **2004,** 104, (10), 4587-4611.
11. Harrison, W. L.; Hickner, M. A.; Kim, Y. S.; McGrath, J. E., Poly(arylene ether sulfone) copolymers and related systems from disulfonated monomer building blocks: Synthesis, characterization, and performance - A topical review. *Fuel Cells* **2005,** 5, (2), 201-212.
12. Schulz, G. O.; Milkovich, R., Graft polymers with macromonomers 1.Synthesis from methacrylate-terminated polystyrene. *Journal of Applied Polymer Science* **1982,** 27, (12), 4773-4786.

13. Balastre, M.; Li, F.; Schorr, P.; Yang, J.; Mays, J. W.; Tirrell, M. V., A study of polyelectrolyte brushes formed from adsorption of amphiphilic diblock copolymers using the surface forces apparatus. *Macromolecules* **2002,** 35, (25), 9480-9486.
14. Guenoun, P.; Davis, H. T.; Tirrell, M.; Mays, J. W., Aqueous micellar solutions of hydrophobically modified polyelectrolytes. *Macromolecules* **1996,** 29, (11), 3965-9.
15. Toomey, R.; Mays, J.; Holley, D. W.; Tirrell, M., Adsorption mechanisms of charged, amphiphilic diblock copolymers: The role of micellization and surface affinity. *Macromolecules* **2005,** 38, (12), 5137-5143.
16. Valint, P. L.; Bock, J., Synthesis and characterization of hydrophbically assiociating block polymers. *Macromolecules* **1988,** 21, (1), 175-179.
17. Yang, J. C.; Jablonsky, M. J.; Mays, J. W., NMR and FT-IR studies of sulfonated styrene-based homopolymers and copolymers. *Polymer* **2002,** 43, (19), 5125-5132.
18. Yang, J. C.; Mays, J. W., Synthesis and characterization of neutral/Ionic block copolymers of various architectures. *Macromolecules* **2002,** 35, (9), 3433-3438.
19. Zhang, Y.; Tirrell, M.; Mays, J. W., Effects of ionic strength and counterion valency on adsorption of hydrophobically modified polyelectrolytes. *Macromolecules* **1996,** 29, (22), 7299-7301.
20. Klein, R. R.; Makowski, H. S. Sulfonating EPDM. 81-301399, 37283, 19810331., 1981.
21. Makowski, H. S.; Bock, J.; Lundberg, R. D. Forming a polymer that contains metalsulfonate. 78-300684, 2353, 19781128., 1979.
22. Makowski, H. S.; Lundberg, R. D.; Agarwal, P. K. Amine-terminated poly(alkylene oxide)-neutralized sulfonated thermoplastic polymers. 82-302463, 66970, 19820514., 1982.
23. Makowski, H. S.; Lundberg, R. D.; Bock, J. Sulfonating elastomeric polymers. 78-300685, 2354, 19781128., 1979.
24. Makowski, H. S.; Lundberg, R. D.; Bock, J. Bulk neutralization of sulfonated elastomeric polymers and compositions thereof. 78-300686, 2355, 19781128., 1979.
25. Makowski, H. S.; Lundberg, R. D.; Bock, J. Sulfonation of an elastomeric polymer. 78-951394, 4184988, 19781016., 1980.
26. Makowski, H. S.; Lundberg, R. D.; Singhal, G. H. Flexible plastic masses. 73-2348842, 2348842, 19730928., 1974.
27. Makowski, H. S.; Lundberg, R. D.; Westerman, L.; Bock, J., Synthesis and properties of sulfonated EPDM. *Advances in Chemistry Series* **1980,** 187, (Ions Polym.), 3-19.
28. De la Fuente, J. L.; Fernandez-Garcia, M.; Madruga, E. L., Characterization and thermal properties of poly(n-butyl acrylate-g-styrene) graft copolymers. *Journal of Applied Polymer Science* **2001,** 80, (5), 783-789.
29. Brandrup, J.; Immergut, E. H., *Polymer Handbook*. 3rd ed.; Wiley: New York, 1989.
30. Mauritz, K. A.; Blackwell, R. I.; Beyer, F. L., Viscoelastic properties and morphology of sulfonated poly(styrene-b-ethylene/butylene-b-styrene) block copolymers (sBCP), and sBCP/[silicate] nanostructured materials. *Polymer* **2004,** 45, (9), 3001-3016.
31. Mokrini, A.; Del Rio, C.; Acosta, J. L., Synthesis and characterization of new ion conductors based on butadiene styrene copolymers. *Solid State Ionics* **2004,** 166, (3-4), 375-381.
32. Shi, Z. Q.; Holdcroft, S., Synthesis and proton conductivity of partially sulfonated poly([vinylidene difluoride-co-hexafluoropropylene]-b-styrene) block copolymers. *Macromolecules* **2005,** 38, (10), 4193-4201.
33. Eisenberg, A.; Hird, B.; Moore, R. B., A new multiplet-cluster model for the morphology of random ionomers. *Macromolecules* **1990,** 23, (18), 4098-4107.
34. Benoit, H.; Hadziioannou, G., Sattering-theory and properties of block copolymers with various architectures in the homogeneous bulk state. *Macromolecules* **1988,** 21, (5), 1449-1464.
35. Shinozaki, A.; Jasnow, D.; Balazs, A. C., Microphase separation in comb copolymers. *Macromolecules* **1994,** 27, (9), 2496-2502.
36. Van Krevelen, D. W.; Hoftyzer, P. J., *Properties of Polymers*. Elsevier: New York, 1976.
37. Kim, B.; Kim, J.; Jung, B., Morphology and transport properties of protons and methanol through partially sulfonated block copolymers. *Journal of Membrane Science* **2005,** 250, (1-2), 175-182.
38. Lu, X. Y.; Weiss, R. A., Development of miscible blends of Bisphenol A polycarbonate and lightly sulfonated polystyrene ionomers from intrapolymer repulsive interactions. *Macromolecules* **1996,** 29, (4), 1216-1221.

39. Tan, N. C. B.; Liu, X.; Briber, R. M.; Peiffer, D. G., Immiscibility in polystyrene sulfonated polystyrene blends. *Polymer* **1995,** 36, (10), 1969-1973.
40. Zhou, N. C.; Xu, C.; Burghardt, W. R.; Composto, R. J.; Winey, K. I., Phase behavior of polystyrene and poly (styrene-ran-styrene sulfonate) blends. *Macromolecules* **2006,** 39, (6), 2373-2379.
41. Fairclough, J. P. A.; Hamley, I. W.; Terrill, N. J., X-ray scattering in polymers and micelles. *Radiation Physics and Chemistry* **1999,** 56, (1-2), 159-173.
42. Guinier, A.; Fournet, G., *Small-angle scattering of x-rays*. John Wiley & Sons: New York, 1955.
43. Yarusso, D. J.; Cooper, S. L., Microstructure of ionomers - Interpretation of small-angle x-ray scattering data. *Macromolecules* **1983,** 16, (12), 1871-1880.
44. Tsujita, Y.; Hayashi, N.; Yamamoto, Y.; Yoshimizu, H.; Kinoshita, T.; Matsumoto, S., SAXS study on ionic aggregates of styrene-isoprene-sulfonated isoprene terpolymer ionomer. *Journal of Polymer Science, Part B: Polymer Physics* **2000,** 38, (10), 1307-1311.
45. Tsujita, Y.; Yasuda, M.; Takei, M.; Kinoshita, T.; Takizawa, A.; Yoshimizu, H., Structure of ionic aggregates of ionomers. 1. Variation in the structure of ionic aggregates with different acid content and degree of neutralization of ethylene and styrene Ionomers. *Macromolecules* **2001,** 34, (7), 2220-2224.
46. Wouters, M. E. L.; Goossens, J. G. P.; Binsbergen, F. L., Morphology of neutralized low molecular weight maleated ethylene-propylene copolymers (MAn-g-EPM) as investigated by small-angle x-ray scattering. *Macromolecules* **2002,** 35, (1), 208-216.
47. Lu, X. Y.; Steckle, W. P.; Weiss, R. A., Morphological-studies of a triblock copolymer ionomer by small-angle x-ray-scattering *Macromolecules* **1993,** 26, (24), 6525-6530.
48. Mani, S.; Weiss, R. A.; Williams, C. E.; Hahn, S. F., Microstructure of ionomers based on sulfonated block copolymers of polystyrene and poly(ethylene-alt-propylene). *Macromolecules* **1999,** 32, (11), 3663-3670.

# Chapter 7: Influence of Site-Specific Sulfonation in Graft Copolymer Architecture

## 7.1 Abstract

This study involves investigating the structure-property relationships of multiphase ionomers as a function of the relative location of sulfonated blocks. Poly(ethylene-*co*-propylene)-*b*-polystyrene (PEP-*b*-PS) diblock macromonomers containing 1000 g/mol PS and 9000 g/mol PEP were synthesized using living-anionic polymerization and subsequent hydrogenation. The macromonomers were copolymerized with methyl methacrylate (MMA) and PS blocks were selectively sulfonated. The sulfonated polystyrene blocks (SPS) were designed either adjacent to the backbone (A) or at the branch terminus (B). The novel site-specific sulfonated graft copolymers, PMMA-*g*-SPS-*b*-PEP (A) and PMMA-*g*-PEP-*b*-SPS (B) were characterized as the weight average molecular weights 90000 - 220000 g/mol, the polydispersity indices 1.5 – 2.2, and 1 – 2 branches on average. Estimated $\chi N$ values predicted the phase separation of each block. Differential scanning calorimetry and dynamic mechanical analysis (DMA) confirmed the phase separation of each block components of the graft copolymers. Two α transitions, $T_g$s of PEP block ($T_g^1$) at approximately -60 °C, and $T_g$ of PMMA block ($T_g^2$) at 80-100 °C, and β transition at around 10 °C were observed in the graft copolymer precursors. The aggregation of sulfonic acid or sodium sulfonate groups at the branch terminus hindered the glass transition of PEP block and glass transition of PEP block was not observed in sulfonated graft copolymer with sulfonated blocks at the branch terminus. This lack of the glass transition of PEP block resulted in higher storage modulus than sulfonated graft copolymer with sulfonated block

adjacent to backbone. This work demonstrated that placing sulfonated block at the branch terminus enhanced the formation of ionic aggregates due to the mobility of the branch ends, while graft copolymers with the sulfonated blocks adjacent to the polymer backbone exhibited little significant formation of ionic aggregates.

## 7.2 Introduction

Graft copolymers possess features of physical blends and random copolymers as well as features similar to block copolymers.[1] Graft copolymers are also looked as chemically linked pairs of homopolymers, which constitute a comb-like structure. The unique macromolecular architecture enables graft copolymers to have a wide variety of emerging applications. Well-defined synthesis and characterization of graft copolymers is necessary to understand their unique structure-property relationships.[2]

A generally accepted strategy for obtaining well-defined graft copolymers involves copolymerization of macromonomers with backbone-forming monomers. A macromonomer is defined as a functional oligomer with a polymerizable end group.[3] Living polymerization strategies for synthesis of macromonomers predetermine the chain length of the macromonomer, which defines the length of branches in the graft copolymer. The choice of monomers and the order of monomer addition also control the composition of the branch and backbone upon subsequent copolymerization.[4]

We are interested in the structure-property relationships of graft copolymers as a function of the relative location of sulfonated blocks, because the location of sulfonated blocks in branched architecture is expected to alter the properties. Understanding this fundamental concept will give an important insight for macromolecular designing and

property tuning. Researchers have predicted that the distribution of sulfonated groups along the chain as well as the acid strength and the linkage to the polymer backbone have a considerable effect on the morphology and the properties.[5] Due to the synthetic difficulties, most synthetic methods that are currently utilized to form ion-containing materials such as proton exchange membranes result in random or statistical placement of sulfonic acid units along the copolymer chain.[5, 6] Therefore, the fundamental study of the structure-property relationships with well-defined branched sulfonated ionomers has rarely been reported.

Our previous study[7] demonstrated that the location of sulfonated blocks in both sulfonic acid and sodium sulfonate graft copolymers significantly affected the thermal and morphological properties. Placing the sulfonated block at the end of the graft chains enhanced the ionomeric character of the grafts due to the mobility of the branches, while those copolymers with the sulfonated blocks adjacent to the polymer backbone exhibited less ionomeric behavior. This demonstrated that the location of ionomeric blocks in branched polymers could significantly affect the subsequent properties and provided insight into the design of branched polymers for their best utilization. However, the brittleness of the sulfonated graft copolymers prevented further mechanical characterization.

This work involves the synthesis and characterization of graft copolymers containing site-specifically sulfonated blocks for improved performance. The structures and schematic representations of the site-specific sulfonated graft copolymers are shown in Figure 7.1. The synthetic methodology that was utilized for controlled graft copolymer synthesis with precise location of sulfonated blocks was the use of preformed

macromonomers.[8] Polyisoprene-*b*-polystyrene (PI-*b*-PS) diblock copolymers were synthesized via living anionic polymerization and polyisoprene blocks were subsequently hydrogenated. The diblock macromonomer contained 1000 g/mol polystyrene and 9000 g/mol poly(ethylene-*co*-propylene) (PEP). Then, PEP-*b*-PS diblock macromonomers were copolymerized with methyl methacrylate (MMA) and polystyrene blocks were selectively sulfonated. The sulfonated blocks were placed either adjacent to the backbone which will be referred to as A or at the branch terminus which will be referred to as B.

A - sulfonated blocks adjacent to backbone

B - sulfonated blocks at the branch terminus

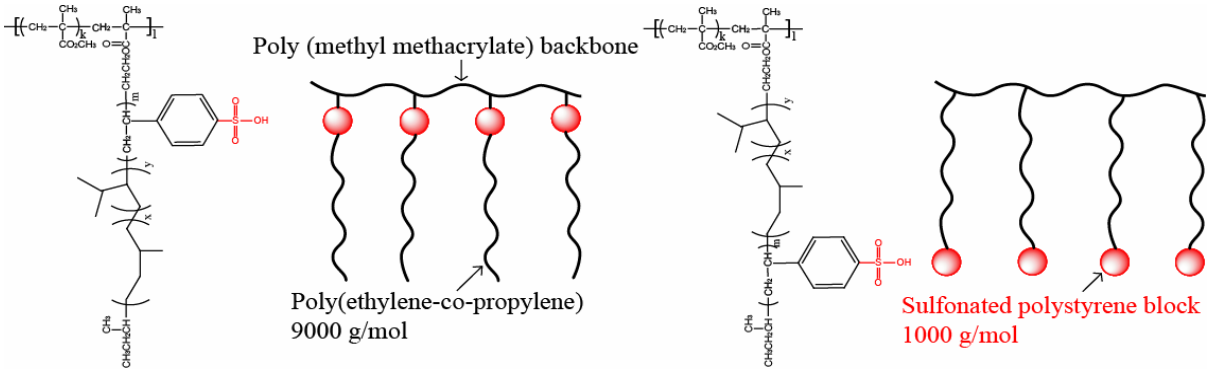


**Figure 7.1** Chemical structures and schematic images of the site-specifically sulfonated graft copolymers

## 7.3 Experimental

### 7.3.1 Materials and Chemicals

Styrene (Aldrich, 99%) and triethylamine (Aldrich, 99%) were dried over calcium hydride (Aldrich, 95%) for 24 h and distilled under vacuum. The distilled styrene and isoprene (Aldrich, 99%) were treated with dibutyl magnesium (Aldrich, 0.10 mM) and distilled under vacuum prior to use. Cyclohexane (Fisher Scientific, HPLC) and tetrahydrofuran (THF, Fisher Scientific, HPLC) were passed through an activated molecular sieve column (Aldrich, 60 Å mesh) and activated alumina column immediately prior to use. Methacryloyl chloride (Aldrich, 96%) was distilled under nitrogen. Methyl methacrylate (MMA, 98%, Aldrich) was de-inhibited via passing through activated basic alumina column. *sec*-Butyllithium (Aldrich, 1.4 M), ethylene oxide (Aldrich, 99.98%), nickel 2-ehtylhexanoate (nickel octoate, Alfa Aesar), 1.0 M triethylaluminum in hexanes (Aldrich), citric acid (Aldrich, 98%), 2,2-azobisisobutyronitrile (AIBN, 99%, Aldrich,) dichloroethane (Aldrich, 99%), acetic anhydride (Aldrich, 98%) and sulfuric acid (Aldrich, 98%) were used as received.

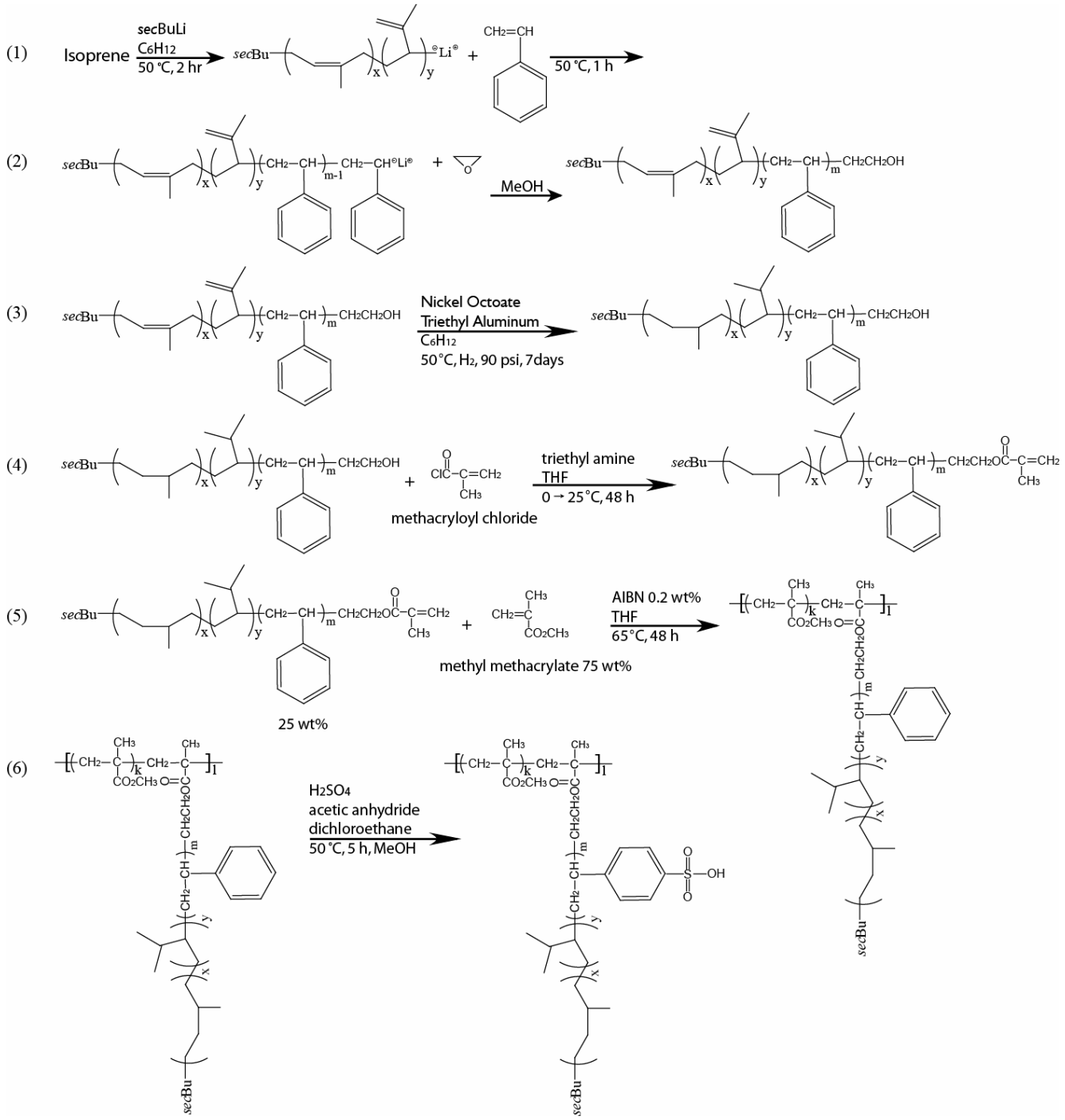


**Scheme 7.1** Synthesis of site-specifically sulfonated graft copolymers

### 7.3.2 Synthesis of Hydroxy-terminated Poly(isoprene-*block*-styrene)

A 600 mL-capacity anionic polymerization reactor was filled with cyclohexane (350 mL) and the temperature was maintained at 50 °C. The glass anionic reactor

consisted of a 600 mL glass bowl, a stainless steel top plate, and stainless steel magnetically coupled mechanical stirrer.[9] In addition, a heat-exchange coil, a thermocouple, a septum sealed port, various stainless steel transfer lines to introduce solvent (cyclohexane), and inlet/vent for purified nitrogen are equipped to the anionic reactor. The anionic reactor system was maintained at a constant nitrogen pressure (40 psi). Isoprene (104 mL, 70.8g) was syringed into the reactor. *sec*-Butyllithium (5.62 mL, 7.87 mmol) was then added to the solution to initiate the anionic polymerization. As illustrated in Scheme 7.1 (1), the first reaction was allowed to proceed 2 h and the second block monomer, styrene (7.79 mL, 7.08 g) was added. After 1 h of polymerization, ethylene oxide was bubbled through the reaction solvent for 2 min and then terminated by adding nitrogen-degassed methanol (Scheme 7.1 (2)). The diblock copolymer solution was passed through a filter to remove lithium salts and the filtered solution was directly used in the next step synthesis. Synthesis of γ-hydroxy-poly(styrene-*block*-isoprene) was also performed with exchanging the first block (isoprene) and the second block (styrene). $^1$H NMR (400 MHz, $CDCl_3$, δ): 0.6 – 0.8 ppm (br, C*H*$_3$CH$_2$CH(C*H*$_3$)-), 1.0 – 2.5 ppm (br, -C*H*$_2$-, -CH$_2$C*H*-, -C*H*$_3$ in polystyrene and polyisoprene units), 3.2 – 3.6 ppm (br, -CH$_2$C*H*$_2$OH), 4.6 – 4.8 ppm (br, -C(CH$_3$)=C*H*$_2$, 3,4-addition), 4.8 – 5.4 ppm (br, -C*H*=C(CH$_3$)-, 1,4-addition), 6.3 – 7.3 ppm (br, aromatic protons in polystyrene).

### 7.3.3 Hydrogenation of Polyisoprene Blocks

Cyclohexane (50 mL) and nickel octoate (1.0g, 2.9 mmol) were added to a flame-dried 100 mL amber bottle equipped with a magnetic stirrer. 1.0 M triethylaluminum solution (8.69 mL, 8.9 mmol) was added dropwise to the nickel solution. An opaque, black colloidal suspension formed immediately and was allowed to sit for 15 min at room

temperature under a nitrogen atmosphere to form a homogeneous solution. Previously described PI-*b*-PS-OH (77 g) cyclohexane solution (500 mL) and the preformed nickel catalyst (30 mL, 1.5 mmol) were added to a 600 mL reactor. The reactor was pressurized with hydrogen and vented three times. The vessel was pressurized with hydrogen (90 psi) and heated to 50 °C for 72 h. Since 100% hydrogenation was not achieved, another preformed nickel catalyst (30 mL, 1.5 mmol) was added. The reactor was again pressurized with hydrogen and vented three times. The vessel was pressurized with hydrogen (90 psi) and heated to 50 °C for 96 h (Scheme 7.1 (3)). The nickel catalyst was extracted from the polymer solution with citric acid washes. The polymer solution was precipitated into methanol, and dried in reduced pressure at room temperature for 72 h. $^1$H NMR (400 MHz, $CDCl_3$, δ): 0.6 – 1.0 ppm (br, -C*H*$_3$), 1.0 – 1.4 ppm (br, -C*H*$_2$-), 1.4 – 2.2 ppm (br, -$CH_2$C*H*-), 3.2 – 3.6 ppm (br, -$CH_2$C*H*$_2$OH), 6.3 – 7.3 ppm (br, aromatic protons in polystyrene).

### 7.3.4 Functionalization of Hydroxy-terminated Diblock Copolymers to Methacrylate Macromonomers

PEP-*b*-PS-OH (70 g) was dissolved in dry THF (1500 mL). Triethylamine (12.41 mL, 78 mmol) was syringed into the reaction vessel. After cooling to 0 °C, methacryloyl chloride (3.81 mL, 39 mmol), which dissolved in THF (70 mL), was added dropwise. The reaction was allowed to proceed for 48 h with warming to room temperature. The macromonomer was precipitated into methanol, re-dissolved in THF and precipitated in methanol. The precipitation step was repeated several times to remove unreacted methacryloyl chloride. The recovered polymer was dried at room temperature in a reduced pressure for 72 h (Scheme 7.1 (4)). $^1$H NMR (400 MHz, $CDCl_3$, δ): 0.6 – 1.0 ppm (br, -C*H*$_3$), 1.0 – 1.4 ppm (br, -C*H*$_2$-), 1.4 – 2.2 ppm (br, -$CH_2$C*H*-), 3.6 – 4.2 ppm

(br, -$CH_2CH_2OC(O)$-), 5.5 ppm (d, $J$ = 16.8 Hz, $CH H_{trans}=C(CH_3)$-), 5.9 ppm (d, $J$ = 16.8 Hz, $CH H_{cis}=C(CH_3)$-), 6.3 – 7.3 ppm (br, aromatic protons in polystyrene).

### 7.3.5 Graft Copolymerization of Methacrylate Macromonomers with Methyl Methacrylate

Methacrylate macromonomer (5.6 g), methyl methacrylate (18.0 mL, 16.8 g) and AIBN (18.4 mg) were dissolved in THF (75 mL). Nitrogen was bubbled through the solution for 10 min. The reaction was allowed to stir for 48 h at 65 °C (Scheme 7.1 (5)). The graft copolymer was precipitated into methanol. The precipitated graft copolymer was filtered and dried at 80 °C in reduced pressure for 24 h. The graft copolymers, poly(methyl methacrylate)-*g*-(polystyrene-*b*-poly(ethylene-*co*-propylene) (PMMA-*g*-PS-*b*-PEP) and poly(methyl methacrylate)-*g*-(poly(ethylene-*co*-propylene)-*b*-polystyrene) (PMMA-*g*-PEP-*b*-PS), were then separated from residual methacrylate macromonomers via heptane extraction for 7 days. The fractionation of the graft copolymers in heptanes was also performed to remove residual methacrylate macromonomers. $^1$H NMR (400 MHz, $CDCl_3$, δ): 0.7 – 1.1 ppm (br, -$CH_3$), 1.1 – 1.5 ppm (br, -$CH_2$-), 1.5 – 2.2 ppm (br, -$CH_2CH$-), 3.4 – 3.8 ppm (br, -$C(O)OCH_3$), 6.3 – 7.3 ppm (br, aromatic protons in polystyrene).

### 7.3.6 Site-specific Sulfonation and $Na^+$ Neutralizaton of Graft Copolymers

1.0 M acetyl sulfate solution was generated via the sequential addition of sulfuric acid (2.1 mL, 0.04 mol) and acetic anhydride (4.7 mL, 0.05 mol) in dichloroethane (33.2 mL) at 0 °C. PMMA-*g*-PS-*b*-PEP (8.3 g) was dissolved in dichloroethane (47.1 mL). Nitrogen was bubbled through the solution for 10 min (Scheme 7.1 (6)). The reaction was maintained at 50 °C and the acetyl sulfate solution (12.5 mL, 1.0 M in dichloroethane) was slowly added. The reaction was allowed to proceed for 5 h at 50 °C

until methanol was added to terminate the reaction. The poly(styrene sulfonic acid)-containing graft polymer was first precipitated in a 1:1 mixture of methanol/water, filtered, re-dissolved in THF, and then precipitated into water. The precipitation and recovery were repeated at least three times. A portion of the dried sulfonic acid-containing graft polymer was re-dissolved in THF and the acid groups were neutralized with one equivalent of NaOH solution (0.01 M). The product polymer was isolated by precipitation in water and dried at 40 °C in reduced pressure for 48 h.

### 7.3.7 Polymer Characterization

$^{1}$H NMR spectra of the polymers were obtained on a Varian Unity spectrometer operating at 400 MHz at ambient temperature. Deuterated chloroform (Cambridge Isotope Laboratories) was used as the solvent. Size exclusion chromatography (SEC) measurements were performed in THF at 40 °C at flow rate 1 mL/min using a Waters size exclusion chromatograph equipped with an autosampler, three 5-mm PLgel Mixed-C columns, a Waters 2410 refractive index (RI) detector operating at 880 nm, and a mini DAWN multiangle laser light scattering (MALLS) detector operating at 690 nm which was calibrated with narrow polydispersity polystyrene standards. The RI increment (dn/dc) was calculated online. Reported weight-average molecular weights were absolute molecular weights, which were obtained using the MALLS detector.

Solvent cast films of the graft polymer precursors and the sulfonic acid graft copolymers were cast from 8 wt% solutions of the polymer (0.387 g) in THF (5 mL) onto a glass slide (5 x 7 cm). The solutions were covered to slow solvent evaporation, and films formed over a period of 2 days. Solvent cast films of the sodium sulfonate graft copolymers were cast from 8 wt% polymer (0.387 g) MeOH/THF (5/95) (5 mL) solution

onto a glass slide (5 x 7 cm), and film formation occurred over a period of 2 days. The sodium sulfonate graft copolymers are insoluble in THF and a polar protic solvent needed to be added.

Glass transition temperatures were determined using a differential scanning calorimeter (DSC) Q200 (TA instruments) at a heating rate of 10 °C/min under nitrogen. Glass transition temperatures are reported as the onset and the transition midpoint during the second heat. Dynamic mechanical analysis (DMA) was performed with a TA Instruments Q800 dynamic mechanical analyzer in tension mode at 5 μm amplitude and at a frequency of 1 Hz with a heating rate of 3 °C/min.

## 7.4 Results and Discussion

### 7.4.1 Synthesis of Methacrylate Macromonomers

PEP-*b*-PS-OH and PS-*b*-PEP-OH, containing 1000 g/mol polystyrene block and 9000 g/mol poly(ethylene-*co*-propylene) block were synthesized via living anionic polymerization and subsequent hydrogenation. The properties of the diblock copolymers are summarized in Table 7.1. Molecular weights ($M_n$ from NMR and SEC) of the diblock copolymers were approximately 10000 g/mol and narrow molecular distributions ($M_w/M_n$) 1.02 – 1.03 were repeatedly obtained. Based on the integration of the $^1$H NMR resonance for the methylene adjacent to the hydroxyl at 3.2 – 3.4 ppm to the integration of the $^1$H NMR resonance for the two methyls in the s*ec*-butyl fragment at 0.6 - 0.8 ppm, 89 - 100% endcapping to the terminal hydroxyl group was achieved. The vinyl peaks in $^1$H NMR at 4.6 – 5.4 ppm from polyisoprene blocks disappeared upon hydrogenation, indicative of quantitative hydrogenation achievement. The hydroxyl end-groups of the

diblock copolymers (PEP-*b*-PS-OH and PS-*b*-PEP-OH) were reacted with methacryloyl chloride to produce methacrylate macromonomers (PEP-*b*-PS-methacrylate and PS-*b*-PEP-methacrylate). Furthermore, quantitative conversion of hydroxyl groups to methacrylate groups were achieved based on $^1$H NMR shifting from alcohol methylene at 3.6 ppm to ester methylene at 4.2 ppm. The functionality of the methacrylate macromonomers was 0.89 – 1.00.

**Table 7.1** Property of PEP-*b*-PS-OH and PS-*b*-PEP-OH

| | $M_n$[a] PEP | $M_n$[a] PS | $M_n$[a] PEP-*b*-PS | $M_n$[b] PEP-*b*-PS | $M_w/M_n$[b] | functionality |
|---|---|---|---|---|---|---|
| PEP-*b*-PS-OH | 9060 | 1160 | 10320 | 11300 | 1.02 | 1.00 |
| PS-*b*-PEP-OH | 8670 | 1220 | 10000 | 9300 | 1.03 | 0.89 |

[a] $^1$H NMR conditions; Varian Unity 400 MHz, $CDCl_3$
[b] Determined using SEC at 40 °C in THF with a MALLS detector

### 7.4.2 Graft Copolymerization of Methacrylate Macromonomer with MMA and Subsequent Sulfonation of Polystyrene Blocks

The results of graft copolymerization of methacrylate macromonomer with MMA via free radical copolymerization are summarized in Table 7.2. Sample A possesses polystyrene blocks adjacent to the PMMA backbone, while sample B has polystyrene blocks at the branch terminus. The weight average molecular weight $M_w$ ranged 90000 - 220000 g/mol, and the polydispersity indices ranged 1.58 – 2.16. The SEC traces of a graft copolymer, PMMA-*g*-PEP-*b*-PS (B1 and B2) and PS-*b*-PEP-methacrylate macromonomer are shown in Figure 7.2. All of SEC traces showed a monomodel signal, indicating that the hexane extraction or fractionation was sufficient to remove the residual macromonomer.

Total conversion of MMA and macromonomer was 50 – 60 % based on the yield and the macromonomer conversion was 30 – 50 %. In the $^1$H NMR spectrum of the graft copolymers, integrations of the methylene region (1.1 – 1.5 ppm) and methoxy

groups in PMMA (3.4 – 3.8 ppm) determined the ratio of PMMA to macromonomers. The amount of incorporated branches ranged approximately 10 wt% in an entire graft copolymer and the polystyrene blocks contributed to approximately 1 wt% in the graft copolymer.

Based on the ratio from $^{1}$H NMR and $M_w$ of the graft copolymers, an average number of branches of the graft copolymers was calculated and listed in Table 7.2. The graft copolymer A and B1 contained one average grafted branch and the graft copolymer B2 contained an average of two grafted branches due to higher molecular weight. Graft copolymerizations of MMA with higher ratio of macromonomers were also attempted to synthesize graft copolymers with higher number of branches; however, higher incorporation of PEP-*b*-PS branches prevented separating the residual macromonomer from the synthesized graft copolymer due to the solubility. Leaving residual macromonomer would lead to ill-defined graft copolymers. Therefore, graft copolymers with higher number of branches could not be prepared, unlike previous study.[7]

Site-specific sulfonation of PS blocks with acetyl sulfate solution was confirmed via acid-base titration for the sulfonic acid content. All of the graft copolymers contained quantitative sulfonation of polystyrene block based on the titration results. Thus, approximately 1 wt% in all of the graft copolymers was sulfonated with precise locations as shown in Figure 7.1. The sulfonic acid graft copolymers, poly(methyl methacrylate)-*g*-(sulfonic acid polystyrene-*b*-poly(ethylene-*co*-propylene) (PMMA-*g*-SPS-*b*-PEP) and poly(methyl methacrylate)-*g*-(poly(ethylene-*co*-propylene)-*b*-sulfonic acid polystyrene) (PMMA-*g*-PEP-*b*-SPS), were successfully synthesized. Finally, a portion of the sulfonic acid graft copolymers were neutralized with an equivalent of NaOH to produce sodium

sulfonate graft copolymers, poly(methyl methacrylate)-*g*-(sodium sulfonate polystyrene-*b*-poly(ethylene-*co*-propylene) (PMMA-*g*-NaSPS-*b*-PEP) and poly(methyl methacrylate)-*g*-(poly(ethylene-*co*-propylene)-*b*-sodium sulfonate polystyrene) (PMMA-*g*-PEP-*b*-NaSPS).

**Table 7.2** Property of Sulfonated Graft Copolymers

| | Number of Branches (λ) | PMMA [wt %] | PEP [wt %] | PS [wt%] | $M_w$[a] | $M_w/M_n$[a] |
|---|---|---|---|---|---|---|
| A | 1 | 89.7 | 9.0 | 1.3 | 92300 | 2.16 |
| B1 | 1 | 91.1 | 7.7 | 1.2 | 129000 | 1.75 |
| B2 | 2 | 92.9 | 6.2 | 0.9 | 206800 | 1.58 |

[a] Determined using SEC at 40 °C in THF with a MALLS detector

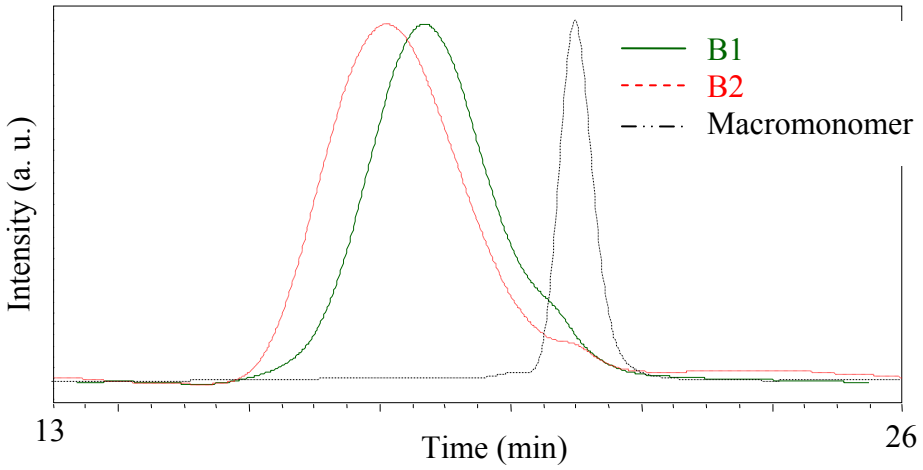


**Figure 7.2** SEC traces of a graft copolymer, PMMA-*g*-PEP-*b*-PS (B1 and B2) and a macromonomer, PS-*b*-PEP-methacrylate
SEC conditions: at 40 °C in THF with RI and MALLS detector

### 7.4.3 Thermal Characterization and Molecular Interaction of Each Block

Non-sulfonated graft copolymers, sulfonic acid graft copolymers, and sodium sulfonate graft copolymers were cast on a glass slide and clear colorless films were obtained. The representative cast films are shown in Figure 7.3. For simplicity, non-sulfonated graft copolymers A, B1, and B2 will be referred to $A_G$, $B1_G$, and $B2_G$, sulfonic

acid graft copolymers will be referred to $A_H$, $B1_H$, and $B2_H$, and sodium sulfonate graft copolymers will be referred to $A_{Na}$, $B1_{Na}$, and $B2_{Na}$.


**Figure 7.3** Cast films of $A_G$, $A_H$, and $A_{Na}$

Glass transition temperatures ($T_g$) of PMMA-*g*-PS-*b*-PEP ($A_G$), PMMA-*g*-PEP-*b*-PS ($B1_G$, $B2_G$), PMMA-*g*-SPS-*b*-PEP ($A_H$), PMMA-*g*-PEP-*b*-SPS ($B1_H$, $B2_H$), PMMA-*g*-NaSPS-*b*-PEP ($A_{Na}$), and PMMA-*g*-PEP-*b*-NaSPS ($B1_{Na}$, $B2_{Na}$) were measured using DSC. All the $T_g$s were determined from the second heating cycle at 10 °C/min. All graft copolymers had a single $T_g$ ranging from 125 – 130 °C, which corresponded to the $T_g$ of the PMMA block. Although $T_g$ of PEP block was not observed, the constant $T_g$ of the PMMA block suggested that each block possessed their own $T_g$ and these graft copolymers were phase separated.

The phase-separation behavior can be estimated using estimated $\chi N/\lambda$, where $\chi$ is Flory-Huggins interaction parameter, and $N$ is the total degree of polymerization. As shown in Chapter 2 and 6, the calculation of $\chi$ follows the equation 2-4:

$$\chi_{12} = \frac{V_0(\delta_2 - \delta_1)^2}{RT} \qquad (2\text{-}4)$$

The molar volumes of PMMA, PEP, PS, and SPS are 85.6 $cm^3/mol$,[10] 81.8 $cm^3/mol$,[10] 99.0 $cm^3/mol$,[10] and 129.1 $cm^3/mol$,[10] respectively, where the molar volume for SPS was calculated using the addition principle of the group contributions and the atomic contributions.[10] The solubility parameters of PMMA, PEP, PS, and SPS are 18.27 $(J/cm^3)^{1/2}$,[11] 16.74 $(J/cm^3)^{1/2}$,[10, 12] 18.66 $(J/cm^3)^{1/2}$,[11] and 33.96 $(J/cm^3)^{1/2}$,[13, 14] respectively.

The calculated $\chi$ values and $\chi N/\lambda$ at $T$ = 298 K are summarized in Table 7.3 and Table 7.4, respectively. The $\chi N/\lambda$ values in Table 7.4 implied the phase separation occurrence between each block except for PMMA/PS. This estimated $\chi N/\lambda$ values supported the obtained trend of $T_g$ values from DSC.

**Table 7.3** $\chi$ values for the each components between PMMA, PS, PEP and SPS at $T$ = 298 K

| $\chi_{PMMA/PS}$ | $\chi_{PMMA/PEP}$ | $\chi_{PEP/PS}$ | $\chi_{PMMA/SPS}$ | $\chi_{PEP/SPS}$ |
|---|---|---|---|---|
| 0.00565 | 0.0791 | 0.127 | 10.4 | 12.9 |

**Table 7.4** Estimation of $\chi N$ values for the PMMA-*g*-PS-*b*-PEP ($A_G$), PMMA-*g*-PEP-*b*-PS ($B1_G$, $B2_G$), PMMA-*g*-SPS-*b*-PEP ($A_H$), PMMA-*g*-PEP-*b*-SPS ($B1_H$, $B2_H$), PMMA-*g*-NaSPS-*b*-PEP ($A_{Na}$), and PMMA-*g*-PEP-*b*-NaSPS ($B1_{Na}$, $B2_{Na}$) at $T$ = 298 K

| | $\chi_{PMMA/PS}N/\lambda$ | $\chi_{PMMA/PEP}N/\lambda$ | $\chi_{PEP/PS}N/\lambda$ | $\chi_{PMMA/SPS}N/\lambda$ | $\chi_{PEP/SPS}N/\lambda$ |
|---|---|---|---|---|---|
| A | 4 | 90 | 18 | 11111 | 1856 |
| B1 | 5 | 99 | 18 | 12468 | 1792 |
| B2 | 6 | 121 | 18 | 15445 | 1792 |

Storage modulus and loss modulus as a function of temperature for PMMA-*g*-PS-*b*-PEP ($A_G$) and PMMA-*g*-PEP-*b*-PS ($B1_G$), PMMA-*g*-SPS-*b*-PEP ($A_H$) and PMMA-*g*-PEP-*b*-SPS ($B1_H$), PMMA-*g*-NaSPS-*b*-PEP ($A_{Na}$), and PMMA-*g*-PEP-*b*-NaSPS ($B1_{Na}$, $B2_{Na}$) are shown in Figure 7.4, 7.5 and 7.6, respectively. Loss modulus peaks determined the transition temperatures, which are summarized in Table 7.5.

Precursor graft copolymers, $A_G$ and $B1_G$ in Figure 7.4 showed three transition temperatures. The $\alpha$ transition ($T_g^1$) at -61 ($A_G$) and -52 °C ($B1_G$) corresponded to the $T_g$ of the PEP block, which ranges from -57 to -63 ºC.[11, 15] The other $\alpha$ transition ($T_g^2$) at 94 ($A_G$) and 91 °C ($B1_G$) implied the $T_g$ of the PMMA blocks. Transition at 8 ($A_G$) or 9 °C ($B1_G$) is assigned to $\beta$ transition. $\beta$ transition of polymethacrylates were reported in the range of 0 ± 40 ºC and $\beta$ transition was attributed to pendant ester chain mobility in

polymethacrylates according to various published data.[16-23] Loss modulus curve at α transition ($T_g^1$) -61 ºC for $A_G$ showed a sharp peak, whereas that for $B1_G$ (-52 °C) gave a broad transition. This difference was presumably due to the location of PS block. As described in Chapter 6, B-type unsulfonated graft copolymer impeded the ability of the graft copolymer to microphase separate and to form an ordered morphology. This was due to the strongly repelled thermodynamic frustration in both ends of P*t*BS block.[7] Similar influence of relative PS block location was seen in these α transitions ($T_g^1$). $A_G$ sample did not possess significant effect of adjacent PS block since PEP block was located at the branch terminus. On the other hand, PS block at the branch terminus in $B_G$ sample seemed to hinder the glass transition of PEP since PEP block was between PMMA backbone and PS block.

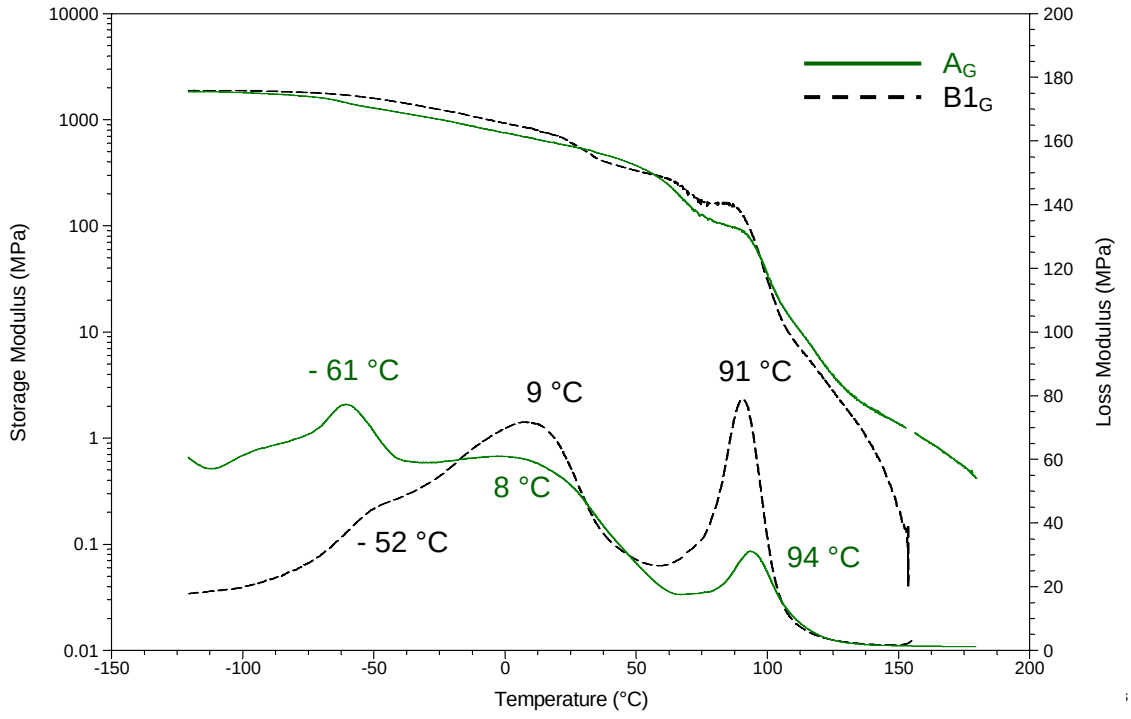


**Figure 7.4** Dynamic mechanical analysis of PMMA-*g*-PS-*b*-PEP ($A_G$) and PMMA-*g*-PEP-*b*-PS ($B1_G$)
DMA condition: tension mode at 2 μm amplitude at a frequency of 1 Hz at a heating rate of 3 °C/min

**Table 7.5** Primary and secondary transition temperatures of PMMA-*g*-PS-*b*-PEP ($A_G$), PMMA-*g*-PEP-*b*-PS ($B1_G$, $B2_G$), PMMA-*g*-SPS-*b*-PEP ($A_H$), PMMA-*g*-PEP-*b*-SPS ($B1_H$, $B2_H$), PMMA-*g*-NaSPS-*b*-PEP ($A_{Na}$), and PMMA-*g*-PEP-*b*-NaSPS ($B1_{Na}$, $B2_{Na}$)

| | $T_g^1$ [°C] | $T_g^2$ [°C] | $T_\beta^1$ [°C] | $T_\beta^2$ [°C] |
|---|---|---|---|---|
| $A_G$ | -61 | 94 | 8 | - |
| $B1_G$ | -52 | 91 | 9 | - |
| $A_H$ | -58 | 87 | 15 | 43 |
| $B1_H$ | - | 94 | 9 | 55 |
| $A_{Na}$ | -58 | 82 | 5 | - |
| $B1_{Na}$ | - | 84 | 9 | - |
| $B2_{Na}$ | - | 80 | 7 | - |

Sulfonic acid graft copolymers, $A_H$ and $B1_H$ in Figure 7.5 showed similar α transitions to precursor graft copolymers ($A_G$ and $B1_G$), which corresponded to $T_g$s of PEP and PMMA block. $B1_H$ sample did not provide clear α transition of PEP block. As seen in Chapter 6, sulfonic acid groups at the branch terminus enhance the formation of ionic aggregates.[7] The aggregation of sulfonic acid groups at the end of graft chain presumably restriced the glass transition of PEP block. The lack of the glass transition of PEP block in $B1_H$ sample also resulted in higher storage modulus in the temperature range between $T_g^1$ and $T_\beta^2$. Interestingly, $A_H$ and $B1_H$ samples showed two β transitions ($T_\beta^1$ and $T_\beta^2$) and the $T_\beta^2$ transition was clearly observed especially in $B1_H$ sample. $T_\beta^1$ corresponded to the above described β transition of PMMA backbone. $T_\beta^2$ appeared to be the β transition of ionic phase, namely the β transition of the branch. Clear second β transition ($T_\beta^2$) in $B1_H$ sample also suggested the formation of ionic aggregates, whereas $A_H$ sample presumably formed sparse ionic aggregates.

Hara et al.'s study[21] supported the observation of the two β transitions. They characterized 0 – 25 mol% PMMA-based ionomer using DMA and reported PMMA-based ionomer possessed two β transitions. The first β transition was attributed to the

rotation of the methoxycarbony side group (-$COOCH_3$), β transition of no ionic phase or ion-poor phase. Pure PMMA provided only this first β transition, whereas the ionomers provided the second β transition. The second β transition was attributed to a rotation in ion-rich phase. The ionic interaction restricted the local motion (β transition) and resulted in the second relaxation peak at higher temperature than the first β transition.

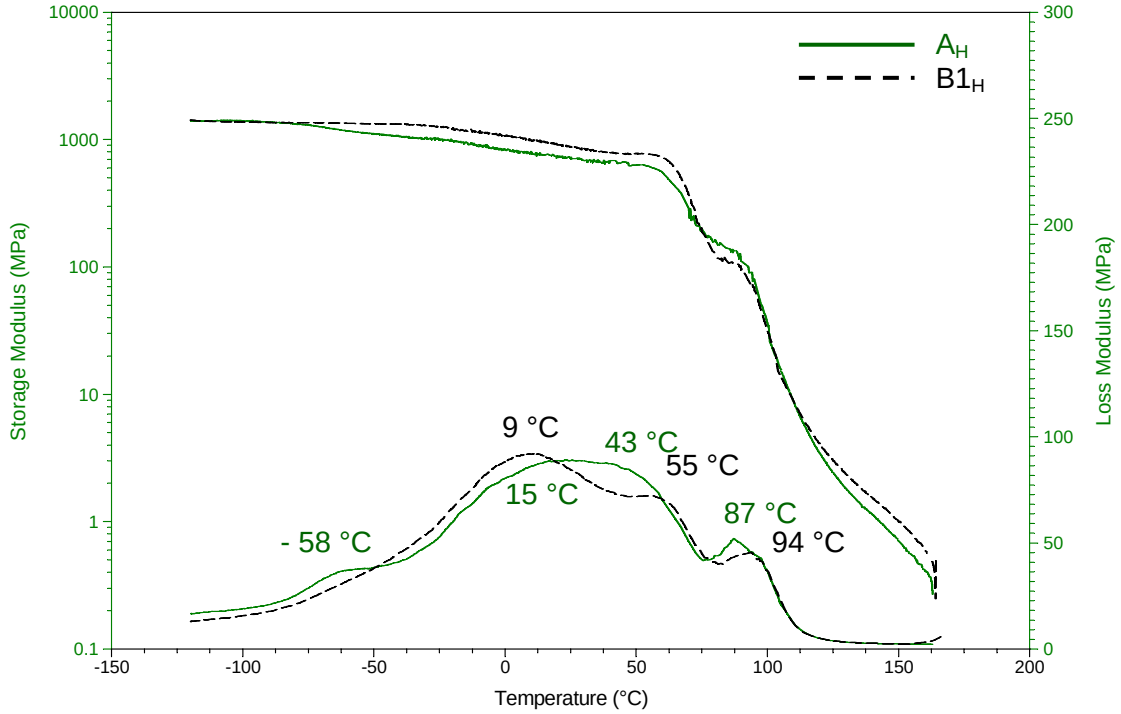


**Figure 7.5** Dynamic mechanical analysis of PMMA-*g*-SPS-*b*-PEP ($A_H$) and PMMA-*g*-PEP-*b*-SPS ($B1_H$)
DMA condition: tension mode at 5 μm amplitude at a frequency of 1 Hz at a heating rate of 3 °C/min

α transitions of sodium sulfonate graft copolymers, $A_{Na}$, $B1_{Na}$, and $B2_{Na}$, in Figure 7.6 resulted in similar to that of sulfonic acid graft copolymers ($A_H$ and $B1_H$). The α transitions corresponded to the $T_g$s of the PEP and PMMA block. As seen in $B1_H$ sample, $B1_{Na}$ and $B2_{Na}$ samples did not provide significant α transition of PEP block. The aggregation of sodium sulfonate groups at the branch terminus restricted the glass

transition of PEP block in the loss modulus curve. This lack of the glass transition of PEP block in $B1_{Na}$ and $B2_{Na}$ samples again resulted in higher storage modulus in the temperature range between $T_g^1$ and $T_g^2$. Although sulfonic acid graft copolymer $A_H$ and $B1_H$ samples showed two β transitions ($T_\beta^1$ and $T_\beta^2$), $A_{Na}$, $B1_{Na}$, and $B2_{Na}$ did not show $T_\beta^2$. $T_\beta^2$ values of $A_{Na}$, $B1_{Na}$, and $B2_{Na}$ were expected to be higher temperature than that of $A_H$ and $B1_H$ due to stronger ionic interaction of sodium sulfonate groups than sulfonic acid groups. The second β transitions ($T_\beta^2$) for $A_{Na}$, $B1_{Na}$, and $B2_{Na}$ were presumably hidden in α transition of $T_g^2$. In addition, $B1_{Na}$, and $B2_{Na}$ did not show significant difference, which implied that the graft copolymer architecture affected the properties rather than the molecular weight.

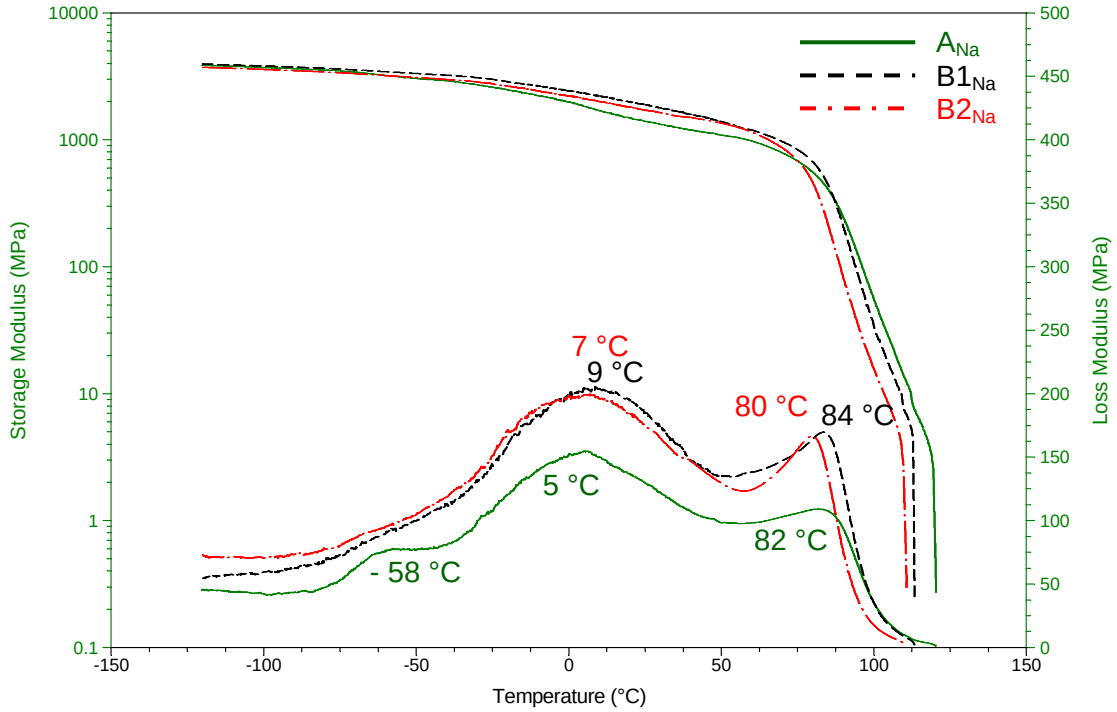


**Figure 7.6** Dynamic mechanical analysis of PMMA-*g*-NaSPS-*b*-PEP ($A_H$) and PMMA-*g*-PEP-*b*-NaSPS ($B1_H$, $B2_H$)
DMA condition: tension mode at 5 μm amplitude at a frequency of 1 Hz at a heating rate of 3 °C/min

## 7.5 Conclusions

Novel selectively-sulfonated graft copolymers, PMMA-*g*-(SPS-*b*-PEP) (A) and PMMA-*g*-(PEP-*b*-SPS) (B) were successfully synthesized. The graft copolymers contained approximately 1-2 average branches and 1 wt% of sulfonic acid or sodium sulfonate blocks adjacent to the backbone (A) or at the branch terminus (B). Estimated $\chi N$ values predicted the phase separation occurrence of each block and the constant $T_g$ values of PMMA block for all graft copolymers upon DSC suggested the phase separation of the graft copolymers, although the $T_g$ values of PEP block in DSC was not observed. DMA experiment also confirmed the phase separation of each block components of the graft copolymers. Precursor graft copolymers, $A_G$ and $B1_G$ showed three transition temperatures. Two α transitions were attributed to the $T_g$s of PEP block ($T_g^1$) and $T_g$ of PMMA block ($T_g^2$). Transitions at around 10 °C were attributed to β transition, which was a rotation of pendant ester chains in PMMA backbone. The aggregation of sulfonic acid or sodium sulfonate groups at the branch terminus restricted the glass transition of PEP block and glass transition of PEP block was not observed in $B1_H$, $B1_{Na}$, and $B2_{Na}$ samples, whereas $A_H$ and $A_{Na}$ showed the glass transition of PEP block in the loss modulus curve. This lack of the glass transition of PEP block in $B1_H$, $B1_{Na}$, and $B2_{Na}$ samples also resulted in higher storage modulus in the temperature range between $T_g^1$ and $T_g^2$ than $A_H$ and $A_{Na}$,.

This work demonstrated that placing sulfonated block at the branch terminus enhanced the formation of ionic aggregates due to the mobility of the branch ends, while copolymers with the sulfonated blocks adjacent to the polymer backbone exhibited little insignificant formation of ionic aggregates. The formation of ionic aggregates in B-type

graft copolymers altered the subsequent thermal transitions. Therefore, location of ionic blocks in molecular architecture plays a significant role in the subsequent properties, and the location of ionic block in molecular architecture can be utilized as a design parameter for utilization of ionomers.

## 7.5 Acknowledgements

This material is based upon work supported by, or in part by, the U.S. Army Research Laboratory and the U.S. Army Research Office under grant number DAAD19-02-1-0275 Macromolecular Architecture for Performance (MAP) MURI.

## 7.6 References

1. McGrath, J. E., Block and graft copolymer. *Journal of Chemical Education* **1981,** 58, (11), 914-921.
2. Jenkins, D. W.; Hudson, S. M., Review of vinyl graft copolymerization featuring recent advances toward controlled radical-based reactions and illustrated with chitin/chitosan trunk polymers. *Chemical Reviews* **2001,** 101, (11), 3245-3273.
3. Hadjichristidis, N.; Pitsikalis, M.; Iatrou, H.; Pispas, S., The strength of the macromonomer strategy for complex macromolecular architecture: Molecular characterization, properties and applications of polymacromonomers. *Macromolecular Rapid Communications* **2003,** 24, (17), 979-1013.
4. Ito, K., Polymeric design by macromonomer technique. *Progress in Polymer Science* **1998,** 23, (4), 581-620.
5. Hickner, M. A.; Ghassemi, H.; Kim, Y. S.; Einsla, B. R.; McGrath, J. E., Alternative polymer systems for proton exchange membranes (PEMs). *Chemical Reviews* **2004,** 104, (10), 4587-4611.
6. Harrison, W. L.; Hickner, M. A.; Kim, Y. S.; McGrath, J. E., Poly(arylene ether sulfone) copolymers and related systems from disulfonated monomer building blocks: Synthesis, characterization, and performance - A topical review. *Fuel Cells* **2005,** 5, (2), 201-212.
7. Saito, T.; Mather, B. D.; Costanzo, P. J.; Beyer, F. L.; Long, T. E., Influence of site-specific sulfonation on acrylic graft copolymer morphology. *Macromolecules* **2008,** in press.
8. Schulz, G. O.; Milkovich, R., Graft polymers with macromonomers 1. Synthesis from methacrylate-terminated polystyrene. *Journal of Applied Polymer Science* **1982,** 27, (12), 4773-4786.
9. McGrath, J. E.; Wilkes, G. L.; Ward, T. C.; Broske, A. D.; Lee, B.; Yilgor, I.; Bradley, D. J.; Hoover, J. M.; Long, T. E., *New Elastomer Synthesis for High Performance Applications*. Noyes Data Corporation Parkridge, New Jersey, 1988; p 118.
10. Van Krevelen, D. W.; Hoftyzer, P. J., *Properties of Polymers*. Elsevier: New York, 1976.
11. Brandrup, J.; Immergut, E. H., *Polymer Handbook*. 3rd ed.; Wiley: New York, 1989.
12. Roth, M., Solubility parameter of poly(dimethyl siloxane) as a function of temperature and chain-length. *Journal of Polymer Science Part B-Polymer Physics* **1990,** 28, (13), 2715-2719.

13. Kim, B.; Kim, J.; Jung, B., Morphology and transport properties of protons and methanol through partially sulfonated block copolymers. *Journal of Membrane Science* **2005,** 250, (1-2), 175-182.
14. Lu, X. Y.; Weiss, R. A., Development of miscible blends of Bisphenol A polycarbonate and lightly sulfonated polystyrene ionomers from intrapolymer repulsive interactions. *Macromolecules* **1996,** 29, (4), 1216-1221.
15. Gotro, J. T.; Graessley, W. W., Model hydrocarbon polymers - Rheological properties of linear polyisoprenes and hydrogenated polyisoprenes. *Macromolecules* **1984,** 17, (12), 2767-2775.
16. Zhou, Z.; Zhang, X.; Xu, P.; Lu, H., Investigation of pendant group and chain segment motions in P(MMA/BA) copolymers by thermally stimulated depolarization current. *Journal of Macromolecular Science, Part B: Physics* **2007,** 46, (5), 1013-1021.
17. Gutierrez-Villarreal, M. H.; Rodriguez-Velazquez, J., The effect of citrate esters as plasticizers on the thermal and mechanical properties of poly(methyl methacrylate). *Journal of Applied Polymer Science* **2007,** 105, (4), 2370-2375.
18. Monnerie, L.; Halary, J. L.; Kausch, H.-H., Deformation, yield and fracture of amorphous polymers: Relation to the secondary transitions. *Advances in Polymer Science* **2005,** 187, (Intrinsic Molecular Mobility and Toughness of Polymers I), 215-364.
19. de Deus, J. F.; Souza, G. P.; Corradini, W. A.; Atvars, T. D. Z.; Akcelrud, L., Relaxations of Poly(methyl methacrylate) Probed by Covalently Attached Anthryl Groups. *Macromolecules* **2004,** 37, (18), 6938-6944.
20. Espadero Berzosa, A.; Gomez Ribelles, J. L.; Kripotou, S.; Pissis, P., Relaxation Spectrum of Polymer Networks Formed from Butyl Acrylate and Methyl Methacrylate Monomeric Units. *Macromolecules* **2004,** 37, (17), 6472-6479.
21. Ma, X.; Sauer, J. A.; Hara, M., Poly(methyl methacrylate) Based Ionomers. 1. Dynamic Mechanical Properties and Morphology. *Macromolecules* **1995,** 28, (11), 3953-62.
22. Lustig, S. R.; Caruthers, J. M.; Peppas, N. A., Dynamic mechanical properties of polymer-fluid systems: characterization of poly(2-hydroxyethyl methacrylate) and poly(2-hydroxyethyl methacrylate-co-methyl methacrylate) hydrogels. *Polymer* **1991,** 32, (18), 3340-53.
23. Clarke, R. L., Dynamic mechanical thermal analysis of dental polymers. I. Heat-cured poly(methyl methacrylate)-based materials. *Biomaterials* **1989,** 10, (7), 494-8.

# Chapter 8: Synthesis and Characterization of Well-Defined Low $T_g$ Diblock Copolymers

## 8.1 Abstract

Well-defined 3000 g/mol hydrogenated PI (poly(ethylene-*co*-propylene), PEP) and symmetric (16000 g/mol each block) and asymmetric (14000 g/mol and 10000 g/mol each block) poly(ethylene-*co*-propylene)-*b*-poly(dimehtyl siloxane) (PEP-*b*-PDMS) were synthesized using living anionic polymerizationa and subsequent hydrogenation. The incorporated amount of each block was consistent with the weight loss of each thermal degradation step in thermogravimetric analysis. The onset of thermal degradation for PEP-*b*-PDMS diblock copolymer was higher than 300 ºC and PEP-*b*-PDMS was more thermally stable than the precursor polyisoprene-*b*-PDMS. Differential scanning calorimetry analysis of PEP-*b*-PDMS provided $T_g$ of PDMS -125 ºC, $T_g$ of PEP -60 or -61 ºC, $T_c$ of PDMS -90 or -91 ºC, and $T_m$ of PDMS -46 and -38 ºC, respectively. Appearance of thermal transitions of each PEP and PDMS block revealed the formation of phase separation. The phase separation was also supported by calculating $\chi N$ of 43 and 33 for 16kPEP-*b*-16kPDMS and 14kPEP-*b*-10kPDMS.

## 8.2 Introduction

The compositional dissimilarity of blocks in block copolymers leads to microphase separation and results in the ordered structure in morphology as described in Chapter 2 and Chapter 6. The chemical architecture and composition of block copolymers results in unique properties and usage in various applications. Block

copolymer melts also exhibit similar behavior to amphiphilic systems such as soaps and surfactants.[1]

Block copolymers have been investigated as compatibilizers for immiscible polymer blends of the block components.[2, 3] The microstructure of the polymer blends during processing influences the resulting properties. The addition of compatibilizers stabilizes a fine microstructure between two phases and the components of compatibilizers affect deformation, break-up and coalescence of droplets during processing.[4, 5] The addition of block copolymers as compatibilizers for the two immiscible polymer blends suppresses droplet coalescence and retains the desired properties of the polymer blends.

Macosko et al. reported an important example of block copolymer compatibilizers. They investigated the effect of block copolymers on the cocontinuous morphology of 50/50 (w/w) polystyrene (PS)/high density polyethylene (HDPE) blends using symmetric polystyrene–polyethylene block copolymers (PS-*b*-PE) with molecular weights varying from 6 to 200 kg/mol.[2] Macosko and Puyvelde et al. also reported the effect of block copolymer architecture on the coalescence and interfacial elasticity in compatibilized polymer blends using polyisoprene-*b*-poly(dimethylsiloxane) (PI-*b*-PDMS). The effect of molecular weight and asymmetry of block copolymers as compatibilizers was studied.[3]

PI-*b*-PDMS possess a characteristic of low $T_g$ values (PI -71 ºC,[6] and PDMS -123 ºC[7]). This low $T_g$ property makes PI-*b*-PDMS a suitable diblock copolymer for a compatibilizer study or a phase behavior study due to the equilibrated phase-separated behavior at room temperature. However, PI block possesses poor oxidative stability[8] and a long time storage or experiment at ambient condition with heat would not produce

reliable data. Therefore, the hydrogenation of PI block to poly(ethylene-*co*-propylene) is the common strategy to alter it to oxidatively stable composition.

Poly(ethylene-*co*-propylene)-*b*-PDMS (PEP-*b*-PDMS), where PEP is hydrogenated PI, has been synthesized and used for various phase behavior studies.[1, 8-20] None of the phase behavior studies described the detail discussion of synthetic scheme or the thermal characterization of PEP-*b*-PDMS. In this chapter, we report the detail synthesis of PEP (hydrogenate PI) and PEP-*b*-PDMS, and thermal characterization using thermogravimetric analysis (TGA) and differential scanning calorimetry (DSC).

## 8.3 Experimental

### 8.3.1 Materials and Chemicals

Isoprene (Aldrich, 99%) was treated with dibutylmagnesium (Aldrich, 0.10 mM) and distilled under vacuum prior to use. Cyclohexane (Fisher Scientific, HPLC) was passed through an activated molecular sieve column (Aldrich, 60 Å mesh) and activated alumina column immediately prior to use. 1.6 M *sec*-butyllithium solution in hexanes (*sec*BuLi, FMC Lithium), nickel 2-ehtylhexanoate (nickel octoate, Alfa Aesar), 1.0 M triethylaluminum in hexanes (Aldrich), citric acid (Aldrich, 98%), triethylamine (Aldrich, 99%), methanol (Fisher Scientific) and deuterated chloroform ($CDCl_3$, Cambridge Isotope Laboratories) were used as received. Hexamethylcyclotrisiloxane ($D_3$, Aldrich, 98%) was dried over calcium hydride (Aldrich, 95%) for 24 h and distilled under vacuum. Chlorotrimethylsilane (Aldrich, 99%) was treated with an aliquot of *sec*-butyllithium (Aldrich, 1.4 M) and distilled under vacuum prior to use. Higher distillation efficiency of $D_3$ was achieved through dissolving $D_3$ in cyclohexane with calcium hydride and distilled

both at once under vacuum. Tetrahydrofuran (THF, Fisher Scientific) were passed through PURE SOLV MD-3 SOLVENT PURIFICATION SYSTEM (Innovative Technology Inc.) immediately prior to use.

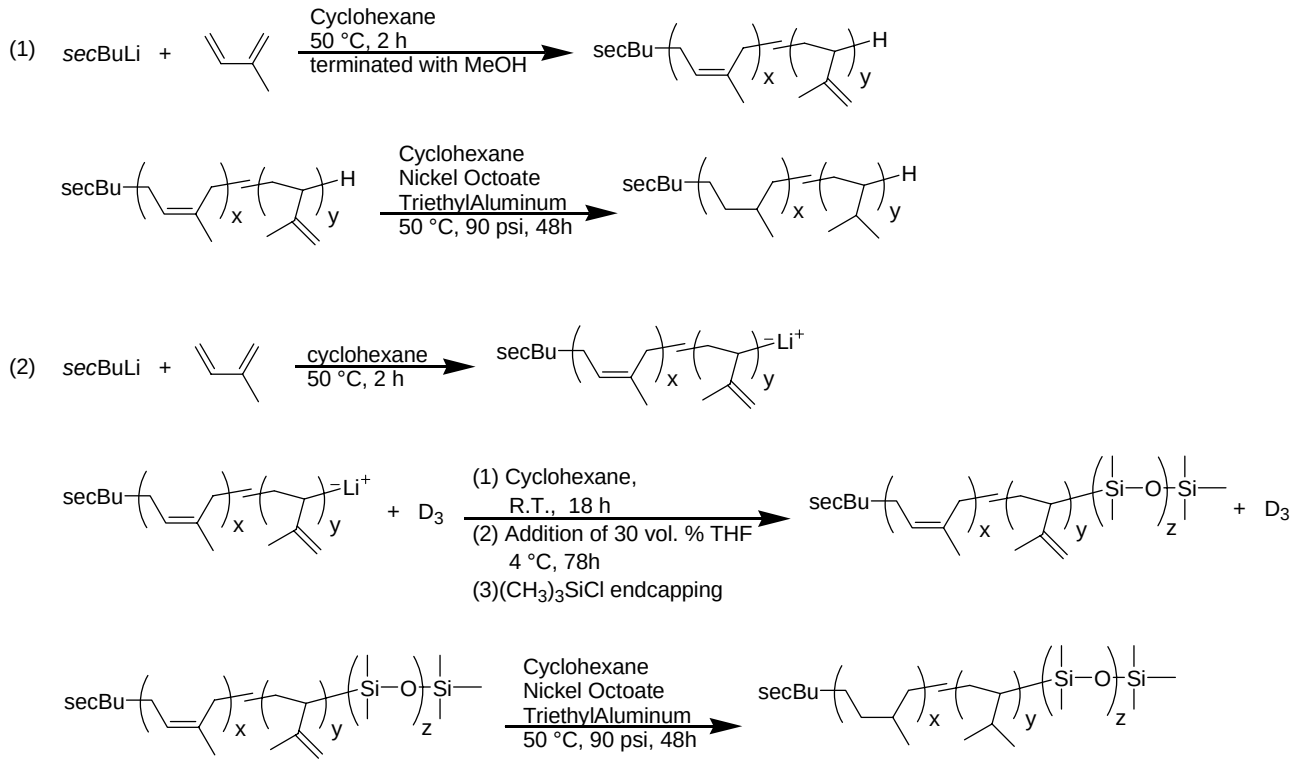


**Scheme 8.1** Synthesis of PEP (1) and PEP-*b*-PDMS (2)

### 8.3.2 Synthesis of PI

A 600 mL-capacity anionic polymerization reactor was filled with cyclohexane (350 mL) and the temperature was maintained at 50 °C. The glass anionic reactor[21] consists of a 600 mL glass bowl, a stainless steel top plate, and stainless steel magnetically coupled mechanical stirrer. In addition, a heat-exchange coil, a thermocouple, a septum sealed port, various stainless steel transfer lines to introduce solvent (cyclohexane), and inlet/vent for purified nitrogen are equipped to the anionic reactor. The anionic reactor system was maintained at a constant nitrogen pressure (40

psi). Isoprene (88 mL, 60 g) was syringed into the reactor. *sec*-BuLi (12.49 mL, 20.0 mmol) was then added to the solution to initiate the anionic polymerization. As illustrated in Scheme 8.1 (1), the reaction was allowed to proceed 2 h and terminated by adding nitrogen-degassed methanol. The PI solution was passed through a filter to remove lithium salts and the filtered solution was directly used in the next step synthesis. $^1$H NMR (400 MHz, $CDCl_3$, δ): 0.8 – 0.9 ppm (br, C*H*$_3$CH$_2$CH(C*H*$_3$)-), 1.1 – 1.2 ppm (br, -C*H*$_3$ in 1,2-polyisoprene units), 1.2 – 1.5 ppm (br, -C*H*$_2$CH-, -CH$_2$C*H*- in 1,2-polyisoprene and 3,4-polyisoprene units), 1.61 ppm (br, -C*H*$_3$ in *trans*-1,4-polyisoprene units), 1.64 ppm (br, -C*H*$_3$ in 3,4-polyisoprene units), 1.68 ppm (br, -C*H*$_3$ in *cis*-1,4-polyisoprene units), 1.8 – 2.2 ppm (br, -C*H*$_2$CH=, -C*H*$_2$C(CH$_3$)= in 1,4-polyisoprene units), 4.6 – 4.8 ppm (br, -C(CH$_3$)=C*H*$_2$ 3,4-polyisoprene units and -CH=C*H*$_2$ 1,2-polyisoprene units), 4.8 – 5.4 ppm (br, -C*H*=C(CH$_3$)- 1,4-polyisoprene units).

### 8.3.3 Synthesis of PI-*b*-PDMS

The reaction procedure for synthesizing PI-*b*-PDMS was modified from Hadjichristidis' previously reported procedure.[22] Cyclohexane (25 mL) was transferred to a flame-dried 100 mL round-bottomed flask equipped with a magnetic stirrer. Isoprene (11.01 mL, 7.5 g) was syringed into the reactor and the temperature was held at 50 ºC. s*ec*-BuLi (0.28 mL, 0.442 mmol) was then added to the solution to initiate the anionic polymerization. The first reaction was allowed to proceed 2 h and a portion of the reaction mixture was taken out for PI characterization. Then, $D_3$ in cyclohexane (18.7 mL of 0.5 g/mL $D_3$ solution, 9.4g $D_3$) was added to the reaction mixture and the reaction mixture was allowed to stir for 18 h at room temperature to ensure the crossover reaction from isoprenyllithium to lithium silanolate. THF (24 mL, 30 vol%) was

transferred to the reaction and the reaction mixture was stirred at 4 ºC in a refrigerator for 78 h. 1.2 fold of chlorotrimethylsilane was syringed into the reaction mixture to terminate the reaction (Scheme 8.1 (2)). After 10 min, aliquot of triethylamine was added to scavenge acid and the solution was precipitated into methanol. The precipitation was repeated three times to remove salts and unreacted $D_3$ monomer. The obtained PI-*b*-PDMS was dried under reduced pressure at room temperature for 72 h. $^1$H NMR (400 MHz, $CDCl_3$, δ): 0 ppm (br, -Si(C*H*$_3$)$_2$O-), 0.8 – 0.9 ppm (br, C*H*$_3$CH$_2$CH(C*H*$_3$)-), 1.1 – 1.2 ppm (br, -C*H*$_3$ in 1,2-polyisoprene units), 1.2 – 1.5 ppm (br, -C*H*$_2$CH-, -CH$_2$C*H*- in 1,2-polyisoprene and 3,4-polyisoprene units), 1.61 ppm (br, -C*H*$_3$ in *trans*-1,4-polyisoprene units), 1.64 ppm (br, -C*H*$_3$ in 3,4-polyisoprene units), 1.68 ppm (br, -C*H*$_3$ in *cis*-1,4-polyisoprene units), 1.8 – 2.2 ppm (br, -C*H*$_2$CH=, -C*H*$_2$C(CH$_3$)= in 1,4-polyisoprene units), 4.6 – 4.8 ppm (br, -C(CH$_3$)=C*H*$_2$ 3,4-polyisoprene units and -CH=C*H*$_2$ 1,2-polyisoprene units), 4.8 – 5.4 ppm (br, -C*H*=C(CH$_3$)- 1,4-polyisoprene units).

### 8.3.4 Hydrogenation of Polyisoprene Blocks

Cyclohexane (50 mL) and nickel octoate (1.0g, 2.9 mmol) were added to a flame-dried 100 mL amber bottle equipped with a magnetic stirrer. 1.0 M triethylaluminum solution (8.69 mL, 8.9 mmol) was added dropwise to the nickel solution. An opaque, black colloidal suspension formed immediately and was allowed to age for 15 min at room temperature under a nitrogen atmosphere to form a homogeneous solution. Previously described PI (60 g) cyclohexane solution (400 mL) or PI-*b*-PDMS (12 g) cyclohexane solution (200mL) and a preformed nickel catalyst (30 mL, 1.5 mmol) were added to a 600 mL reactor. The reactor was pressurized with hydrogen and vented three

times. The vessel was pressurized with hydrogen (90 psi) and heated to 50 °C. The reaction mixture was allowed to stir for 24 h. Another preformed nickel catalyst (30 mL, 1.5 mmol) was added. The reactor was again pressurized with hydrogen and vented three times. The vessel was pressurized with hydrogen (90 psi), heated to 50 °C, and stirred for another 24 h (Scheme 8.1 (2)). The nickel catalyst was extracted from the polymer solution with citric acid washes. The polymer solution was precipitated into methanol, and dried in vacuo at room temperature for 72 h. $^1$H NMR (400 MHz, $CDCl_3$, δ) for hydrogenated PI (PEP): 0.7 – 1.0 ppm (br, -C*H*$_3$), 1.0 – 1.6 ppm (br, -C*H*$_2$-). $^1$H NMR (400 MHz, $CDCl_3$, δ) for PEP-*b*-PDMS: 0 ppm (br, -Si(C*H*$_3$)$_2$O-), 0.7 – 1.0 ppm (br, -C*H*$_3$), 1.0 – 1.6 ppm (br, -C*H*$_2$-).

### 8.3.5 Polymer Characterization

$^1$H NMR spectra of the polymers were obtained on a Varian Unity spectrometer operating at 400 MHz at ambient temperature. $CDCl_3$ was used as the solvent. Size exclusion chromatography (SEC) measurements were performed in THF at 40 °C at flow rate 1 mL/min using a Waters size exclusion chromatograph equipped with an autosampler, three 5-mm PLgel Mixed-C columns, a Waters 410 refractive index (RI) detector operating at 880 nm, and a miniDAWN multiangle laser light scattering (MALLS) detector operating at 690 nm which was calibrated with narrow polydispersity polystyrene standards. The RI increment (*dn*/*dc*) was calculated online. Glass transition temperatures, crystallization temperatures, and melting temperatures were determined using a differential scanning calorimeter (DSC) Q100 (TA instruments) at a heating rate of 10 °C/min under helium. Glass transition temperatures are reported as the transition midpoint during the second heat. Thermogravimetric analysis (TGA) measurements

were conducted using a TA Instruments Hi-Res TGA 2950 thermogravimetric analyzer under $N_2$ at a heating rate of 10 ºC/min.

## 8.4 Results and Discussion

### 8.4.1 Synthesis of PEP and PEP-*b*-PDMS

PEP (target MW 3000 g/mol) was synthesized via living anionic polymerization and subsequent hydrogenation. The integration of the $^1$H NMR resonances for two methyl groups in the s*ec*-butyl group (A) at 0.8 - 0.9 ppm and the integrations of C($CH_3$)=C$H_2$ 3,4-polyisoprene units and -CH=C$H_2$ 1,2-polyisoprene units at 4.6 – 4.8 ppm and -C*H*=C($CH_3$)- 1,4-polyisoprene units at 4.8 – 5.4 ppm were used to calculate the number-average molecular weight. The microstructure of the polyisoprene was estimated using the integration for a methyl group in 1,2-polyisoprene units at 1.15 ppm, a methyl group in *trans*-1,4-polyisoprene units at 1.61 ppm, a methyl group in 3,4-polyisoprene units at 1.64 ppm, and a methyl group in *cis*-1,4-polyisoprene units at 1.68 ppm. The molecular weights and microstructure are summarized in Table 8.1. The molecular weights ($M_n$ from NMR and SEC) were approximately 3000 g/mol and narrow molecular distributions ($M_w/M_n$) 1.04 were obtained. SEC analysis for both PI and PEP exhibited monomodel curves, which indicated no side reaction occurrence upon hydrogenation.

**Table 8.1** Molecular weights and microstructure of 3000 g/mol PI and PEP

| | Microstructure [%] | | | | | | |
|---|---|---|---|---|---|---|---|
| | *cis*-1,4 | *trans*-1,4 | 3,4 | 1,2 | $M_n$[a] | $M_n$[b] | $M_w/M_n$[b] |
| PI | 70 | 24 | 5 | 1 | 3030 | 2930 | 1.04 |
| PEP | | | | | | 3100 | 1.04 |

[a] $^1$H NMR conditions; Varian Unity 400 MHz, $CDCl_3$
[b] Determined using SEC at 40 °C in THF with a MALLS detector

Symmetric PI-*b*-PDMS (target molecular weight, 16kPI-*b*-16kPDMS) and asymmetric PI-*b*-PDMS (target molecular weight, 16kPI-*b*-12kPDMS) were synthesized via living anionic polymerization. The molecular weight calculation from $^1$H NMR followed the above described $^1$H NMR assignments for PI and used the integration of -Si(C$H_3$)$_2$O- from PDMS block at $^1$H NMR resonance 0 ppm. Molecular weights of PI-*b*-PDMS are summarized in Table 8.2. $^1$H NMR of 16kPI-*b*-16kPDMS is shown in Figure 8.1 (1) and SEC trace of 16kPI-*b*-16kPDMS is depicted in Figure 8.2 (1). Molecular weight from $^1$H NMR agreed well with the SEC molecular weight and narrow polydispersity indices less than 1.1 were obtained. The symmetric and asymmetric PI-*b*-PDMS were prepared in the range of the target molecular weight. As shown in SEC curve in Figure 8.2 (1), a partial termination of PI block occurred for 16kPI-*b*-16kPDMS, while 14kPI-*b*-10kPDMS did not show the partial termination. This was due to the impurity upon second block $D_3$ monomer addition. $D_3$ monomer final conversion ranged 75 – 80 % whereas isoprene gave quantitative conversion. The amount of $D_3$ monomer addition for PDMS block utilized the assumption of 80% $D_3$ conversion to obtain the target molecular weight. The microstructure of PI block for both 16kPI-*b*-16kPDMS and 14kPI-*b*-10kPDMS resulted in 70% *cis*-1,4, 25% *trans*-1,4, and 5% 3,4 microstructure, which were consistent with the microstructure of PI homopolymer in Table 8.1.

Hydrogenation of symmetric and asymmetric PI-*b*-PDMS was conducted. $^1$H NMR and SEC curve of 16kPEP-*b*-16kPDMS are shown in Figure 8.1 (2) and Figure 8.2 (2). The molecular weights of 16kPEP-*b*-16kPDMS and 14kPEP-*b*-10kPDMS are tabulated in Table 8.3. As shown in $^1$H NMR in Figure 8.1, the double bond of isoprene block at 4.6 – 5.4 ppm disappeared, which indicated achievement of the quantitative

hydrogenation. The molecular weights and of PEP-*b*-PDMS in Table 8.3 retained the precursor molecular weights of PI-*b*-PDMS in Table 8.2 and the narrow polydispersity indices were maintained. In addition, the reduction of tailing in SEC curve in Figure 8.2 (2) was observed, which suggested that the fractionation upon precipitation in methanol removed the PEP homopolymer in the 16kPEP-*b*-16kPDMS sample.

**Table 8.2** Molecular weights of PI-*b*-PDMS

| Target MW | $M_n$ PI[a] | $M_n$ PDMS[a] | $M_n$ PI-*b*-PDMS[a] | $M_n$ PI[b] | $M_n$ PI-*b*-PDMS[b] | $M_w/M_n$ PI-b-PDMS[b] |
|---|---|---|---|---|---|---|
| 16kPI-*b*-16kPDMS | 15500 | 15800 | 31400 | 15500 | 31000 | 1.03 |
| 16kPI-*b*-12kPDMS | 14100 | 9700 | 23800 | 13300 | 24200 | 1.09 |

[a] $^1$H NMR conditions; Varian Unity 400 MHz, $CDCl_3$
[b] Determined using SEC at 40 °C in THF with a MALLS detector

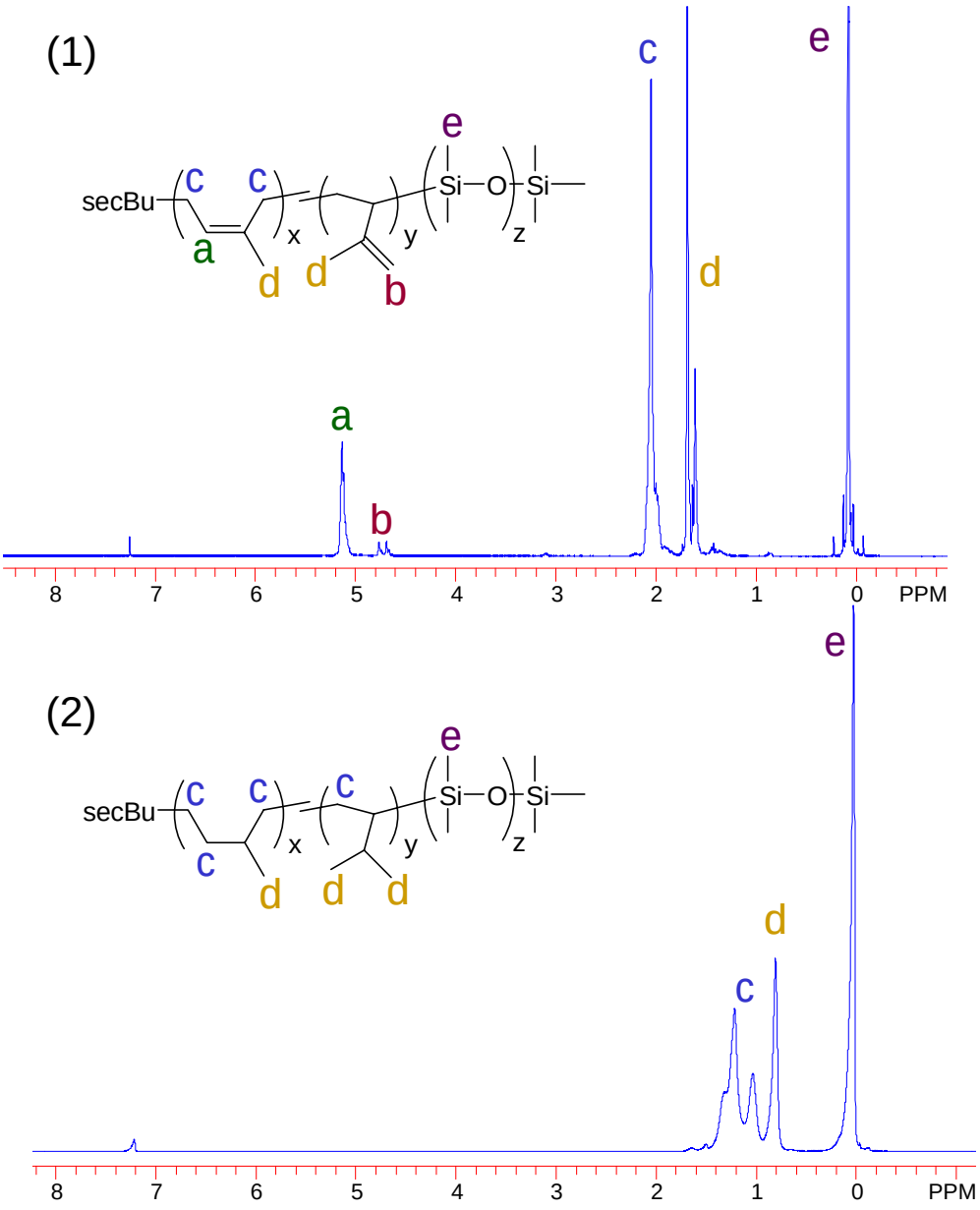


**Figure 8.1** $^{1}$H NMR of 16kPI-*b*-16kPDMS (1) and 16kPEP-*b*-16kPDMS (2)

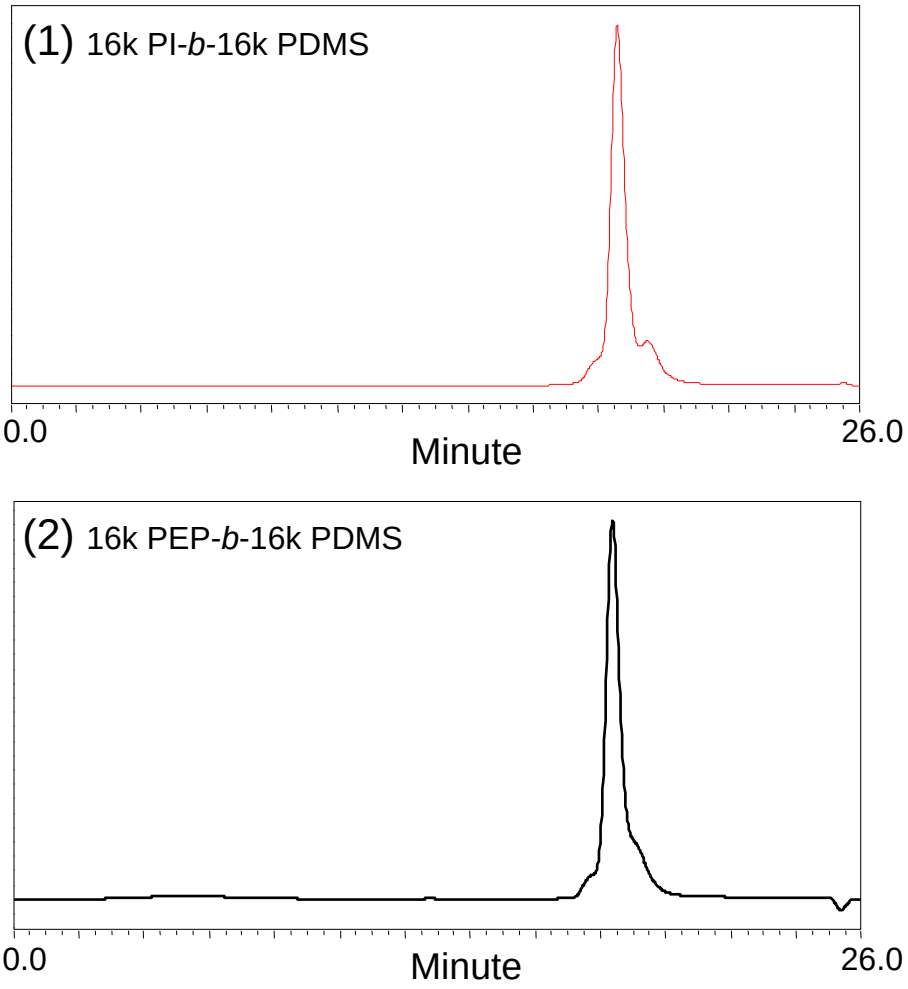


**Figure 8.2** SEC curves of 16kPI-*b*-16kPDMS (1) and 16kPEP-*b*-16kPDMS (2)

**Table 8.3** Molecular weights of PEP-*b*-PDMS

| | $M_n$* | $M_w/M_n$* |
|---|---|---|
| 16kPEP-*b*-16kPDMS | 32000 | 1.04 |
| 14kPEP-*b*-10kPDMS | 25300 | 1.04 |

*Determined using SEC at 40 °C in THF with a MALLS detector

### 8.4.2 Thermal Characterization and Phase Separation of PI- *b*-PDMS and PEP-*b*-PDMS

Thermal degradation behavior of PI-*b*-PDMS and PEP-*b*-PDMS diblock copolymers was studied using a TGA analyzer. TGA and derivative TGA of 16kPI, 16kPI-*b*-16kPDMS and 14kPI-*b*-10kPDMS are shown in Figure 8.3 and the data are

summarized in Table 8.4. The first step degradation of the diblock copolymer corresponded to the degradation of PI block, where $T_{max1}$ ranged 351 – 354 ºC. The $T_{max1}$ range of PI was consistent with the degradation study of PI and other analogues.[23] The second transition with $T_{max2}$ corresponded to the thermal degradation of PDMS block. Thermal degradation study of polysiloxanes[24] reported the onset of degradation of PDMS ranged 370 – 380 ºC in both in air and nitrogen and the previously reported degradation behavior of polysiloxanes[24-27] was consistent with the degradation of PDMS block in these PI-*b*-PDMS diblock copolymers.

Two step thermal degradations of PI-*b*-PDMS also indicated the incorporated amount of each block. The first degradation of PI block appeared to become a plateau around 425 ºC. 16kPI-*b*-16kPDMS and 14kPI-*b*-10kPDMS showed 53% and 38% residual weight at 425 ºC, respectively. The residual weights were in good agreement with the incorporated amount of PDMS block in 16kPI-*b*-16kPDMS and 14kPI-*b*-10kPDMS. Determination of the amount of block in diblock copolymer incorporated using thermal transition in TGA was also previously reported, e.g. in PDMS-*b*-poly(alkyl methacrylic acid)[28] and this TGA study showed the similar trend to the previous example.[28]

Thermal degradation behavior between 16kPI-*b*-16kPDMS and 16kPEP-*b*-16kPDMS was compared and the TGA curves are shown in Figure 8.4. PEP (or PE, PP) is more thermally stable than PI.[25-27] The derivative maximum of the thermal degradation in the first step, $T_{max1}$, resulted in 417 ºC (Table 8.4), which was approximately 65 ºC higher than that of PI block. The first degradation of PEP block showed a plateau around 437 ºC and the residual weight of 16kPEP-*b*-16kPDMS at 437

ºC resulted in 50% (Table 8.4), which is consistent with incorporated amount of PDMS. The onset 5 wt% degradation temperature of 16kPEP-*b*-16kPDMS resulted in 345 ºC. This implies that PEP-*b*-PDMS diblock copolymer is thermally stable over 300 ºC.

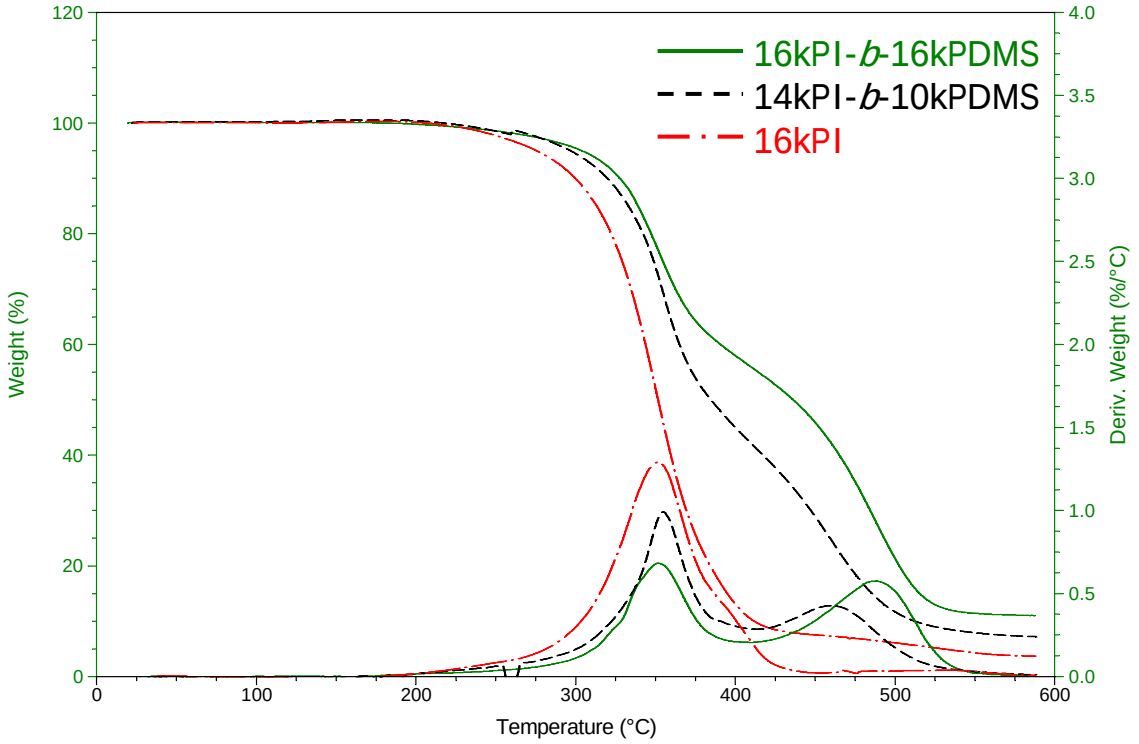


**Figure 8.3** TGA analysis of 16kPI, 16kPI-*b*-16kPDMS and 14kPI-*b*-10kPDMS

**Table 8.4** Thermal degradation of 16kPI, 14kPI-*b*-10kPDMS, 16kPI-*b*-16kPDMS, and 16kPEP-*b*-16kPDMS

| | $T_{max1}$ [ºC] | $T_{max2}$ [ºC] | Weight % at 425 ºC | Weight % at 437 ºC |
|---|---|---|---|---|
| 16kPI | 352 | - | 8 | - |
| 14kPI-*b*-10kPDMS | 354 | 459 | 38 | - |
| 16kPI-*b*-16kPDMS | 351 | 488 | 53 | - |
| 16kPEP-*b*-16kPDMS | 417 | 515 | - | 50 |

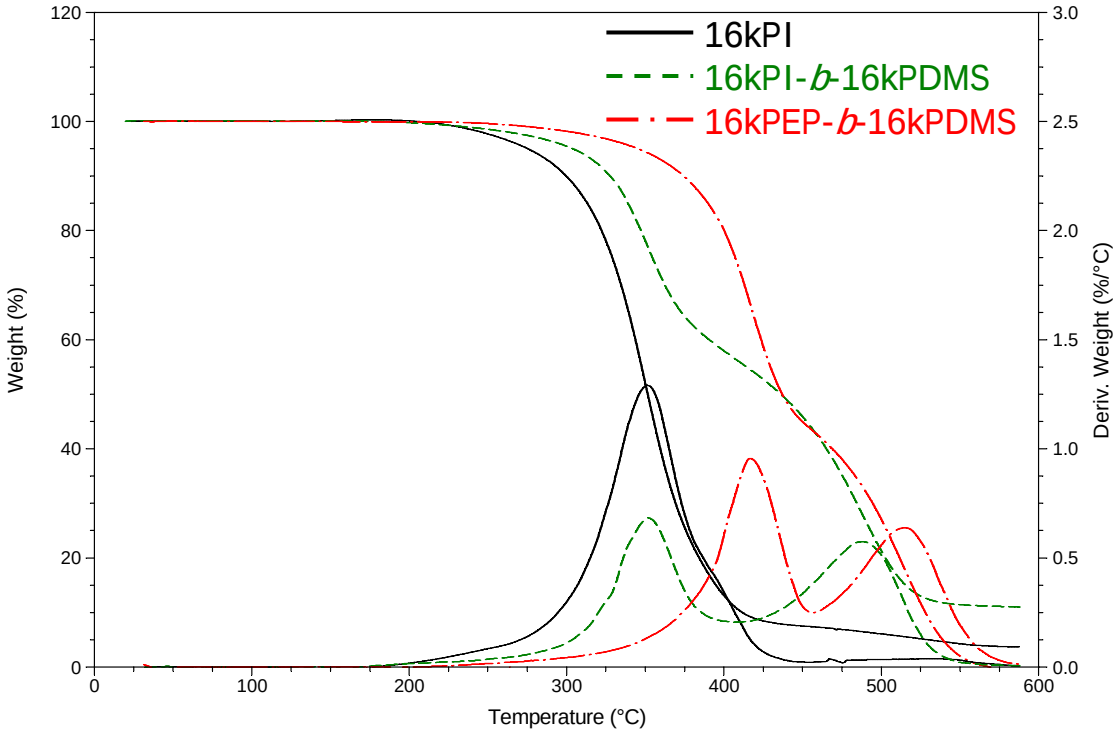


**Figure 8.4** TGA analysis of 16kPI, 16kPI-*b*-16kPDMS and 16kPEP-*b*-16kPDMS

DSC analysis of 16kPEP-*b*-16kPDMS and 14kPEP-*b*-10kPDMS were performed and the DSC curves are shown in Figure 8.5 and 8.6. The observed glass transition temperature ($T_g$), crystallization temperature ($T_c$), and melting temperature ($T_m$) are shown in Figure 8.5 and 8.6 as well as tabulated in Table 8.5. Both 16kPEP-*b*-16kPDMS and 14kPEP-*b*-10kPDMS provided the same temperature range of four transitions, which were glass transition ($T_g$), an exothermal crystalline formation (cold crystallization, $T_c$), and melting of two different crystalline form ($T_m$).[29]

PDMS block showed $T_g$ – 125 ºC, $T_c$ -90 or -91 ºC, and $T_m$ -46 and -38 ºC. The transition values of PDMS block were consistent with the previously reported values.[7, 29-36] Existence of two $T_m$ was due to crystallites of different size and perfection or different crystal forms of PDMS.[29, 33, 36] These two $T_m$ transition changes to one $T_m$ if PDMS is cooled at slow rate such as -2 ºC/min.[33] On the other hand, PEP block showed $T_g$ -60 or

-61 ºC, while $T_m$ was not observed in either block copolymer. These $T_g$ values are good agreement with a $T_g$ value in literatures, -57 to -63 ºC.[7, 37]

Both PDMS block and PEP block gave own $T_g$ values, which indicated the synthesized PEP-*b*-PDMS block copolymers were phase-separated. The phase-separation behavior was confirmed estimating $\chi N$, where $\chi$ is Flory-Huggins interaction parameter, and $N$ is the total degree of polymerization. The calculation of $\chi$ followed the equation 2-4:

$$\chi_{12} = \frac{V_0(\delta_2 - \delta_1)^2}{RT} \qquad (2\text{-}4)$$

The molar volumes of PDMS and PEP are 73.5 $cm^3/mol$[38] and 81.8 $cm^3/mol$,[38] respectively. The solubility parameters of PDMS and PEP are 14.97 $(J/cm^3)^{1/2}$ [7, 39] and 16.74 $(J/cm^3)^{1/2}$,[38, 40] respectively. These values were plugged into the equation 2-4 and the calculated $\chi_{PDMS/PEP}$ value at $T$ = 298 K resulted in 0.098. Utilizing the component molecular weight of 16kPEP-*b*-16kPDMS and 14kPEP-*b*-10kPDMS in Table 8.2, $N$ for 16kPEP-*b*-16kPDMS and 14kPEP-*b*-10kPDMS were estimated as 441 and 337, respectively. Therefore, $\chi N$ for 16kPEP-*b*-16kPDMS and 14kPEP-*b*-10kPDMS are 43 and 33, respectively, which are large enough to produce phase separation between PEP block and PDMS block.

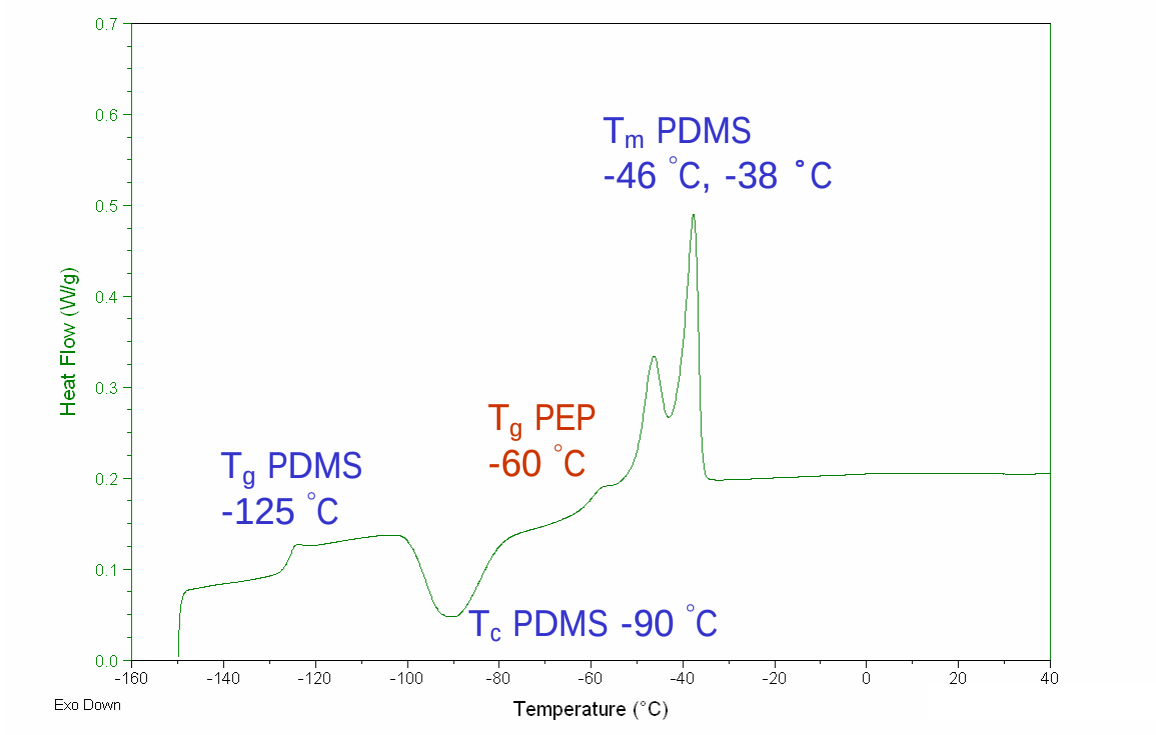


**Figure 8.5** DSC analysis of 16kPEP-*b*-16kPDMS

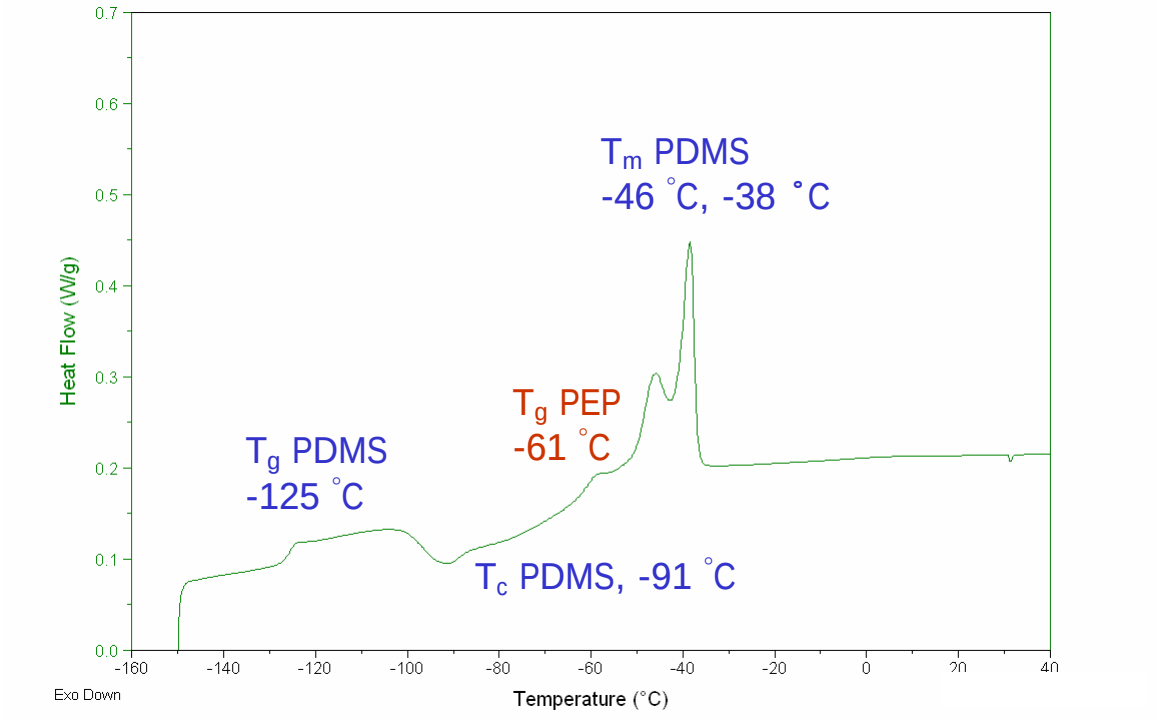


**Figure 8.6** DSC analysis of 14kPEP-*b*-10kPDMS

**Table 8.5** Thermal transition of 14kPEP-*b*-10kPDMS and 16kPEP-*b*-16kPDMS

| | $T_{gPDMS}$ [ºC] | $T_{gPEP}$ [ºC] | $T_{cPDMS}$ [ºC] | $T_{mPDMS1}$ [ºC] | $T_{mPDMS2}$ [ºC] |
|---|---|---|---|---|---|
| 14kPEP-*b*-10kPDMS | -125 | -60 | -90 | -46 | -38 |
| 16kPEP-*b*-16kPDMS | -125 | -61 | -91 | -46 | -38 |

## 8.5 Conclusions

The synthesis of PEP (hydrogenated PI) and PEP-*b*-PDMS were performed using living anionic polymerization and subsequent hydrogenation. PEP and PEP-*b*-PDMS with well-defined molecular weight and narrow polydispersity indices were successfully achieved. In TGA measurements, the initial thermal degradation of PI-*b*-PDMS and PEP-*b*-PDMS corresponded to that of PI and PEP, and the second thermal degradation corresponded to that of PDMS. The residual weight at between two degradation steps agreed well with the incorporated amount of the PDMS block. The PEP-*b*-PDMS diblock copolymer was thermally stable over 300 ºC and this thermal and oxidative stability made PEP-*b*-PDMS diblock copolymer a good candidate for various applications. DSC analysis of PEP-*b*-PDMS provided $T_g$, $T_c$, and $T_m$ of each PEP and PDMS block, and the values were consistent with the reported values earlier. Appearance of $T_g$ for each PEP and PDMS block indicated the formation of phase separation. The calculation of $\chi N$ supported the phase separation between PEP and PDMS block.

## 8.6 Acknowledgements

The authors would like to thank NSF for financial support of this research.

## 8.7 References


1. Almdal, K.; Mortensen, K.; Ryan, A. J.; Bates, F. S., Order, disorder, and composition fluctuation effects in low molar mass hydrocarbon-poly(dimethylsiloxane) diblock copolymers. *Macromolecules* **1996,** 29, (18), 5940-5947.
2. Galloway, J. A.; Jeon, H. K.; Bell, J. R.; Macosko, C. W., Block copolymer compatibilization of cocontinuous polymer blends. *Polymer* **2005,** 46, (1), 183-191.
3. Van Hemelrijck, E.; Van Puyvelde, P.; Macosko, C. W.; Moldenaers, P., The effect of block copolymer architecture on the coalescence and interfacial elasticity in compatibilized polymer blends. *Journal of Rheology* **2005,** 49, (3), 783-798.
4. Sundararaj, U.; Macosko, C. W., Drop breakup and coalescence in polymer blends - The effects of concentration and compatibilization. *Macromolecules* **1995,** 28, (8), 2647-2657.
5. Ramic, A. J.; Stehlin, J. C.; Hudson, S. D.; Jamieson, A. M.; Manas-Zloczower, I., Influence of block copolymer on droplet breakup and coalescence in model immiscible polymer blends. *Macromolecules* **2000,** 33, (2), 371-374.
6. Kow, C.; Morton, M.; Fetters, L. J.; Hadjichristidis, N., Glass - transition behavior of polyisoprene - the influence of molecular-weight, terminal hydroxy-groups, microstructure, and chain-branching. *Rubber Chemistry and Technology* **1982,** 55, (1), 245-252.
7. Brandrup, J.; Immergut, E. H., *Polymer Handbook*. 3rd ed.; Wiley: New York, 1989.
8. Simon, P.; Cibulkova, Z.; Thomas, P., Accelerated thermooxidative ageing tests and their extrapolation to lower temperatures. *Journal of Thermal Analysis and Calorimetry* **2005,** 80, (2), 381-385.
9. Gadegaard, N.; Almdal, K.; Larsen, N. B.; Mortensen, K., The lamellar period in symmetric diblock copolymer thin films studied by neutron reflectivity and AFM. *Applied Surface Science* **1999,** 142, (1-4), 608-613.
10. Krishnan, K.; Chapman, B.; Bates, F. S.; Lodge, T. P.; Almdal, K.; Burghardt, W. R., Effects of shear flow on a polymeric bicontinuous microemulsion: Equilibrium and steady state behavior. *Journal of Rheology (New York, NY, United States)* **2002,** 46, (2), 529-554.
11. Papadakis, C. M.; Almdal, K.; Mortensen, K.; Vigild, M. E.; Stepanek, P., Unexpected phase behavior of an asymmetric diblock copolymer. *Journal of Chemical Physics* **1999,** 111, (9), 4319-4326.
12. Rittig, F.; Karger, J.; Papadakis, C. M.; Fleischer, G.; Stepanek, P.; Almdal, K., Self-diffusion investigations on a series of PEP-PDMS diblock copolymers with different morphologies by pulsed field gradient NMR. *Physical Chemistry Chemical Physics* **1999,** 1, (17), 3923-3931.
13. Schwahn, D.; Frielinghaus, H.; Mortensen, K.; Almdal, K., Temperature and pressure dependence of the order parameter fluctuations, conformational compressibility, and the phase diagram of the PEP-PDMS diblock copolymer. *Physical Review Letters* **1996,** 77, (15), 3153-3156.
14. Schwahn, D.; Mortensen, K.; Frielinghaus, H.; Almdal, K.; Kielhorn, L., Thermal composition fluctuations near the isotropic Lifshitz critical point in a ternary mixture of a homopolymer blend and diblock copolymer. *Journal of Chemical Physics* **2000,** 112, (12), 5454-5472.
15. Rittig, F.; Kaerger, J.; Papadakis, C. M.; Fleischer, G.; Almdal, K.; Stepanek, P., Self-diffusion in a lamellar and gyroid (ordered) diblock copolymer investigated using pulsed field gradient NMR. *Macromolecules* **2001,** 34, (4), 868-873.
16. Papadakis, C. M.; Almdal, K.; Mortensen, K.; Rittig, F.; Fleischer, G.; Stepanek, P., The bulk dynamics of a compositionally asymmetric diblock copolymer studied using dynamic light scattering. *European Physical Journal E: Soft Matter* **2000,** 1, (4), 275-283.
17. Rittig, F.; Fleischer, G.; Kaerger, J.; Papadakis, C. M.; Almdal, K.; Stepanek, P., Anisotropic self-diffusion in a hexagonally ordered asymmetric PEP-PDMS diblock copolymer studied by pulsed field gradient NMR. *Macromolecules* **1999,** 32, (18), 5872-5877.

18. Fleischer, G.; Rittig, F.; Karger, J.; Papadakis, C. M.; Mortensen, K.; Almdal, K.; Stepanek, P., Self-diffusion of an asymmetric diblock copolymer above and below the order-to-disorder transition temperature. *Journal of Chemical Physics* **1999,** 111, (6), 2789-2796.
19. Fleischer, G.; Rittig, F.; Stepanek, P.; Almdal, K.; Papadakis, C. M., Self-diffusion of a symmetric PEP-PDMS diblock copolymer above and below the disorder-to-order transition. *Macromolecules* **1999,** 32, (6), 1956-1961.
20. Vigild, M. E.; Almdal, K.; Mortensen, K.; Hamley, I. W.; Fairclough, J. P. A.; Ryan, A. J., Transformations to and from the gyroid phase in a diblock copolymer. *Macromolecules* **1998,** 31, (17), 5702-5716.
21. McGrath, J. E.; Wilkes, G. L.; Ward, T. C.; Broske, A. D.; Lee, B.; Yilgor, I.; Bradley, D. J.; Hoover, J. M.; Long, T. E., *New elastomer synthesis for high performance applications*. Noyes Data Corporation Parkridge, New Jersey, 1988; p 118.
22. Bellas, V.; Iatrou, H.; Hadjichristidis, N., Controlled anionic polymerization of hexamethylcyclotrisiloxane. Model linear and miktoarm star co- and terpolymers of dimethylsiloxane with styrene and isoprene. *Macromolecules* **2000,** 33, (19), 6993-6997.
23. Chiantore, O.; Guaita, M.; Lazzari, M.; Hadjichristidis, N.; Pitsikalis, M., Thermal degradation of model linear and star-shaped polyisoprene molecules. *Polymer Degradation and Stability* **1995,** 49, (3), 385-92.
24. Jovanovic, J. D.; Govedarica, M. N.; Dvornic, P. R.; Popovic, I. G., The thermogravimetric analysis of some polysiloxanes. *Polymer Degradation and Stability* **1998,** 61, (1), 87-93.
25. Jana, R. N.; Nando, G. B., Thermogravimetric analysis of blends of low-density polyethylene and poly(dimethyl siloxane) rubber: The effects of compatibilizers. *Journal of Applied Polymer Science* **2003,** 90, (3), 635-642.
26. Jana, R. N.; Mukunda, P. G.; Nando, G. B., Thermogravimetric analysis of compatibilized blends of low density polyethylene and poly(dimethyl siloxane) rubber. *Polymer Degradation and Stability* **2003,** 80, (1), 75-82.
27. Deshpande, G.; Rezac, M. E., Kinetic aspects of the thermal degradation of poly(dimethyl siloxane) and poly(dimethyldiphenyl siloxane). *Polymer Degradation and Stability* **2002,** 76, (1), 17-24.
28. Lim, K. T.; Webber, S. E.; Johnston, K. P., Synthesis and characterization of poly(dimethyl siloxane)-poly[alkyl (meth)acrylic acid] block copolymers. *Macromolecules* **1999,** 32, (9), 2811-2815.
29. Clarson, S. J.; Dodgson, K.; Semlyen, J. A., Studies of cyclic and linear poly(dimethylsiloxanes). 19. Glass transition temperatures and crystallization behavior. *Polymer* **1985,** 26, (6), 930-4.
30. Lue, S.; Yang, S.; Chang, Y., Sorption of organic solvents in poly(dimethyl siloxane) membrane. II. Effect of sorption on the polymer crystals upon cooling. *Journal of Macromolecular Science, Part B: Physics* **2006,** 45, (3), 417-430.
31. Beigbeder, A.; Bruzaud, S.; Spevacek, J.; Brus, J.; Grohens, Y., Dynamics and crystallization in polydimethylsiloxane nanocomposites. *Macromolecular Symposia* **2005,** 222, (Polymer-Solvent Complexes and Intercalates V), 225-231.
32. Jiao, J.; Rak, S.; Polak, A., The effect of crystallization on the modulus of thermally conductive silicone adhesives. *Thermochimica Acta* **2000,** 357-358, 313-319.
33. Soutzidou, M.; Panas, A.; Viras, K., Differential scanning calorimetry (DSC) and Raman spectroscopy study of poly(dimethylsiloxane). *Journal of Polymer Science, Part B: Polymer Physics* **1998,** 36, (15), 2805-2810.
34. Aranguren, M. I., Crystallization of polydimethylsiloxane: effect of silica filler and curing. *Polymer* **1998,** 39, (20), 4897-4903.
35. Okamoto, S.; Hasegawa, H.; Hashimoto, T.; Fujimoto, T.; Zhang, H.; Kazama, T.; Takano, A.; Isono, Y., Morphology of model three-component three-arm star-shaped copolymers. *Polymer* **1997,** 38, (21), 5275-5281.
36. Wang, B.; Krause, S., Properties of dimethylsiloxane microphases in phase-separated dimethylsiloxane block copolymers. *Macromolecules* **1997,** 20, 2201-2208.
37. Gotro, J. T.; Graessley, W. W., Model hydrocarbon polymers - Rheological properties of linear polyisoprenes and hydrogenated polyisoprenes. *Macromolecules* **1984,** 17, (12), 2767-2775.
38. Van Krevelen, D. W.; Hoftyzer, P. J., *Properties of Polymers*. Elsevier: New York, 1976.

39. Roth, M., Solubility parameter of poly(dimethyl siloxane) as a function of temperature and chain-length. *Journal of Polymer Science Part B-Polymer Physics* **1990,** 28, (13), 2715-2719.
40. Krishnamoorti, R.; Graessley, W. W.; Dee, G. T.; Walsh, D. J.; Fetters, L. J.; Lohse, D. J., Pure component properties and mixing behavior in polyolefin blends. *Macromolecules* **1996,** 29, (1), 367-376.

# Chapter 9: Overall Conclusions

Introducing non-covalent interactions altered polymer properties. Placing functional groups (hydrogen-bonding or ionic groups) in a specific location on macromolecular architecture played a significant role in the resulting thermal, mechanical and morphological properties.

Novel sulfonated graft copolymers, with precise location of the sulfonated blocks, either adjacent to the backbone or at the branch termini, were successfully synthesized using living anionic polymerization, free radical graft copolymerization, and post-sulfonation. The location of sulfonated blocks in both sulfonic acid and sodium sulfonate graft copolymers significantly affected the thermal, mechanical and morphological properties. The mobility of the sulfonated blocks located at the branch termini enabled the sulfonated blocks to more readily interact and form ionic aggregates. The glass transition temperatures ($T_g$) of the sulfonated graft copolymers with sulfonated blocks at the branch termini were higher than that of graft copolymers with sulfonated blocks adjacent to the backbone. The appearance of ionomer peaks in SAXS also demonstrated more facile aggregation of sulfonated blocks at the branch termini. The aggregation of sulfonic acid or sodium sulfonate groups at the branch termini restricted the glass transition of the PEP block in DMA. Molecular architecture plays a significant morphological role, and can be used as a design parameter for utilization of ionomers.

Living anionic polymerization methodology also enabled synthesis of well-defined various macromolecular architectures. 1000 g/mol 60% 1,2-liquid polybutadiene homopolymer was prepared using conventional anionic polymerization and anionic telomerization. Maintaining both the initiation and reaction temperatures at lower than

70 °C minimized the chain transfer and synthesized well-defined liquid PBs with narrow polydispersity indices. MALDI-TOF MS also verified that liquid PBs synthesized from anionic telomerization possessed one benzyl and one proton end groups.

Synthesis of well-defined PEP (hydrogenated PI) and PEP-*b*-PDMS with narrow polydispersity indices was successfully achieved. PEP-*b*-PDMS diblock copolymer was thermally stable over 300 ºC. This thermal and oxidative stability broadened its application of PEP-*b*-PDMS diblock copolymer. Appearance of $T_g$ for each PEP and PDMS block in DSC demonstrated the formation of phase separation, which was also supported by calculated $\chi N$.

Furthermore, 2-ureido-4[*1H*]-pyrimidone (UPy) quadruple hydrogen-bonding was successfully introduced to telechelic poly(ethylene-*co*-propylene) (PEP) and styrene-butadiene rubbers. Introducing UPy groups to SBRs or PEP drastically altered the physical properties of these materials. The hydrogen-bonding networks served as mechanically effective crosslinks, which raised $T_g$ and enhanced the mechanical performance. The composites with UPy-functionalized carbon nanotubes further enhanced the mechanical properties and the UPy-UPy association between the matrix polymer and carbon nanotubes prevented the decrease of an elongation at break.

# Chapter 10: Suggested Future Work

## 10.1 Site-specific Sulfonated Graft Copolymers: Study in Mixed Solvent System

In Chapter 6, poly(methyl methacrylate)-*g*-(poly(sulfonic acid styrene)-*b*-poly(*tert*-butyl styrene)), poly(methyl methacrylate)-*g*-(poly(*tert*-butyl styrene)-*b*-poly(sulfonic acid styrene)), and the corresponding sodium sulfonate salts were synthesized, and thermal and morphological characterization were performed. These sulfonated graft copolymers also showed unique solubility property in THF/MeOH mixture. Figure 10.1 depicts the solubility of the sulfonic acid graft copolymers and sodium sulfonate graft copolymers in THF/MeOH mixture.

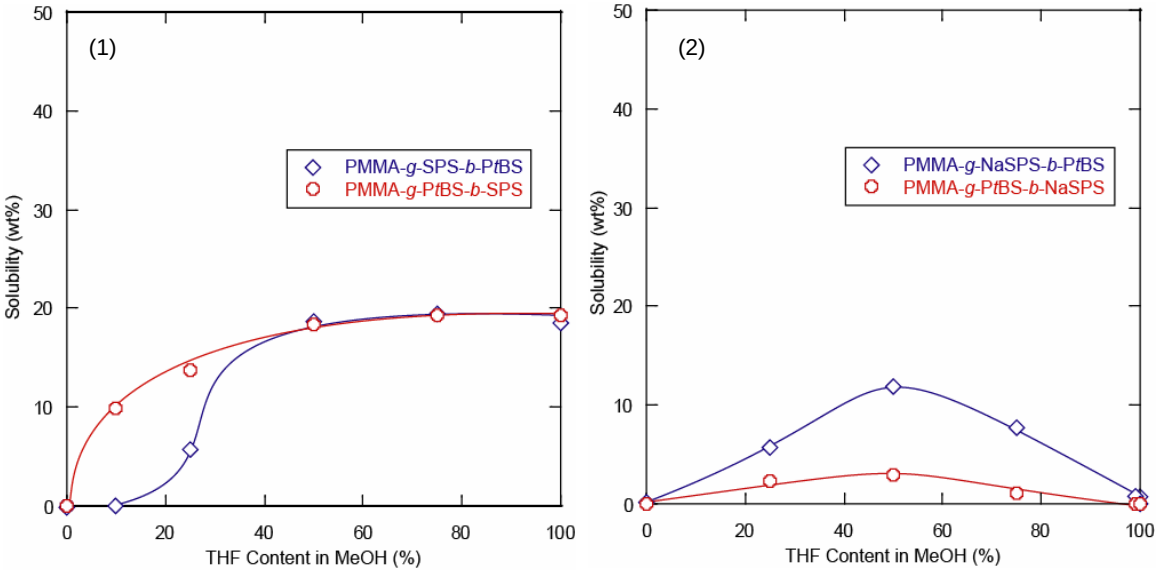


**Figure 10.1** Solubility of the sulfonic acid graft copolymers (1) and sodium sulfonate graft copolymers (2) in THF/MeOH mixture.

Further investigation of the site-specific sulfonated graft copolymer properties in the mixed solvent has not been performed. The suggested future work will include:

1. Solution rheology of site-specific sulfonated graft copolymers in various THF/MeOH ratio.
2. Investigation of the aggregation behavior using dynamic light scattering (Preliminary study was already performed.)
3. Morphological study of spin-coated films from various THF/MeOH graft copolymer solution. (Preliminary study was already performed.)

## 10.2 Site-specific Sulfonated Graft Copolymers with Low $T_g$ Fluorinated Backbone

Chapter 7 described the development of site-specific sulfonated graft copolymers for improved performance. Exchanging P*t*BS block to PEP improved the mechanical properties; however, large number of branches could not be incorporated due to the solubility of the resulting graft copolymers. To overcome this issue, a fluorinated polyisoprene backbone is proposed as a future work.

Synthesis and characterization of site-specific sulfonated graft copolymers with fluorinated polyisoprene backbone will be;

1. (1) Graft copolymerization of isoprene with P*t*BS-*b*-PS diblock macromonomer or PI-*b*-PS diblock macromonomer. (2) Metalation graft polymerization[1] of P*t*BS-*b*-PS from PI backbone; *n*-BuLi/TMEDA complex metalates allylic C-H bonds in isoprene units (Scheme 10.1 above) and graft polymerization occurs from the PI backbone.
2. Fluorination of PI backbone using difluorocarbene ($:CF_2$) generated from thermolysis of hexafluoropropyleneoxide (HFPO)[2]
3. Post sulfonation of the fluorinated graft copolymers

4. Morphological characterization using AFM, TEM and SAXS
5. Proton conductivity measurement (sulfonated PS block should be designed to be longer than that of previous study in Chapter 6 and 7)
6. Investigation of water uptake and swelling relating to the measured proton conductivity
7. Mechanical testing of the site-specific sulfonated graft copolymers with various counter ions using DMA and tensile measurement.

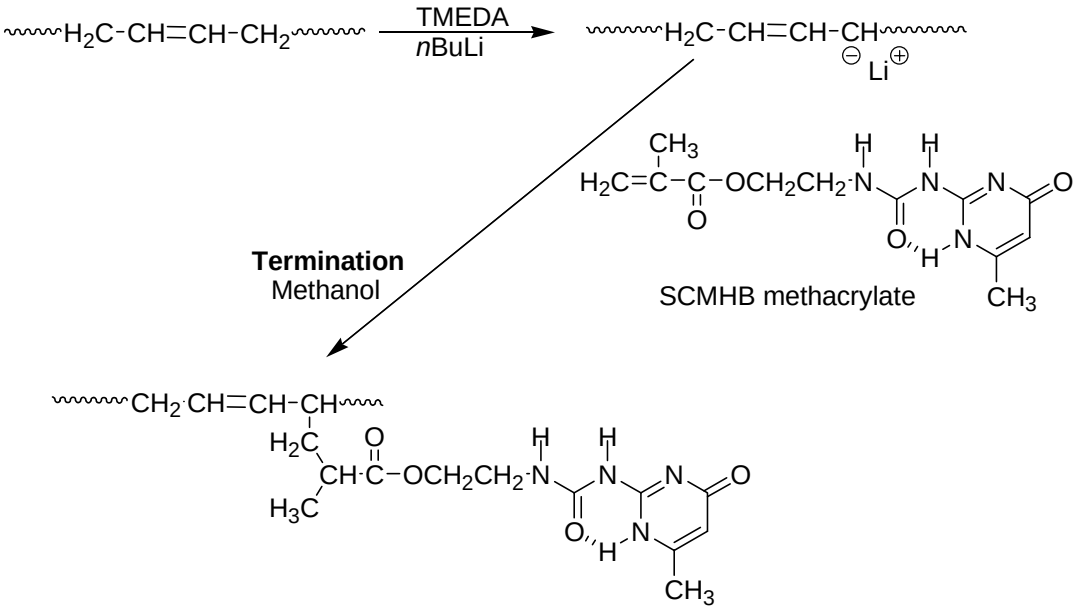


**Scheme 10.1** Introducing UPy groups to butadiene backbone: Metalation of allylic carbon and subsequent Michael reaction

## 10.3 Another Strategy for Introducing SCMHB to SBR Backbone

Chapter 5 described multiple step functionalizations of SBRs. To achieve facile UPy-functionalization of SBRs, another proposed strategy uses one step functionalization. The first step involves metalation of allylic carbon using TMEDA/*n*BuLi.[1] The second step utilizes Michael reaction with UPy-methacrylate[3] as shown in Scheme 10.1. UPy-

groups might prevent the Michael reaction, thus, preliminary experiments will be necessary to confirm that this chemistry works. The suggested future work includes:

1. Introduction of UPy-methacrylate to SBRs
2. Determination of incorporated amount of UPy groups using NMR and TGA
3. Mechanical testing using DMA and tensile measurement
4. Melt rheology to understand the thermoreversibility
5. Tensile experiment to measure the elastic property

## 10.4 Supramolecular Polymers Containing SCMHB

Novel UPy-containing isocyanate, MIC-IDPI, was synthesized in Chapter 5. Introducing MIC-IPDI to functional ends of oligomers will form thermoreversible supramolecular polymers. For example, the reaction of MIC-IPDI with phosphonium-diol was attempted. The reaction scheme and schematic image is shown in Figure 10.2.

Synthesis of novel thermoreversible supramolecular polymers involves:

1. Introduction of UPy-IPDI to various diols or diamines
2. Determination of incorporated amount of UPy groups using TGA
3. Mechanical testing using DMA and tensile measurement
4. Melt rheology to understand the thermoreversibility
5. Morphological characterization using AFM
6. Melt or solution electrospinning

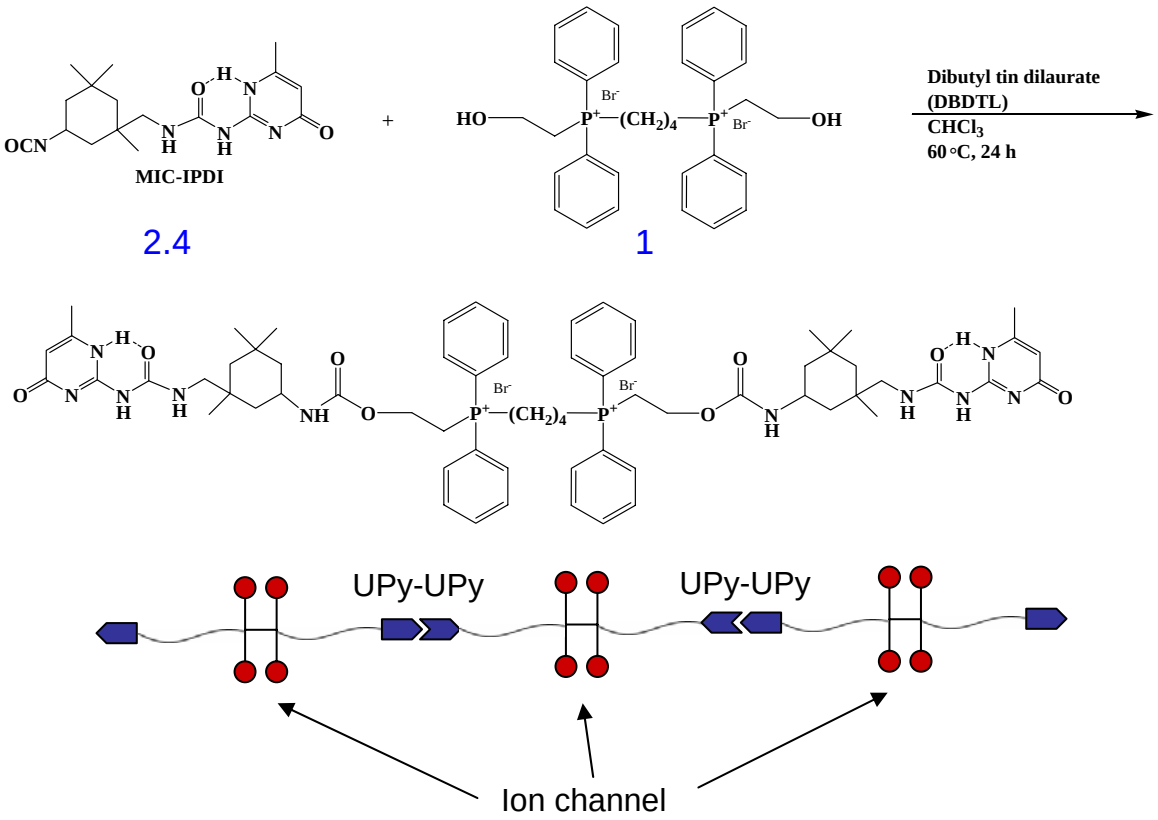


**Figure 10.2** Reaction of MIC-IDPI with phosphonium-diol and resulting supramolecular polymer

## 10.5 References


1. Hsieh, H. L.; Quirk, R. P., *Anionic Polymerization*. Marcel Dekker, Inc.: New York, Basel, Hong Kong, 1996.
2. Huang, T.; Messman, J. M.; Mays, J. W., A new fluorinated polymer having two connected rings in the main chain: Synthesis and characterization of fluorinated poly(1,3-cyclohexadiene). *Macromolecules* **2008,** 41, (1), 266-268.
3. Yamauchi, K.; Lizotte, J. R.; Long, T. E., Thermoreversible poly(alkyl acrylates) consisting of self-complementary multiple hydrogen bonding. *Macromolecules* **2003,** 36, (4), 1083-1088.